Evaluation and prediction of cohesive soil erosion parameters among varying soil properties and testing procedures: Implications for river bed scour at bridge piers

A Dissertation Presented for the
Doctor of Philosophy
Degree
The University of Tennessee, Knoxville

Badal Mahalder
May 2018

Copyright © 2018 by Badal Mahalder
All rights reserved.

DEDICATION

This dissertation is dedicated to my grandparents Nagendra Nath Mahalder (late) and Sarala Mahalder (late), my wife Mollika Roy, my parents Kanchan Mahalder and Amar Mahalder, and my son Adrik Borno Mahalder.

ACKNOWLEDGEMENTS

I would like to extend my deepest gratitude to Dr. John S. Schwartz my major advisor and Dr. Angelica M. Palomino my co major advisor for developing the initial scope for the research, securing funding and bringing me into the project. Their knowledge, expertise, encouragement and guidance have been invaluable. Without their continuous suggestions and knowledgeable feedbacks, this work would not be possible to accomplish. I would also like to express the appreciation to my committee members Dr. Athanasios N. Papanicolaou, Dr. Daniel C. Yoder and Dr. Tess M. Thompson for their willingness to serve as committee members. Their experience and broad knowledge base, insightful suggestions, and feedback have been a great resource.

I would like to thank Tennessee Department of Transportation (TDOT), especially Mr. Jon Zirkle and its board of directors for approving and providing the funding for this research work.

A special thanks to Ms. Nancy Roberts for helping me schedule time for use of the department lab equipment and facilities. I would also like to express my gratitude to Dr. Chris Cox for extending his helping hand in quick laboratory flume construction process for finishing my experimental work. My special gratitude is to Mr. Andy Baker and Mr. Larry Roberts for their tireless help for the outdoor flume construction.

I would also like to acknowledge the Hydraulics and Sedimentation Laboratory, special thanks to Dr. Athanasios N. Papanicolaou for letting me use the pressurized flume to complete one of my research objectives.

I would also like to appreciate the efforts of Jordan Hicks, Zachariah Seiden, Bijoy K. Halder, Adrian Gonzalez, Cyrus Jedari, Robert Woockman, Brandy Manka, Payton Smith, Alex Hollman, Maxwell Carter, Alan Jolly and Michael Walton. Their supports in the field and/or laboratory have been instrumental for achieving the research objectives.

The encouragement of my parents and family members are also instrumental for my dedication to accomplish this research work and was another key.

Finally, I would like to thank my wife Mollika Roy for her sacrifice, time, and the physical and mental support in the field and at home. I don’t have any words to express her contributions.

ABSTRACT

Sediment entrainment in cohesive soils is influenced by interactions among the soil physical, geochemical and biological properties, which eventually define the inter-particle forces. Research was conducted for better understanding cohesive soil erosion using an in-situ mini-jet device for estimating erodibility parameters: critical shear stress (τ_c) and erodibility coefficient (k_d), and develop a modified field operational and data analysis procedure to more consistently predict these parameters. This newly developed procedure accounted for sediment property changes in surface and subsurface layers on stream beds/banks. Field data were collected from 21 streams using this method among geologically diverse formations across Tennessee, USA and identified that geological origin affected the erodibility parameters estimation. Predictive models were also developed among four physiographic provinces based on controlling soil physicochemical properties, in which a comprehensive suite of soil properties were assessed.

Because existing studies report a wide variability in estimating erodibility parameters per device, research compared results between two fundamentally different devices: conduit flume and mini-jet device. Estimated results showed a reasonable correlation between the two devices for τ_c (R^2 = 0.58) but deviated for k_d. This fundamental research on measurements of the erodibility parameters with relationships to soil properties were applied to a civil infrastructure issue of scour at highway road bridges. Through an extensive hydrological modeling effort, the influence of cumulative effective stream power on scour depth around piers in cohesive sediments was explored. It was identified that shear duration, number of flow events above critical, and age of foundation were significantly affecting the observed scour depths around bridge piers.

In addition, a laboratory flume experiment was also conducted using natural cohesive sediments around cylinder. The effect of multiple flow events on scour depth propagation and the stress history (memory effect) were studied. Results from these experiments showed significant influence on final scour depths based on the flow sequence. Finally the available scour depth predictive equations were also used to compare the results from this study. In general, findings from this research expand the body of knowledge on improving our understanding of erosion behavior and associated processes in cohesive soils in stream banks/beds.

TABLE OF CONTENTS

CHAPTER I INTRODUCTION 1

1.1 General 1

1.2 Problem statement 2

1.2.1 Issues with critical shear stress measurement in cohesive soil 2

1.2.2 Scour depth prediction and consequences 4

1.2.3 Equilibrium scour behavior for cohesive soil 4

1.3 Background 5

1.4 Research Objectives 7

1.5 Organization of this Dissertation 8

1.6 References 10

CHAPTER II PROPOSED NEW METHOD FOR JET DEVICE 12

Abstract 13

2.1 Introduction 13

2.2 Background for jet test data analysis 18

2.3 Materials and Methods 20

2.3.1. Study Design 20

2.3.2. Study Area 21

2.3.3. Field data collection and computational procedures 22

2.4. Results and Discussion 29

2.4.1. Comparison of SPS and MPS methods for estimating critical shear stress 29

2.4.2. Comparison of MPS method and computational procedures for erodibility parameters 33

2.4.3. Qualitative observations in scour-hole development and morphology 39

2.5. Conclusions 41

2.6 References 44

CHAPTER III RELATIONSHIPS BETWEEN SOIL PROPERTIES AND ERODIBILITY 48

Abstract 49

3.1 Introduction 49

3.2 Review: Predictive Relationships for Soil Erodibility 52

3.3 Study Area 54

3.4 Methodology 56

3.4.1 Data collection 56

3.4.2 Laboratory analysis 59

3.4.3 Parameters prediction for excess shear stress equation 60
3.4.4 Multicollinearity in the dataset 60
3.4.5 Cluster analysis 61
3.4.6 Statistical model development for variable selection 61
3.5 Results 64
3.5.1 Soil Properties 64
3.5.2 Properties of the cluster groups 67
3.5.3 Statistical correlation and model variable selection 67
3.6 Discussion 76
3.6.1 Correlation pattern of significant variables 78
3.6.2 Relationship of critical shear stress with the erodibility coefficient 83
3.7 Conclusions 84
3.8 References 86
CHAPTER IV IDENTIFICATION OF DEVICE DEPENDENT VARIABILITY 92
Abstract 93
4.1 Introduction 93
4.2 Theoretical Background 97
4.2.1 In-situ jet test device 97
4.2.2 Mini-jet test device design specifications 98
4.2.3 Device hydraulic principles 100
4.2.4 Laboratory conduit flume 101
4.2.5 Bed shear stress calculations 103
4.2.6 Comparative study rationale 104
4.3 Methodology 106
4.3.1 Sites locations for soil collections 106
4.3.2 Soil sample collection 108
4.3.3 Soil sample testing in laboratory conduit flume 109
4.3.4 Data analysis 111
4.4 Results 112
4.4.1 Physical properties of soil samples 112
4.4.2 Chemical properties of sediment-water mix 113
4.4.3 Critical shear stress measurement 116
4.4.4 Statistical data analysis 116
4.5 Discussion 124
4.6 Conclusions 132
4.7 References 133
CHAPTER V SCOUR DEPTH PREDICTION IN COHEISVE SOIL 137
Abstract 138
5.1 Introduction 138

5.2 Methods 142
5.2.1 Study Design 142
5.2.2 Erodibility index calculation 146
5.2.3 Hydrologic flow simulation 147
5.2.4 Field measurements of stream bank/bed soil critical shear stress 149
5.2.5 Effective stream power calculation 150
5.3 Results 151
5.3.1 Behavior of the data 151
5.3.2 Case study for Pond Creek site on scour pattern 156
5.4 Discussion 156
5.5 Conclusions 164
5.6 References 166
CHAPTER VI SCOUR STUDY IN COHESIVE SOILS 169
Abstract 170
6.1 Introduction 170
6.2 Experimental Set-up and Procedures 172
6.2.1 Flume construction 172
6.2.2 Properties of natural cohesive sediment 172
6.2.3 Sediment bed preparation 173
6.2.4 Procedure of experiment 178
6.2.5 Available equilibrium scour depth predicting equations for cohesive soil 179
6.3 Results and Discussion 182
6.3.1 Scour depth evolution 182
6.3.2 Influence of multi-flow on scour propagation 186
6.3.3 Influence of stress history on scour propagation 190
6.3.4 Comparison between different scour depth equations 191
6.4 Conclusions 195
6.5 References 197
CHAPTER VII CONCLUSIONS AND FUTURE RECOMMENDATIONS 199
7.1 Summary and Conclusions 199
7.2 Limitations and Recommendations 202
APPENDIX 204
VITA 215

LIST OF TABLES

Table 2.3.1 Procedural summaries for field data collection and computation for erodibility parameters using the mini-jet device 24

Table 2.3.2 Mini-jet test conditions comparing single pressure setting (SPS) and multiple pressure settings (MPS) field data procedures at the Gist Creek study site, including soil properties among the five test locations per upper and lower bank areas..... 27

Table 2.4.1 Statistical summary of erodibility parameters computed using different computational methods: SPS-BM, MPS-BM, SPS-SDP, MPS-SDP, SPS-IP, and MPS-IP (as defined in Table 2.3.1) 33

Table 3.4.1 Study sites with identifying information on location, geological formation and rock characteristics (Miller, 1974), and watershed drainage area (km^2)..... 58

Table 3.4.2 Soil tests and method standards used to characterize soil properties..... 59

Table 3.4.3 Statistical description of the measured variables for the dataset consisting of 128 soil samples among the different Tennessee physiographic provinces 63

Table 3.5.1 Degree of dispersion for the tested soils according to the US Army Corps of Engineers (USACE, 1970) classification criteria 65

Table 3.5.2 Multiple regression models for prediction of critical shear stress (τ_c) based on soil properties. Models included all possible regression (APR), McHenry algorithm (MHA), least angle regression (LAR), and stepwise multiple linear regression (STR). R^2, p-value, and PRESS statistics are shown for each model..... 70

Table 3.5.3 Coefficient p-values for individual variables and corresponding correlation sign among the predictive models for each cluster representing an unique physiographic province and surficial geology..... 75

Table 3.5.4 Predictive models in each cluster for erodibility coefficient (k_d) as a function of critical shear stress (τ_c) for the entire dataset, and individually for the four identified data clusters 77

Table 4.4.1 Physical properties of test soil samples from West Tennessee..... 112

Table 4.4.2 Range variation of water chemistry during the conduit flume tests..... 113

Table 4.4.3 Experimental conditions from the conduit flume test for four example samples and the corresponding parameter calculations..... 117

Table 4.4.4 Estimated critical shear stress (τ_c) using jet test and conduit flume test for four West Tennessee study sites 119

Table 5.2.1 Study sites characters including the watershed and bridge..... 144

Table 5.2.2 Statistical error calculation and validation targets 149

Table 5.3.1 Soil properties, erodibility index parameters, critical shear stress and critical stream power per unit width of channel, and channel slope for the nine study sites 152

Table 6.2.1 Properties of Crooked Creek sediment 175

Table 6.2.2 Experimental condition 177

Table 6.3.1 Scour depth development around circular pier for different flow and soil condition 188

Table 6.3.2 Comparison of observed and predicted scour depth 193

Table A.1.1 Custer 1 data 205

Table A.1.2 Cluster 2 data 207

Table A.1.3 Cluster 3 data 209

Table A.1.4 Cluster 4 data 212

LIST OF FIGURES

Figure 1.2.1: Conceptual model of the sediment properties and processes that affect sediment erodibility (Grabowski et al., 2011) 3

Figure 2.3.1: Study site locations using the mini-jet test device in Tennessee, where Gist Creek is shown as a black square and the sites used for the multiple-pressure test among the different physiographic provinces (Miller, 1974) are shown as green circles 22

Figure 2.3.2: Response patterns of critical shear stress (τ_c) and erodibility coefficient (k_d) to jet-test device pressure head setting. Data represented are identified for τ_c: (**a**) concave-down shape, (**b**) linear, (**c**) scattered points and for k_d: (**d**) concave-up shape, (**e**) linear, and (**f**) scattered points 28

Figure 2.4.1: Using the SPS method, estimates of critical shear stress (τ_c) with different pressure heads are shown for the: (**a**) lower bank and (**b**) upper bank, based on the following computational procedures: BM = Blaisdell method, IP = iterative principle, SDP = scour depth principle, and BMM = modified Blaisdell method 30

Figure 2.4.2: Based on the MPS method at the Gist Creek study site, critical shear stress (τ_c) estimates for the: (**a**) lower bank and (**b**) upper bank among the five test locations (Loca-1, -II, -III, -IV, and -V) and shown for the MPS-BM, MPS-IP, and MPS-SDP computational procedures 31

Figure 2.4.3: Estimates of critical shear stress (τ_c) at the five Gist Creek test locations for the: (**a**) lower bank and (**b**) upper bank area (Loca. -I, -II, - III, -IV, and -V). Computational methods: BM, BMM, and MPS-BM were compared 32

Figure 2.4.4: Relationship between critical shear stress (τ_c) and erodibility coefficient (k_d) using the MPS method data from this study 34

Figure 2.4.5: (**a**) Critical shear stress, and (**b**) erodibility coefficient using the field methods and computation procedures: MPS-BM, SPS-BM, SPS-SDP, and SPS-IP (as defined in Table 2.3.1) 35

Figure 2.4.6: A comparison of (**a**) critical shear stress and (**b**) erodibility coefficient using the MPS method for the computational procedures: MPS-BM, MPS-SDP, and MPS-IP (as defined in Table 2.3.1) 36

Figure 2.4.7: Pairwise differences between different solution techniques for: (**a**) critical shear stress (τ_c), and (**b**) erodibility coefficient (k_d) estimations between: MPS-BM and SPS-BM; MPS-BM and SPS-SDP; MPS-BM and SPS-IP; MPS-BM and MPS-SDP; and MPS-BM and MPS-IP procedures 37

Figure 2.4.8: Comparison of (**a**) critical shear stress (τ_c) and (**b**) erodibility coefficient (k_d) using the SPS-BM, SPS-SDP and SPS-IP methods based on data from Daly et al. (2013, 2015a)38

Figure 2.4.9: Photos of scour hole formation in different soil physical conditions (**a**) wide and shallower, and (**b**) narrow and deeper 40

Figure 3.3.1: Physiographic map of Tennessee with study sites (physiographic classifications from Miller, 1974) 56

Figure 3.5.1: Relationship between critical shear stress and erodibility coefficient with erosion index (after Hanson and Simon, 2001) 66

Figure 3.5.2: Four cluster groups using the "Ward" method and non-hierarchical "k-means" approach based on soil properties including critical shear stress..... 68

Figure 3.5.3: Measured and predicted critical shear stress (a) Cluster 1, (b) Cluster 2, (c) Cluster 3, and (d) Cluster 4 (using transformed data) 74

Figure 4.2.1: (a) Mini jet device components, (b) jet operation in the field..... 99

Figure 4.2.2: Conduit flume showing: a) photo of flume with testing box, and b) details of flume dimensions (Sutarto et al., 2014) 102

Figure 4.3.1: Study area with in-situ jet testing and soil collection locations in West Tennessee 107

Figure 4.3.2: For use the laboratory conduit flume photos show: a) the testing tray and b) the rectangular metal box to field collect soil samples..... 108

Figure 4.3.3: In-situ mini-jet testing and sample collection at the Black Creek site..... 109

Figure 4.4.1: Variation of a) electric conductivity, b) water pH, c) SAR, and d) KIF. Here "Before" stands for after completing test with first flow rate and "After" stands for after completing test with last flow rate 114

Figure 4.4.2: Variation of ion concentrations of conduit flume water during sample testing, where "Before" represents for the period after completing test with first flow rate and "After" represents the period for after completing test with last flow rate..... 115

Figure 4.4.3: Conduit flume test results from four samples as presented in Table 4.4.3; the τ_c is determined as the y-intercept where E = 0. These plots represent the sample identifier: a) COCRSP-2, b) COCRSP-3, c) COCRSP-7, and d) CRCRSP-5..... 118

Figure 4.4.4: a) Critical shear stress (τ_c), and b) erodibility coefficient (k_d) comparisons using conduit flume test and jet test results..... 120

Figure 4.4.5: Critical shear stress comparison with conduit flume test results: a) using multiple pressure settings (MPS), b) using Blaisdell method (BL), c) using scour depth principle (SDP), and d) using iterative principle (IP). Red circles in a) indicate the samples with WC < 18.5%..... 122

Figure 4.4.6: Erodibility coefficient comparison with conduit flume test results: a) using multiple pressure settings (MPS), b) using Blaisdell method (BL), c) using scour depth principle (SDP), and d) using iterative principle (IP)..... 123

Figure 4.5.1: Relationship between critical shear stress (τ_c) and erodibility coefficient (k_d): a) conduit flume, b) jet test (MPS), c) jet test (BL), and d) jet test (IP) 127

Figure 4.5.2: Erosion pattern of tested soil sample in conduit flume: a) before test, b) after test, erosion pattern from field observations: c) at bottom of creek, and d) around structures .. 131

Figure 5.1.1: Erosion in cohesive soils: a) around bridge piers in Crooked Creek, Shelby County, TN, b) undercutting at the bottom of creek in Coal Creek, Tipton County, TN... 141

Figure 5.2.1: Study watersheds showing locations of bridge sites in western Tennessee..... 145

Figure 5.2.2: Simulated flow for gaged watershed (Stokes Creek): a) model calibration, b) model validation..... 148

Figure 5.2.3: Example flow simulation for Pond Creek in Dyer County, West Tennessee, and the flow threshold at critical shear stress 150

Figure 5.3.1: Relationship between critical stream power and erodibility index. Where probability of erosion was calculated using the Wibowo et al. (2005) proposed probabilistic approach using logistic regression method 153

Figure 5.3.2: Relationship between cumulative effective stream power and scour depth measurement. Circled data points represent measurements at the Crooked Creek site..... 154

Figure 5.3.3: Relationship between relative scour depth and the number of flow events above the critical flow for the studied stream sites. Solid circles = regular scour data points, diamonds = scour data before 2004 with longer duration flow events; and squares = scour data after 2004 with short duration flow events..... 155

Figure 5.3.4: Long-term scour depth data and the number of flow events above critical flow at the bridge pier for Pond Creek showing three different scour rate over a 20-year period.. 157

Figure 5.4.1: Protective wooden logs at the vicinity of the pier in Crooked Creek 162

Figure 6.2.1: Detail of the flume: a) plan view, and b) long section of the flume (not to scale)174

Figure 6.2.2: a) Prepared sediment bed with the Plexiglas circular pier, b) placement of underwater camera during experiments for periodic scour depth measurement 176

Figure 6.2.3: Velocity distribution with depth: a) low flow (run no. 3), b) medium flow (run no. 4), and b) high flow (run no. 5)..... 179

Figure 6.3.1: Scour hole development for: a) run 16, V = 80.68 cm/s, WC = 37.45%, b) run 14, V = 80.10 cm/s, WC = 38.12%, c) run 10, V = 90.26 cm/s, WC = 31.25%, and d) run 9, V = 102.40 cm/s, WC = 31.25%..... 184

Figure 6.3.2: Scour hole development and the soil removal erosion pattern at the wake zone of the pier: run 14, V = 80.10 cm/s, WC = 38.12% 185

Figure 6.3.3: The evolution of maximum scour depth: a) for High-Medium-Low (H-M-L) flow sequence at 270° and 90° of the pier, b) for Low-Medium-High (L-M-H) flow sequence at 90° and 45° of the pier 187

Figure 6.3.4: The evolution of maximum scour depth: (a) for High-High-High (H-H-H) flow sequence at 270° and 90° of the pier, b) for Low-Low-Low (L-L-L) flow sequence at 90° and 270° of the pier..... 189

Figure 6.3.5: Observed and predicted scour depths after each experimental run..... 194

Figure A.2.1: Soil textures for tested soil samples (figure compiled using USDA soil texture calculator, http://www.nrcs.usda.gov/wps/portal/nrcs/detail/soils/survey) 213

Figure A.2.2: Soil classification according to the Unified Soil Classification System (USCS) Plasticity Chart..... 213

Figure A.2.3: Particle size distribution of the natural cohesive sediment 214

CHAPTER I
INTRODUCTION

1.1 General

The ever growing trend of human struggles in daily life for the vast growing population of the world and their basic needs to extract naturally grown resources requires more technological development and refinement of the existing techniques. Since natural processes are so complex, details of each and every phenomenon are difficult to fathom. The inter-dependent and inter-relational behavior of these complex environmental systems results in system of self-adjustments regulated by many controlling factors serving human demands. Due to expanding civilization demands, expanding the transportation system and its development are immediate needs, consequently the ever growing development of infrastructures. These structures on open channels cause major hydrological, ecological, and hydraulic disturbances in the aquatic environment. In particular, constructed structures in water bodies influence the sediment morphodynamics and the stability of structures. These structures may be prone to catastrophic failure if the design is not done accordingly. On the other hand, an overly cautious engineering design could be prohibitively expensive when the exact nature of the sediment transport around structures is not completely understood. Therefore, the nature of sediment movement, which is also known as erosion, is the foremost important factor to be investigated prior to starting any sustainable and economically viable engineering design. However, predicting the erosional behavior is not a straightforward task as it is an intriguing phenomenon resulting from the interaction between the flow dynamics around the structures and the erosive resistance of the earth material.

It is well known that sediment detachment and its transport process significantly affect the evolution of river morphology. For non-cohesive sediments, sediment detachment or initiation of movement and the transport behavior due to in-stream hydraulics, known as bed load and suspended load are reasonably well understood. However, particle/aggregate detachment or initiation in cohesive material is yet to be understood completely and is an ongoing research area. The importance of understanding this process in cohesive soils is necessary for solving numerous engineering problems. Successful implementation and sustainability of some engineering projects, such as: embankment stability, navigation, bank erosion, local and contraction scour around bridge piers and abutments on cohesive soils, are also heavily dependent on the understanding of the detachment process of cohesive soils.

1.2 Problem statement

1.2.1 Issues with critical shear stress measurement in cohesive soil

Inter-particle attraction forces play a critical role in the erosion behavior of cohesive sediments. These inter-particle attraction forces are dependent on soil physical, geochemical and biological properties, consequently, the erodibility of cohesive sediments (Figure 1.2.1). Therefore, cohesive soil erodibility is a function of sediment geotechnical, geochemical and biological properties (e.g., unit weight, plasticity, clay mineral type and content, cation exchange capacity, inter-particle forces, water and sediment temperature, sodium adsorption ratio (SAR), pH, organic content, biogenic structures, etc.). Yet, there remains a lack of reliable predictive relationships between erodibility and these soil properties.

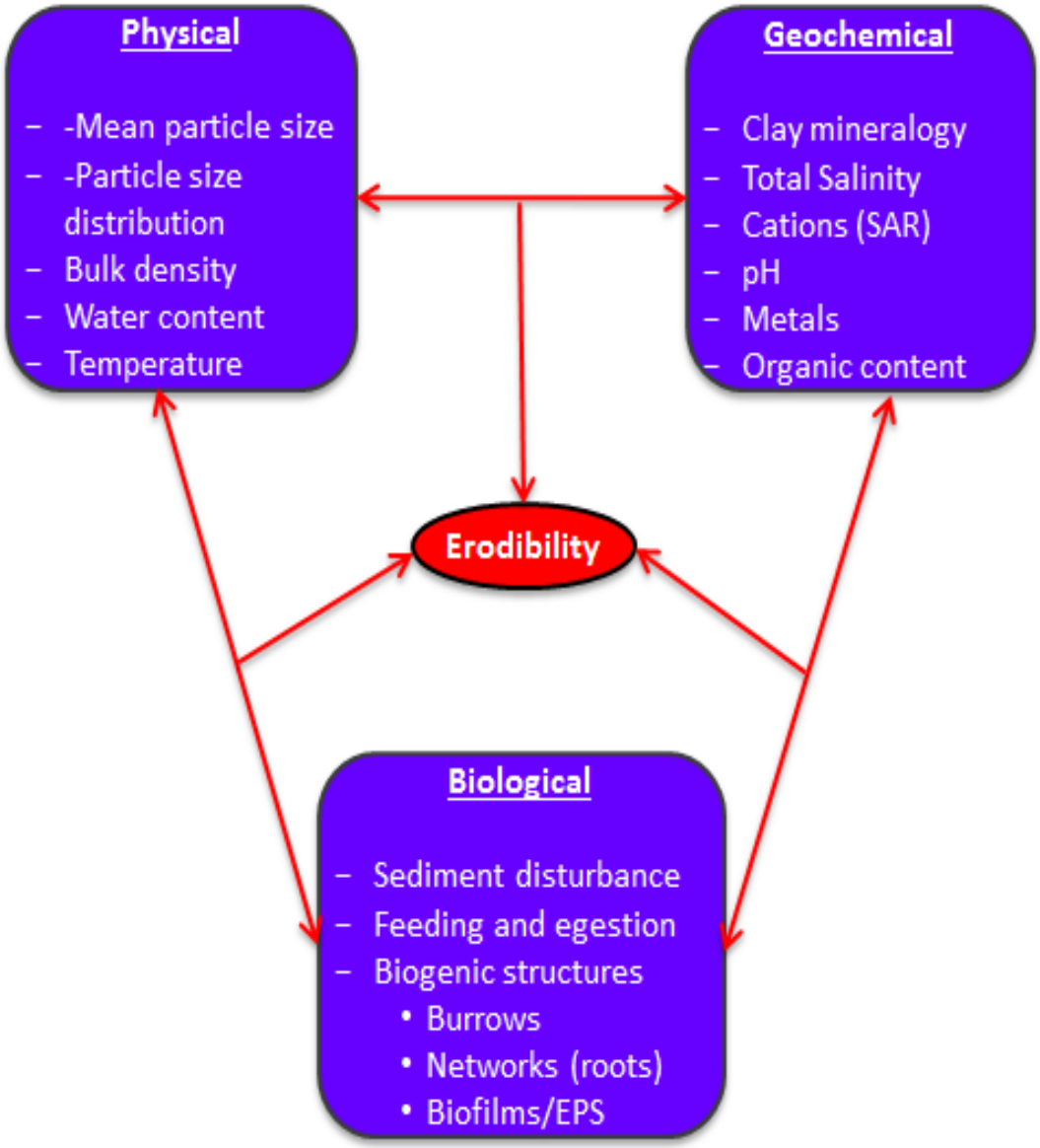


Figure 1.2.1: Conceptual model of the sediment properties and processes that affect sediment erodibility (Grabowski et al., 2011)

1.2.2 Scour depth prediction and consequences

Soil is grossly classified into coarse grained (non-cohesive) and fine grained (cohesive). In water body, structures such as bridges and culverts foundations are constructed on different soils to a certain depth based on equilibrium scour depth prediction using the available equations. Current practice for equilibrium scour depth calculation is to use the Hydraulic Engineering Circular No. 18 (HEC-18, 5th edition, 2012) equations developed by the Federal Highway Administration for bridge piers and contractions in river beds in non-cohesive, i.e. coarse-grained sediments. There are approximately 610,749 bridges in the United States and about 500,000 of them are over water (National Bridge Inventory, 2017). During the last 30 years, about 1000 bridges have failed and about 60% of those failures are due to scour (Shirole and Holt, 1991; Cook, 2014). The average cost for flood damage repair of highways on the federal aid system is $50 million per year (Lagasse et al., 1995). Therefore, efficient bridge design is necessary for avoiding any catastrophic bridge failure but must also remain cost effective to reduce construction costs. Recently, a study conducted by the South Carolina Department of Transportation (SCDOT) and the US Geological Survey found HEC-18 equations over-predicted scour depth in cohesive sediments for 84% of bridge sites surveyed, with over-predicted depths ranging from 0.1 to 13.4 ft (Benedict and Caldwell, 2009). The study also showed 16% of the surveyed sites under-predicted the scour depth, which were a function of local bed sediment and geological conditions with high hydraulic resistance properties.

1.2.3 Equilibrium scour behavior for cohesive soil

The behavior of cohesive soil erosion around bridge piers and abutments is different compared to non-cohesive soils, and there is no widely accepted approach for erosion prediction for cohesive sediments. During a large storm event, the peak flood velocity may last for a few hours or days and is likely sufficient for maximum scour generation for non-cohesive soils. This

the major difference between non-cohesive soils and cohesive soils erosion properties (TRB, 2004). Hence, knowing the peak flow or peak flow velocity is necessary for maximum or equilibrium scour depth calculations in non-cohesive soils. On the other hand, in cohesive soils, scour and erosion rate can be 1000 times slower than in non-cohesive soils. In cohesive soils, a few days may generate only a small fraction of the maximum scour depth, and so is termed a time dependent phenomena (Briaud et al., 2001).

1.3 Background

Based on a review of the existing literature, resistance to scour and scouring rates of cohesive sediments are controlled by a number of interacting and interrelated factors such as cohesion, water stability, density, specific gravity, mechanical composition, structure and texture, fissuring, plastic properties, mineralogical composition and saturation with cations, chemical composition and salinity, piping properties, moisture before exposure to flow, total moisture capacity, permeability, vegetal cover and species of plants, meteorological conditions, chemical composition of water and its turbidity, in-plane and cross-sectional geometry of the channel, roughness of the channel, flow depth, turbulence characteristics (scale intensity, frequency), etc. (Dunn, 1959; Smerdon and Beasley, 1959; Lyle and Smerdon, 1965; Alizadeh, 1974; Raudkivi, 1990; Wynn, 2004; Julian and Torres, 2006; Mostafa et al., 2008; Thoman and Niezgoda, 2008; Grabowski et al., 2011).

The abundance of these factors explains the inadequate description of scour processes in cohesive soils. However, some of these parameters are correlated. Nonetheless, the number of soil and environmental parameters affecting the repulsive forces, attractive forces and the inherent van der Waals forces are more significant in cohesive (clay minerals) soils than in granular materials where the submerged gravitation force and the packing and orientation of the

particles could be sufficient to predict the incipient erosion. Therefore, scour prediction formulas for cohesive soils are inconsistent and not widely acceptable compared to granular materials. Studies related to cohesive soil erosion either concentrates on a particular soil, pore water conditions, or highlighted the influence of sample type such as natural field samples (both remolded and undisturbed), pure cohesive materials mixed with granular materials. In those studies, the main goals were to attain the desired test conditions for flume or other laboratory tests. Some in-situ experiments were also conducted by several researchers to capture the environmental variability.

Laboratory experiments are often preferred over field measurements due to the ability to control the study design. However, in-situ results are more realistic as the complex compositional structure of natural cohesive sediments may not be accurately replicated in laboratory experiments (Paterson and Black, 1999). On contrary, samples used in laboratory experiments may not adequately represent the field condition as sediment properties may be altered significantly during transportation from the field to the laboratory (Black and Paterson, 1997). This may result in an erroneous estimation of erosion threshold parameters. Nevertheless, laboratory determination of erosion threshold and scour potential are needed when experiments cannot be performed in the field. It is also understood that experiments such as local scour and contraction scour of bridge structure studies are difficult or impossible to conduct in the field. Therefore, the in-situ measurement of critical erodibility parameters, and the use of those predicted parameters in laboratory experiments could be useful alternative for scour prediction around structures in cohesive sediments. It was also identified that variability associated with operational procedures and data analyses methods for the popular in-situ devices.

Scour phenomenon around bridge piers has been studied by numerous investigators. Shen et al. (1969) described the scour phenomena as i) clear-water scour (no sediment transport from upstream flow), and ii) live-bed scour (sediment supply from upstream flow). Few studies have been conducted in cohesive soil to study the local scour around bridge piers (Hosny, 1995; Briaud et al., 1999; Ansari et al., 2002; Li, 2002; Mostafa, 2003; Oh, 2009; Debnath and Chaudhuri, 2010a,b). Experimental study of local pier scour in cohesive soil is difficult due to the complex erosion characteristics of fine-grained soils and the difficulty in scaling their properties. Therefore, the erosion rate prediction or the critical erodibility parameters prediction may vary widely for different soils and geological locations/origins as soil properties are widely varying in natural environments. It has been also identified from the literature that commercially available clay materials were extensively used in pervious scour studies using constant flow velocity during experiment. In natural streams flow hydrograph is not constant, so the influence of flow sequence on scour propagation should be investigated.

1.4 Research Objectives

Investigation of cohesive soil erosion studies started back in 1926. Conducting a through literature review, it was identified that improvements are required to quantify the erosional process in cohesive sediments. The supporting literature on cohesive soil erosion studies was found to be site-specific, varying little in the soil properties and geology of the parent material. Therefore, the main objectives of this dissertation are: i) Develop a new methodology for in-situ device operational and data analyses procedures, ii) Develop predictive equations for erodibility parameters estimation in natural cohesive sediments, iii) Identify the device dependent variability in erodibility parameter estimation, iv) Develop scour depth prediction equation based on

cumulated effective stream power, and v) Investigate scour propagation around cylinders in natural cohesive sediments using laboratory flume experiments.

These research objectives are intended to improve our understanding of cohesive soil erosion processes and the linkages with soil properties. This research will eventually enhance the capabilities in solving numerous engineering problems including catchment level soil erosion mitigation, sedimentation process in reservoirs, channel design, aggradation and deposition of sediments from the channel bed, affect of fine grain sediments on aquatic environment, water quality, basin managements and cost effective structural design. Although current research has made promising steps towards providing comprehensive knowledge in understanding the complex erosional behavior of cohesive soils in varying geology, there remains a lack of adequate information on aquatic properties affecting the cohesion properties in fine sediments.

1.5 Organization of this Dissertation

This dissertation is written based on field tests and laboratory flume experiments for understanding the erosion behavior in cohesive sediments and observe scour depth evolution around cylinders in natural cohesive sediments. The field tests were conducted among 21 streams across the state of Tennessee, which is geologically diverse. Laboratory flume experiments were conducted in an outdoor flume on the ETREC Plant Sciences Unit premises.

During the study design stage of this research, it was identified that the use of in-situ device would be best options for measuring erosion parameters. Therefore, a popular in-situ device “mini-jet” was used for the field tests. It was identified that there are issues associated with the device regarding the operation and data analysis procedure. For addressing these issues, a new field operational and data analysis procedures have been developed and discussed in detail in Chapter II. In Chapter III, the influence of soil physical and geochemical properties on

cohesive soil erodibility are presented based on the 128 in-situ jet test results. This chapter also represents how the critical shear stress prediction equations varied in a diverse geological formation. Device dependent variability on erosion parameters estimation in cohesive sediments is a concern for the researchers. Chapter IV represents the estimated erodibility parameters using two devices: an in-situ mini-jet and a pressurized conduit flume for cohesive soil. The probable agreement and/or disagreements identified from these tests are also discussed in detail. Effective cumulative stream power is a surrogate measure of shear duration above a critical value for scour depth prediction in cohesive soils. In Chapter V, based on simulated daily stream flow data, field measured critical shear stress, and long term scour depths measurement around bridge piers the relationship between effective cumulative stream power and scour depth has been developed. The influence of flow events on scour depth propagation also been discussed. Chapter VI represents the results from the outdoor laboratory flume experiments. This chapter details the experimental setup, properties of soil used in the flume tests, and test procedures for scour depths propagation under multi-flow events around cylinder in natural cohesive soil.

1.6 References

Alizadeh A. 1974. Amount and type of clay and pore fluid influences on the critical shear stress and swelling of cohesive sediments. Ph.D. Dissertation, University of California, Davis, CA, USA

Ansari SA, Kothyari UC, Ranga Raju KG. 2002. Influence of cohesion on scour around bridge piers. J. Hydraul. Research 40 (6): 717-729

Benedict ST, Caldwell AW. 2009. Development and evaluation of live-bed pier and contraction scour envelope curves in the coastal plain and piedmont provinces of South Carolina, U.S. Geological Survey Scientific Investigations, Report 2009-5099

Black KS, Paterson DM. 1997. Measurement of the erosion potential of cohesive marine sediments: A Review of Current in situ Technology. J. Marine Environ. Eng. 4: 43-83

Briaud JL, Ting FCK, Chen HC, Gudavalli R, Perugu S, Wei G. 1999. SRICOS: Prediction of scour rate in cohesive soils at bridge piers. J. Geotechnical Eng., ASCE 125 (4): 237-246

Briaud J, Ting F, Chen HC, Gudavilli R, Kwak K, Philogene B, Han S, Perugu S, Wei G, Nurtjahyo P, Cao Y, Li Y. 2001. SRICOS: Prediction of scour rate at bridge piers. Report 2937-1, Texas Transportation Institute, The Texas A&M University, College Station, Texas, USA

Cook W. 2014. Bridge failure rates, consequences, and predictive trends. PhD Dissertation, Civil and Environmental Engineering, Utah State University, Logan, Utah, USA

Debnath K, Chaudhuri S. 2010a. Bridge pier scour in clay-sand mixed sediments at near-threshold velocity for Sand. J. Hydraul. Eng. 136 (9): 597-609

Debnath K, Chaudhuri S. 2010b. Laboratory experiments on local scour around cylinder for clay and clay–sand mixed beds. Engineering Geology 111: 51-61.

Dunn IS. 1959. Tractive resistance of cohesive channels. J. Soil Mechanics and Foundations, ASCE 85(SM3, Part 1): 1-24

Grabowski RC, Droppo IG, Wharton G. 2011. Erodibility of cohesive sediment: The importance of sediment properties. Earth Sci. Rev. 105 (1): 101-120

Hosny MM. 1995. Experimental study of local scour around circular bridge piers in cohesive soils. Ph.D. Dissertation, Civil Engineering Department, Colorado State University, Fort Collins, Colorado, USA

Julian J, Torres R. 2006. Hydraulic erosion of cohesive riverbanks. Geomorphology 76 (1): 193–206

Lagasse PF, Schall JD, Johnson F, Richardson EV, Chang F. 1995. Stream stability at highway structures. Rep. No. FHWAIP-90-014 (HEC 20), Federal Highway Administration, Washington, D.C., USA

Li Y. 2002. Bridge pier scour and contraction scour in cohesive soils on the basis of flume tests. Ph. D. Dissertation, Department of Civil Engineering, Texas A&M University, College Station, TX, USA

Lyle W, Smerdon E. 1965. Relation of compaction and other soil properties to erosion resistance of soils. Transactions of the American Society of Agricultural Engineers 8 (3): 419-422

Mostafa TMS. 2003. Experimental modeling of local scour in cohesive soils. PhD Dissertation, Dept. of Civil and Environ. Eng., Univ. of South Carolina, Columbia, SC, USA

Mostafa TMS, Imran J, Chaudhry MH, Khan IB. 2008. Erosion resistance of cohesive soils. J. Hydraul. Research 46 (6): 777-787

Oh SJ. 2009. Experimental study of bridge scour in cohesive soil. Ph.D. Dissertation, Department of Civil Engineering, Texas A&M University, College Station, TX, USA

Paterson DM, Black KS. 1999. Water flow, sediment dynamics and benthic biology. Adv. Ecological Res. 29: 155-193

Raudkivi AJ. 1990. Loose boundary hydraulics. 3rd edition, Pergamon Press, New York, USA.

Thoman RW, Nieggoda SL. 2008. Determining erodibility, critical shear stress, and allowable discharge estimates for cohesive channels: Case study in the Powder River basin of Wyoming. J. Hydraul. Eng. 134 (12): 1677-1687

TRB 2004. NCHRP Report 516. Pier and Contraction Scour in Cohesive Soils. Transportation Research Board, Washington D.C., USA.

Shen HW, Schneider VR, Karaki S. 1969. Local scour around bridge piers. Proc. ASCE 95 (6): 1919-1940

Shirole AM, Holt RC. 1991. Planning for a comprehensive bridge safety assurance program. Transp. Res. Rec. 1290, Transportation Research Board, Washington, D.C.; 137-142

Smerdon ET, Beasley RP. 1959. The tractive force theory applied to stability of open channels in cohesive sediments. University of Missouri, College of Agriculture, Agricultural Experiment Station, Columbia, MO, USA

Wynn TM. 2004. The effects of vegetation on stream bank erosion. Ph.D. Dissertation, Biological Systems Engineering, Virginia Polytechnic Institute and State University, Blacksburg, VA, USA

CHAPTER II
PROPOSED NEW METHOD FOR JET DEVICE

This article has been published by Badal Mahalder, John S. Schwartz, Angelica M. Palomino, and Jon Zirkle.

Badal Mahalder, John S. Schwartz, Angelica M. Palomino, and Jon Zirkle: **"Estimating Erodibility Parameters for Streambanks with Cohesive Soils Using the Mini Jet Test Device: A Comparison of Field and Computational Methods."** Journal of Water, 10(3), 304 (2018)

Badal Mahalder, the senior author generated this manuscript as a part of his Ph.D. dissertation, and co-authors John Schwartz, Angelica Palomino, and Jon Zirkle supervised his research, in addition to direct text contributions to his study's manuscript.

Abstract

The jet test device has been predominantly used for in situ critical shear stress (τ_c) and erodibility coefficient (k_d) measurements of cohesive streambanks/beds using three analytical procedures: the Blaisdell method (BM), the iterative approach (IP), and the scour depth approach (SDP). Existing studies have reported that τ_c and k_d estimates can be influenced by the computational procedure, time intervals for scour-hole depth measurements, and the pressure head selection. This study compared estimates of τ_c and k_d among the three computational procedures using single and multiple pressure settings (SPS, MPS). A new method is introduced applying incrementally increasing pressure heads, hypothesizing depth-averaged erodibility parameters would be generated that better represent bank and fluvial erosion. Estimates of τ_c applying the MPS-BM procedure were greater by 17% to 100% compared with SPS-BM procedures and k_d estimates were lower with less variability ($\sigma = 3.54$) compared with other procedures from 126 jet tests among 21 Tennessee stream sites. This finding supports the hypothesis of increasing τ_c and decreasing k_d with greater soil depths into the bank, suggesting the MPS-BM procedure can improve the estimation of τ_c and k_d using the mini-jet test device. Overall, this study demonstrates the need to standardize field and computational procedures.

2.1 Introduction

Concept development of a jet device for estimating erosion rates for cohesive soils was first introduced by Dunn (1959), where critical shear stress (τ_c) and the erodibility coefficient (k_d) are measured and used in the excess shear stress equation. The excess shear stress equation is expressed as: $\varepsilon_T = k_d(\tau_b - \tau_c)^m$, where ε_T is the erosion rate ($cm \cdot s^{-1}$), k_d ($cm^3 \cdot N^{-1} \cdot s^{-1}$), τ_c (Pa), τ_b is the hydraulic boundary shear stress (Pa), and m is an empirical exponent (Arulanandan et al., 1980; Hanson, 1990; Hanson and Simon, 2001; Sanford and Maa, 2001). In the 1990s, researchers with the US Department of Agriculture further developed the jet device consisting of a large submergence tank (test chamber) 30.0 cm in diameter and height (Hanson, 1990; Hanson and Cook, 1997,2004). They provided operational guidance for the in situ field data collection, in

which depths of the scour hole formed by the impinging jet are measured over time. Commonly referred to as the "original" jet tester, it has been the dominant measurement tool for estimating in situ erodibility of cohesive streambank soils (Hanson and Cook, 1997,2004). In the 2010s, the mini-jet test device was developed and first used by Simon et al. (2010), where its submergence tank is 101.6 mm in diameter and 7.0 cm in height. Due to its smaller size, light weight, and the ease of field operation, the mini-jet device is more applicable for in situ testing on bed and bank surfaces. Al-Madhhachi et al. (2013) compared results from the original and mini-jet devices and found that k_d values were not significantly different, whereas τ_c values were consistently lower from the mini-jet compared with the original jet tester.

Mini-jet operational guidance was provided by Al-Madhhachi et al. (2013) where a constant pressure head setting with a pre-defined time interval were specified to measure the depth of the developing scour hole independent of soil type. However, their study noted that selection of the pressure head setting for a specific field test appeared to be dependent on soil type and the experience of the jet operator. Using the mini-jet device, Khanal et al. (2016) recently investigated the influence of data collection time intervals and test termination times on erosion parameter estimations. They also suggested that an interactive effect of pressure head setting relative to the data collection intervals and length of the test may have influence on τ_c and k_d estimations for different natural sediment types. It was hypothesized that inappropriate test selection of the pressure head setting could affect the τ_c and k_d estimations significantly. Khanal et al. (2016) identified the importance of the measurement time interval and pressure head selection; however, they did not report on the potential effect of changing soil properties with depth on τ_c and k_d estimations. Differences in soil properties from the streambank surface inward into the bank material (subsurface) have the potential to influence the rate of scour hole

development by the impinging jet. Therefore, critical research is needed to better understand how device operational procedures and streambank soil properties jointly affect the computation of erodibility parameters, and how operational procedures can be improved.

Many environmental factors affect streambank soil erodibility. It is well known that physical and geochemical properties of cohesive soils can affect erodibility, including bulk density, water content, dispersion ratio, percent clay and clay activity, plasticity index, organic matter content, pore water pH, and sodium adsorption ratio (Arulanandan et al., 1980; Briaud et al., 2001; Julian and Torres, 2006; Wynn and Mostaghimi, 2006; Thoman and Nieggoda, 2008; Grabowskiet al., 2011; Mahalder et al, 2017). In general, cohesive soil properties consisting of clay, sand, silt, and gravel can be highly variable in natural riverine environments as a function of long-term geomorphic processes (Lick et al., 1994; Zreik et al., 1998; Midgley et al., 2013). Mahalder et al. (2017) found varying relationships to controlling erodibility parameters among different physiographic regions in Tennessee. Daly et al. (2015a) characterized variability of erodibility parameters within an Oklahoma watershed. At the local streambank scale, erodibility parameters varied among different surfaces vertically from the top of bank to the toe where an increase in bulk density and water content was observed, and thus, an increase in τ_c apparently associated with soil consolidation (McNeil et al., 1996; Taylor and Lick, 1996; Jepsen et al., 1997; Roberts et al., 1998; Perkins et al., 2003; Perkins et al., 2004; Sutarto et al., 2014; Daly et al., 2015b; Daly et al., 2016). Soil bulk density appears to also increase at a point on the bank inward from the surface into the bank due to subaerial processes, the wetting and drying action in association with seasonal climate variations, where erosion rates reduce consequently inward from the bank surface (McNeil et al., 1996; Zreik et al., 1998; Lick and McNeil, 2001). It is thought that any in situ soil test on the thin surficial layers will therefore substantially influence estimation of

erodibility parameters compared with the deeper bank soil layers. Several studies reported that τ_c of the upper surface (about 0–3 cm) is 3 to 5 times lower compared to underneath soil layers in both laboratory remolded and undisturbed soil samples (McNeil et al., 1996; Jepsen et al., 1997; Zreik et al., 1998). The importance of bank point-scale variability is that it can affect the time-dependent measurements of scour hole depths during the jet device operation, particularly for the first few readings of a given test.

In order to improve operational procedures, the possible influence of soil property changes with depth of scour-hole development must be recognized, in addition to how data from the test measurements are used to compute τ_c and k_d parameters. The computational procedure developed for the original jet device per Hanson and Cook (1997) used the Blaisdell method (BM). More recent computational procedures have included the iterative principle (IP) described by Simon et al. (2010) and the scour depth principle (SDP) described by Daly et al. (2013). Inconsistencies in τ_c and k_d estimations have been reported using the same measured test data from the mini jet device (Khanal et al., 2016; Karamigolbaghi et al., 2017; Mahalder et al., 2018). Results from several studies have shown that the BM solution technique generally under-predicted τ_c compared with the IP and SDP methods (Simon et al., 2010; Daly et al., 2013; Daly et al., 2015a; Karamigolbaghi et al., 2017). A limited number of study results using the IP and SDP solution methods showed very high k_d values corresponding to both higher and lower τ_c values. In addition to the solution technique, inconsistencies in τ_c and k_d estimations are likely due to interdependent factors of soil property changes, and highly complex hydrodynamics and turbulence in the device test chamber as the scour hole shape develops (Gibson et al., 1978; Craft et al., 1993; Mercier et al., 2014; Karamigolbaghi et al., 2017). Karamigolbaghi et al. (2017) suggested that the head loss coefficient in the Blaisdell equation should be modified (BMM),

accounting for jet confinement in the mini-jet device test chamber and its effect on scour hole development. Field observations reveal that depending on the soil type, soil physical conditions and resistance properties, and the jet characteristics, scour hole shape and formation alter with time and applied fluid forces. Similar observations were also reported by other studies (Clark and Wynn, 2007; Bonelli and Brivois, 2008; Bonelli et al., 2012; Mercier et al., 2014). These findings suggest that advances in the operational procedures for jet test devices need greater consideration of in situ soil properties, selection of appropriate test pressure head settings and measurement time intervals, and the computational methods for τ_c and k_d estimation.

The objectives of this study were to: (1) investigate the influence of device pressure head selection on τ_c estimates leading to development of an alternative field procedure using multiple pressure settings during a test, (2) compare differences in τ_c and k_d estimations from three computational procedures, the BM, IP, and SDP for single pressure (SPS) and multiple pressure (MPS) field procedures, and (3) qualitatively describe differences in scour hole development and morphology per varying soil types and the resulting patterns for τ_c and k_d versus jet device pressure setting. The rationale for investigating the influence of pressure setting is that it is hypothesized that jet procedures with a single pressure head may lead to erodibility parameter estimates heavily influenced by the surficial soil layer. Theoretically, scour hole depth changes over time during a jet test vary with soil cohesion, bulk density and/or other soil conditions, and those rate and field measurement differences ultimately influence estimations of τ_c and k_d per computational method selected. If τ_c and k_d parameters derived by the jet test device using a single pressure setting reflect the erodibility of surficial bank surface to a greater extent, when used in the excess shear equation they may over-predict streambank erosion rates. This research uniquely applies a multiple-pressure setting procedure to improve the mini-jet test device's field

data collection and computational procedures for greater consistency in τ_c and k_d estimations. Among research and practitioner river engineers there is a general understanding that erodibility measurements need to follow a standard procedure, and this study supports that effort.

2.2 Background for jet test data analysis

Estimating τ_c and k_d from jet device test data has used the following computational procedures: BM (Hanson and Cook, 1997, 2004), IP (Simon et al., 2010), and SDP (Daly et al., 2013). These procedures are based on the theoretical understanding that shear stress can be computed from dispersion principles by a submerged fluid jet projected normal to an erodible surface developing a scour hole. Background on the computational procedures relevant to this study is described in this section. Hanson and Cook (1997) developed an analytical procedure to calculate the erosion index parameter from jet test data based on jet diffusion principles developed by Stein and Nett (1997). This method was developed for the original submerged jet tester; however, the governing principles are consistent for both the original and mini-jet devices. The major assumption considered for this device was that the rate of scour depth or erosion rate (*dJ/dt*) is a function of maximum stress at boundary. Therefore, the jet erosion rate equation was organized as (Hanson and Cook, 1997, 2004):

$$\frac{dJ}{dt} = k_d \left[\frac{\tau_0 J_P^2}{J^2} - \tau_c\right], for\ J \geq J_P \qquad (2.1)$$

where J is the scour depth (cm); J_p is the potential core length from jet origin (cm); k_d is the erodibility coefficient ($cm^3 \cdot N^{-1} \cdot s^{-1}$); τ_0 is the applied bottom shear stress (Pa); and τ_c is the critical shear stress (Pa).

Based on soil type and conditions, the initial erosion rate may be substantial approaching zero asymptotically for the jet device (Stein and Nett, 1997). The depth at which the applied

shear stress on the soil surface does not produce any erosion (dJ/dt = 0) is termed as the equilibrium scour depth (J_e) and the shear stress to that depth is termed as τ_c.

$$\tau_c = \tau_0 \left(\frac{J_P}{J_e}\right)^2 \tag{2.2}$$

where $\tau_0 = C_f \rho_w U_0^2$ is the maximum shear stress due to the jet velocity at the nozzle (Pa); C_f = 0.00416 is the friction coefficient; ρ_w is water density (kg·m^{-3}); $U_0 = C\sqrt{2gh}$ is the velocity of jet at orifice (cm·s^{-1}); C is discharge coefficient; h is the applied head (cm) or pressure head; $J_P = C_d d_0$; d_0 is the nozzle diameter (cm); and C_d = 6.3 is the diffusion constant. Writing a dimensionless form, Equations (2.1) and (2.2) were formed as follows (Hanson and Cook, 1997):

$$\frac{dJ^*}{dT^*} = \frac{(1-J^{*2})}{J^{*2}} \tag{2.3}$$

where $J^* = J/J_e$; and $J_P^* = J_P/J_e$. The dimensional time (T*) was also expressed as:

$$T^* = \frac{t}{T_r} \tag{2.4}$$

where t is the time of data measurement during the test; and $T_r = J_e/k_d\,\tau_c$ is the reference time. Integrating Equation (2.3), the following form was developed (Hanson and Cook, 1997):

$$T^* - T_P^* = -J^* + 0.5 \ln\left(\frac{1+J^*}{1-J^*}\right) + J_P^* - 0.5 \ln\left(\frac{1+J_P^*}{1-J_P^*}\right) \tag{2.5}$$

Using Equations (2.3) to (2.5), τ_c and k_d can be calculated using an Excel™ spreadsheet. However, Blaisdell et al. (1981) showed that the time required to attain J_e is excessively high, hence, the calculation of τ_c becomes impractical for efficient field testing. Therefore, they proposed a technique to calculate J_e by fitting scour depth data versus time as a hyperbolic function. The general form as proposed by Blaisdell et al. (1981) of the equation was:

$$A = (f - f_0)^2 - x^2 \tag{2.6}$$

$$= \log\left(\frac{J}{d_0}\right) - \log\left(\frac{U_0 t}{d_0}\right) \tag{2.7}$$

$$f_0 = \log\left(\frac{J_e}{d_0}\right) \quad (2.8)$$

$$x = \log\left(\frac{U_0 t}{d_0}\right) \quad (2.9)$$

The coefficients A and f_o can be determined using spreadsheet solver by fitting the scour depth data based on the plotting of f versus x, consequently, J_e was calculated $J_e = d_0 10^{f_0}$.

The IP and SDP approaches for estimating τ_c and k_d are variations of the BM (Daly et al., 2015a). In the IP approach, initially τ_c and k_d values are estimated from the Blaisdell solution based on T^* and J^* values. The erodibility parameters are then simultaneously solved in an iterative manner. The ultimate goal for this iterative solution method is to minimize the root-mean-square error between the measured and predicted time, where an upper bound of τ_c is included to prevent the solution from exceeding the equilibrium scour depth. In the IP, τ_c is a function of shear stress at the jet nozzle and maximum observed scour depth during jet test. Daly et al. (2013) developed another spreadsheet routine that also solved for τ_c and k_d iteratively, which is known as the SDP method. In this method, observed scour depth data from the jet test are fitted to the predicted scour depth data using the excess shear stress equation using initial guessed values of τ_c and k_d. In this simultaneous solution method, by minimizing the sum of squared errors between measured and predicted scour depth data from the excess shear stress equation, final τ_c and k_d values are estimated. Results of these recently developed solution techniques suggest a better fit with the measured scour depth data, though the reported k_d values were found to be much higher and unrealistic in some cases.

2.3 Materials and Methods

2.3.1. Study Design

In order to meet the study objectives, two separate field operations were conducted for this study using the mini-jet test device. In the first field operation, the MPS approach was used at 21

sites across Tennessee from July 2014 through August 2015. The rationale for site selection was to obtain data across multiple physiographic regions (Mahalder et al., 2017), in which geographical details of these study sites are described below in Section 2.3.2. The second operation consisted of collecting scour hole depth measurements for a single pressure setting (SPS), and at the same site location collecting scour hole depth measurements using an alternative MPS approach. This comparative field operation was conducted during July 2017 on Gist Creek, Sevier County, Tennessee to provide sufficient justification for the MPS approach (Objective 1). Both field datasets applied the BM, IP, and SDP computational procedures in order to assess any differences between them (Objective 2). The Gist Creek dataset was collected after the main study which included the 21 statewide field sites to provide greater justification for applying the MPS procedure to improve the consistency of measured erodibility parameters. Field data collection and computational methods are described below in Section 2.3.3.

2.3.2. Study Area

The Gist Creek study site is located in the Ridge and Valley Physiographic Province in eastern Tennessee (Figure 2.3.1). Gist Creek is a third order stream with a bank full width of 20 m. Five test locations including the upper and lower bank positions were investigated (designated as Loca.-I, -II, -III, -IV, and -V), totaling 10 tests per SPS and MPS field procedures. The field operation that used the MPS procedure for 21 sites was conducted across the state of Tennessee in four physiographic provinces: Valley and Ridge, Central Basin, West Highland Rim, and Coastal Plain, each with diverse geological settings with different dominant soil properties that govern estimates for the erodibility parameters (Mahalder et al., 2017). Among these regions, five stream sites were located in the Valley and Ridge Physiographic Province, three sites in the West Highland Rim and the Central Basin, and 13 sites in the West Tennessee Plain and West Tennessee Uplands, sub-regions of the Coastal Plain physiographic province (Figure 2.3.1). The

majority of the sites were from the western part of Tennessee, which has predominantly cohesive (silt/clay) type materials. Mahalder et al. (2017) have described the soil properties of each site in detail.

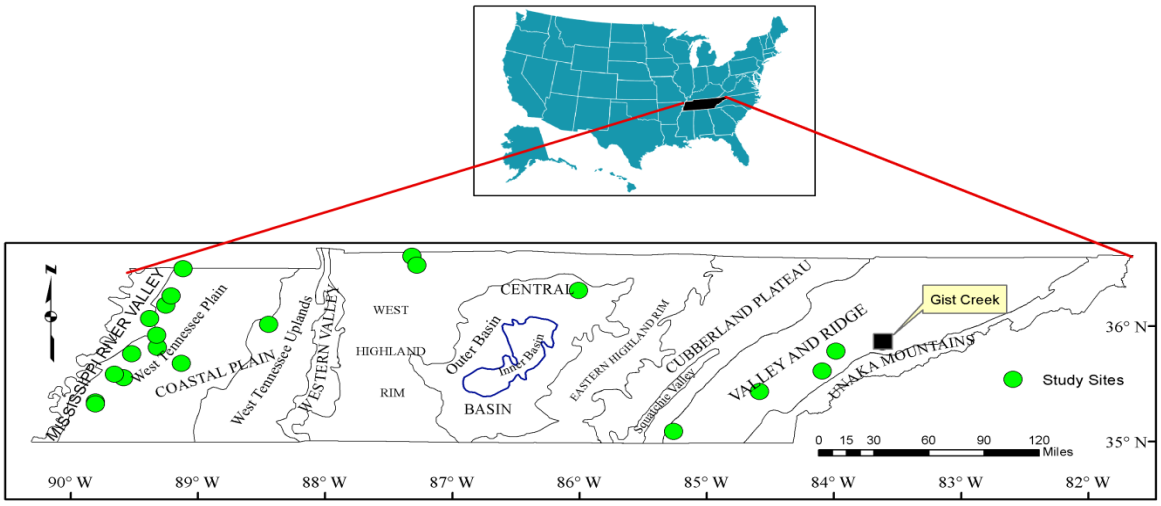


Figure 2.3.1: Study site locations using the mini-jet test device in Tennessee, where Gist Creek is shown as a black square and the sites used for the multiple-pressure test among the different physiographic provinces (Miller, 1974) are shown as green circles

2.3.3. Field data collection and computational procedures

In general, site preparation for all mini-jet test locations consisted of taking care to maintain the ambient moisture content by avoiding days with rainfall. Test locations were visually selected so that soil was homogenous in character, and free from pebbles or rocks, vegetation, and root systems. Each test location was cleaned very gently using a shovel prior to conducting a test, and the bottom ring of the jet device was inserted into the soil using uniform pressure on the top of the bottom ring to minimize disturbances at the soil surface. After completing each test, two core samples near the test location were collected using a cylindrical coring device, which were analyzed in the University of Tennessee' Geotechnical Laboratory for bulk density, water content, and unconfined compressive strength (UCS). Approximately 1.4 kg of soil was also

collected from the inside of the jet's bottom ring at each test location to measure selected physiochemical soil properties. Collectively, soil samples represented a wide variation in moisture content and bulk density associated with the diverse geological settings.

The jet operation procedure using the SPS follows the guidelines outlined by Hanson and Cook (2004) and Al-Madhhachi et al. (2013) with a slight modification, where scour-hole depth readings were measured at one-minute intervals. A centrifugal pump powered by a 2000-W portable generator provided water flow from the nearby stream through the jet device, and a constant pressure head was regulated by a ball valve and monitored by an inline pressure gage. The terminal test time was 46 min for a set pressure for the SPS method. These data were then used to estimate τ_c and k_d by three computational methods: BM, SDP, and IP (Table 2.3.1).

The jet operation procedure using the MPS generally followed the field guidance by Hanson and Cook (2004) and Al-Madhhachi et al. (2013); however, in the MPS procedure five different pressure settings were applied, starting from a lower to a higher pressure at each testing location. Selected pressures were adjusted based on testing location, soil type and condition, and test erosion rates. The applied pressure ranged from 4.14 kPa to 44.12 kPa. In some testing locations, the initial pressure was set as high as 27.58 kPa because lower pressure settings did not produce a scour hole due to the resistant soil erosion properties.

Table 2.3.1 Procedural summaries for field data collection and computation for erodibility parameters using the mini-jet device

Procedures	Description/Working Principles
	Field Data Collection Procedures
Single Pressure Setting (SPS)	A single pressure setting is chosen in which scour depth readings are collected at pre-defined time intervals. Finally, equilibrium scour depth is assumed based on different computational methods (BM, SDP, and IP) and used in τ_c and k_d calculation.
Multiple Pressure Settings (MPS)	Incrementally five different pressure heads are used at a test location starting from lower to higher. At each pressure head, test duration is about 12–20 min, where three different intervals are used for recording the scour depth readings.
	Computational Procedures
Blaisdell Method (BM)	The Blaisdell et al. (1981) approach is used for equilibrium scour depth calculation and subsequently τ_c and k_d are calculated (Hanson et al., 2002).
Modified Blaisdell Method (BMM)	The Blaisdell et al. (1981) approach is used for equilibrium scour depth calculation and subsequently τ_c and k_d are calculated (Hanson et al., 2002), however a head loss coefficient of 0.39 was applied as per Karamigolbaghi et al. (2017) where 0.16 is typically used. The adjusted coefficient addresses the jet confinement in the mini-jet's submergence (tank) test chamber.
Scour Depth Principle (SDP)	Solved for τ_c and k_d iteratively by plotting the original scour depth versus predicted scour depth using excess shear stress equation. In this simultaneous solution method, by minimizing the sum of squared errors between the measured scour data and the predicted scour depth data τ_c and k_d values are estimated. Single pressure head is used for jet operation (Daly et al., 2013).
Iterative Principle (IP)	In the IP approach, τ_c and k_d values are estimated from Blaisdell solution approach based on T^* and J^* values. Initial τ_c and k_d values are estimated from Blaisdell method and simultaneously solved for erosion parameters iteratively by minimizing root-mean-square error between the measured and predicted time. In this method an upper limit is employed for the iteration of τ_c values and similar to the other two methods, the jet device is operated using a single pressure head (Simon et al., 2010).
	Computational Procedures for Erodibility Parameters Estimation
Multiple Pressure Settings using the BM (MPS-BM)	Solution approach follows the BM method for equilibrium scour depth prediction. However, MPS field data are used for the final τ_c and k_d values estimation, where a spreadsheet is run separately using the scour depth readings for each applied pressure head. The estimated τ_c and k_d values obtained from each pressure head and the corresponding scour depths data are then plotted on a normal graph against the corresponding pressure head. Finally, erodibility parameters at a test location are estimated based on the shape of plots (see Figure 2.3.2).
Multiple Pressure Settings using the SDP (MPS-SDP)	Solution approach follows the SDP method for equilibrium scour depth prediction using the MPS field procedures and data. A similar approach is followed for the final τ_c and k_d values estimation as the MPS-BM method.
Multiple Pressure Settings using the IP (MPS-IP)	Solution approach follows the IP method for equilibrium scour depth prediction using the MPS field procedures and data. A similar approach is followed for the final τ_c and k_d values estimation as the MPS-BM method.

For each pressure head setting, the test duration at each location was about 12–20 min, where three different time intervals were selected during the tests for the scour-hole depth measurements. The different time intervals during a MPS test were: (i) 30-s intervals for the first two readings, (ii) one-minute time intervals for 2–6 min, and (iii) two-minute time intervals for depth measurements until test termination. The applied pressure head was then increased to the next pressure increment after 12 min if the measured scour-hole depth difference between two consecutive readings was not more than one millimeter. If the difference between two consecutive scour-hole depth readings was greater than one millimeter, the test was continued for the next two-minute interval. These procedures were repeated for each incremental increased pressure head settings at the same test location. The total run time for a test at each location (applying all the five pressure heads) was about 60–100 min, depending on the progression of the scour depth. MPS mini-jet testing was conducted at upper, middle, and lower bank positions where possible for the 21 sites across Tennessee. These data were then used to estimate τ_c and k_d by three computational methods: BM, SDP, and IP (Table 2.3.1).

The SPS procedure was only used at the Gist Creek study site where the MPS procedure was concurrently conducted for a method comparison (Objective 1). For accomplishing this objective, ten tests were conducted, five per upper and lower bank locations (Table 2.3.2). For each of the upper bank test locations, five different pressures heads were applied they were: 11.72 kPa, 16.55 kPa, 20.68 kPa, 27.58 kPa, and 33.09 kPa. For the lower bank the selected pressures heads were: 13.79 kPa, 20.68 kPa, 27.58 kPa, 33.78 kPa, and 41.37 kPa. These pressure heads were also used incrementally for the MPS method by following similar procedures as discussed in the previous paragraph. In the MPS procedure, τ_c and k_d values were calculated individually for each pressure head setting and corresponding scour depth values. As

summarized in Table 2.3.1, these data were used to estimate the erodibility parameters by the three computational methods: BM, SDP, and IP. Estimates for τ_c and k_d using the BM was completed using a spreadsheet routine developed at the USDA National Sedimentation Laboratory. This spreadsheet routine was based on Hanson and Cook (1997, 2004). Erodibility parameters from the other two computational methods (SDP and IP) were also calculated using another spreadsheet provided per Daly et al. (2013). Therefore, using the MPS data and different computational procedures, τ_c and k_d values were estimated and are denoted as: MPS-BM, MPS-SDP, and MPS-IP. Per test pressure setting and associated individual computations of τ_c and k_d, the erodibility parameters were plotted on normal graph paper. By doing so, three patterns were observed from these plots.

Using selected data from the 21 stream sites across Tennessee, those patterns are demonstrated in Figure 2.3.2. The three distinct patterns were: (i) a concave-down shape (76 observations), (ii) a nearly linear pattern (20 observations), and (iii) scattered points (30 observations) using the MPS-BM method. For the concave-down shape, the critical shear stress (τ_c) was calculated by drawing an asymptotic line on the concave-down shaped curve (Figure 2.3.2a), and average values were taken for the scattered patterns. For the linearly increasing pattern, the maximum value was read from the plot as the τ_c value. The majority of the tests demonstrated the concave-down shape. Similar procedures were followed for k_d value calculations. It is interesting to note that using MPS-SDP and MPS-IP methods, similar patterns were also observed. Though Figure 2.3.2 was provided in this paper only to demonstrate the computational procedures using MPS field collected data, these patterns appear to reflect a test response to the different soil properties.

Table 2.3.2 Mini-jet test conditions comparing single pressure setting (SPS) and multiple pressure settings (MPS) field data procedures at the Gist Creek study site, including soil properties among the five test locations per upper and lower bank areas

Bank Position	Test Identifier	Test Location	Selected Pressure Head (kPa)	Test Duration (min)	Water Content (%)	Bulk Density (gm/cm^3)
Upper Bank	SPS-1	I	11.72	46	17.73	1.77
	MPS-1		11.72–33.09	80	18.58	1.77
	SPS-2	II	16.55	46	21.20	1.79
	MPS-2		11.72–33.09	78	20.89	1.78
	SPS-3	III	20.68	46	19.42	1.78
	MPS-3		11.72–33.09	100	20.89	1.79
	SPS-4	IV	27.58	46	20.89	1.76
	MPS-4		11.72–33.09	100	21.12	1.78
	SPS-5	V	33.09	46	20.80	1.79
	MPS-5		11.72–33.09	100	21.85	1.78
Lower Bank	SPS-1	I	13.79	46	30.83	1.92
	MPS-1		13.79–41.37	80	31.83	1.90
	SPS-2	II	20.68	46	31.45	1.90
	MPS-2		13.79–41.37	80	32.14	1.90
	SPS-3	III	27.58	46	30.14	1.90
	MPS-3		13.79–41.37	90	29.54	1.90
	SPS-4	IV	33.78	46	29.51	1.92
	MPS-4		13.79–41.37	100	29.96	1.91
	SPS-5	V	41.37	46	31.28	1.90
	MPS-5		13.79–41.37	100	31.27	1.91

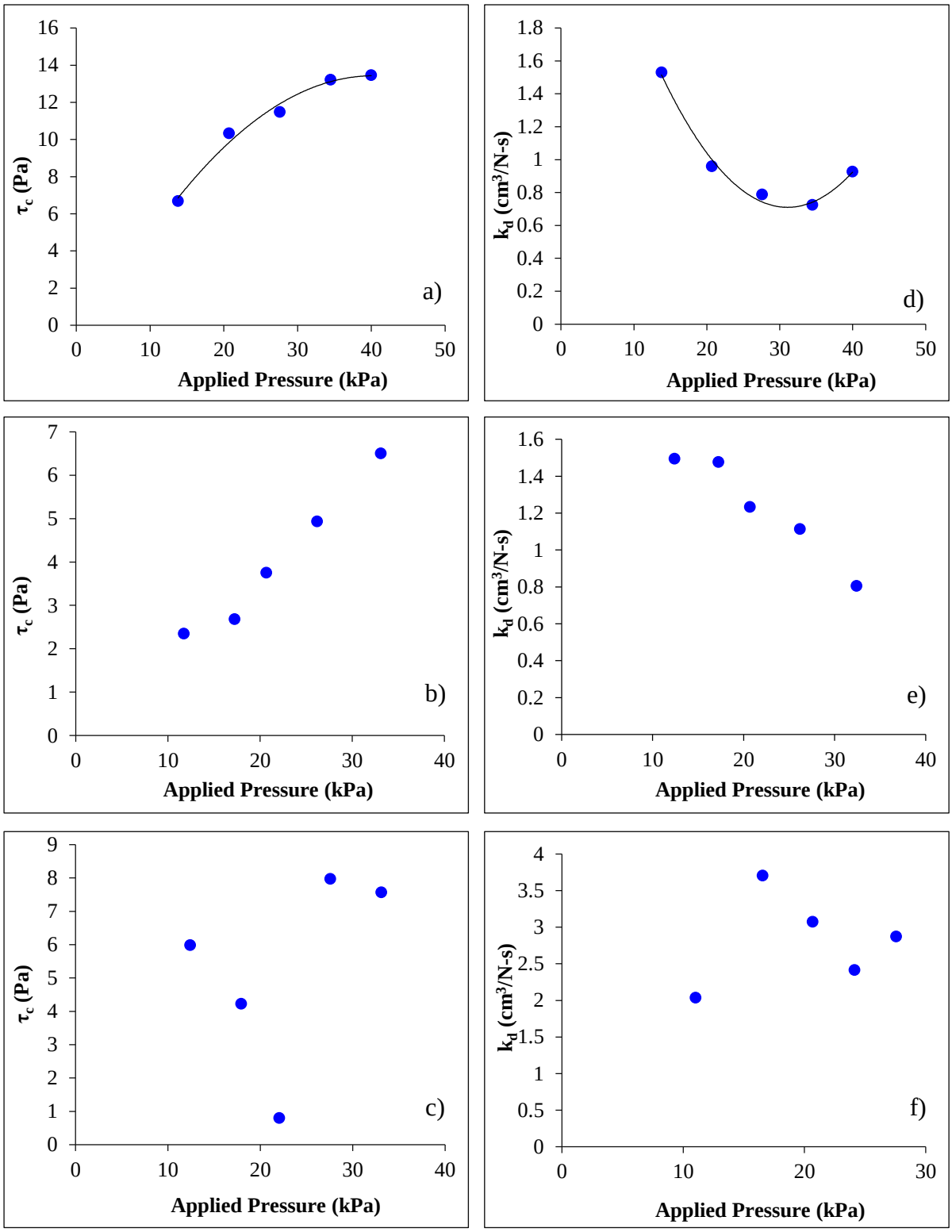


Figure 2.3.2: Response patterns of critical shear stress (τ_c) and erodibility coefficient (k_d) to jet-test device pressure head setting. Data represented are identified for τ_c: (**a**) concave-down shape, (**b**) linear, (**c**) scattered points and for k_d: (**d**) concave-up shape, (**e**) linear, and (**f**) scattered points

These patterns will be discussed further to supplement field observations related to dissimilarities in scour-hole development per different soil types (Objective 3). It is important to note that these plots in Figure 2.3.2 do not represent the same jet test data, rather the shapes are representative of different jet tests for the purpose of depicting the observed unique patterns.

2.4. Results and Discussion

2.4.1. Comparison of SPS and MPS methods for estimating critical shear stress

Test locations on Gist Creek and jet device pressure settings for SPS and MPS methods are summarized in Table 2.3.2. Soil properties were generally consistent among the five test locations but differed between the upper and lower bank areas (Table 2.3.2). The soil of the upper bank was predominantly found as semi-cohesive with the D_{50} value ranging between 75 µm to 95 µm with clay content 15%, and the PI value was about 5%. Lower bank soil was found as cohesive, the D_{50} value was between 33 µm to 40 µm, clay content was 25%, and the PI value was 10%. Bulk density averaged 1.78 g·cm^{-3} for the upper bank and 1.91 g·cm^{-3} for the lower bank. Using the SPS method, selection of pressure head influenced τ_c estimates for different computational procedures for both lower and upper bank areas (Figure 2.4.1). BM results also found that estimated τ_c values were significantly different from the SDP and IP methods over the range of applied test pressures for the lower bank ($p = 0.008$), and upper bank ($p < 0.001$). Lower banks soils were more cohesive with higher bulk densities than the upper bank locations, and as expected, τ_c was greater. Regardless of soil type, τ_c values were considerably higher at lower pressure heads. The computational method appears to have a greater effect on τ_c estimates than individually per method, where for τ_c on the lower bank area the SDP procedure was substantially greater than the BM and IP procedures. However, for the upper bank soils, τ_c estimates were in similar ranges for the SDP and IP procedures.

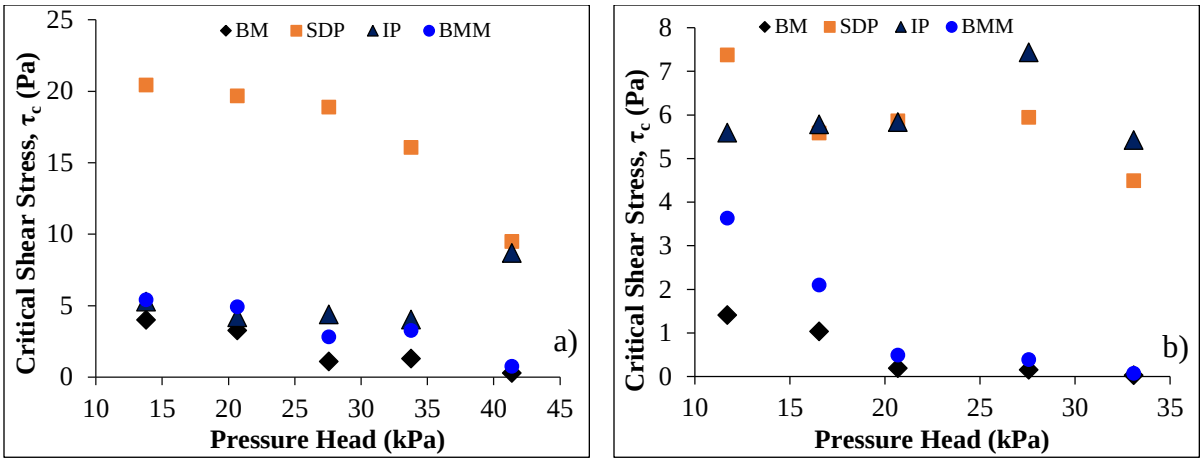


Figure 2.4.1: Using the SPS method, estimates of critical shear stress (τ_c) with different pressure heads are shown for the: (**a**) lower bank and (**b**) upper bank, based on the following computational procedures: BM = Blaisdell method, IP = iterative principle, SDP = scour depth principle, and BMM = modified Blaisdell method

Karamigolbaghi et al. (2017) reported that jet confinement could influence the jet test results and proposed a new value for the coefficient of $C_f{*}C_d^2$ as 0.39 instead of 0.16, which is also introduced in the jet test data analyses equations. Using this new coefficient, test data were also analyzed and termed as modified Blaisdell method (BMM). In Figure 2.4.1, the BMM was compared with the three methods (BM, SDP, and IP), which applied the original coefficient value of 0.16. The τ_c estimates for BM and BMM procedures were similar among the pressure settings for the lower bank locations, which were more cohesive soils compared with the upper bank locations (Figure 2.4.1). Among the upper bank locations, τ_c estimates using the BMM procedure were considerably higher than the BM procedure at the lower pressures (less than about 17 kPa). This result suggests pressure head setting and jet hydraulics affect τ_c estimates to a greater extent, especially at lower pressure settings. Using the MPS methods at the same Gist Creek test locations, τ_c values were generally more consistent among the five locations using the MPS-BM procedures (σ = 0.36 and 1.17 for lower and upper bank, respectively) compared with the MPS-SDP (σ = 0.91, and 5.51 for lower and upper bank, respectively) and MPS-IP (σ = 1.16,

and 3.32 for lower and upper bank, respectively) procedures (Figure 2.4.2). Differences in estimated τ_c values between the lower and upper banks align with other studies (Sutarto et al., 2014; Daly et al., 2015b; Daly et al., 2016). Relationships between τ_c and corresponding pressure heads resulted in concave-down patterns (as demonstrated in Figure 2.3.2a) regardless of computational procedures.

These findings also suggest that the τ_c of the upper soil surface in both laboratory remolded and undisturbed soil samples could be lower compared to soil underneath the surface layer (McNeil et al., 1996; Jepsen et al., 1997; Zreik et al., 1998). Therefore, using the SPS method, estimated τ_c and k_d values likely represent that of the surficial soil layer, whereas the MPS method estimated τ_c and k_d values represent depth-averaged parameters for the bank soil. Estimates for τ_c using the BM and BMM procedures were also compared with the MPS-BM procedure (Figure 2.4.3). From these results, it was identified that pressure head selection could significantly influence τ_c estimates regardless of the analysis method.

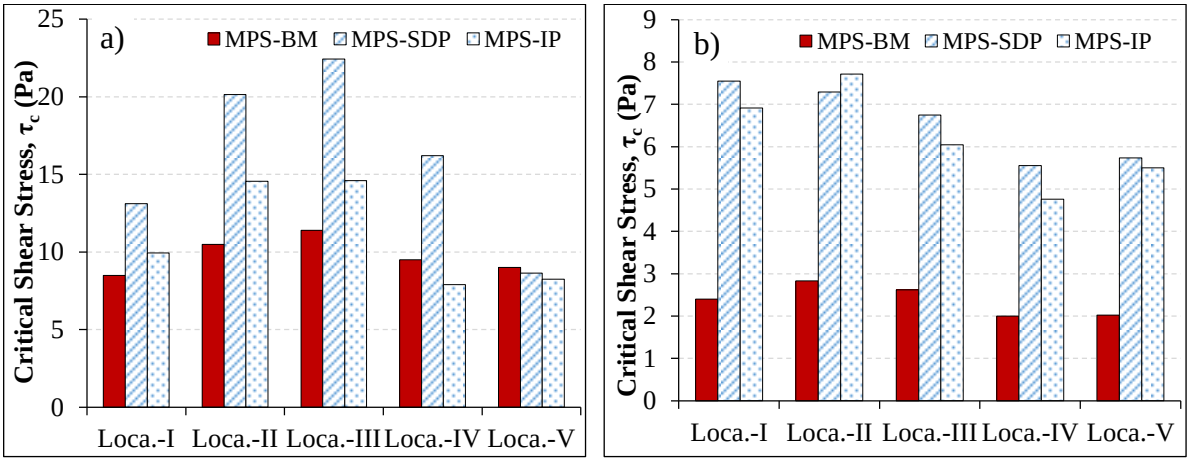


Figure 2.4.2: Based on the MPS method at the Gist Creek study site, critical shear stress (τ_c) estimates for the: (**a**) lower bank and (**b**) upper bank among the five test locations (Loca-1, -II, -III, -IV, and -V) and shown for the MPS-BM, MPS-IP, and MPS-SDP computational procedures

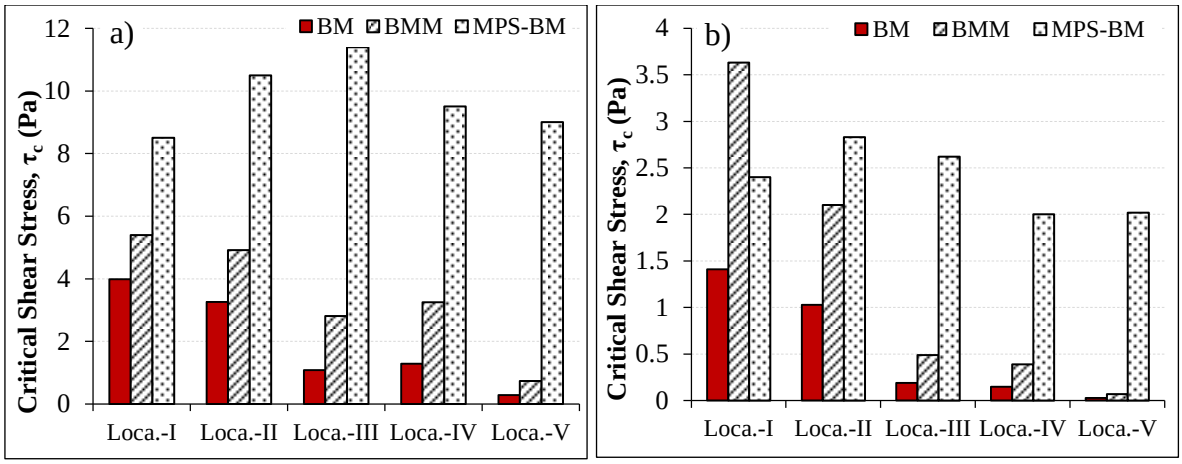


Figure 2.4.3: Estimates of critical shear stress (τ_c) at the five Gist Creek test locations for the: (**a**) lower bank and (**b**) upper bank area (Loca. -I, -II, - III, -IV, and -V). Computational methods: BM, BMM, and MPS-BM were compared

However, τ_c estimates using the MPS-BM procedure were generally more consistent among the five test locations, for both the upper and lower banks. This supports the hypothesis that pressure head selection could significantly affect the τ_c estimation using the jet device, as was also observed by Khanal et al. (2016).

The influence of the termination time interval on τ_c and k_d estimation was investigated among the Gist Creek mini-jet test locations. Results from the data analyses found that if the test was terminated after 12–26 min, where the difference between two consecutive scour depth readings was less than 1 mm, estimated τ_c and k_d values were similar with values from the full-length test. Therefore, in the new jet test operational protocol (MPS), a time interval of 12–20 min was selected for an applied pressure head by observing the difference between two consecutive scour depth readings at the end of any test. As noted earlier, subaerial processes appear to decrease bulk density at the bank surface compared to soil into the bank. In the operational protocol for the original jet tester as outlined by Hanson and Cook (2004) and Al-Madhhachi et al. (2013), scour hole depth measurements are recorded at five-minute intervals.

Using the MPS method developed for this study, it was observed that if we arbitrarily change the initial six readings inside the first five-minute time interval compared to the published interval for scour depth readings, τ_c and k_d varied significantly. Results from this study indicate the initial and termination time intervals can substantially influence τ_c and k_d estimates. Similar observations were also reported by Khanal et al. (2017) but greater details are provided in this study.

2.4.2. Comparison of MPS method and computational procedures for erodibility parameters

Potential differences in τ_c and k_d estimations from the newly developed MPS method were compared with the SPS method among the three computational procedures BM, IP, and SDP (Objective 2). Because no field tests were conducted using the SPS method among the 21 Tennessee sites, to compute τ_c and k_d values per the SPS method scour depth readings corresponding to the first selected pressure head at each jet test were used and identified as: SPS-BM, SPS-IP, and SPS-SDP (Table 2.4.1).

Table 2.4.1 Statistical summary of erodibility parameters computed using different computational methods: SPS-BM, MPS-BM, SPS-SDP, MPS-SDP, SPS-IP, and MPS-IP (as defined in Table 2.3.1)

Methods	Critical Shear Stress, τ_c (Pa)				Erodibility Coefficient, k_d ($cm^3 \cdot N^{-1} \cdot s^{-1}$)			
	Min	Max	Mean	Std. Dev	Min	Max	Mean	Std. Dev
Single Pressure Setting (SPS-BM)	0.00	12.43	2.48	2.25	0.53	24.28	3.84	3.84
Multiple Pressure Settings (MPS-BM)	0.09	26.80	5.13	3.82	0.56	24.28	3.26	3.54
Scour Depth Principle (SPS-SDP)	0.00	19.09	6.88	3.78	0.93	81.13	12.28	13.02
MPS using SDP method (MPS-SDP)	0.00	21.97	8.51	4.32	0.89	81.13	9.44	10.48
Iterative Principle (SPS-IP)	1.99	12.76	7.07	2.09	3.73	102.12	23.92	16.77
MPS using IP method (MPS-IP)	1.99	15.20	8.12	2.61	3.73	102.12	24.27	15.98

Among the 21 stream sites (126 jet tests), soil textures varied but generally were predominantly silty-loam and silty-clay-loam (Figure 2.3.1). Atterberg limit tests indicated the presence of cohesiveness in the soil samples since the PI values were between ~3 and 21. The LL and PL values were between 24% and 43%, and 17% and 31%, respectively. Some of the soil samples had a low PI (3.4–7.5), even though the material met the criteria for cohesive soils (minimum clay content of 5–10% by weight) as defined by Raudkivi (1990) and Mitchell and Soga (2005). Bulk density of the tested soils was between 1.52 g·cm^{-3} and 2.12 g·cm^{-3}, and the D_{50} value was between 3.7 µm and 40 µm. Soil cohesion ranged from 8.55 kPa to 107.90 kPa. Details of other physical and geochemical properties of these soil samples were summarized in Mahalder et al. (2017). The relationship between τ_c and k_d from the MPS-BM for the jet device dataset among the 21 Tennessee sites showed an inverse power relationship (Figure 2.4.4). The linear relationship between τ_c and k_d is consistent with others (Hanson and Simon, 2001; Thoman and Nieggoda, 2008; Simon et al., 2010), however the MPS result in this study scales higher for the erodibility parameters.

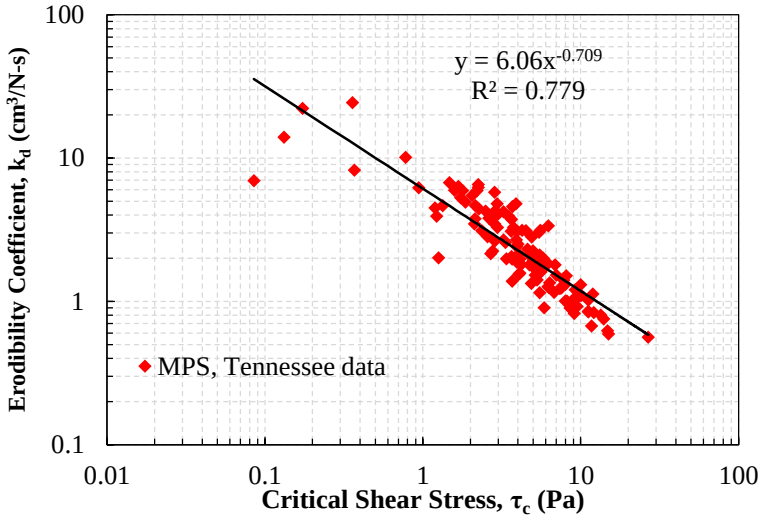


Figure 2.4.4: Relationship between critical shear stress (τ_c) and erodibility coefficient (k_d) using the MPS method data from this study

Mean τ_c using the MPS-BM method was 5.13 Pa, over twice the mean of 2.48 Pa from the SPS-BM method (Table 2.4.1, Figure 2.4.5a). Estimates of τ_c between the MPS-BM and SPS-BM methods were statistically different ($p < 0.001$, Mann-Whitney U test, SPSS- v.23.0). Mean k_d was 3.26 $cm^3 \cdot N^{-1} \cdot s^{-1}$ using the MPS-BM method and 3.84 $cm^3 \cdot N^{-1} \cdot s^{-1}$ from the SPS-BM method (Figure 2.4.5b); they were not significantly different ($p = 0.116$). Similarly, τ_c estimates from the MPS-BM procedure also compared with the SPS-SDP and SPS-IP procedures (Figure 2.4.5a).

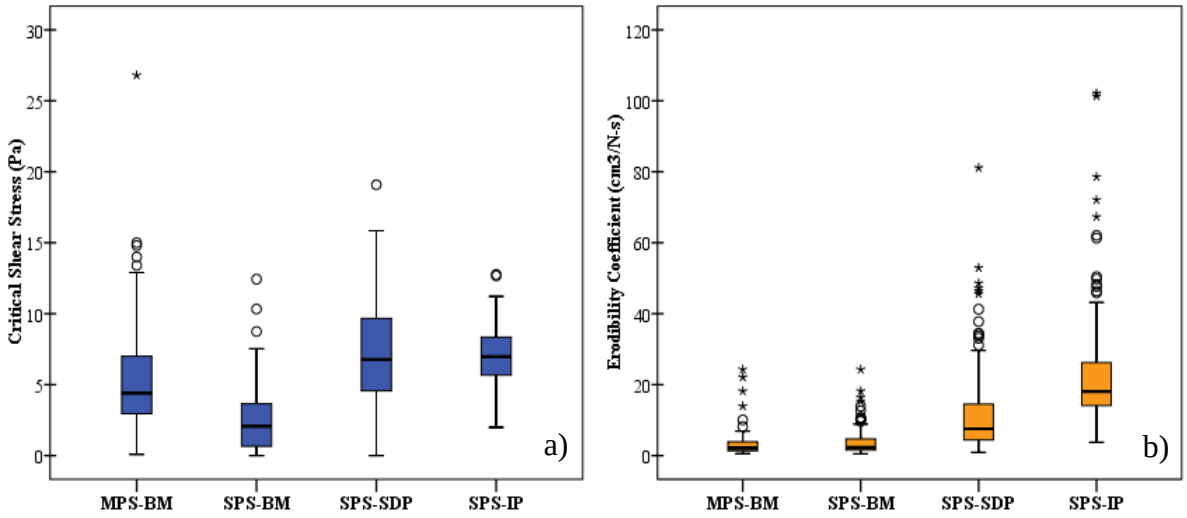


Figure 2.4.5: (**a**) Critical shear stress, and (**b**) erodibility coefficient using the field methods and computation procedures: MPS-BM, SPS-BM, SPS-SDP, and SPS-IP (as defined in Table 2.3.1)

The mean τ_c values using the MPS-BM method were found to be 5.13 Pa, and for the SPS-SDP and SPS-IP the mean values were found to be 6.88 Pa and 7.07 Pa, respectively. The median τ_c using the MPS-BM method was statistically different from both the SPS-SDP and SPS-IP procedures ($p < 0.001$). Estimated k_d values were significantly less for both the MPS-BM and SPS-BM procedures compared with the SPS-SDP and SPS-IP procedures (Table 2.4.1; Figure 2.4.5b). This result identified a major anomaly using these solution approaches where k_d

values increased with increasing τ_c values, and was similarly reported by Karamigolbaghi et al. (2017). It is important to note that a wide range (about 1 to 3 orders of magnitude difference) in the estimated τ_c and k_d values were observed among this dataset using different computational procedures.

Erodibility parameters estimated from the 126 jet test dataset using the MPS-BM, MPS-SDP, MPS-IP procedures were also compared (Figure 2.4.6). The mean τ_c values were 8.51 Pa and 8.12 Pa, and mean k_d values were 9.44 $cm^3 \cdot N^{-1} \cdot s^{-1}$ and 24.27 $cm^3 \cdot N^{-1} \cdot s^{-1}$ for MPS-SDP and MPS-IP procedures, respectively. The erodibility parameters (τ_c and k_d) from the MPS-BM procedures were statistically different from the estimates using the MPS-SDP and MPS-IP procedures ($p < 0.001$, Mann-Whitney U test, SPSS v.23.0).

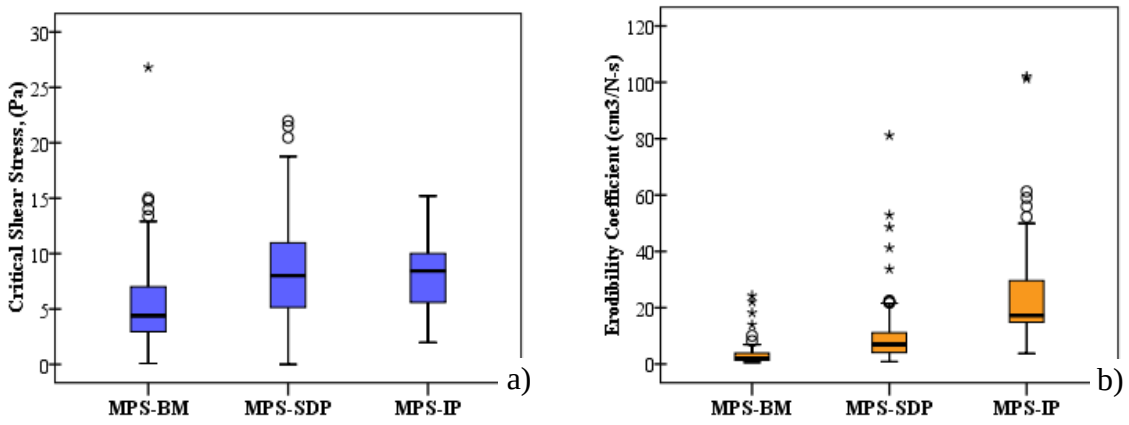


Figure 2.4.6: A comparison of (**a**) critical shear stress and (**b**) erodibility coefficient using the MPS method for the computational procedures: MPS-BM, MPS-SDP, and MPS-IP (as defined in Table 2.3.1)

Overall, τ_c and k_d values were greater for both the MPS-SDP and MPS-IP procedures compared with SPS-SDP and SPS-IP. As defined in Figure 2.3.2, more discrete relationships between τ_c and the corresponding pressure heads were observed with MPS-SDP (58 observations) and MPS-IP (42 observations) procedures. Also, based on field observations, discrete relationships

between τ_c and pressure head from the MPS method appeared to be dependent on the soil's physical properties. Therefore, these relationships for MPS-SDP and MPS-IP procedures deviated from the hypothesis that τ_c increases with soil depth.

Pairwise differences for τ_c estimates between the MPS-BM and the other computational procedures were above and below a zero difference, though the median differences for these comparisons were negative except for the SPS-BM procedure (Figure 2.4.7a). The pairwise difference of τ_c between the MPS-BM and SPS-BM procedures was positive with a range between 0.0 and 14.32 Pa, which indicates the MPS-BM procedure predicted 17% to 100% higher τ_c values compared with the SPS-BM procedure. Of the 126 field tests only 29 resulted in positive τ_c pairwise differences between MPS-BM and SPS-SDP, and SPS-IP procedures. When comparing the pairwise differences for τ_c between MPS-BM and MPS-SDP, and MPS-IP procedures, only 13 and 18 observations were positive, respectively. The greater τ_c values for the MPS method apparently accounts for the increased cohesive properties of soil as the scour hole develops during the field test.

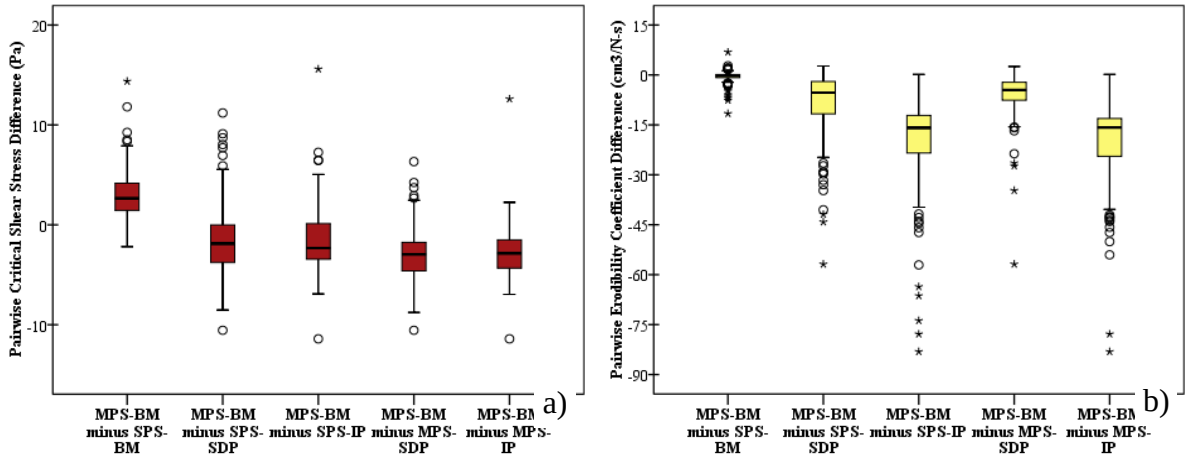


Figure 2.4.7: Pairwise differences between different solution techniques for: (**a**) critical shear stress (τ_c), and (**b**) erodibility coefficient (k_d) estimations between: MPS-BM and SPS-BM; MPS-BM and SPS-SDP; MPS-BM and SPS-IP; MPS-BM and MPS-SDP; and MPS-BM and MPS-IP procedures

Pairwise differences for k_d between MPS-BM and SPS-SDP, SPS-IP, MPS-SDP, and MPS-IP procedures were generally negative (Figure 2.4.7b). Therefore, both the SDP and IP procedures (using both the SPS and MPS methods) predicted much higher k_d values compared with the MPS-BM procedure. In general, these variations among all the procedures demonstrate how both field protocols and computational procedures greatly influence in situ τ_c and k_d values. Using the published datasets from the Daly et al. (2013, 2015a) studies, a slight increase in τ_c values were associated with significantly higher k_d values (Figure 2.4.8). Therefore, significantly higher erosion rates are expected using the linear erosion model with the SPS-SDP and SPS-IP computational results. Karamigolbaghi et al. (2017) showed that the SPS-SDP and SPS-IP procedures predicted physically unrealistic erosion rates (negative erosion rate) using the Hanson and Cook (2004) data. Likewise, the MPS-SDP and MPS-IP procedures did not physically improve the uncertainty associated with these two methods. Furthermore, this study found inconsistent k_d values using the SPS-SDP and SPS-IP procedures, which was also reported in previous studies (Simon et al., 2010; Daly et al., 2013, 2015a).

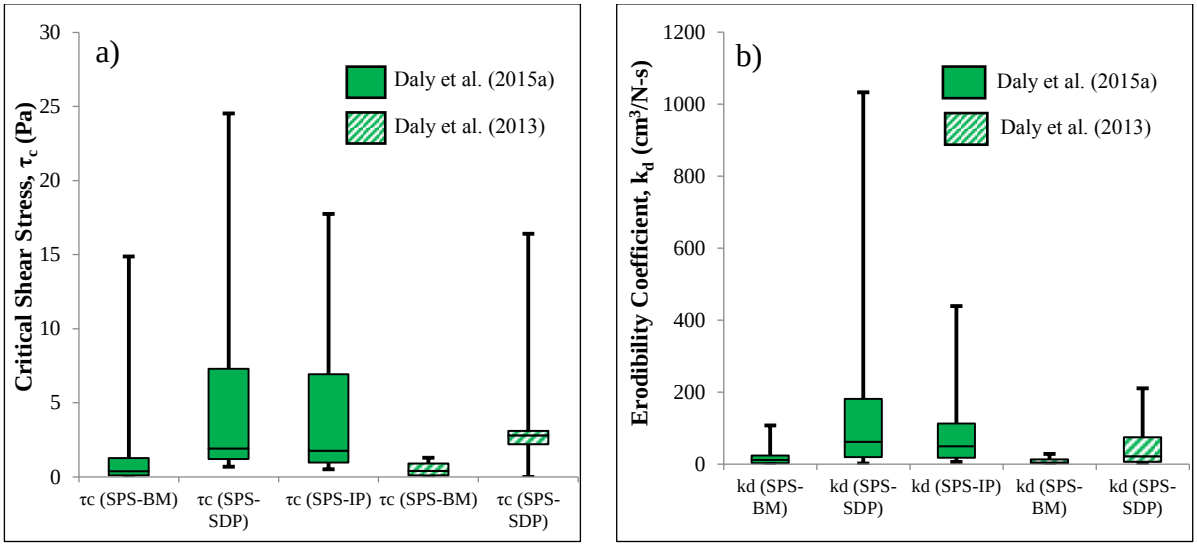


Figure 2.4.8: Comparison of (**a**) critical shear stress (τ_c) and (**b**) erodibility coefficient (k_d) using the SPS-BM, SPS-SDP and SPS-IP methods based on data from Daly et al. (2013, 2015a)

Daly et al. (2016) suggested that a reduction factor (α) in the excess shear stress equation to estimate erosion parameters using the SPS-SDP and SPS-IP computational procedures, could alleviate the problem to some extent, expressed as follows in Equation (2.10):

$$\varepsilon_T = k_d(\alpha\,\tau_b - \tau_c) = \alpha\,k_d\left(\tau_b - \frac{\tau_c}{\alpha}\right) \quad (2.10)$$

However, the acceptability of these two computational procedures may be limited if a reduction factor is required for erosion prediction, because it is understood that the reduction factor is site specific and also dependent on the expertise of the person who is operating the jet device in different regions and soil properties. Thus, further research is needed to address this issue using these two methods.

2.4.3. Qualitative observations in scour-hole development and morphology

Based on field observations, development and morphology of a scour hole subjected to jet hydraulic forces were dependent on several soil properties, which affected depth measurements over prescribed test time intervals. It has been demonstrated in this study how the time interval of scour-hole depth measurements, and the use of different computation procedures influence the estimation of the τ_c and k_d parameters (Simon et al., 2010; Daly et al., 2013, 2015b). Thus, computed values of τ_c and k_d are interdependent on soil properties, scour hole morphological development and depth measurements over time, and computational procedure using the depth measurements. As observed from this study, it was found that comparatively dry and loose soils (with higher D_{50}) resulted in discrete patterns between pressure head settings and erodibility parameters (Figure 2.3.2c,f). By observing the position of the tested soil on the creek, it appeared that the soil formation age and cohesion had a substantial effect on the concave and linear increasing patterns (Figure 2.3.2a,b,d,e). It was also observed that a wider and shallower scour

hole (Figure 2.4.9a) was observed for the concave and linear increasing patterns and a narrower deep scour hole (Figure 2.4.9b) was observed for the discrete pattern (Figure 2.3.2c,f).



Figure 2.4.9: Photos of scour hole formation in different soil physical conditions (**a**) wide and shallower, and (**b**) narrow and deeper

Nonlinear patterns appeared to occur as the scour depth increased with time and higher applied shear stress from increased device pressure (Figure 2.3.2a,d). Khanal et al. (2016) attempted to correlate erodibility parameters with applied pressure heads, though no specific patterns were reported in their study conducted on laboratory remolded soils and a limited number of tests utilizing only three pressure heads per test. The use of laboratory remolded soils limits the range of τ_c and k_d estimates that can be obtained for multiple pressure settings which generated different response patterns based on soil conditions (as observed in Figure 2.3.2). In addition, remolded soils add to uncertainty in parameter estimation associated with whether adequate time for consolidation has occurred, which over time may affect soil cohesion.

Khanal et al. (2016) did observe that the initial time interval and the termination time interval significantly influenced the estimates for erodibility parameters based on soil properties.

In this study, it was found that a change in an initial few scour depth data points (4–5 data points) significantly affected the computed erodibility parameter values. This observation suggests estimation of erodibility parameters with the jet device using a single pressure setting can be greatly influenced by soil properties at the test surface. Because the bulk density and cohesion of the soil strata generally increases with depth into the streambank, applying multiple pressure settings with the jet device can alleviate some of these issues with over-predicting τ_c and k_d for streambanks with cohesive soil. In addition, for the dataset applied in this study, it appears that estimates of τ_c and k_d using the MPS-BM procedure were comparatively more consistent with the SPS-SDP, MPS-SDP, SPS-IP and MPS-IP procedures.

2.5. Conclusions

This study investigated the effect of different pressure settings on the mini-jet device using three published computational procedures (BM, SDP, and IP) for estimating the τ_c and k_d erodibility parameters, in which a unique MPS procedure was developed and tested. The effect of time interval selection for scour-hole depth measurements during an in situ test was also examined for the different field and computational procedures. The experimental study was based on the hypothesis that streambank soil cohesion and bulk density increases from the near surface into the bank, differing due to subaerial processes and other environmental factors, therefore τ_c and k_d are affected as the jet device forms the scour hole at a test location. It was also hypothesized that by incrementally increasing device pressure settings during the test that it would compensate for the assumed change in soil properties as the scour hole develops. Collectively from 21 streambank sites across different Tennessee physiographic regions (a dataset of 126 jet tests), τ_c estimates applying the MPS-BM procedure were 17–100% greater than those applying the SPS-BM procedure, though the SPS-SDP, SPS-IP, MPS-SDP, and MPS-

IP procedures generally estimated higher values. With k_d estimates, MPS-BM showed lower values and less variation ($\sigma = 3.54$) in the dataset compared with the SPS-BM, SPS-SDP, SPS-IP, MPS-SDP, and MPS-IP procedures. These findings support the hypothesis of increasing τ_c and decreasing erodibility as the soil depth increases for cohesive soils, whereas the SPS-SDP, MPS-SDP, SPS-IP, and MPS-IP procedures estimated results contradicted the hypothesis. The MPS-BM procedure generated more consistent results for τ_c and k_d estimates (smaller ranges for the same applied dataset) compared with the SPS methods and the three computational procedures (BM, SDP, and IP).

It appears that the MPS field methodology provides an alternative to the reduction factor (α) suggested by others to be incorporated in the excess shear stress equation to address the over-prediction of soil erosion on streambanks when τ_c and k_d estimates are used from the SPS method. The advantage of using the MPS is that τ_c and k_d estimates are determined in situ whereas α requires a known relationship as a function of soil properties. It was shown in this study, those relationships between applied device pressure, and τ_c and k_d estimates were dependent on soil properties at the test location, which in turn affected the developmental morphology of the scour hole. Distinct patterns from these relationships were observed with different soil properties where it appears that with greater cohesion a concave-down to linear patterns were prominent in contrast to scattered patterns for less cohesive soils. This finding also suggests that the MPS method produces more consistent τ_c and k_d estimates with more diverse soil properties.

Overall, it appears that the MPS method, in which incrementally increasing device pressure settings are applied for estimating τ_c and k_d values, may better reflect fluvial erosion processes along a streambank/bed during a flood event. Consequently, average erodibility parameter values

are represented rather than that of the surficial soil layer. The BM computational procedure appeared to generate more consistent estimates of τ_c and k_d compared with the SDP and IP procedures, therefore the best results appear to be the MPS-BM procedure. More consistent procedures for estimating the erodibility parameters are a benefit to stream restoration practitioners improving on project designs that incorporate bank protection structures. Findings from this study suggest further research is needed to demonstrate its implications for improving the prediction of streambank erosion, in addition to an important and essential goal to standardize both field and computation methodologies.

2.6 References

Al-Madhhachi AT, Hanson GJ, Fox GA, Tyagi AK, Bulut R. 2013. Measuring soil erodibility using a laboratory "mini" JET. Trans. ASABE 56(3): 901-910

Arulanandan K; Gillogley E; Tully R. 1980. Development of a quantitative method to predict critical shear stress and rate of erosion of natural undisturbed cohesive soils. USACE, Waterways Experiment Station Technical Report, GL-80-5, Vicksburg, MS, USA

Blaisdell FW, Clayton LA, Hebaus CG. Ultimate dimension of local scour. J. Hydraul. Division-ASCE 107(3): 327-337

Bonelli S, Brivois O. 2008. The scaling law in the hole erosion test with a constant pressure drop. International Journal for Numerical and Analytical Methods in Geomechanics 32: 1573-1595. DOI: 10.1002/nag.683

Bonelli S, Golay F, Mercier F. 2012. Chapter 6 - On the modelling of interface erosion. Erosion of Geomaterials Wiley/ISTE: 187-222

Briaud J, Ting F, Chen HC, Gudavilli R, Kwak K, Philogene B, Han S, Perugu S, Wei G, Nurtjahyo P, Cao Y, Li Y. 2001. SRICOS: Prediction of scour rate at bridge piers. Report 2937-1, Texas Transportation Institute, The Texas A&M University, College Station, Texas, USA

Clark LA, Wynn TM. 2007. Methods for determining streambank critical shear stress and soil erodibility: implications for erosion rate predictions. Transactions of the ASABE 50(1): 95-106. DOI: http://dx.doi.org/10.13031/2013.22415

Craft T, Graham L, Launder B. 1993. Impinging jet studies for turbulence model assessment-II. An examination of the performance of four turbulence models. Int. J. Heat Mass Transfer 36(10): 2685-2697. DOI: https://doi.org/10.1016/S0017-9310(05)80205-4

Daly ER, Fox GA, Al-Madhhachi AT, Miller RB. 2013. A scour depth approach for deriving erodibility parameters from jet erosion tests. Trans. ASABE 56(6): 1343-1351. DOI 10.13031/trans.56.10350

Daly ER, Fox GA, Enlow HK, Storm DE, Hunt SL. 2015a. Site-scale variability of streambank fluvial erodibility parameters as measured with a jet erosion test. J. Hydrol. Processes 29: 5451-5464. DOI: 10.1002/hyp.10547

Daly ER, Miller RB, Fox GA. 2015b. Modelling streambank erosion and failure along protected and unprotected composite streambanks. Advances in Water Resources, Special Issue on Fluvial Eco-Hydraulics and Morphodynamics: New Insights and Challenges 81: 114-127. DOI: 10.1016/j.advwatres.2015.01.004

Daly ER, Fox GA, Fox AK. 2016. Correlating site-scale erodibility parameters from jet erosion tests to soil physical properties. Transactions of the ASABE 59(1): 115-128. DOI: 10.13031/trans.59.11309

Dunn IS. 1959. Tractive resistance of cohesive channels. Journal of the Soil Mechanics and Foundations, ASCE 85(SM3, Part 1): 1-24

Gibson MM, Launder BE. 1978. Ground effects on pressure fluctuations in the atmospheric boundary layer. J. Fluid Mech. 86: 491-511

Golay F, Lachouette D, Bonelli S, Seppecher P. 2011. Numerical modelling of interfacial soil erosion with viscous incompressible flows. Computer Methods in Applied Mechanics and Engineering 200: 383-391. DOI: https://doi.org/10.1016/j.cma.2010.09.002

Grabowski RC, Droppo IG, Wharton G. 2011. Erodibility of cohesive sediment: the importance of sediment properties. Earth Sci. Rev. 105(1): 101-120. DOI:10.1016/j.earscirev.2011.01.008

Hanson GJ. 1990. Surface erodibility of earthen channels at high stresses. Part I-Open Channel Testing. Trans. ASAE 33(1): 127-131

Hanson GJ; Cook KR. 1997. Development of excess shear stress parameters for circular jet testing. ASAE Paper No. 97-2227, St. Joseph, MI, USA

Hanson GJ; Simon A. 2001. Erodibility of cohesive streambeds in the Loess area of the Midwestern USA. Hydrol. Process 15: 23-28. DOI: 10.1002/hyp.149

Hanson GJ, Robinson KM, Cook KR. 2002. Scour below an overfall: Part II. Prediction. Trans. ASAE 45(4): 957-964

Hanson GJ; Cook KR. 2004. Apparatus, test procedures, and analytical methods to measure soil erodibility in-situ. Appl. Eng. Agric. 20(4): 455-462

Jepsen R, Roberts J, Lick W. 1997. Effects of bulk density on sediment erosion rates. Water Air Soil Pollution 99: 21-31. DOI: https://doi.org/10.1007/BF02406841

Julian J, Torres R. 2006. Hydraulic erosion of cohesive riverbanks. Geomorphology 76(1): 193-206. DOI: 10.1016/j.geomorph.2005.11.003

Karamigolbaghi M, Ghaneeizad SM, Atkinson JF, Bennett SJ, Wells RR. 2017. Critical assessment of jet erosion test methodologies for cohesive soil and sediment. Geomorphology 295: 529-536. DOI: http://dx.doi.org/10.1016/j.geomorph.2017.08.005

Khanal A, Fox GA, Al-Madhhachi AT. 2016. Variability of erodibility parameters from laboratory mini jet erosion tests. J. Hydrol. Eng. 21(10). DOI: 10.1061/(ASCE)HE.1943-5548.0001404

Lick W, McNeil J, Xu YJ, Taylor C. 1994. Measurements of the resuspension and erosion of sediments in rivers. Rep. Department of Mechanical and Environmental Engineering, University of California, Santa Barbara, CA, USA

Lick W, McNeil J. 2001. Effects of sediment bulk properties on erosion rates. The science of the total environment, Elsevier 266: 41-48. DOI: https://doi.org/10.1016/S0048-9697(00)00747-6

Mahalder B, Schwartz JS, Palomino AM, Zirkle J. 2017. Relationships between physical-geochemical soil properties and erodibility of streambanks among different physiographic provinces of Tennessee, USA. Earth Surface Processes and Landforms 43:401-416. DOI: https://doi.org/10.1002/esp.4252

Mahalder, B, Schwartz JS, Papanicolaou AN, Palomino AM, Zirkle J. 2018. Comparison of erodibility parameters for cohesive streambank soils between an in-situ jet test device and laboratory conduit flume. J. Hydraul. Eng. (under review)

McNeil J, Taylor C, Lick W. 1996. Measurements of erosion of undisturbed bottom sediments with depth. J. Hydraul. Eng. 122: 316-324. DOI: https://doi.org/10.1061/(ASCE)0733-9429(1996)122:6(316)

Mercier F, Bonelli S, Pinettes P, Golay F, Anselmet F et al. 2014. Comparison of CFD simulations with experimental jet erosion tests results. J. Hydraul. Eng. 140(5). DOI: 10.1061/(ASCE)HY.1943-7900.0000829, 04014006

Midgley TL, Fox GA, Wilson GV, Heeren DM, Langendoen E, Simon A. 2013. Streambank erosion and instability induced by seepage: In-situ constant-head experiments. J. Hydrol. Eng. 18(10): 1200-1210. DOI: 10.1061/(ASCE)HE.1943-5584.0000685

Miller RA. 1974. The Geologic history of Tennessee: Tennessee Division of Geology, Bulletin 74

Mitchell JK, Soga K. 2005. Fundamentals of soil behavior. 3rd Edition, John Wiley & Sons, Inc, Hoboken, New Jersey, USA

Perkins RG, Honeywill C, Consalvey M, Austin HA, Tolhurst TJ, Paterson DM. 2003. Changes in Microphytobenthic Chlorophyll a and EPS resulting from sediment compaction due to de-watering: opposing patterns in concentration and content. Continental Shelf Research 23: 575-586. https://doi.org/10.1016/S0278-4343(03)00006-2

Perkins RG, Sun H, Watson J, Player MA, Paterson DM.2004. In-line laser holography and video analysis of eroded flocs from engineered and estuarine sediments. Environmental Science & Technology 38: 4640-4648. DOI: 10.1021/es040011i

Raudkivi AJ. 1990. Loose boundary hydraulics. 3rd edition, Pergamon Press, New York, USA

Roberts J, Jepsen R, Gotthard D, Lick W. 1998. Effects of particle size and bulk density on erosion of quartz particles. J. Hydraul. Eng. 124(12): 1261-1267. DOI: https://doi.org/10.1061/(ASCE)0733-9429(1998)124:12(1261)

Sanford LP; Maa JPY. 2001. A unified erosion formulation for fine sediments. Marine Geology 179(1-2): 9-23. DOI: https://doi.org/10.1016/S0025-3227(01)00201-8

Simon A, Thomas RE, Klimetz L. 2010. Comparison and experiences with field techniques to measure critical shear stress and erodibility of cohesive deposits. In Proceedings of the 2nd Joint Federal Interagency Conference on Sedimentation and Hydrologic Modeling, U.S. Geological Survey: Reston, VA, USA

Stein OR, Nett DD. 1997. Impinging jet calibration of excess shear sediment detachment parameters. Trans. ASAE 40(6): 1573-1580

Sutarto T, Papanicolaou AN, Wilson CG, Langendoen EJ. 2014. Stability analysis of semicohesive streambanks with CONCEPTS: Coupling field and laboratory investigations to quantify the onset of fluvial erosion and mass failure. J. Hydraul. Eng. 140(9). DOI: 10 .1061/(ASCE)HY.1943-7900.0000899

Taylor C, Lick W. 1996. Erosion properties of reat Lakes sediments. Report, Department of Mechanical and Environmental Engineering, University of California, Santa Barbara, CA, USA

Thoman RW, Nieggoda SL. 2008. Determining erodibility, critical shear stress, and allowable discharge estimates for cohesive channels; case study in the Powder River Basin of Wyoming. J. Hydraul. Eng. 134(12): 1677-1687. DOI: 10.1061/(ASCE)0733-9429(2008)134:12(1677)

Wynn TM, Mostaghimi S. 2006. The Effects of vegetation and soil type on streambank erosion, Southwestern Virginia, USA. Journal of the American Water Resources Association (AWARA) 42(1): 69-82. DOI: 10.1111/j.1752-1688.2006.tb03824.x

Zreik DA, Krishnappan BG, Germaine JT, Madsen OS, Ladd CC. 1998. Erosional and mechanical strengths of deposited cohesive sediments. J. Hydraul. Eng. 124(11): 1076-1085

CHAPTER III
RELATIONSHIPS BETWEEN SOIL PROPERTIES AND ERODIBILITY

This chapter was published by Badal Mahalder, John S. Schwartz, Angelica M. Palomino and Jon Zirkle.

Badal Mahalder, John S. Schwartz, Angelica M. Palomino and Jon Zirkle: **"Relationships between physical-geochemical soil properties and erodibility of streambanks among different physiographic provinces of Tennessee, USA."** Earth Surface Processes and Landforms (2017), pp 401-416, DOI: 10.1002/esp.4252.

Badal Mahalder, the senior author generated this manuscript as a part of his Ph.D. dissertation, and co-authors John Schwartz, Angelica Palomino, and Jon Zirkle supervised his research, in addition to direct text contributions to his study's manuscript.

Abstract

Erosion of cohesive soils in fluvial environments is dependent on physical, geochemical and biological properties, which govern inter-particle attraction forces and control detachment rates from stream beds and banks. Most erosion rate models are based on the excess shear stress equation where the soil erodibility coefficient (k_d) is multiplied by the difference between the boundary hydraulic shear stress (τ_b) and the soil critical shear stress (τ_c). Both k_d and τ_c are a function of soil properties and must be obtained through in situ field or laboratory testing. Many studies have generated predictive relationships for k_d and τ_c derived from various soil properties. These studies typically were conducted in watersheds within a single physiographic region with a common surficial geology and/or investigated a limited number of soil properties, particularly geochemical properties. With widely reported differences in relationships between τ_c and soil properties, this study investigated differences in predictive relationships for τ_c among different physiographic provinces in Tennessee, USA. Erodibility parameters were determined in the field using a mini-jet test device. Among these provinces, statistically four unique clusters were identified from a dataset of 128 observations and these data clusters were used to develop predictive models for τ_c to identify dominant properties governing erosion. In these clusters, 16 significant physical and geochemical soil properties were identified for τ_c prediction. Among these soil properties, water content and passing #200 sieve (percentage soil less than 75 μm) were the dominant controlling parameters to predict τ_c in addition to clay percentage (< 2 μm), bulk density, and soil pore water chemistry. This study suggests that unique relationships exist for physiographic provinces that are likely due to soil physical-geochemical processes associated with surficial geology that determine minerology of the cohesive soil.

3.1 Introduction

Erosion of cohesive soils in fluvial environments has been extensively studied in order to better predict streambank scour and failure as well as equilibrium scour depth on the channel bed near bridge piers and other civil infrastructures. In addition, erosion is studied to estimate model parameters for stream restoration design and excessive sediment yields to streams that can cause biological impairment (Arulanandan et al., 1980; Berlamont et al., 1993; McNeil et al., 1996; Molinas et al., 1999; Papanicolaou, 2001; Black et al., 2002; Mostafa, 2003; Wynn, 2004; Julian

and Torres, 2006; Clark and Wynn, 2007; Mostafa et al., 2008; Thoman and Niezgoda, 2008; Wynn et al., 2008; Oh, 2009; Debnath and Chaudhuri, 2010; Karmaker and Dutta, 2011; Daly et al., 2015a; Schwartz et al., 2015). Within these studies, the excess shear stress equation has been predominantly used to predict erosion rates, which is expressed as:

$$\varepsilon_T = k_d (\tau_b - \tau_c)^m \quad (3.1)$$

where ε_T is the erosion rate (cm s^{-1}), k_d is the erodibility coefficient (cm^3 N^{-1} s^{-1}), τ_b is the average hydraulic boundary shear stress (Pa), τ_c is the critical shear stress (Pa), and m is an empirical exponent (Arulanandan et al., 1980; Hanson, 1990a,b; Hanson and Simon, 2001; Sanford and Maa, 2001). Use of this equation requires measurement of k_d and τ_c, where m is generally assumed equal to unity. To achieve these measurements in situ, the jet test device by Hanson (1990b) has been widely applied in erosion studies (Hanson and Simon, 2001; Hanson and Cook, 2004; Simon et al., 2010; Al-Madhhachi et al., 2013a) though other devices have been developed and used. Estimates for k_d and τ_c can vary widely, for example τ_c has been reported from near 0 to 400 Pa (Dunn, 1959; Hanson and Simon, 2001; Wynn and Mostaghimi, 2006; Debnath et al., 2007; Mostafa et al., 2008; Thoman and Niezgoda, 2008; Daly et al., 2015a, b). Parameter variability depends on many factors including the measurement approach; the soil physical and geochemical properties; bank conditions related to subaerial processes, root density, and percent cover of riparian vegetation; and spatial variability of boundary shear stress along the bank and bed (Kamphuis and Hall, 1983; Allen et al., 1999; Briaud et al., 1999; Wynn, 2004; Julian and Torres, 2006; Wynn and Mostaghimi, 2006; Thoman and Niezgoda, 2008; Wynn et al., 2008; Grabowski et al., 2011). Though many factors may affect estimates of k_d and τ_c, a more comprehensive understanding is needed specifically on how physical and geochemical properties influence predictability of erosion utilizing the excess shear stress equation.

There have been several studies identifying various physical and geochemical properties that influence estimates of k_d and τ_c, the results of which are not consistent. Properties that have been found to influence erodibility include: percent clay, organic matter, dispersion ratio, water content, clay activity, pore water pH, sodium adsorption ratio (SAR), soil bulk density, and plasticity index (Arunlanandan et al., 1980; Briaud et al., 2001; Wynn, 2004; Julian and Torres, 2006; Thoman and Niezgoda, 2008; Grabowski et al., 2011). Several of these properties appear to be due to inter-particle forces of cohesive soils and their control of detachment rates (Johnson et al., 1994; Droppo et al., 2008). Soil classification schemes characterizing physical properties have been applied to better predict k_d and τ_c with some success (Smerdon and Beasley, 1961; Allen et al., 1999; Clark and Wynn, 2007; Utley and Wynn, 2008). However, these studies were based on measured data from a single physiographic province and surficial geology (Hanson and Simon, 2001; Clark and Wynn, 2007; Thoman and Niezgoda, 2008; Daly et al., 2015a). In addition, estimates of the erodibility parameters were generally derived from a limited number of soil properties and/or study site samples (Dunn, 1959; Kamphuis and Hall, 1983; Allen et al., 1999; Thoman and Niezgoda, 2008; Daly et al., 2016). A review of published equations for cohesive soil erodibility, presented below, suggests that the erodibility parameters governed by the surficial geology within a given physiographic province.

The objectives of this study were to develop predictive relationships for erodibility parameters for use with the excess shear stress equation, investigate which physical-geochemical properties govern erodibility of cohesive soils, and determine whether governing properties vary among different surficial geologies. We hypothesized that the erodibility parameters k_d and τ_c are largely dependent on mineralogy and soil cohesion, which are a function of surficial geology and

soil genesis (Mitchell and Soga, 2005). This study applied jet tests to collect field-based k_d and τ_c data across diverse physiographic provinces within the state of Tennessee, USA.

3.2 Review: Predictive Relationships for Soil Erodibility

The erodibility parameters k_d and τ_c are dependent on soil physical, geochemical and biological parameters (Grabowski et al., 2011). In several studies, researchers have developed relationships between erodibility parameters and different soil properties. Most relationships have included multiple regression models for prediction of τ_c, and power functions between the erodibility parameters k_d and τ_c.

One of the earliest equation developments for predicting erodibility parameters was based on a laboratory flume study conducted by Smerdon and Beasley (1961). They suggested relationships for τ_c (Pa) are related to the median grain size in mm (d_{50}) and clay percentage (F_{clay}) according to:

$$\tau_c = 3.54 \times 10^{-28.1 d_{50}} \quad (3.2)$$

$$\tau_c = 0.493 \times 10^{0.0182 F_{clay}} \quad (3.3)$$

In cohesive soils, the relationship between k_d and τ_c is typically reported as an inverse power law. Hanson and Simon (2001) proposed an inverse relationship of k_d with τ_c based on 83 jet tests conducted in the western United States (US). In their dataset, they showed 64% variation, which was recently incorporated into the Bank Stability and Toe Erosion Model (BSTEM) for estimating k_d and τ_c:

$$k_d = 0.2 \tau_c^{-0.5} \quad (3.4)$$

This relationship was later modified by Simon et al. (2011) by conducting hundreds of jet tests across the US in different streams:

$$k_d = 1.62\ \tau_c^{-0.838} \quad (3.5)$$

Similar to these relationships, Daly et al. (2015a) developed another set of relationships based on different solution techniques using an in-situ jet test device. Their proposed relationships were developed based on jet test data from 13 sites, and all of the tests were conducted in the same geological region, the Illinois River basin in Oklahoma:

$$k_d = 4.62\ \tau_c^{-0.207} \quad (3.6)$$

$$k_d = 84.32\ \tau_c^{-1.17} \quad (3.7)$$

Equation 3.6 was based on the Blaisdell et al. (1981) solution method with R^2 value of 0.08, and subsequently Equation 3.7 was developed based on scour depth principle (Daly et al., 2013) with R^2 value of 0.47. The above reported studies were limited in that they were either investigated only a few soil physical properties (mean grain size, water content, and plasticity index) or focused on individual watersheds.

Julian and Torres (2006) also conducted a similar type of study, where they found that silt-clay (SC) content was the only governing soil property for the τ_c rating curve. The τ_c was maximum at 100% SC and minimum at 0% SC, and their proposed relationship was derived as a third-order polynomial equation:

$$\tau_c = 0.1 + 0.1779\ (SC\ \%) + 0.0028\ (SC\ \%)^2 - 2.34\ e^{-5(SC\ \%)^3} \quad (3.8)$$

In southwest Virginia, correlation between cohesive soil parameters and τ_c was developed based on data from 25 sites with a total of 140 jet tests (Wynn and Mostaghimi, 2006). They reported that soil bulk density, potassium intensity factor, soil/water pH, and water temperature were the most significant properties with R^2 = 0.569. To note, the stream banks considered in this study were mostly covered with vegetation. It is well known that vegetation cover and root

systems in the soil can significantly affect the τ_c compared to vegetation-free cohesive soils (Simon and Collison, 2002).

Thoman and Niezgoda (2008) conducted a comparable study in northeast Wyoming on five different creeks with a total of 25 observations. They found that activity of clay (CA), dry density of soil (DD), specific gravity (SG), pH, and water content (WC) of soil were significant soil parameters affecting cohesive soil τ_c, and reported τ_c range was between 0.11 Pa to 15.35 Pa. Their relationship from this geological region was developed as:

$$\tau_c = 77.28 + 2.20(CA) + 0.26(DD) - 13.49(SG) - 6.4(pH) + 0.12(WC) \quad (3.9)$$

Regazzoni and Marot (2011) proposed a new way for expressing the cohesive soil erodibility expressed as erosion resistance (I_α). They developed multivariate relationships for dispersive and non-dispersive cohesive soils, respectively, as follows:

$$I_\alpha = -1.36 + 8.96\,\Delta_{wL} + 2.68\,c + 2.08\,S_r \quad (3.10)$$

$$I_\alpha = -2.31 + 0.69\,\Delta_{wL} + 1.41\,c + 6.07\,S_r \quad (3.11)$$

where $c = \rho_d / \rho_s$; ρ_d dry density and ρ_s solid density of soil; Δ_{wL} clay water content, $\Delta_{wL} = LL - w_{clay}$, $w_{clay} = WC / F_{clay}$, w_{clay} clay water content, WC soil water content, F_{clay} clay fraction of the soil and S_r is the saturation ratio. Their study was conducted on remolded soils in a controlled laboratory environment using a jet test device. The sample size was 11 and 27 for dispersive and non-dispersive soils, respectively.

3.3 Study Area

In this study, 21 streams were selected across Tennessee. The geology of Tennessee is diverse and divided into eight major physiographic provinces (Figure 3.3.1). The topography of Tennessee also ranges between the Appalachian Mountains in the east to Mississippi River

bottoms in the west (Miller, 1974). Among these eight major physiographic provinces, in situ erodibility tests were conducted among four provinces and compared for differences in erodibility properties. The detail descriptions of these physiographic provinces are presented below (Figure 3.3.1, Table 3.4.1):

1) the Valley and Ridge physiographic province, characterized by elongate ridges and valleys, represents the remnants of an ancient fold-and-thrust belt formed during Alleghany orogeny. Erosion, beginning the Mesozoic Era, has resulted in the modern-day topography where more erosion-resistant rock (e.g., sandstone and shale) forms ridges and less resistant rock (e.g., limestone, dolomite, siltstone) forms the valleys (Miller, 1974);
2) the Highland Rim physiographic province, which is divided by the Central Basin physiographic province into two subregions: the Eastern and Western Highland Rims. The Eastern Rim is marked by a dissected escarpment composed of Paleozoic carbonate rock and the Western Rim is marked with rolling hill topography created by differential erosion of Mississippian sandstone, shale, and limestone. This physiographic province also consists of karst terrain in Mississippian, Devonian, Silurian, Ordovician, and Cambrian limestones;
3) the Central Basin province was formed from the erosion of the Nashville Dome, which exposed less resistant underlying limestones forming a topography with rolling hills consisting of limestone, shale, dolomite, siltstone, and claystone;
4) within the western area of Tennessee, a relatively flat and low elevation landscape is identified as the Coastal Plain physiographic province. It is divided into the West Tennessee Uplands and the West Tennessee Plain subregions. This physiographic province was formed during the Mesozoic and the Cenozoic Eras with predominantly sand, silt, clay, gravel and loess surficial materials (Safford, 1869; Miller, 1974).

In this study, five stream sites were selected from the eastern region of Tennessee in the Valley and Ridge physiographic province. Three sites each were selected from the West Highland Rim and the Central Basin from the middle region of Tennessee. The majority of the selected sites were from the western region of Tennessee, which stream bed and banks dominantly had cohesive (silt/clay) type soils. Selected sites from west Tennessee were: (i) West Tennessee Plain (11 sites), and (ii) West Tennessee Uplands (one site), areas of the Coastal Plain physiographic province. Table 3.4.1 lists the study sites and their location, study site physiographic province, drainage area, and geological formation and rock characteristics.

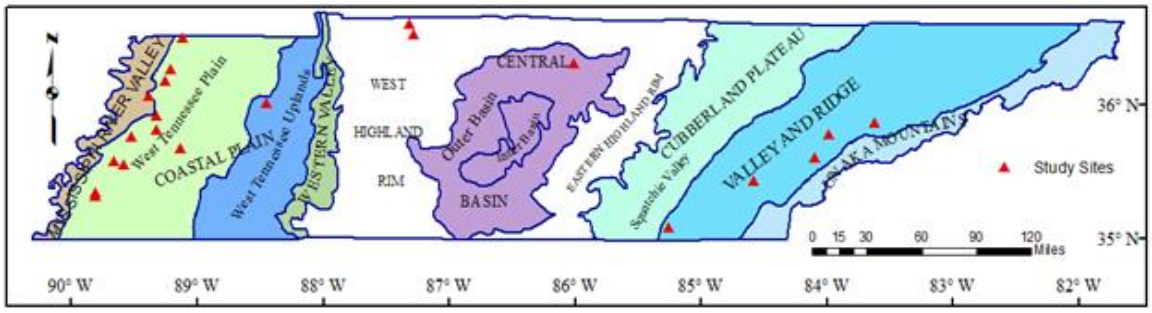


Figure 3.3.1: Physiographic map of Tennessee with study sites (physiographic classifications from Miller, 1974)

3.4 Methodology

3.4.1 Data collection

In this study, in-situ jet test data and soil samples were collected from the selected streams (Table 3.4.1). Data were collected from the five sites in east Tennessee from July 2014 to April 2015, and the remaining sixteen sites from May 2015 to August 2015. Soil natural moisture content prior to in-situ testing was relatively similar as fieldwork was not conducted within 24 hours after precipitation. Test locations were also visually free from pebbles or rocks, vegetation, and root systems. Test data were collected from six locations for each stream study

site, approximated at higher, middle, and lower bank positions. In a few cases, rocks or vegetation prevented testing along all vertical positions, or both banks. In two streams (Lewis Creek and Pond Creek), 11 jet tests were conducted at bank failure locations to compare whether there were soil property differences between the failed material and the exposed bank surface.

Prior to each test, the soil surface was cleaned gently using a shovel and the bottom ring of the jet test device was inserted into the soil using uniform pressure to minimize surface disturbances. The jet test device was then operated following the procedures outlined by Hanson and Cook (2004) and Al-Madhhachi et al. (2013a,b) but with modification as discussed in detail by Mahalder et al. (2018) and presented in Chapter II. A constant head at each pressure was maintained using a pump that delivered stream water powered by a 2000 W portable generator. Before starting any test, the soil WC, electrical conductivity (EC), and soil temperature (T) were measured using a Decagon 5TE probe (Decagon Device Inc., Washington, US). This probe was factory calibrated and rechecked for WC and temperature in the laboratory before field use. Accuracy for WC readings were ±3%, ±10% for EC readings, and ±1°C for temperature measurements. Water pH was measured using a portable Orion 250 A+ pH meter (Thermo Electron Corporation, Massachusetts, US) with an accuracy of ±0.2 pH units. Prior to each measurement, the pH probe was calibrated using the autocalibration mode with two buffer solutions (4.01 and 7.00 pH solutions). After completing each test, two core samples near the test location were collected using a 5.08 cm dia. cylindrical stainless steel coring instrument. These core samples were used to measure bulk density (BD), WC and unconfined compression (UC) strength. The core cylinders were immediately end capped and sealed in an air-tight plastic bag to minimize moisture loss.

Table 3.4.1 Study sites with identifying information on location, geological formation and rock characteristics (Miller, 1974), and watershed drainage area (km^2)

Creek Name	County	Physiographic Province	Geological Formation and Rock Characteristics		Latitude	Longitude	Watershed Area (km^2)
Pistol Creek	Blount	Valley and Ridge	Ordovician and Cambrian System • Knox Group • Chilhowee Group Conasauga Group	Shale, dolomite, limestone, sandstone, conglomerate, quartzite, arkose, greywacke, and siltstone	35.781954	-83.984316	77.67
Nine Mile Creek					35.609316	-84.093183	117.25
Gist Creek	Sevier				35.8613667	-83.619066	26.89
South Chickamauga Creek	Hamilton				35.0873194	-85.260766	1204.76
Oostanaula Creek	McMinn				35.4325810	-84.585825	149.66
Spring Creek	Montgomery	Western Highland Rim	Mississippian and Pennsylvanian System	Limestone, sandstone, shale, siltstone, and dolomite	36.604722	-87.318056	195.34
Red River					36.526111	-87.279444	1344.16
Peyton Creek	Smith	Central Basin			36.308889	-86.007778	128.85
Beaver Creek	Carrol	West Tennessee Uplands (suregion)	Cretaceous in age Neogene and Quaternary System Deposit from both marine and nonmarine sand, silt and clay with sand dominant	Sand, silt, clay, gravel and loess	36.013041	-88.445056	58.39
Lewis Creek	Dyer	West Tennessee Plain (subregion)			36.064388	-89.379583	66.95
Pond Creek					35.921027	-89.325277	139.96
Reeds Creek					36.179666	-89.25400	134.10
Mud Creek	Haywood				35.678261	-89.132721	64.60
Cane Creek	Lauderdale				35.759750	-89.522583	87.60
North Reelfoot Creek	Obion				36.495533	-89.118099	9.02
Richland Creek					36.262007	-89.212328	45.28
Big Creek	Shelby				35.342108	-89.806569	83.29
Crooked Creek					35.323894	-89.807139	44.63
Coal Creek	Town				35.552611	-89.585556	19.00
Town Creek					35.581445	-89.657422	29.15
Black Creek	Crockett				35.815902	-89.320778	151.22

The sealed samples were then stored in a cooler. Approximately 1.4 kg of soil was also collected per test site from inside the jet device's bottom ring for laboratory analyses of other soil physical and geochemical properties (Table 3.4.2). After completing the fieldwork, a GIS base map was prepared for the studied watersheds including: a digital elevation model (DEM) from U.S. Geological Survey (USGS), topographic data, and Natural Resources Conservation Service (NRCS) Soil Survey Geographic (SSURGO) data. For all the study sites, the SSURGO soil database was used for identifying the soil horizons and source of parent materials.

Table 3.4.2 Soil tests and method standards used to characterize soil properties

Test	Measurement Method
Liquid Limit	BS1377
Plastic Limit	ASTM D4318
Median Grain Size (D_{50})	ASTM D422
Specific Gravity of soil	ASTM D854
Dispersion Ratio	ASTM D4221
Specific Surface	Modified European Spot Method (Santamarina et al., 2002)
Organic Content	LOI method (USDA 2011)
Saturated paste preparation	USDA 2011
Extract from saturated paste	Centrifuging and vacuum filtration (0.45 μm filter)
Soil pore water pH	Direct measurement from the soil extract
Pore water electric conductivity	Direct measurement from the soil extract
Cations (Na^+, K^+, Ca^{2+}, Mg^{2+})	IC Analysis on soil paste extract
USCS Classification	ASTM D2487

3.4.2 Laboratory analysis

The collected cores and soil samples from each test location were used for determining mechanical, physical, and geochemical properties. The core samples were extruded and analyzed for BD (ASTM D2937) and WC (ASTM D7263). Extruded cylindrical samples were then trimmed and subjected to UC tests using a triaxial testing device (Loadframe 1, GEOTAC) (ASTM D2166). Soil samples collected from each test location for measuring soil physical and

geochemical properties were air dried and ground. A summary of the performed tests and corresponding protocols are presented in Table 3.4.2.

3.4.3 Parameters prediction for excess shear stress equation

The erodibility parameter τ_c and k_d were calculated by the Blaisdell et al. (1981) approach with modification as discussed by Mahalder et al. (2018) and presented in Chapter II. These two parameters were correlated utilizing the 128 soil samples, and compared with Simon et al. (2011) developed equations to validate the existing model for this dataset. Tested soils were also classified based on the erodibility index described by Hanson and Simon (2001).

3.4.4 Multicollinearity in the dataset

Multicollinearity is the existence of near-linear relationships among the independent variables violating basic assumptions for regression analyses. It may also create inaccurate regression coefficients estimation and inflation of the standard errors of the regression coefficients, deflate the partial t-tests for the regression coefficients, compute false, nonsignificant p-values, and/or reduce model predictability (Statistical software package NCSS v.9.0 Tutorial). Working with comprehensive datasets for soil properties substantially increases the possibility of multicollinearity due to various tests measuring similar characteristics. However, in this study, multicollinearity was minimized by removing co-varying variables from the original dataset. For example, the variable DD was calculated from the measured BD and WC, which caused multicollinearity. Plasticity index (PI) is calculated from liquid limit (LL) and plastic limit (PL), so this variable obviously showed strong collinearity. Porosity (n) of soil is calculated from the void ratio (e), which showed strong collinearity as well. The percent sand, silt, and clay content was calculated from the grain size distribution curve; therefore, these variables have a significant linear relationship. Hence, the variable selection process using regression may encounter division by zero or by a very small quantity causing biased results

(NCSS v.9.0 Tutorial). Thus, DD, e, PI and sand% variables were omitted during the variable selection procedure.

Multicollinearity among the independent variables was also checked by following Belsley et al. (1980) criteria in NCSS, and a cluster analysis (as described below) was used to assess selected variables within data clusters. Using statistical software package SPSS v.23.0, the variable inflation factor (VIF) for individual variables and Durbin-Watson coefficient value for each model were calculated for each data cluster. Results of these analyses showed that the VIF for each variable in each cluster was less than 10 (O'Brian, 2007), and the Durbin-Watson values were between 1.67 and 2.23. Therefore, possible multicollinearity issues for this dataset were addressed in a systematic manner.

3.4.5 Cluster analysis

A two-stage non-parametric and non-hierarchical cluster analysis (CLA) was used to identify statistically significant cluster groupings of sites based on similar soil properties and results assessed for similarity in surficial geology. CLA was performed in statistical software package SAS v.9.4 where the non-parametric clustering method "Ward" and non-hierarchical "k-means" approach were used. The pattern of the individual observation classified into a particular cluster, based on the corresponding probability value was also validated by the two-stage CLA using both SAS v.9.4 and NCSS v.9.0. The non-hierarchical clustering method identified the misclassification of observations in any cluster and reassigned them into the appropriate cluster from individual observation probabilities.

3.4.6 Statistical model development for variable selection

Multiple regression equations were developed for the entire dataset and unique site groupings from the cluster analysis as described above. Different variable selection algorithms are available for the multivariate statistical data analysis because each may generate different

regression models with significant predictor variables based on data type. Four different variable selection algorithms were used for this study and the role of those algorithms was evaluated for variable selection on erodibility parameters prediction. Variable transformations were performed when necessary to convert values within similar orders of magnitude (Table 3.4.3). Transformations aided in reducing the dataset skewness. In order to identify the dominant independent variables related to erodibility, a systematic approach to the statistical analyses followed these steps:

1) all possible regression (APR) analyses were performed for significant variables selection due to the large number of independent variables; the possible number of outliers in the dataset were also identified using NCSS v.9.0 for decision making prior to conducting the variable selection analyses;
2) the variables found to be significant from the APR were compared with the McHenry algorithm (MHA) variable selection technique, the least angle regression (LAR) (Efron et al., 2004) analysis, and stepwise multiple linear regression (STR) method; the LAR analysis was conducted using a Matlab routine developed by Chen (2012), and the APR, MHA and STR analyses were conducted using NCSS v.9.0;
3) the selected variables found to be significant using these variable selection procedures were used for a multiple regression equation for developing a prediction model for τ_c prediction;
4) the corresponding p-value of the individual variables were examined from the analysis; the variable(s) with coefficient p-value greater than 0.05 were omitted from the model; depending on the resulting change in the R^2 value, the predictive model was either kept intact or modified by excluding the non-significant variable(s); and

Table 3.4.3 Statistical description of the measured variables for the dataset consisting of 128 soil samples among the different Tennessee physiographic provinces

Variables	Range	Min	Max	Mean	Std. Deviation	Data Transformation Technique Used
Critical Shear Stress (Pa)	26.72	0.08	26.8	5.17	3.81	SQRT
k_d (cm^3/N-s)	23.84	0.56	24.4	3.51	4.11	SQRT
Water Content, WC (%)	24.76	17.6	42.36	29.03	5.16	Decimal
Bulk Density, BD (g/cm^3)	0.60	1.52	2.12	1.88	0.11	None
Dry Density, DD (g/cm^3)	0.78	0.98	1.76	1.45	0.14	None
Median Grain Size, D_{50} (µm)	36.3	3.7	40.0	15.52	6.71	Log
Dispersion Ratio (DR)	0.48	0.15	0.63	0.36	0.10	None
Specific Gravity (SG)	0.21	2.49	2.7	2.62	0.04	None
Cohesion, CC (psi)	14.42	1.24	15.65	5.12	2.78	Log
Strain, Str (%)	20.45	2.45	22.9	10.82	4.48	Decimal
Void Ratio (e)	1.11	0.50	1.61	0.82	0.18	None
Porosity (n)	0.38	0.24	0.61	0.44	0.06	None
Liquid Limit (LL)	18.9	23.6	42.5	31.66	4.15	Decimal
Plastic Limit (PL)	13.89	16.76	30.65	22.74	3.21	Decimal
Plasticity Index (PI)	17.23	3.44	20.66	8.93	3.63	Decimal
Organic Content (%)	7.17	1.48	8.65	3.28	1.55	Decimal
Sodium Adsorption Ratio (SAR)	25.19	0.32	25.51	4.67	5.21	SQRT
Potassium Intensity Factor (KIF)	1.23	0.02	1.25	0.19	0.2	None
Passing # 200 sieve (%)	39.0	60.0	99.0	89.9	8.35	Decimal
Geometric Standard Deviation (σ_g)	25.25	2.04	27.29	10.46	6.16	Log
Sand (%)	48.0	2.0	50.0	12.48	9.83	Decimal
Silt (%)	50.0	30.0	80.0	63.37	11.41	Decimal
Clay (%)	33.0	10.0	43.0	24.15	7.48	Decimal
pH	3.29	4.83	8.12	7.0	0.64	Log
Specific Surface, SS (m^2/g)	141.29	12.84	154.14	50.35	22.82	Log
T (^oC)	17.7	16.8	34.5	26.63	4.02	Log
Clay Activity (CA)	0.41	0.20	0.61	0.37	0.07	None
Electric Conductivity, EC (µS/cm)	684.93	7.07	692.0	263.42	187.17	Log
Consistency (Con)	3.95	-2.07	1.88	0.15	0.63	None

5) the residual distribution patterns were checked for normality in NCSS v.9.0; VIF and Durbin-Watson values were also checked using SPSS v.23.0.

PRESS statistics were computed for each regression model developed using SPSS v.23.0. PRESS statistic, or predicted residual sum of squares is the sum of the squared deleted residuals, which is a cross-validation technique approach for the performance analysis of a predictive model.

3.5 Results

3.5.1 Soil Properties

As classified by the USDA (Foth, 1990), the soil samples consisted of a variety of soil textures including: loam, clay-loam, silty-clay, silty-loam and silty-clay-loam, but were predominantly silty-loam and silty-clay-loam. Atterberg limit tests indicated the presence of cohesiveness in the soil samples since the PI values were between 3.40 and 20.70 (Table 3.4.3). The LL and PL values were between 23.6% and 42.5%, and 16.80% and 30.70%, respectively. Some of the soil samples had a low PI, even though the material met the criteria for cohesive soils (minimum clay content of 5%-10% by weight) as defined by Raudkivi (1990) and Mitchell and Soga (2005). Soil BD ranged from 1.52 g cm^{-3} to 2.12 g cm^{-3} and D_{50} was between 3.7 μm and 40 μm. The size geometric standard deviation (σ_g) of the tested soils ranged between 2.04 and 27.29 with a mean of 10.46, indicating widely varying grain sizes. The range of soil cohesion (CC) was between 8.55 kPa and 107.90 kPa, and organic content (OC) ranged between 1.48% and 8.65%. The soil dispersion ratio (DR) ranged from 0.15 to 0.63. The dispersive behavior of clay was classified and identified according to the US Army Corps of Engineers (USACE, 1970) classification criteria as presented in Table 3.5.1. The majority of the soil samples were either non-dispersive or in the intermediate range. Results also suggested the studied soils were mostly inactive (Skempton, 1953) based on a maximum CA value of 0.61 and

specific surface (SS) values of 12.8 m^2 g^{-1} to 154.1 m^2 g^{-1}. Some of the tested soils (43 observations) had a negative consistency value, which was thought to be influenced by the presence of organic matter and/or possibly precipitation events before conducting the field tests.

Table 3.5.1 Degree of dispersion for the tested soils according to the US Army Corps of Engineers (USACE, 1970) classification criteria

Percent Dispersion	Count	Degree of Dispersion
< 35%	66	Non-dispersive
35-50%	51	Intermediate
> 50%	11	Dispersive

The physiochemical properties of the soil samples in bank failure locations were not found statistically different from the in-situ bank material (p = 0.58). However, erodibility parameters τ_c and k_d were found different for the failed bank materials compared to the in-situ bank material (p = 0.002, 0.030, respectively).

The τ_c and k_d values were calculated by the methods developed in Chapter II, in which values for τ_c ranged from 0.08 Pa to 26.82 Pa with a mean of 5.17 Pa and standard deviation of 3.81 Pa (Table 3.4.3). The k_d ranged between 0.56 and 24.4 cm^3 N^{-1} s^{-1}, with a mean of 3.51 cm^3 N^{-1} s^{-1} and standard deviation of 4.11. The τ_c and k_d values were strongly correlated as shown in Figure 3.5.1 (R^2 = 0.78; p <0.001). The erodibility index of the tested soil was also plotted on the same figure. Results showed the tested soils were very erodible to erodible based on the Hanson and Simon (2001) classification scheme.

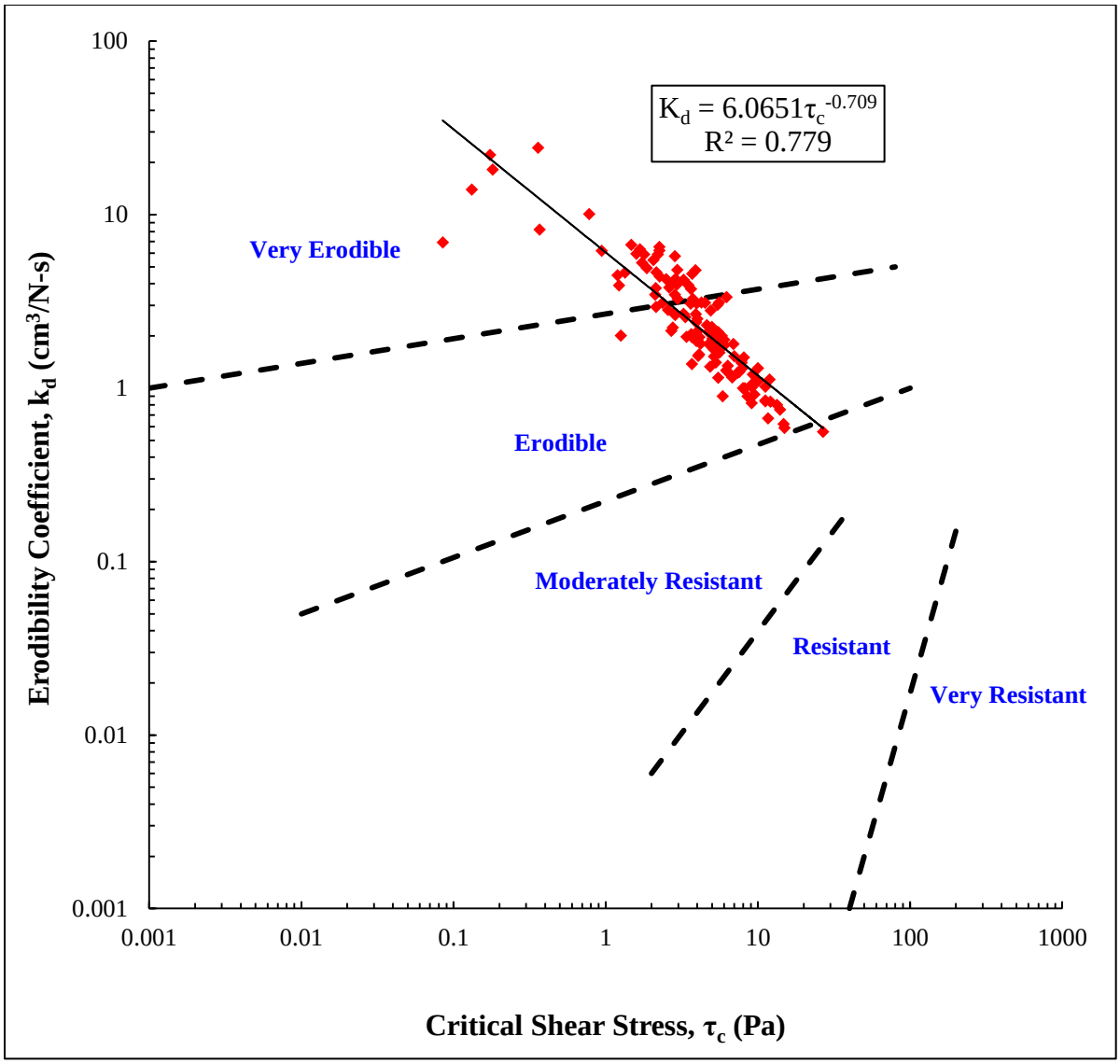


Figure 3.5.1: Relationship between critical shear stress and erodibility coefficient with erosion index (after Hanson and Simon, 2001)

3.5.2 Properties of the cluster groups

In order to observe whether soil properties were distinct among Tennessee physiographic providences, CLA was performed using complete dataset (Table 3.4.3). Four cluster groups were significantly identified using CLA (Figure 3.5.2). It is important to note that these clusters highlight the important association with different surficial geologies among the physiographic provinces. In Cluster 1, 32 observations were found and a majority of the observations (25) were from the Valley and Ridge physiographic province. Cluster 2 was formed with 30 observations from two border counties (Dyer and Obion) of the West Tennessee Plain, subregion of Coastal Plain (Table 3.4.1). In Cluster 3, observations were assigned from six counties (Carroll, Crockett, Haywood, Obion, Shelby, and Town) of West Tennessee in the Coastal Plain physiographic province with 49 observations. The remaining 17 observations were classified into Cluster 4 from the West Highland Rim and Central Basin physiographic provinces. The results of the CLA indicated that τ_c was dependent on a comprehensive set of soil physical and geochemical properties that appear to be inherently related to the associated surficial geology (Table 3.4.1). Acceptability of the cluster data was verified by applying MANOVA tests using SPSS v.23.0. Results showed the significance level of Pillai's Trace value as 0.0001, so the groups were significantly different for an α value of 0.05.

3.5.3 Statistical correlation and model variable selection

Development of statistical models for predicting τ_c as a function of significant independent variables was completed using APR, MHA, LAR, and STR methods. These analyses were performed on the complete transformed dataset (Table 3.4.3), and separately on the four clusters identified in Figure 3.5.2 and as described above. The normality and independence assumptions were met for each significant regression variable from visual assessments of residual plots.

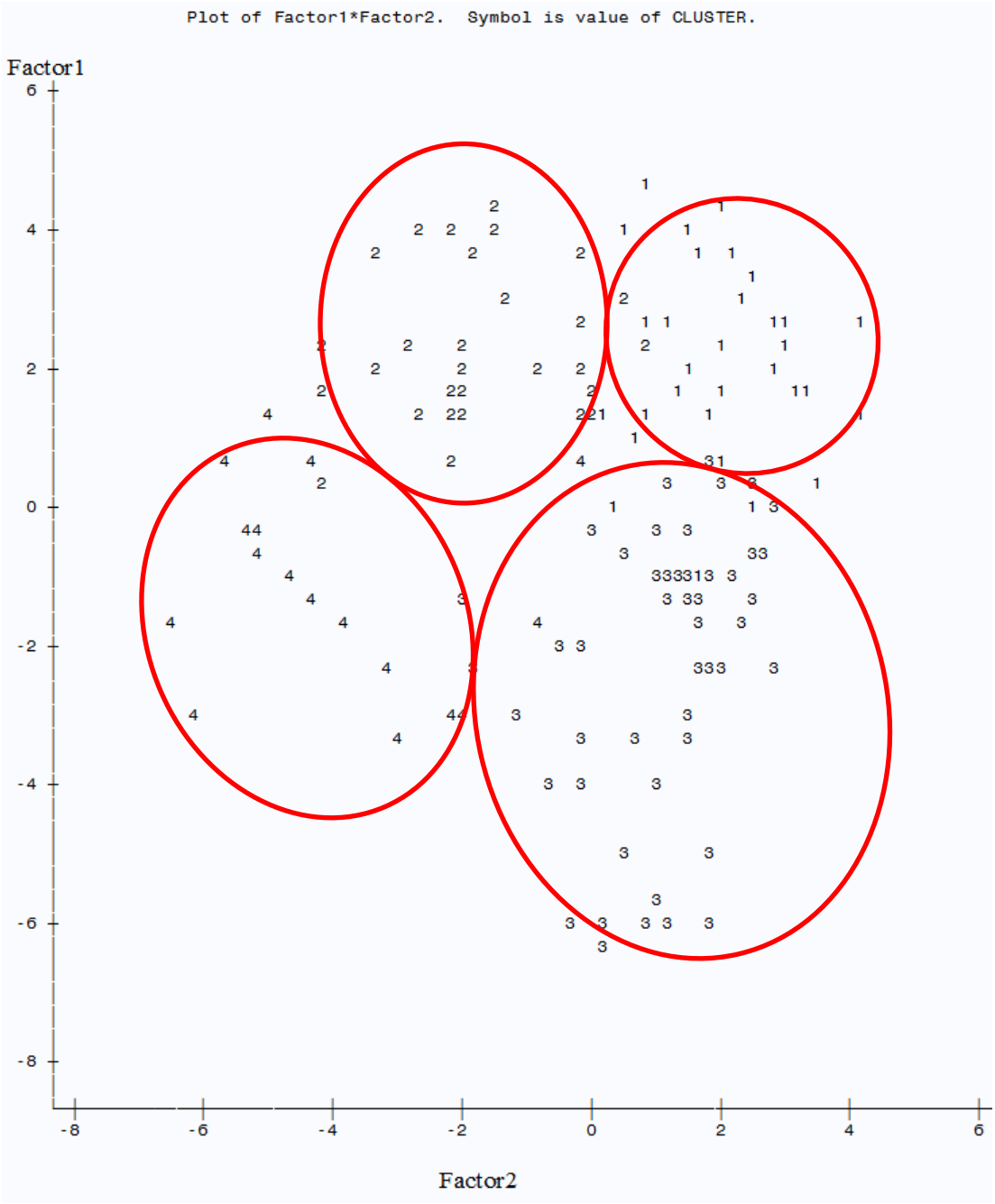


Figure 3.5.2: Four cluster groups using the "Ward" method and non-hierarchical "k-means" approach based on soil properties including critical shear stress

Predictive statistical models as presented in Table 3.5.3 showed statistically significant selected variables using the above mentioned methods and corresponding regression p-values. Changes in R^2 value and adjusted R^2 value were also examined by omitting variables with coefficient-p value > 0.05 in order to obtain the best-fit model. As stated earlier, four different statistical techniques were used for significant variable selection. Based on PRESS statistics value and nature of the dataset, predictive statistical model using LAR method was adopted for variable selection for the entire dataset of 128 observations. Among these suite of regression models, three variables: CC, DR, and SAR were common (Table 3.5.2). However, in the best predictive multiple regression model, seven variables: BD, CC, DR, OC, SAR and σ_g were found statistically significant (adjusted $R^2 = 0.29$; $p < 0.001$):

$$\tau_c = -3.798 + 1.784 * BD + 1.082 * CC + 1.45 * DR + 12.292 * OC + 0.18 * SAR + 0.53 * \sigma_g \quad (3.12)$$

Variables selected in the model showed high significance (coefficient $p < 0.05$) except σ_g (coefficient $p = 0.078$). Though, the inclusion of σ_g increased the correlation of the model. The plot of the predicted versus observed τ_c and the residuals plot showed variation from the normal probability distribution patterns. Statistical data analysis also showed models using the entire dataset differed from the models when developed individually per data from each cluster representing different physiographic provinces (Figure 3.5.2). Those models are described below.

Of the 32 observations classified into Cluster 1, the soil samples consisted mostly of non-dispersive inactive clay materials. The majority of the observations were from the Valley and Ridge physiographic province consisting of geological formations comprised of shales, limestone, and sandstone (Table 3.4.1).

Table 3.5.2 Multiple regression models for prediction of critical shear stress (τ_c) based on soil properties. Models included all possible regression (APR), McHenry algorithm (MHA), least angle regression (LAR), and stepwise multiple linear regression (STR). R^2, p-value, and PRESS statistics are shown for each model

Data type	Predicting Model	Method	N	R^2	p-value	PRESS
All data	$\tau_c = -4.853 + 2.519 * BD + 1.171 * CC + 1.183 * DR + 20.242 * OC + 0.189 * SAR$	APR	128	0.21	0.0001	57.38
	$\tau_c = -4.20 + 1.304 * CC - 0.733 * D_{50} + 2.13 * DR + 0.154 * SAR + 1.06 * \sigma_g + 2.424 * T + 2.72 * WC$	MHA	128	0.30	0.0001	56.06
	$\tau_c = -3.798 + 1.784 * BD + 1.082 * CC + 1.45 * DR + 12.292 * OC + 0.18 * SAR + 0.53 * \sigma_g$	LAR	128	0.29	0.0001	56.38
	$\tau_c = -2.533 + 1.063 * CC - 0.619 * D_{50} + 2.06 * DR + 0.15 * SAR + 0.93 * \sigma_g + 1.93 * T$	STR	128	0.28	0.0001	57.12
Cluster 1	$\tau_c = -1.927 + 1.348 * CC + 1.921 * Clay - 0.568 * Con + 2.032 * DR - 1.926 * KIF + 5.151 * LL + 0.562 * \sigma_g$	APR	32	0.72	0.0001	5.44
	$\tau_c = -1.927 + 1.348 * CC + 1.921 * Clay - 0.568 * Con + 2.032 * DR - 1.926 * KIF + 5.151 * LL + 0.562 * \sigma_g$	MHA	32	0.72	0.0001	5.44
	$\tau_c = -0.97 + 0.98 * CC + 2.77 * Clay + 2.06 * DR - 1.956 * KIF + 4.146 * WC$	LAR	32	0.61	0.0001	6.16
	$\tau_c = -1.916 + 1.334 * CC + 2.267 * Clay + 1.79 * DR - 1.78 * KIF + 0.265 * SAR + 0.573 * \sigma_g + 3.93 * WC$	STR	32	0.67	0.0001	6.17
Cluster 2	$\tau_c = 3.94 + 2.76 * CC - 2.335 * D_{50} - 2.72 * Pass\ 200 + 0.24 * SAR - 1.49 * SS + 6.13 * Str + 8.1 * WC$	APR	30	0.45	0.0033	11.30
	$\tau_c = 3.94 + 2.76 * CC - 2.335 * D_{50} - 2.72 * Pass\ 200 + 0.24 * SAR - 1.49 * SS + 6.13 * Str + 8.1 * WC$	MHA	30	0.45	0.0033	11.30
	$\tau_c = 6.644 + 2.492 * CC - 1.70 * D_{50} + 1.362 * DR - 4.12 * Pass\ 200 - 6.06 * pH + 0.343 * SAR + 10.48 * WC$	LAR	30	0.44	0.0045	11.63
	$\tau_c = 5.352 + 1.676 * CC - 5.682 * pH$	STR	30	0.42	0.0002	10.00
Cluster 3	$\tau_c = -33.802 + 14.161 * BD + 5.643 * CA - 18.84 * LL + 69.1 * OC + 8.545 * Pass\ 200 - 3.49 * pH + 21.0 * WC$	APR	49	0.54	0.0001	19.12
	$\tau_c = -27.63 + 10.96 * BD - 0.812 * Con + 1.13 * DR - 0.433 * EC + 49.33 * OC + 7.97 * Pass\ 200 + 0.605 * SS$	MHA	49	0.48	0.0001	22.86
	$\tau_c = -10.42 + 5.035 * BD + 0.261 * CC - 1.272 * D_{50} + 1.86 * DR + 1.06 * KIF + 2.614 * Pass\ 200 + 0.665 * SS$	LAR	49	0.38	0.0002	26.09
	$\tau_c = -30.03 + 12.29 * BD - 0.769 * Con + 57.516 * OC + 8.042 * Pass\ 200$	STR	49	0.46	0.0001	20.65
Cluster 4	$\tau_c = -7.698 + 14.161 * CA - 12.678 * n - 21.39 * OC + 9.38 * Pass\ 200 - 0.548 * SAR + 12.90 * WC$	APR	17	0.80	0.0005	2.32
	$\tau_c = 25.318 - 0.374 * DR + 2.316 * KIF + 44.394 * LL - 59.53 * PL - 0.68 * SAR - 9.32 * SG + 10.03 * Str$	MHA	17	0.65	0.0117	5.95
	$\tau_c = 8.77 + 1.223 * CC + 8.8 * DR + 4.3 * EC + 3.955 * KIF - 9.61 * n + 13.99 * Pass\ 200 - 20.466 * T$	LAR	17	0.74	0.0032	6.07
	$\tau_c = 0.904 + 4.56 * DR$	STR	17	0.18	0.0489	7.06

$\tau_{c(actual)} = (\tau_c)^2$, Critical Shear Stress; BD = Bulk Density (g/cm^3); CC = log (CC_{actual}), Cohesion; DR = Dispersion Ratio; OC = Organic Content; σ_g = Geometric Standard Deviation; D_{50} = log($_{D50(actual)}$), Sediment Diameter (μm); SAR = SQRT (SAR_{actual}), Sodium Adsorption Ratio; T = log(T), Water Temperature (^{0}C); WC = Water Content; Clay = Clay Content in the soil; Con = Soil Consistency (PI/Clay Content); KIF = Potassium Intensity Factor; LL = Liquid Limit; Pass200 = Sediment Passing 200 Sieve; SS = log(SS_{actual}), Specific Surface (m^2/g); Str = Strain Rate from UC Test; CA = Clay Activity; n = Porosity; PL = Plastic Limit; SG = Specific Gravity of Soil.

Though seven observations were also grouped into Cluster 1 from western Tennessee with calcareous type soils composed of fine siliceous loam with the presence of lime concretions. Calcium was thought to be the key geochemical property governing the statistical similarity with observations from the Valley and Ridge physiographic province. APR, MHA and STR methods identified seven significant variables for predicting τ_c. APR and MHA methods predicted models were found to have the best correlation (adjusted $R^2 = 0.72$; Table 3.5.2):

$$\tau_c = -1.927 + 1.348 * CC + 1.921 * Clay - 0.568 * Con + 2.032 * DR - 1.926 * KIF + 5.151 * LL + 0.562 * \sigma_g \quad (3.13)$$

The inclusion of σ_g increased the correlation most significantly though the coefficient p = 0.083. DR was identified the second most significant variable.

In Cluster 2, 30 observations were grouped from two counties (Dyer and Obion County) from the West Tennessee Plain, a subregion of the Coastal Plains physiographic province. Grain size distribution curve for these soils showed sand, silt, and clay in the soil formation with no gravel. This cluster group showed a higher number of outliers (30% observations) compared to other clusters. The LAR model resulted in the best-fit model after variable selection with adjusted $R^2 = 0.44$ (Table 3.5.2).

$$\tau_c = 6.644 + 2.492 * CC - 1.70 * D_{50} + 1.362 * DR - 4.12 * Pass\ 200 - 6.06 * pH + 0.343 * SAR + 10.48 * WC \quad (3.14)$$

WC explained most variance in this dataset as it significantly affected the R^2 value. Pass200 and pH were the second and third most significant variables, respectively, to predict τ_c.

Within Cluster 3, 49 observations were from the West Tennessee Plain and the West Tennessee Uplands (subregions of the Coastal Plain physiographic province). Similar to Cluster 2, in this cluster no gravel material was found from the grain size distribution curves. The overall soil characteristics were found as laminated sands and clays, with well-marked beds of bluff

loams with beds of clay with poor drainage. In this cluster, three observations were identified as outliers due to the presence of dispersive clay. APR, MHA and LAR methods identified seven significant variables for the model. Based on the coefficient p-value of individual variables and significance of the correlation, APR method generated the best-fit model with (adjusted R^2 = 0.55; $p < 0.001$) (Table 3.5.2):

$$\tau_c = -33.802 + 14.161 * BD + 5.643 * CA - 18.84 * LL + 69.1 * OC + 8.545 * Pass\ 200 - 3.49 * pH + 21.0 * WC \quad (3.15)$$

In this model, the Pass200 variable explained most variance in this dataset as the inclusion of this variable increased the correlation and WC was the second most significant variable.

Within Cluster 4, 17 observations were from Middle Tennessee covering the Western Highland Rim and the Central Basin physiographic provinces. The geologic rock at study sites in this cluster included limestone, siltstone, sandstone and sandy shales, and interstratified with layers of chert. In this region, soil samples consisted of a higher percentage of coarse silt (wider grain size distribution curve in the silt range was observed) compared to other clusters and the average PI value was less than the other three clusters. In Cluster 4, the APR variable selection method generated the best-fit model for τ_c (adjusted R^2 = 0.80; Table 3.5.2):

$$\tau_c = -7.698 + 14.61 * CA - 12.678 * n - 21.39 * OC + 9.38 * Pass\ 200 - - 0.548 * SAR + 12.90 * WC \quad (3.16)$$

The variable OC with coefficient $p = 0.083$ significantly increased the model's correlation. WC and CA were the two other most significant variables.

PRESS statistic values for each predicted models using different variable selection algorithms are also presented in Table 3.5.2. It is expected that the PRESS statistics would be lower for a better predictive model, which was found analogous with the reported best predictive models as developed per multivariate regression analyses. However, in Cluster 2, the PRESS

statistic value for the selected predictive model was found to be slightly higher compared to other predictive models.

Using these four predictive models, unique for each cluster, the correlation between measured τ_c and predicted τ_c for different clusters are presented in Figure 3.5.3. In summary, 16 soil physiochemical parameters were identified as significant among the developed predictive models for τ_c. Four variable selection algorithms were used in this study to identify significant soil physiochemical parameters to predict τ_c in the four cluster groups. However, based on the data characteristics, one algorithm was usually found to be the best predictive model. In this study, APR, MHA, and LAR predicted 3 to 5 common variables in the predictive models in each cluster group with similar correlation and adjusted R^2 values (Table 3.5.2). Statistically, it was interesting to note that STR showed overall lower R^2 and adjusted R^2 values and different sets of variables compared to other three methods. Differences were observed in coefficient p-values for individual variables among the dominant models (Equations 3.13-3.16).

The coefficient p-values for individual variables and the correlation sign to τ_c among the predictive models are presented in Table 3.5.3. WC and Pass200 were selected as a significant model variable among three clusters, and CC, DR, LL, SAR, and OC were selected for at least two of the four cluster models. In this study, no analyses were completed for k_d prediction rather, empirical equations were developed among the four clusters using the study's jet test data (Table 3.5.4). Highly significant relationships were developed for all clusters ($p < 0.001$).

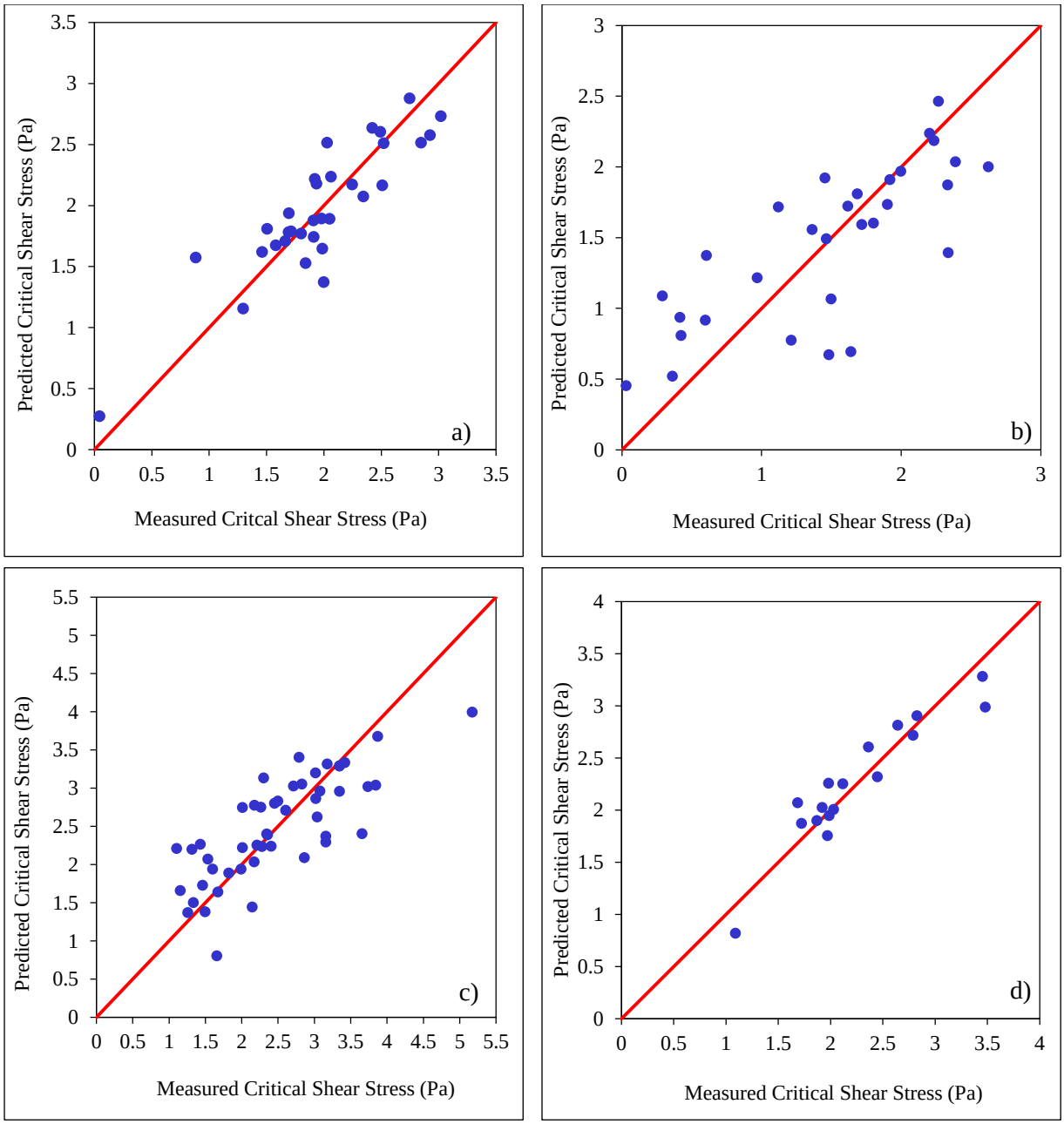


Figure 3.5.3: Measured and predicted critical shear stress (a) Cluster 1, (b) Cluster 2, (c) Cluster 3, and (d) Cluster 4 (using transformed data)

Table 3.5.3 Coefficient p-values for individual variables and corresponding correlation sign among the predictive models for each cluster representing an unique physiographic province and surficial geology

Name of Variables	**Cluster 1 (Eq. 3.13)**	**Cluster 2 (Eq. 3.14)**	**Cluster 3 (Eq. 3.15)**	**Cluster 4 (Eq. 3.16)**
Passing # 200 sieve (Pass200)	-	(-) 0.215	(+) < 0.001	(+) < 0.001
Water Content (WC)	-	(+) 0.014	(+) < 0.001	(+) < 0.001
Cohesion (CC)	(+) < 0.001	(+) 0.026	-	-
Dispersion Ratio (DR)	(+) 0.014	(+) 0.025	-	-
Liquid Limit (LL)	(+) 0.008	-	(-) 0.003	-
pH	-	(-) 0.100	(-) 0.083	-
Sodium Adsorption Ratio (SAR)	-	(+) 0.010	-	(-) < 0.001
Clay Activity (CA)	-	-	(+) 0.026	(+) < 0.001
Organic Content (OC)	-	-	(+) < 0.001	(-) 0.083
Consistency (Con)	(-) < 0.001	-	-	-
Potassium Intensity Factor (KIF)	(-) < 0.001	-	-	-
Clay Content (Clay)	(+) 0.043	-	-	-
Geometric Standard Deviation (σ_g)	(+) 0.083	-	-	-
Bulk Density (BD)	-	-	(+) < 0.001	-
Median Grain Size (D_{50})	-	(-) 0.018	-	-
Porosity (n)	-	-	-	(-) < 0.001

+/- Sign indicates the correlation to the τ_c

3.6 Discussion

The importance of developing predictive relationships for the erodibility parameters (k_d and τ_c) was highlighted in the background section summarizing the different empirical models developed from numerous published studies. Existing models for τ_c, differed widely for various reasons, which included the set of physical-geochemical properties selected as independent variables. Few field studies used a more comprehensive variable dataset of soil properties, and the studies were generally conducted in a single geologic region. The primary interest of this study was to provide better insight into which physical-geochemical properties dominantly control soil erodibility, and knowing that these properties are derived from the parent soils material. The state of Tennessee with its many physiographic provinces and diverse geology provided a unique US region to examine the differences in the erodibility parameters among different surficial geologies.

With an in situ testing apparatus, the mini-jet, results from this study provided evidence that different governing physical-geochemical soil properties dominate among different physiographic provinces. The key finding from our study suggests that a single universal equation for predicting erodibility parameters is highly unlikely, and predictive relationships need to be developed per province. A physiographic province consists of a distinct surficial geology, and climate and vegetation conditions that control soil genesis, and the existing physical-geochemical properties. The possible effect of geology on the empirical erodibility coefficient prediction models was also reported by Clark and Wynn (2007), but was not researched among different physiographic provinces. Therefore, it was necessary to assess a comprehensive set of the soil properties because of the possibility of varying controlling properties per province. In addition, our approach to predictive model development utilized four separate logistic regression techniques to find the best-fit model where we found that statistical

method did influence the results. Observing the differences in predictive models for τ_c, our study compared a predictive model developed from the entire dataset to that of four statistically significant site groups that correlated with unique surficial geologies.

Table 3.5.4 Predictive models in each cluster for erodibility coefficient (k_d) as a function of critical shear stress (τ_c) for the entire dataset, and individually for the four identified data clusters

Cluster	Empirical Equation	R^2 value	Model p-value
Entire Data	$k_d = 6.065\ \tau_c^{-0.709}$	0.78	< 0.0001
1	$k_d = 8.708\ \tau_c^{-1.009}$	0.79	< 0.0001
2	$k_d = 5.561\ \tau_c^{-0.538}$	0.70	< 0.0001
3	$k_d = 7.822\ \tau_c^{-0.876}$	0.87	< 0.0001
4	$k_d = 9.524\ \tau_c^{-0.899}$	0.73	< 0.0001

As reported earlier, in the four clusters, different soil physiochemical properties were controlling the τ_c prediction equation consisting similar geology. In Cluster 1, as reported in the results section, seven observations were grouped from western Tennessee containing lime concretions. Miller (1991) reported that lime concretions in this area were not the carbonate rather a silicate precipitate or an infilling of silt, which deposited later. Soil horizons in Cluster 1 from the SSURGO soil database were identified as Hamlin (Hb), Dekoven (De), Etowah loam (Eo), Newark (Ne), Sequatchie loam (Sc), and Steadman (Su) from silty loam parent material originated from limestone, sandstone, and calcareous shale. In this cluster, since sand percentage was higher compared to other three clusters, dispersive nature of the soil with clay content influenced the τ_c prediction equation (Equation 3.12).

Cluster 2 and Cluster 3 were formed from the same physiographic province. Soil horizons: Calloway (Ca), Collins (Cl), Waverly silt (Ws), and Waverly (Wv) were found in Cluster 2 and parent material type was silty alluvium. In Cluster 3, silty alluvium and loess

parent material were present with Adler (Ad), Ca, Wolftever (Wo), and Wv soil horizons. Though similar in texture, material of Cluster 2 was generally softer and more friable than the underlying deposits, commonly breaking to fine crumbs between the fingers compared to Cluster 3 (William and Diehl, 1993). They also reported that the upper 5-20 feet in the region of Cluster 2 were deposited in the past few hundred years compared to the area of Cluster 3, which was formed during Quaternary period. William and Diehl (1993) also reported that the presence of water table influenced the cohesiveness of the soil. In this study it was identified that τ_c values were lower in Cluster 2 compared to Cluster 3, which supported the findings of William and Diehl (1993) study. The presence of outliers in Cluster 2 also supported the hypothesis that the local soil deposition pattern and age of deposition influenced the formation of two distinct clusters from the same physiographic province.

In Cluster 4, soil horizons were found as Arrington (Ar), Atkins (At), Amanda (AmD2) from silty alluvium material originating from limestone and siltstone. In this cluster, since coarse silt with higher σ_g was observed the presence of OC and WC in the soil significantly affected the cohesion, consequently the τ_c values (Equation 3.16). These findings supported the hypothesis that the clusters were formed based on geological formation, rock type, and the characteristics of parent material.

3.6.1 Correlation pattern of significant variables

Six soil physiochemical parameters were identified as statistically significant to predicting τ_c when using the entire dataset among four physiographic provinces (Equation 3.12; adjusted $R^2 = 0.29$; $p < 0.001$); included: BD, CC, DR, OC, SAR, and σ_g. All the significant variables showed a positive correlation with τ_c and the adjusted R^2 value was lower than individual predictive models for data groups clustered by physiographic province (Table 3.5.2). It is also important to note that the PRESS statistics values were much higher for the models

developed with complete dataset compared to the clustered datasets. Therefore, this regression model with complete dataset was considered to have a higher level of uncertainty comparatively with the models based on clustered datasets that aligned with similar geological and soil properties (Figure 3.5.2).

Statistical analyses in this study showed that Pass200 and WC (Table 3.5.3) were the most significant variables among the cluster groups to predict $\tau_{c,}$ consistent with other findings (Hanson and Robinson, 1993; Allen et al., 1999; Briaud et al., 1999; van Ledden et al., 2004; Thoman and Niezgoda, 2008). Briaud et al. (1999) reported that the percentage Passing #200 sieve has a positive correlation with τ_c, which was found to be consistent with the findings in this study for Clusters 3 and 4 (Equations 3.15 and 3.16). However, in Cluster 2, a negative correlation with τ_c was observed (Equation 3.14). The behavior of clay minerals likely affected the characteristics of the cohesive sediments; hence, a detailed clay mineralogical analysis would provide some insight to these results.

WC directly affects the mechanical properties of clay (Gillott, 1987; van Ledden et al., 2004; Grabowski et al., 2011) as well as the plastic deformation. Therefore, a positive correlation with τ_c (Equations. 3.14, 3.15 and 3.16) was expected, which is supported by several other researchers (Hanson and Robinson, 1993; van Ledden et al., 2004; Thoman and Niezgoda, 2008). However, Allen et al. (1999), and Wynn and Mostaghimi (2006) reported a negative correlation between WC to τ_c and reported that for non-plastic soils, WC significantly affect the erosion behavior. The inconsistency could be related to the presence of organic matter and root systems that significantly enhanced the stability of those studied soils and could have altered the behavior of granular material to resemble that of cohesive soil when water coats the granular particles.

The second most significant set of variables was found to be BD, CA, CC, DR, LL, OC, pH and SAR (Table 3.5.3). However, BD and CC were interrelated and these variables showed a positive correlation with τ_c for the complete dataset and in the cluster groupings. Previous researchers have reported that soil erosion rates decreased with increasing BD (Hanson and Robinson, 1993; Allen et al., 1999; Wynn, 2004, Wynn and Mostaghimi, 2006 and Grabowski et al., 2011). Therefore, it is expected that an increase in BD or CC will significantly increase the τ_c of the tested soils. In this study, results showed a positive correlation between DR and τ_c (Equations 3.13 and 3.14), which was supported by other study results. Thoman and Niezgoda (2008) found a similar relationship between DR and τ_c in their study, and the tested soils of the study were also non-dispersive and unsaturated. Shaikh et al. (1988) and Lim (2006) reported similar findings though they did not propose any direct correlation with τ_c. The positive correlation between DR and τ_c identified from this study is also supported by the results as reported by Smerdon and Beasley (1959) and Lyle and Smerdon (1965).

In this study, the tested clay was found to be inactive, so, clay content dominated the ratio (CA = PI/clay content), which is used to define the clay activity for the studied soils (Skempton, 1953). Therefore, the increase in percent clay and the decrease of CA were found to be analogous for a specific clay type. Positive correlations between τ_c and these two parameters (Clay and CA) were identified from this study (Equations 3.13, 3.15 and 3.16). The increase in clay content for these soils (since the tested soil was inactive) increased the probability that the clay would be more inactive. In addition, experimental results suggest that an increase in clay content increases the erosion threshold (increase in τ_c) due to the combination of hydrodynamic smoothing, clay/sand adhesion and clay cohesion (Lick et al., 2004; Grabowski et al., 2011). The

positive correlation between τ_c and clay content is also supported by the field investigation of erosion resistance for different clay minerals (Dickhudt et al., 2011).

Inverse relationships between τ_c and soil pore water pH were identified from the multiple linear regression equations for both Cluster 2 and 3 datasets (Equations 3.14 and 3.15). As the pH increases, the concentration of H^+ ions decreases resulting in an increase in the double layer thickness. Consequently, a greater repulsive force was expected (Winterwerp and van Kesteren, 2004) and the τ_c values reduced with increasing pH. The formation of surface crusting was also reported as another significant physical change on the soil surface due to increase in pH (Wischmeier and Mannering, 1969; Wynn, 2004). These negative correlations were also supported by other studies (Wynn, 2004; Wynn and Mostaghimi, 2006; Thoman and Niezgoda, 2008). However, the variable OC showed both positive and negative correlations with τ_c (Equations 3.15 and 3.16). Depending on the nature of the organic matter and the pore water chemistry for different clay minerals, the erodibility may increase or decrease significantly (Morgan, 2005; Ravisangar et al., 2005). In this study, OC was measured by the LOI method (at 550 °C) for air-dried samples, which did not differentiate between living or dead organisms, fecal material, and the extracellular organic compounds. However, for natural riverine environments, a positive correlation between OC and τ_c has been reported as the inter-particle attraction forces are affected by the presence of organic matter in the natural soil (Gerbersdorf et al., 2007). Therefore, both positive and negative correlations may be observed, which was found in this study.

Similar to OC, both positive and negative correlations with τ_c were observed in the predicting model (Equations 3.13, 3.14, 3.15, and 3.16) for LL and SAR. Clay minerology, the environment to which the soil is exposed, and pore water chemistry were found to be the

defining parameters for τ_c (Liou, 1970; Alizadeh, 1974; Arulanandan, 1975). A negative correlation between SAR and τ_c were reported by Alizadeh (1974), Arulanandan (1975) and Lim (2006). According to the above-mentioned study results, as the SAR increased the repulsive forces increased, consequently influencing the erosion potential. Using different clay minerals and pore fluid conditions, Liou (1970) also reported a positive correlation between SAR and τ_c. Therefore, identifying the mineral type and pore water chemistry are necessary to conclusively define the relationship between these two parameters. A similar explanation was also applicable to the LL, as the ratio of LL for Na-montmorillonite to Ca-montmorillonite clay is about 6 times (522% and 90% respectively; Shaikh et al., 1988). The presence of kaolinite or porcelain clay can reduce the LL value significantly. Henceforth, based on the clay minerology, both positive and negative correlations between LL and τ_c were expected.

The contribution of four other variables, Con, KIF, D_{50} and σ_g, were found only once in the predicting models as shown in Table 3.5.3 (Equations 3.13 and 3.14). In the Cluster 1 dataset, the sand percentage was greater compared to the other three cluster groups. In this cluster, a positive correlation between τ_c and σ_g was found, which is similar to Wynn and Mostaghimi's (2006) findings. The sediment size range is higher for a larger σ_g value, which reduces the possibility of interaction between hydraulic forces and larger particles as the smaller particles fill the open spaces in the soil array. Therefore, the soil entrainment rate is reduced or the τ_c increases. The remaining three variables showed negative correlations with τ_c. Fine natural sediment (D_{50} < 120 μm) showed a significant negative correlation with τ_c (Roberts et al., 1998), which was later supported by Thomsen and Gust (2000) in an estuarine environment. A similar result was also found in this study. However, the D_{50} value was not found to be as significant to τ_c prediction in cohesive soils compared to granular sediments.

Soil consistency, which is the state of the soil (liquid, semiliquid or solid), showed a negative correlation with τ_c. Therefore, the change in state of the soil changes the BD and CC, which supported the negative correlation. A negative correlation between KIF and τ_c was also found for the Cluster 1 data, which was in agreement with Wynn and Mostaghimi (2006). Soils with higher KIF values indicate the sources were primarily micas and illite. Therefore, soils with high KIF values were typically friable and eroded away easily. Consequently, a negative correlation was expected (Wynn and Mostaghimi, 2006).

Variable selection procedures appeared to be dependent on the properties of the dataset and the statistical procedures, influencing the resulting predictive models, which have lead to the observed differences from other studies (e.g., Wynn, 2004; Wynn and Mostaghimi, 2006; Thoman and Niezgoda, 2008). This analysis also showed that the STR variable selection method was the least influential method as this method is dependent on the probability of including and omitting a variable from the model and the defining criteria (coefficient p-value; Akaike information criterion, AIC; or Bayesian information criterion, BIC). In this study, predictive models for τ_c (Equations. 3.13-3.16) for the four clusters showed 16 total variables as statistically significant (Table 3.5.3). Some variables were found positively correlated to τ_c, and some variables were found negatively correlated. However, some variables were showed both positive and negative correlation to τ_c.

3.6.2 Relationship of critical shear stress with the erodibility coefficient

In this study, a strong inverse correlation between k_d and τ_c was identified (Figure 3.5.1), which followed similar trends to those in other studies (Hanson and Simon, 2001; Wynn, 2004; Thoman and Niezgoda, 2008; Karmaker and Dutta, 2011; Simon et al., 2011; Layzell and Mandel, 2014; Daly et al., 2015a). The trend line of the entire dataset followed a power law relationship to estimate k_d as a function of τ_c with an R^2 value of 0.78 (Table 2.5.4). However,

unique relationships were found for the four different data clusters that represent different physiographic provinces. In this study, the updated Simon et al. (2011) relationship was also evaluated to its prediction of k_d based on τ_c. The Simon et al. (2011) model predicted lower k_d values for the same τ_c, or a downward shift of the trend line compared to the results in this study. Therefore, use of these empirically derived models for the erodibility coefficient should be used with the understanding that geologic region in conjunction with soil geochemical properties and field testing protocols may play a significant role in their relationships. Knowing that predictive models for k_d and τ_c may differ based on geologic and regional differences, these results can assist in improving outputs from bank erosion models that incorporate the excess shear stress equation (Equation 3.1), e.g., the BSTEM, Water Erosion Prediction Project (WEPP), Soil and Water Assessment Tool (SWAT), and Conservational Channel Evolution and Pollutant Transport Systems (CONCEPTS) (Langendoen, 2000; Abaci and Papanicolaou, 2009; NEH, 2011; Neitsch et al., 2011).

3.7 Conclusions

Unique relationships for the prediction of τ_c were determined among four physiographic provinces in Tennessee associated with different surficial geologies. They were: Ridge and Valley, West Highland Rim, Central Basin, and Coastal Palin bordering the Mississippi River Valley in the loess depositional area. Among these provinces, four data clusters were statistically identified through multivariate cluster analysis. Per regional cluster, predictive models were developed by multivariate regression utilizing a suite of 27 soil physical-geochemical properties, removing variables with multicollinearity. The final variable set of soil properties with statistically significant model coefficients included 16 variables. The key findings from this study suggests that no one soil property, or a common group of a select few properties will form

a universal equation for predicting τ_c. Controlling soil properties for τ_c appear to be dependent on the overall soil composition based on the regional surficial geology, which determine the properties that will dominate.

Within the four physiographic regions, the soil properties WC and Pass200 were found to control τ_c prediction among three of the four regions. The properties CC, DR, LL, SAR, and OC were also found to be dominant variables within the predictive models among the four provinces. It is interesting to observe that D_{50} is the least significant variable in predicting τ_c in cohesive soils. The relationship between τ_c and k_d were highly correlated, which is consistent with other studies. Within the entire dataset τ_c ranged from 0.08 to 26.82 Pa with a mean of 5.17 Pa, and k_d ranged from 0.56 to 24.4 $cm^3\ N^{-1}\ s^{-1}$ with a mean of 3.51 $cm^3\ N^{-1}\ s^{-1}$.

Overall, findings from this study identified dominant physiochemical variables that control erosion behavior of cohesive soils. With these findings, it suggests that individual equations need to be developed based on physiographic provinces. However our findings also illustrated that statistical methodology appears to influence resulting predictive models, and likely also contributes to the diverse number of published predictive models for τ_c. Further research through a study design specifically targeting the relationships among unique geologies, soil properties, and erosion behavior are necessary to better understand the significant variables, which were selected from the statistical models.

3.8 References

Abaci O, Papanicolaou AN. 2009. Long-term effects of management practices on water-driven soil erosion in an intense agricultural sub-watershed: Monitoring and modeling. Hydrological Processes 23: 2818-2837. DOI: 10.1002/hyp.7380

Allen PM, Arnold J, Jakubowski E. 1999. Prediction of stream channel erosion potential. Environ. Eng. Geosci. 5(3): 339-351

Al-Madhhachi AT, Hanson GJ, Fox GA, Tyagi AK, Bulut R. 2013a. Measuring soil erodibility using a laboratory "mini" JET. Trans. ASABE 56(3): 901-910

Al-Madhhachi AT, Hanson GJ, Fox GA, Tyagi AK, Bulut R. 2013b. Deriving parameters of a fundamental detachment model for cohesive soils from flume and jet erosion tests. Trans. ASABE 56(2): 489-504

Alizadeh A. 1974. Amount and type of clay and pore fluid influences on the critical shear stress and swelling of cohesive sediments. Ph.D. Dissertation, University of California, Davis, CA, USA

Arulanandan K. 1975. Fundamental aspects of erosion of cohesive sediments. Journal of Hydraulics Division, ASCE 101(HY5): 635-639, USA

Arulanandan K, Gillogley E, Tully R. 1980. Development of a quantitative method to predict critical shear stress and rate of erosion of natural undisturbed cohesive Soils. USACE, Waterways Experiment Station Technical Report GL-80-5, Vicksburg, MS, USA

ASTM. 2007. Standard test method for particle-size analysis of soils-ASTM Standard D422. ASTM International, West Conshohocken, PA, USA

ASTM. 2009. Standard test methods for laboratory determination of density (Unit Weight) of soil specimens-ASTM Standard D7263. ASTM International, West Conshohocken, PA, USA

ASTM. 2010. Standard test methods for liquid limit, plastic limit, and plasticity index of soils-ASTM Standard D4318. ASTM International, West Conshohocken, PA, USA

ASTM. 2010. Standard test method for density of soil in place by the drive-cylinder method-ASTM Standard D2937. ASTM International, West Conshohocken, PA, USA

ASTM. 2011. Standard practice for classification of soils for engineering purposes (Unified Soil Classification System) -ASTM Standard D2487. ASTM International, West Conshohocken, PA, USA

ASTM. 2011. Standard test method for dispersive characteristics of clay soil by double hydrometer-ASTM Standard D4221. ASTM International, West Conshohocken, PA, USA

ASTM. 2013. Standard test method for unconfined compressive strength of cohesive soil-ASTM Standard D2166. ASTM International, West Conshohocken, PA, USA

ASTM. 2014. Standard test methods for specific gravity of soil solids by water pycnometer-ASTM Standard D854. ASTM International, West Conshohocken, PA, USA

Belsley DA, Kuh E, Welsch RE. 1980. Regression diagnostics: Identifying influential data sources and sources of collinearity, Wiley, New York

Berlamont JE, Ockenden MC, Toorman EA Winterwerp JC. 1993. The characterization of cohesive sediment properties. Coastal Eng. 21(1–3): 105–128

Black KS, Tolhurst TJ, Paterson DM, Hagerthey SE. 2002. Working with natural cohesive sediments. J. Hydraul. Eng., ASCE 128(1): 2-8

Blaisdell FW, Clayton LA, Hebaus CG. 1981. Ultimate dimension of local scour. Journal of Hydraulics Division-ASCE 107(3): 327-337

Briaud JL, Ting F, Chen HC, Gudavalli R, Kwak K, Philogene B, Han SW, Perugu S, Wei GS, Nurtjahyo P, Cao YW, Li Y. 1999. SRICOS: Prediction of scour rate at bridge piers, TTI Report no. 2937-1 to the Texas DOT, Texas A&M University, College Station, Texas, USA

Briaud JL, Ting FCK, Chen HC, Cao Y, Han SW, Kwak KW. 2001. Erosion function apparatus for scour rate prediction. Geochem. J. 127Z(2): 105-113. DOI: 10.1061/(ASCE)1090-0241(2001)127:2(105)

BS, 1990. British standard methods of test for soils for civil engineering purposes-BS 1377-2. British Standards Institution, Milton Keynes

Clark LA, Wynn TM. 2007. Methods for determining streambank critical shear stress and soil erodibility: Implications for erosion rate predictions. Transactions of the ASABE 50(1): 95-106. DOI: http://dx.doi.org/10.13031/2013.22415

Chen X. 2012. Matlab code for the LARS algorithm. University of Illinois, Urbana-Champaign, Illinois. https://publish.illinois.edu/xiaohuichen/code/lars/

Daly ER, Fox GA, Al-Madhhachi AT, Miller RB 2013. A scour depth approach for deriving erodibility parameters from jet erosion tests. Trans. ASABE 56(6): 1343-1351

Daly ER, Fox GA, Al-Madhhachi AT, Storm DE. 2015a. Variability of fluvial erodibility parameters for streambanks on a watershed scale. Geomorphology 231: 281-291

Daly ER, Fox GA, Enlow HK, Storm DE, Hunt SL. 2015b. Site-scale variability of streambank fluvial erodibility parameters as measured with a jet erosion test. DOI: 10.1002/hyp.10547

Daly ER, Fox GA, Fox AK. 2016. Correlating site-scale erodibility parameters from jet erosion tests to soil physical properties. American Society of Agricultural and Biological Engineers, ASABE 59(1): 115-128. DOI 10.13031/trans.59.11309

Debnath K, Nikora V, Aberle J, Westrich B, Muste M. 2007. Erosion of cohesive sediments: resuspension, bed load, and erosion patterns from field experiments. J. Hydraul. Eng., ASCE 133 (5): 508-520. DOI: 10.1061/(ASCE)0733-9429(2007)133:5(508)

Debnath K, Chaudhuri S. 2010. Bridge pier scour in clay-sand mixed sediments at near-threshold velocity for Sand. J. Hydraul. Eng., ASCE 136(9): 597-609. DOI: 10.1061/(ASCE)HY.1943-7900.0000221

Dickhudt PJ, Friedrichs CT, Sanford LP. 2011. Mud matrix solids fraction and bed erodibility in the York River Estuary, USA, and other Muddy Environments. Continental Shelf Research 31: S3-S13. DOI: 10.1016/j.csr.2010.02.008

Droppo IG, Exall K, Stafford K. 2008. Effects of chemical amendments on aquatic floc structure, settling and strength. Water Research 42(1-2): 169-179. DOI: 10.1016/j.watres.2007.06.054

Dunn IS. 1959. Tractive resistance of cohesive channels. Journal of the Soil Mechanics and Foundations, ASCE 85(SM3, Part 1): 1-24

Efron B, Hastie T, Johnstone I, Tibshirani R. 2004. Least angle regression. Annals of Statistics 32(2): 407-499

Foth, HD. 1990. Fundamentals of soil science, 8th Edition. John Wiley & Sons, Canada

Gerbersdorf SU, Jancke T, Westrich B. 2007. Sediment properties for assessing the erosion risk of contaminated riverine sites. Journal of Soils and Sediments 7(1): 25-35. DOI: http://dx.doi.org/10.1065/jss2006.11.190

Gillott JE. 1987. Clay in engineering geology. Elsevier, Amsterdam

Grabowski RC, Droppo IG, Wharton G. 2011. Erodibility of cohesive sediment: the importance of sediment properties. Earth Sci. Rev. 105(1): 101-120. DOI:10.1016/j.earscirev.2011.01.008

Hanson GJ. 1990a. Surface erodibility of earthen channels at high stresses. I: Open channels testing. Trans. ASAE 33(1): 127-131

Hanson GJ. 1990b. Surface erodibility of earthen channels at high stresses. II: Developing an in-situ testing device. Trans. ASAE 33(1): 132-137

Hanson GJ, Simon A. 2001. Erodibility of cohesive streambeds in the loess area of the midwestern USA. Hydrol. Process 15: 23-28

Hanson GJ, Cook KR. 2004. Apparatus, test procedures, and analytical methods to measure soil erodibility in-situ. Appl. Eng. Agric. 20(4): 455-462

Hanson GJ, Robinson KM. 1993. The influence of soil moisture and compaction on spillway erosion. Trans. ASAE 36(5): 1349-1352

Johnson BD, Kranck K, Muschenheim DK. 1994. Physicochemical factors in particle aggregation. In: Wotton, R.S. (Ed.), The biology of particles in aquatic systems. Lewis, Boca Raton: 75-96

Julian J, Torres R. 2006. Hydraulic erosion of cohesive riverbanks. Geomorphology 76(1): 193-206. DOI: 10.1016/j.geomorph.2005.11.003

Kamphuis JW, Hall KR. 1983. Cohesive material erosion by unidirectional current. J. Hydraul. Eng. 109: 39-62

Karmaker T, Dutta S. 2011. Erodibility of fine soil from the composite river bank of Brahmaputra in India. Hydrol. Process 25: 104-111. DOI: 10.1002/hyp.7826

Langendoen EJ. 2000. CONCEPTS-Conservational channel evolution and pollutant transport system, Stream Corridor Version 1.0. U.S. Department of Agriculture, Agricultural Research Service, Oxford, MS, USA

Layzell AL, Mandel RD. 2014. An assessment of the erodibility of Holocene Lithounits comprising streambanks in northeastern Kansas, USA. Geomorphology 213: 116-127. http://dx.doi.org/10.1016/j.geomorph.2014.01.003

Lick W, Jin LJ, Gailani J. 2004. Initiation of movement of quartz particles. J. Hydraul. Eng., ASCE 130 (8): 755–761. DOI: 10.1061/(ASCE)0733-9429(2004)130:8(755)

Lim SS. 2006. Experimental investigation of erosion in variable saturated clay soils. Ph.D. Dissertation, School of Civil and Environmental Engineering, The Univ. of New South Wales, Sydney, Australia

Liou, YD. 1970. Hydraulic erodibility of two pure clay systems. Ph.D. Dissertation, Colorado State University, Fort Collins, CO, USA

Lyle W, Smerdon ET. 1965. Relation of compaction and other soil properties to Eerosion resistance of soils. Transactions of the American Society of Agricultural Engineers 8(3): 419-422

Mahalder B, Schwartz JS, Palomino AM, Zirkle J. 2018. Estimating erodibility parameters for streambanks with cohesive soils using the mini jet test device: A comparison of field and computational methods. Water, 10(3), 304. DOI: 10.3390/w10030304

McNeil J, Taylor C, Lick W. 1996. Measurements of erosion of undisturbed bottom sediments with depth. J. Hydraul. Eng., ASCE 122(6): 316-324. DOI: http://dx.doi.org/10.1061/(ASCE)0733-9429(1996)122:6(316)

Miller RA. 1974. The geologic history of Tennessee: Tennessee Division of Geology Bulletin 74

Miller JH. 1991. Surficial geology of the Cane Creek Basin, Lauderdale County, Tennessee, U.S. Geological Survey, Water-Resources Investigation Report 90-4139, Nashville, TN, USA

Mitchell JK, Soga K. 2005. Fundamentals of soil behavior. 3rd Edition, John Wiley & Sons, Inc, Hoboken, New Jersey, USA

Molinas A, Jones S, Hosny M. 1999. Effects of cohesive material properties on local scour around piers. Transportation Research Record, 1690, Paper No. 99-1275

Morgan RPC. 2005. Soil erosion and conservation. Blackwell, Oxford

Mostafa TMS. 2003. Experimental modeling of local scour in cohesive soils. PhD Dissertation, Dept. of Civil and Environ. Eng., Univ. of South Carolina, Columbia, SC, USA

Mostafa TMS, Imran J, Chaudhry MH, Khan IB. 2008. Erosion resistance of cohesive soils. J. Hydraul. Research 46(6): 777-787. DOI:10.3826/jhr.2008.2794

National Engineering Handbook (NEH). 2011. Erodibility parameter selection for soil material horizons (surface detachment coefficient and headcut erodibility index)

Neitsch SL, Arnold JG, Kiniry JR, Williams JR. 2011. Soil and water assessment tool theoretical documentation version 2009, Texas Water Resources Institute Technical Report No. 406, College Station, TX, USA

O'brien RM. 2007. A Caution regarding rules of thumb for variance inflation factors. Quality & Quantity, Springer, 41:673–690. DOI 10.1007/s11135-006-9018-6

Oh SJ. 2009. Experimental study of bridge scour in cohesive soil. Ph.D. Dissertation, Department of Civil Engineering, Texas A&M University, College Station, TX, USA

Papanicolaou AN. 2001. Erosion of cohesive streambeds and banks, State Wash. Water Res. Cent. Rep. WRR-08, Washington. State University, Pullman, Washington, USA

Raudkivi AJ, 1990. Loose boundary hydraulics. 3rd edition, Pergamon Press, New York, USA

Ravisangar V, Sturm TW, Amirtharajah A. 2005. Influence of sediment structure on erosional strength and density of kaolinite sediment Beds. J. Hydraul. Eng.-ASCE 131(5): 356-365. DOI: 10.1061/(ASCE)0733-9429(2005)131:5(356)

Regazzoni PL, Marot D. 2011. Investigation of interface erosion rate by jet erosion test and statistical analysis. EJEC 15:1167-1185. DOI: 10.3166/EJECE.15.1167-1185

Roberts J, Jepsen R, Gotthard D, Lick W. 1998. Effects of particle size and bulk density on erosion of quartz particles. J. Hydraul. Eng.-ASCE 124(12): 1261-1267. DOI: http://dx.doi.org/10.1061/(ASCE)0733-9429(1998)124:12(1261)

Safford JM. 1869. Geology of Tennessee, State of Tennessee, Nashville, USA

Sanford LP, Maa JPY. 2001. A unified erosion formulation for fine sediments. Marine Geology 179(1-2): 9-23. PII: S0025-3227(01)00201-8

Santamarina JC, Klein KA, Wang YH, Prencke E. 2002. Specific surface: Determination and relevance. Can. Geotech. Journal 39: 233-241. DOI: 10.1139/T01-077

Schwartz JS, Neff KJ, Dworak FJ, Woockman RR. 2015. Restoring riffle-pool structure in an incised, straightened urban stream channel using an ecohydraulic modeling approach. Ecological Engineering 78: 112-126. DOI: http://dx.doi.org/10.1016/j.ecoleng.2014.06.002

Shaikh A, Ruff JF, Wayne CA, Abt SA. 1988. Erosion rate of dispersive and nondispersive Clays. J. Geotech. Engrg. 114(5): 589-600

Simon A, Collison AJC. 2002. Quantifying the mechanical and hydrologic effects of vegetation on streambank stability. Earth Surface Processes and Landforms 27: 527-546

Simon A, Thomas RE, Klimetz L. 2010. Comparison and experiences with field techniques to measure critical shear stress and erodibility of cohesive deposits. In Proceedings of the 2nd Joint Federal Interagency Conference on Sedimentation and Hydrologic Modeling. U.S. Geological Survey: Reston, VA, USA

Simon A, Pollen-Bankhead N, Thomas RE. 2011. Development and application of a deterministic bank stability and toe erosion model for stream restoration. In: Simon, A., Bennett, S.J., Castro, J.M. (Eds.), Stream Restoration in Dynamic Fluvial Systems. American Geophysical Union, Washington, D.C., USA

Skempton AW. 1953. The colloidal activity of clays. Proc., 3rd Int. Conf. of Soil Mechanics and Foundation Engineering 1(1): 57-61

Smerdon ET, Beasley RP. 1959. The tractive force theory applied to stability of open channels in cohesive sediments. University of Missouri, College of Agriculture, Agricultural Experiment Station, Columbia, Mo, USA

Smerdon ET, Beasley R. 1961. Critical tractive forces in cohesive Soil. Agric. Eng. 42(1): 26-29

Thoman RW, Niezgoda SL. 2008. Determining erodibility, critical shear Stress, and allowable discharge estimates for cohesive channels; Case study in the Powder River basin of Wyoming. J. Hydraul. Eng.-ASCE 134(12): 1677-1687. DOI: 10.1061/(ASCE)0733-9429(2008)134:12(1677)

Thomsen L, Gust G. 2000. Sediment erosion thresholds and characteristics of resuspended aggregates on the western European continental margin. Deep-Sea Research Part I-Oceanographic Research Papers 47(10): 1881-1897

USACE. 1970. Laboratory soils testing. Engineer manual, EM1110-2-1906, Washington, D.C., USA

USDA. 2011. Soil survey laboratory manual methods. Soil Survey Investigations Report No. 45, Version 2.0. US Department of Agriculture, Natural Resources Conservation Service, National Soil Survey Center: Lincoln, NE, USA

Utley B, Wynn TM. 2008. Cohesive soil erosion: Theory and Practice. World Environmental and Water Resources Congress: 1-10

van Ledden M, van Kesteren WGM, Winterwerp JC. 2004. A conceptual framework for the erosion behaviour of sand–mud mixtures. Continental Shelf Research 24(1): 1-11. DOI:10.1016/j.csr.2003.09.002

William JW, Diehl, TH. 1993. Recent sedimentation and surface-water flow patterns on the flood plain of the North Fork Forked Deer River, Dyer County, Tennessee, U.S. Geological Survey, Water-Resources Investigations Report 92-4082, Nashville, TN, USA

Winterwerp JC, van Kesteren WGM. 2004. Introduction to the physics of cohesive sediment in the marine environment. Elsevier, Amsterdam, the Netherlands

Wischmeier WH, Mannering JV. 1969. Relation of soil properties to its erodibility. Soil Sci. Soc. Am. Proc. 33(1): 131-137

Wynn TM. 2004. The effects of vegetation on stream bank erosion. Ph.D. dissertation, Biological Systems Engineering, Virginia Polytechnic Institute and State University, Blacksburg, VA, USA

Wynn TM, Mostaghimi S. 2006. The effects of vegetation and soil type on streambank erosion, southwestern Virginia, USA. Journal of the American Water Resources Association (AWARA) 42(1): 69-82

Wynn TM, Henderson MB, Vaughan DH. 2008. Changes in streambank erodibility and critical shear stress due to subaerial processes along a headwater stream, southwestern Virginia, USA. Geomorphology 97: 260-273. DOI:10.1016/j.geomorph.2007.08.010

CHAPTER IV
IDENTIFICATION OF DEVICE DEPENDENT VARIABILITY

A version of this chapter is in preparation for publication by Badal Mahalder, John S. Schwartz, A.N. Thanos Papanicolaou, Angelica M. Palomino, and Jon Zirkle.

Badal Mahalder, John S. Schwartz, A.N. Thanos Papanicolaou, Angelica M. Palomino, and Jon Zirkle: **"Comparison of erodibility parameters for cohesive streambank soils between an in-situ jet test device and laboratory conduit flume."** Journal of Hydraulics Engineering (2018)

Badal Mahalder, the senior author generated this manuscript as a part of his Ph.D. dissertation, and co-authors John Schwartz, Angelica Palomino, and Jon Zirkle supervised his research, in addition to direct text contributions to his study's manuscript.

Abstract

Several methods have been developed to estimate erodibility parameters for cohesive streambanks, critical shear stress τ_c and the erodibility coefficient k_d. This research compares estimates of these parameters between an in situ mini-jet device and a pressurized laboratory conduit flume. Operation of the mini-jet device applied a unique multiple pressure setting (MPS) procedure that accounts for the change in soil properties into the bank matrix from the surface. Both the mini-jet MPS approach and the conduit flume using the Sutarto et al. approach remove the effect of surface subaerial process on erodibility parameter estimations, and resulted in similar τ_c and k_d estimates from the same bank soils. Estimates for τ_c between the two devices were in general agreement compared to k_d especially for shear magnitudes greater than 5 Pa and consolidated soil with moisture contents greater than 20%. Erodibility estimates between devices differed likely due to the aggregate failure behavior of cohesive soils. Findings suggest τ_c and k_d estimates are dependent on the device hydraulics, computational method, and soil properties.

4.1 Introduction

Erodibility parameters for cohesive soils, namely the critical shear stress (τ_c) and erodibility coefficient (k_d), can range over orders of magnitude depending on the different measurement devices used in the analysis. These devices and associated computational methods include the following: laboratory flume type tests (Briaud et al., 2001; Mostafa et al., 2008; Sutarto et al., 2014), laboratory hole erosion tests (Wan and Fell, 2004), in-situ direct measurements using submersible flumes (Amos et al., 1992; Houwing and van Rijn, 1998), rotating cylinder test (Moore and Masch, 1962; Arulanandan et al., 1973; Chapuis and Gatien, 1986), and jet test devices (Hanson, 1990; Hanson and Cook, 2004; Simon et al., 2010; Al-Madhhachi et al., 2013a). Each device has advantages and disadvantages related to its operational principles and analytical procedures for measuring τ_c and k_d and estimating

streambank erosion rates with applicability (Tolhurst et al., 2000; Aberle et al., 2003; Debnath et al., 2004; Debnath et al., 2007; Hobson, 2008; Weidner, 2012; Bones, 2014; Sutarto et al., 2014). Further research is needed to advance our understanding of the interrelationships between device-induced erosion and entrainment behavior leading to measurement inconsistences among different devices.

A critical review of different devices and their inherent theoretical and operational principles provides a foundation to assess potential measurement inconsistences. Of particular interest among research has been a comparison of erosion measurements using in-situ jet and flume devices in cohesive soil, though only a limited number of studies have been completed (Hanson, 1990; Hanson and Cook, 2004; Hanson and Hunt, 2007; Al-Maddhachi et al., 2013b). With a focus on comparing k_d values, Hanson (1990) related soil erodibility values at different water contents from both flume tests and in-situ jet tests assuming negligible τ_c values. Similar to the Hanson (1990) study, assuming fixed τ_c values, erosion rates were measured from the flume tests and the corresponding k_d values were compared to the jet test results considering the excess shear stress equation (Hanson and Cook, 2004; Hanson and Hunt, 2007; Al-Maddhachi et al., 2013b). Soil samples in these studies consisted of different textures (e.g., silty clay, lean clay, or silty sand) and were compacted at different water contents. Yet, no direct comparisons between τ_c and k_d values estimation have been reported using two independent devices to date in the literature. Several studies also identified that analytical solution methods can significantly influence the erodibility parameters estimated from jet test data (Daly et al., 2015; Khanal et al., 2016, Karamigolbaghi et al., 2017), although an acceptable fit to the scour depth data from those solution methods were identified with a wide range in estimated τ_c and k_d values. Currently, using the linear excess shear stress principle, three analytical solution methods are available to

predict τ_c and k_d using jet test data: Blaisdell solution (BL) method, iterative solution (IP) method, and scour depth solution (SDP) method. Recently, Karamigolbaghi et al. (2017) showed that physically unrealistic values of erosion rates resulted from both the IP and SDP solution methods using data from the Hanson and Cook (2004).

Wahl et al. (2008) compared the hole erosion test (HET) and jet erosion test (JET) for different soil types at different soil moisture conditions using remolded soil. In the HET, flow is directed through a pre-drilled hole using a constant head for a soil sample causes erosion, where the hole diameter is inferred from the flow properties. From the HET test, suing the hole diameter over time and the hydraulic gradient across soil sample, erosion rates and applied shear stresses are calculated in order to compute the erodibility parameters (Wan and Fell, 2004). Wahl et al. (2008) identified that moisture content and soil compaction significantly affects τ_c and k_d estimation. They also suggested that device dependent variations of results are associated with the simplified stress description procedures and in the erosion mechanism for each test. The range of τ_c using the JET was reported between 0.08 Pa and 18.82 Pa, and using the HET, the range was between 2.0 Pa and 402 Pa for different soil moisture conditions and soil types. Regazzoni and Marot (2013) proposed an alternative erosion index parameter calculation procedure and compared the results using both the HET and JET device. They identified a good correlation (R^2 = 0.78) between the results from these two devices. These tests were conducted on laboratory remolded soil with optimum moisture content and optimum dry density containing 7% to 40% clay content by weight.

Briaud et al. (2001) developed the erosion function apparatus (EFA) to assess soil erodibility to model scour around bridge piers using pressurized flow principles. In the EFA, a soil test sample is exposed to pressurized flow by controlling movement of the sample into the

flow field from the apparatus bottom. However, the applied forces on the sample is both shear and drag where the drag force acts predominantly on the exposed soil sample protruded face consequently affecting the erosion rate. Papanicolaou (2001) and Papanicolaou et al. (2007) developed a field-laboratory testing protocol in which relatively undisturbed soil samples are collected from the field in a 30 cm by 10 cm open box and placed in a free-surface flume exposed to shear forces only. Similar to results found by Mallison (2008), an open channel flume limited the maximum applied shear that could be generated. Thus, Sutarto et al. (2014) developed a new pressurized flume to measure τ_c and k_d integrating concepts from Briaud et al. (2001) and Papanicolaou et al. (2007). According to the working principle of this conduit flume, it is capable of applying a wide range of applied shear stresses parallel to the soil test surface compared to other devices such as the jet tester, annular flumes, EFA, and free-surface channels (Sutarto et al., 2014). The fact that the flow in the conduit is pressurized allows the use of the flume on resistant soil surfaces where the applied shear stress values for erosion to occurs requires values up to nearly 60 Pa.

The arguments between laboratory flume and in-situ devices have been well documented in literature for τ_c and k_d estimation in cohesive soils. It is well known that laboratory flume tests provide greater degree of control over the experimental conditions compared to in-situ field devices. However, it is understood that "undisturbed" soil sample collection is challenging since during sample collection and transport to the laboratory, soil microstructures can be altered significantly. In addition to this, other possible changes in soil physical properties (e.g., soil moisture) could significantly alter the erosion behavior of the collected soil samples compared to the source soil. In lieu, in-situ test devices preserve the original in-field conditions better

(Houwing and van Rijn 1998; Hanson and Cook, 2004; Debnath et al., 2007), but it is difficult to maintain precision on specific controls during tests.

The objectives of this research were to compare estimates for erodibility parameters (τ_c and k_d) and quantify the variability between a pressurized conduit flume and a mini-jet device using the available jet operation and data analyses approaches. Device comparisons are discussed in terms of their fundamental theoretical and operational principles governing erosion. During each test, changes in the chemical composition of the sediment and water mix were also monitored for quantifying possible influence on inter-particle attraction forces in cohesive soils. This comparative study provides context in which to evaluate results from previously published cohesive soil erosion studies thereby enhancing our ability to interpret data derived from these two measurement devices.

4.2 Theoretical Background

4.2.1 In-situ jet test device

The submerged jet device was developed for measuring soil erodibility parameters in-situ, but it can also be used in the laboratory (Hanson, 1990; Hanson and Cook, 1997; Hanson and Simon, 2001) based on Dunn (1959). The jet device has two models (i) the original jet (Hanson, 1990; Hanson and Cook, 1997; Hanson and Simon, 2001), and (ii) the mini jet (Simon et al., 2010; Al-Madhhachi et al., 2013a). Detailed descriptions of the original jet can be found in numerous studies (Hanson, 1990; Hanson and Cook, 1997; Hanson and Simon, 2001; Hanson and Hunt, 2007; Al-Madhhachi et al. 2013a). Previous studies comparing the original and mini jet devices reported similar values for both the τ_c and k_d estimation, though adjusted factor was also proposed (Simon et al., 2010; Al-Madhhachi et al. 2013b). The mini jet device is much smaller and lighter compared to the original jet device and easier to use both in the laboratory

and in the field, this device is generally preferred over the original jet device and was used in this study.

4.2.2 Mini-jet test device design specifications

The mini jet device is a scaled down version of the original jet device, and consists of a submergence tank with a water inlet nozzle and outlet port, an internal rotating plate, a pressure gage to determine the flow velocity, a valve, a depth gage, hoses and a base metal ring (Figure 4.2.1a). A high-velocity jet of water is projected normal to the soil surface through a 3.18 mm diameter nozzle. The rotating plate prevents the water jet from impinging upon the soil surface at the test initiation and during the scour-hole measurements at different time intervals. A water pump supplies water directly from the stream to the desired pressure heads by regulating the valve for conducting in-situ tests on stream bed or banks.

The mini jet device in operation in the field is shown in Figure 4.2.1b. The submergence tank is a cylindrical, clear Plexiglas, conduit that is 70 mm in height, 101.6 mm in diameter, and 6.4 mm in thickness. Before starting any test, a steel base ring (180 mm diameter) is inserted into ground about 51 mm with a uniform pressure applied to the top in order to avoid any water loss from the bottom of the tank. During the tests (Figure 4.2.1b), a water jet impacts the soil surface through the water and diffuses radially, which produces a shear stress on the soil surface to initiate scour. By recording the applied pressure during the test and the corresponding scour depth at different time intervals, an equilibrium scour depth is estimated and τ_c and k_d can be calculated.

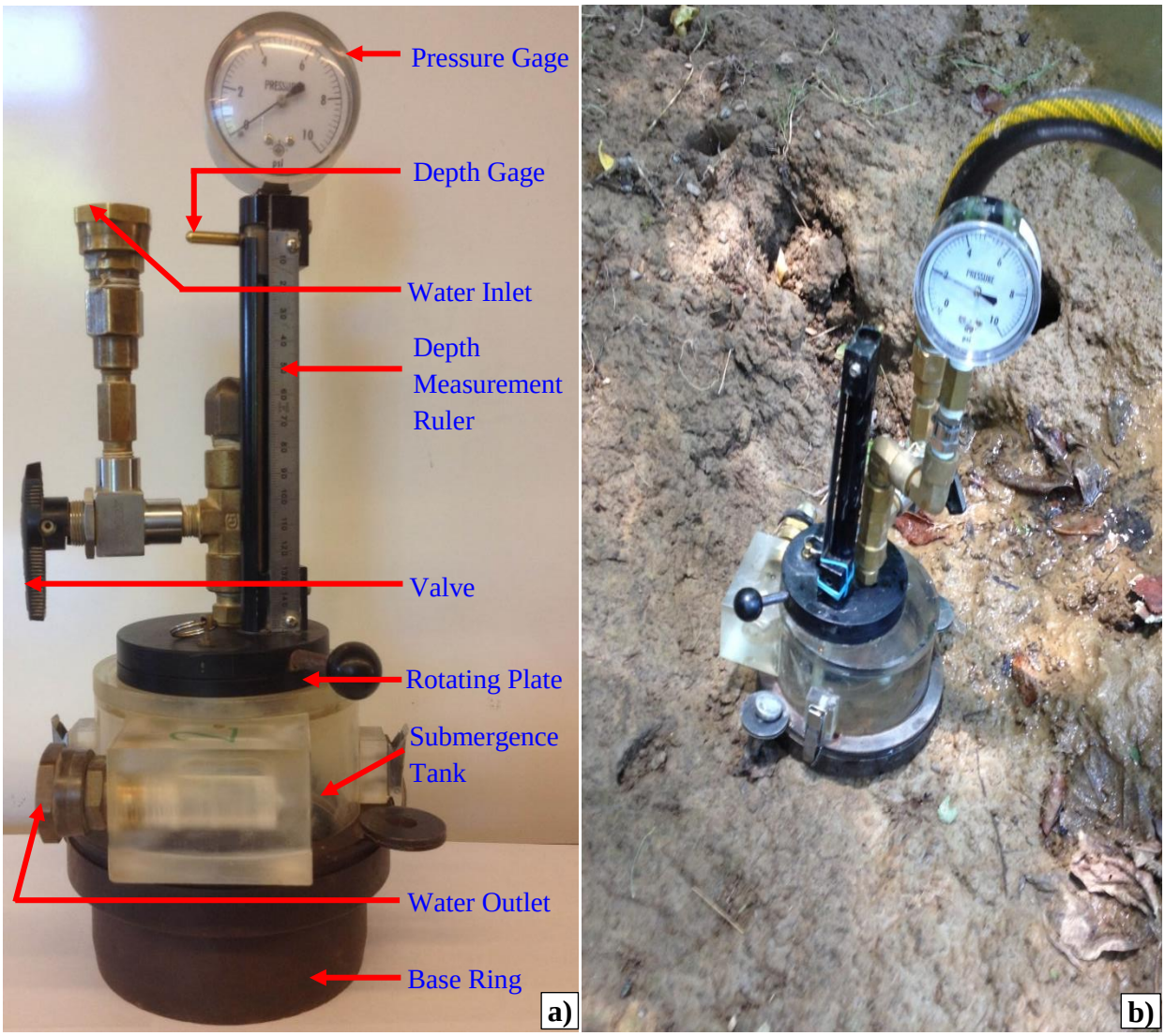


Figure 4.2.1: (a) Mini jet device components, (b) jet operation in the field

4.2.3 Device hydraulic principles

Hanson and Cook (1997) developed an analytical procedure to calculate the erosion index parameter from jet test data based on the jet diffusion principles of Stein and Nett (1997). This method was developed for the original submerged jet test apparatus; however, the governing principles are consistent for both devices. The major assumption associated with this device is the rate of scour or the erosion rate (dJ/dt) is a function of the maximum stress at the boundary. Therefore, the jet erosion rate equation expressed by Hanson and Cook (1997, 2004) is the following:

$$\frac{dJ}{dt} = k_d \left[\frac{\tau_0 J_p^2}{J^2} - \tau_c \right], \text{ for } J \geq J_p \tag{4.1}$$

where J is the scour depth (cm); J_p is the potential core length from jet origin (cm); k_d is the erodibility coefficient ($cm^3\ N^{-1}\ s^{-1}$); τ_0 is the applied bottom shear stress (Pa); and τ_c is the critical shear stress (Pa).

Based on the soil type and water conditions, the initial erosion rate could be substantial and approaches zero asymptotically for the jet device (Stein and Nett, 1997). In addition, the depth at which the applied shear stress on the soil surface does not produce any erosion (dJ/dt = 0) is termed as equilibrium scour depth (J_e) and the shear to that depth is termed as τ_c.

$$\tau_c = \tau_0 \left(\frac{J_p}{J_e} \right)^2 \tag{4.2}$$

where $\tau_0 = C_f \rho_w U_0^2$ is the maximum shear stress due to the jet velocity at the nozzle (Pa); C_f = 0.00416 is the friction coefficient; ρ_w is water density ($kg\ m^{-3}$); $U_0 = C\sqrt{2gh}$ is the velocity of jet at orifice ($cm\ s^{-1}$); C is discharge coefficient; h is the applied head (cm) or pressure head; $J_p = C_d d_0$; d_0 is the nozzle diameter (cm); and C_d = 6.3 is the diffusion constant. Blaisdell et al.

(1981) showed that the time required to attain J_e is excessively high, hence, the calculation of τ_c can be problematic. Therefore, they proposed calculating J_e by fitting the scour depth data versus time as a hyperbolic function. This method is identified as BL in this article.

Two other solution techniques IP and SDP methods were reported recently based on linear excess shear stress equation (Simon et al., 2010; Daly et al., 2013) to estimate τ_c and k_d values. In the IP approach, initial values of τ_c and k_d are estimated from the BL method. Then, erosion parameters are iteratively and simultaneously solved by minimizing the root mean square error between the measured and estimated time. In the SDP approach, a generalized gradient reduction method is used to reduce the sum-of-square errors between the measured and estimated scour depth using the excess shear stress equation. Daly et al. (2015) reported that the BL method under-predicts τ_c and k_d compared to IP and SDP approaches. Therefore, the jet solution is dependent not only on operational protocol but also the solution approaches used for data analyses.

4.2.4 Laboratory conduit flume

The laboratory conduit flume is a straight, recirculating, pressurized device with a useful length of 305 cm and a rectangular cross section of 10 × 5 cm. A sample tray is placed 215 cm downstream from the flow entrance (Figure 4.2.2) to ensure fully developed flow. A conical water storage tank is attached to the 7.5 hp variable-speed pump, which passes water through a 7.62-cm ID galvanized pipe into a 50 cm^2 rectangular Plexiglas conduit. Varying the pump frequency regulates the flow rates (Q). Q is recorded from a magnetic flow meter in-line with the galvanized supply pipe. This flume has a wide range of operational flow rates from 0.0025 $m^3 s^{-1}$ to 0.0157 $m^3 s^{-1}$, flow velocities (0.5-3.10 m s^{-1}), and the corresponding shear stresses (1-32 Pa) for testing different soil types (Sutarto et al., 2014).

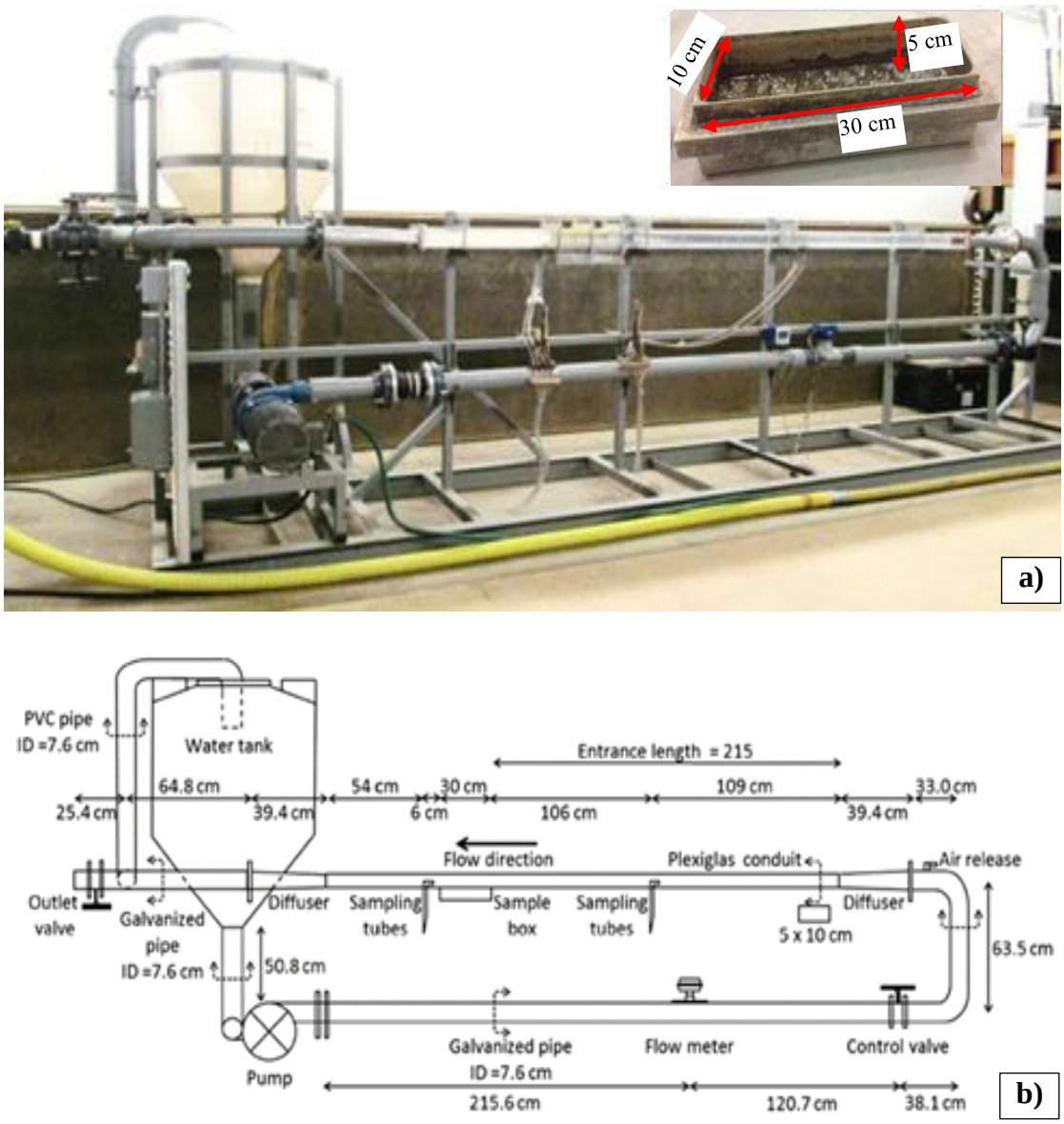


Figure 4.2.2: Conduit flume showing: a) photo of flume with testing box, and b) details of flume dimensions (Sutarto et al., 2014)

Specific sample collection and flume operational protocols have been established for this flume (Sutarto et al., 2014). Relatively undisturbed soil samples are collected from the field and tested either in the field or in the laboratory. The sample is cut with a wire saw to fit in the sample tray. The dimensions of the tray are 30 cm in length, 10 cm in width, and 5 cm in depth (Figure 4.2.2). The sample tray location is over 40 times the height of the conduit from the upstream diffuser to ensure a fully developed boundary layer over the sediment sample (McNeil et al., 1996). Approaching the tray, the conduit bed and ceiling is covered with fine sand paper for replicating micro-roughness of soil surface. Soil samples in the tray can be adjusted using the jack screws underneath the tray for any necessary minor adjustments to ensure the flume bed and soil surface are at the same elevation.

4.2.5 Bed shear stress calculations

In an open channel laboratory flume, the applied bed shear is calculated using $\tau_b = \rho g h S$, where ρ is the fluid density (kg m^{-3}), g is the gravitational acceleration (m s^{-2}), h is the flow depth (m), and S is the slope of the channel. However, the conduit flume is based on pressurized conduit flow and the Darcy-Weisbach equation can be used (Sutarto et al., 2014):

$$\tau_b = \frac{\rho U^2}{8} f \tag{4.3}$$

where U is the flow velocity (m s^{-1}); and f is the Darcy-Weisbach friction factor calculated from Haaland (1983) equation:

$$\frac{1}{\sqrt{f}} = -1.8 \log \left[\frac{6.9}{R_e} + \left(\frac{\varepsilon}{3.7 d} \right)^{1.11} \right] \tag{4.4}$$

where ε is the wall relative roughness height; and R_e is the Reynolds Number ($R_e = Ud/\upsilon$ with υ being the kinematic viscosity of water and d is the effective diameter of the rectangular conduit calculated using hydraulic diameter (d_h) (0.0667 m for this flume). White (2008) proposed d =

*1.029*d_h*, which was used for this flume's calculations. The corresponding erosion rate for each applied shear stress due to the flow was determined by the following equation as proposed by Sutarto et al. (2014):

$$E = \frac{\Delta C_{avg} Q}{A} \tag{4.5}$$

where ΔC_{avg} is the average sediment concentration difference between two consecutive flows (kg m^{-3}); Q is the flow rate (m^3 s^{-1}), and A is the surface area of the soil sample (m^2). Equations 4.3-4.5 were used to compute applied shear stress and the corresponding erosion rate. Erosion rate was plotted against the applied shear stress on a normal graph, where τ_c was identified as the y-intercept corresponding to zero erosion rate from the best-fit line (Papanicolaou et al., 2007). From those plots, slope was also calculated for each sample to estimate the k_d value by considering linear erosion model.

4.2.6 Comparative study rationale

Fluvial erosion, especially in cohesive soils, is complex where many process factors contribute to soil detachment over time lending to the difficulty in developing standard test measurements for τ_c and k_d parameters. It is understood that selection of device to measure τ_c in association with the data analyses protocols significantly affects estimating these parameters as discussed in the Introduction. In this study, τ_c and k_d measurements obtained using both the mini-jet device and the pressurized conduit flume are compared. The working principles and operational protocols of these two devices are different as discussed in the previous section. However, barring these differences, these two devices possess some unique attributes to assess erosion processes in the field and in the laboratory environment, and provide better insight to uncertainties associated with τ_c and k_d measurements.

The jet device was developed based on the diffusion principle for calculating τ_c values, which produces highly complex hydrodynamic forces and turbulence inside the submergence tank during development of the simple scour configuration (Craft et al., 1993; Mercier et al., 2014). Due to the flexibility associated to jet operation in the field, the ASTM Standard D5852 "Standard Test Method for Erodibility Determination of Soil in the Field or in the Laboratory by the Jet Index Method" was developed using the original jet device, which was withdrawn in 2016 with no complementary replacement. It is understood that the lack of a methodological replacement for the proposed ASTM standard is due to inconsistencies in both jet operation and analytical solution procedures among different soil types (Wahl, 2016).

With the unique nature of operation on literally any surface condition in a riverine environment, the jet device has become a popular tool to estimate erosion parameters in-situ. However, as noted earlier, several study findings reported that the jet test data analysis procedures could have significant influence on erosion rate estimation consequently three solution methods (BL, IP, and SDP) have been developed. Several studies reported that τ_c values, estimated from the IP and SDP methods are greater than the BL estimated τ_c values (Simon et al., 2010; Daly et al., 2013, 2015; Regazzoni and Marot, 2013; Karamigolbaghi et al., 2017). It is important to note that a single pressure head is used for jet operation following the guidelines as Hanson and Cook (2004) outlined. Recently, Khanal et al. (2016) identified the influence of data collection time interval and termination time interval on erosion parameters estimation, which were not considered in the standard jet operation protocol. They also identified the importance of pressure head selection for erosion parameters estimation during jet testing on different soil types, though they did not report that explicitly in their study.

In order to critically analyze the issues related to the jet operation and data analysis procedures, a comparative study is necessary to investigate whether the erodibility parameters estimated using the available jet operation protocols and solution methods are similar to those obtained using a more traditional laboratory flume. As reported earlier, in a conduit flume, a greater range of shear stresses can be applied to a soil sample parallel to the surface (similar to the natural flow condition). While the erosion rate is assumed linear for both conduit flume and jet devices, greater control during the sample testing and the mode of stress applied to the sample surface can be advantageous when using the flume compared to the jet device. However, flume erosion measurements are assumed to use relatively undisturbed samples, which may not be the case during field collection. Sample disturbance affects the estimation of the erodibility parameters. Considering all these aspects related to these two devices, and since no direct comparative study of erosion parameters estimation currently exists, the authors identified that a direct comparison between the results from these fundamentally different devices is critical to cohesive soil erosion studies.

4.3 Methodology

4.3.1 Sites locations for soil collections

In-situ mini-jet tests were conducted in the same locations from which soil samples were collected for the conduit flume experiments. The locations included the stream banks of Pond Creek, Coal Creek, Crooked Creek and Black Creek, all of which are in West Tennessee, USA (Figure 4.3.1). These creeks are in Dyer County, Tipton County, Shelby County and Crockett County, respectively. In this study, the bank soils were classified as cohesive because greater than 94% of the soil particles were finer than 0.074 mm (#200 sieve) and the clay content ranged between 18% and 39%.

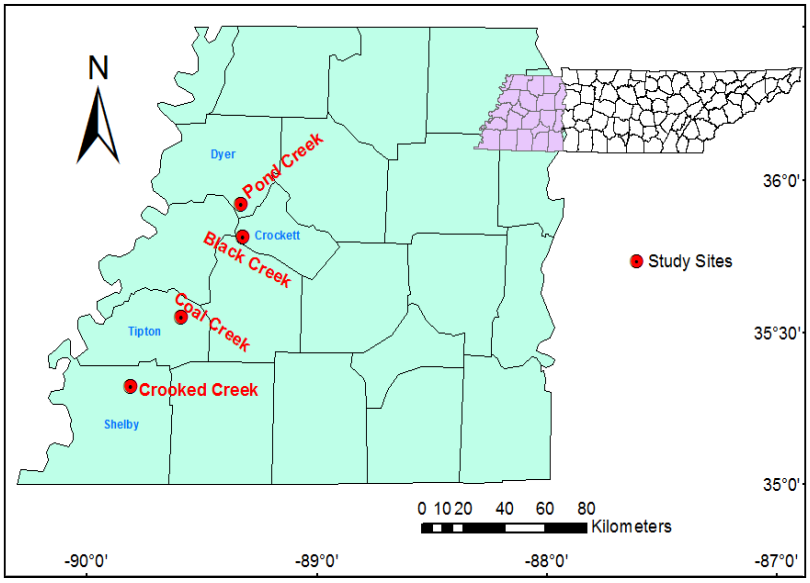


Figure 4.3.1: Study area with in-situ jet testing and soil collection locations in West Tennessee

The measurements and sample collection took place in November 2016. Soil samples were collected when local temperatures were about 16-20°C to avoid any freeze-thaw cycle effects. It is also important to note that during the sample collection, no significant change in soil moisture content was expected since the weather was dry. In this study, multiple pressure heads were used for jet testing instead of using a single pressure head. In a jet test location, pressure heads were increased from a lower head to higher (pressure head range was 12.40 kPa to 41.37 kPa). For a pressure head, test was continued for 15-20 minutes and then the pressure head was increased when the difference between two consecutive scour depth readings was less than one mm. This new jet operational protocol is termed as multiple pressure settings (MPS) method (Mahalder et al., 2018). A total of 26 in-situ jet tests were conducted and a corresponding number of relatively undisturbed soil samples were collected for the flume testing. Additional soil was also collected to measure soil physical properties including bulk density (BD), grain size distribution, moisture content (WC), Atterberg limits, and dispersion ratio (DR).

4.3.2 Soil sample collection

Several studies have reported that with increasing bed slope, τ_c decreased and the force balance for gravity with respect to slope complicates erosion estimates (Luque and Beek, 1976; Whitehouse and Hardisty, 1988; Chiew and Parker, 1994; Dey et al., 1999; Dey, 2003). Therefore, in this study, jet tests were conducted on relatively horizontal plane on bank/bed and soil samples were collected from those locations for conduit flume tests to negate the effects of gravity in erosion parameters estimation. Soil sample collections for the conduit flume were modified from the protocols as described in Sutarto et al. (2014) to further reduce disturbances from placing the collected sample in the flume's testing tray. A metal frame was used matching the dimensions of the sample tray (Figure 4.3.2). Two polymer filler end caps were also manufactured to fill the gaps at the testing tray ends. Roughness at the top surface of these polymer end caps was similar to coarse sand paper. The surficial area of a test soil sample inside the rectangular box was 0.0254 m^2.



Figure 4.3.2: For use the laboratory conduit flume photos show: a) the testing tray and b) the rectangular metal box to field collect soil samples

After finishing each jet test, the rectangular frame was driven into the ground close to the jet test location using uniform pressure at the top of the rectangular box (Figure 4.3.3). The top

soil surace was kept undisturbed to capture the natural soil formation to replicate the exact roughness conditions for erosion process. The four sides of the frame were then carefully excavated using a long taping knife. The soil underneath the box was cut using a wire saw with extreme care to avoid any possible disturbances. The frame with the soil sample was then removed from the ground and immediately wrapped with plastic wrap and aluminum foil paper to avoid any moisture loss from the soil surface and stored in a cooler. After finishing the sample collections, coolers containing soil samples were stored in a climate controlled room to avoid further moisture loss from the soil sample before starting the flume tests.



Figure 4.3.3: In-situ mini-jet testing and sample collection at the Black Creek site

4.3.3 Soil sample testing in laboratory conduit flume

Before starting a sample test, the conical storage tank and the flume pipes were filled and flushed several times to remove any deposits from the flume conduit and pipes. After cleaning the conduit flume system, the testing tray was removed and soil sample was placed into it. The tray was remounted in the flume with the same orientation as in the channel. Two filler end caps were also inserted at the upstream and downstream side of sample box as discussed in the previous section. The conical storage tank and flume were then filled again slowly using tap water. The pump was started at a very low frequency to remove all the air bubbles from the

conduit flume without triggering the onset of erosion. The initial flow rate was adjusted by the variable speed frequency control to set levels corresponding to increasing applied shear stress. The flume was kept at the same applied shear for about 10 minutes allowing the flow to stabilize after the increase. After 10 minutes, two 1-L water-eroded sediment samples were drawn from the conduit flume using four Tygon tubes downstream side of the sample testing tray (Sutarto et al., 2014). When the sediment-water samples were collected, the flow rate was increased to the next test level. Five to six flow rates were applied for each soil sample test in the conduit flume.

Inter-particle forces in cohesive soils are dependent not only on the physical properties of the soil but on the exposed environmental conditions such as pore water chemistry, flowing water chemistry, and physical conditions. In the jet test, water is pumped from the creek and subsequently passed through the outlet from the submersible tank. Therefore, it is expected that only minor changes in chemical compositions would occur to the running water during the test. On the contrary, in conduit flume since it is a recirculating system, the water chemistry could alter considerably when compared to that of the stream water and consequently affect the erosional behavior of the tested cohesive soils. Henceforth, some chemical properties of the sediment-water mix were measured and the variations were observed during the sample testing as discussed in the Methodology. In the conduit flume, since tap water was used the properties of the tap water were also measured along with the stream water used for the jet test. The cation concentrations (CC), water pH (pH), and the electric conductivity (EC) of flume water were measured to detect changes during the experiments. Water pH and EC were measured using an automated titration system (Mantech PC-Titrate® system) and the CC was measured by ion chromatography (IC) using Dionex 2100/1100 dual column system with background suppression following standard methods (Eaton et al., 2005). The chemical compositions were measured at

the beginning and end of each test. These measurements were compared to the stream water used in the jet device.

Suspended sediment concentrations in the sediment-water samples were measured through filtration using pre-weighed glass microfiber filters with 0.75 µm pore opening. Filter papers with soil particles were oven-dried at 60^0C for about 48 hrs until a constant weight was observed. Average suspended sediment concentrations (C_{avg}) were computed for the paired set of bottles collected for each flow rate. Using flow rate readings, applied shear stresses on the soil surface were calculated as described in the previous section. For calculating τ_c, erosion rate (E) was plotted against the applied shear stress (τ_b) on a normal graph paper. τ_b and E were calculated using Equations 4.3-4.5. From these plots, τ_c was estimated as the shear stress corresponding to E = 0 by drawing a best fitted line through the data points for a soil sample (Sutarto et al., 2014). In this study, filtered water samples were also preserved for future chemical analysis to observe the possible chemical composition changes in the tested water during sample testing. It was hypothesized that a possible chemical composition changes in the sample water could affect erosion behavior of the test soils.

4.3.4 Data analysis

Mini-jet test data analysis was conducted using the MPS method as described by Mahalder et al. (2018). In this method, scour depth data corresponding to the applied pressure head was analyzed individually and τ_c and k_d values were estimated. These estimated τ_c and k_d values were plotted on a normal graph against the corresponding pressure head. Finally, τ_c and k_d values for a specific test location were calculated from the shape of the plots. The MPS method is new for jet operation and data analysis, so the authors of this article suggest the readers to review the MPS method in detail as reported by Mahalder et al. (2018) for further clarification. Erosion parameters were also calculated by using the BL approach and the newly developed IP

and SDP methods with the single pressure head (traditional jet operation protocol), where the initial pressure head at each test location and the corresponding scour depths data were taken for the analyses. The analyses were conducted using a spreadsheet developed by Daly et al. (2013, *personal communication*).

Statistical differences for τ_c between the results from these two devices were compared using mean separation ANOVA. Statistical correlations between the conduit flume tests data and jet tests data (using all the four solution techniques) for τ_c was developed. Similar to the τ_c, statistical correlation for k_d was also developed. Changes in the water chemistry during soil tests were investigated from the water chemistry analyses. Statistical analyses were conducted with SPSS v.23.0.

4.4 Results

4.4.1 Physical properties of soil samples

The soil samples tested in this study were silty-clay-loams and clay-loams. Greater than 94% of the grains passed through a #200 sieve (opening 0.074 mm). BD ranged between 1.65 g cm^{-3} to 2.25 g cm^{-3} and the median grain size (D_{50}) was between 7.0 µm to 22 µm (Table 4.4.1).

Table 4.4.1 Physical properties of test soil samples from West Tennessee

Properties	**Minimum**	**Maximum**	**Mean**	**Standard Dev.**
Bulk density, BD (g cm^{-3})	1.65	2.25	1.97	0.14
D_{50} (µm)	7.00	22.00	13.76	3.31
Liquid Limits, LL (%)	24.10	40.60	32.54	4.34
Plastic Limit, PL (%)	17.80	25.60	21.88	2.33
Plasticity Index, PI (%)	5.60	19.97	10.65	3.63
Water Content, WC (%)	17.60	33.25	24.22	4.06
Dispersion Ratio, DR	0.22	0.55	0.33	0.08
Clay Content, Clay (%)	18.00	39.00	25.58	5.31
Clay Activity, CA	0.31	0.56	0.41	0.06
% Passing # 200 sieve, Pass200	93.00	98.00	96.15	1.32

Results also showed that DR range was between 0.22 and 0.55, and the clay content ranged between 18% and 39% for the soil samples. Details of other soil physical properties are presented in Table 4.4.1.

4.4.2 Chemical properties of sediment-water mix

The changes in the physical and chemical compositions of recirculating water during sample test in conduit flume were found relatively low from before the test to after (Figure 4.4.1). Overall the EC values increased but the pH values were similar. Two other properties: sodium adsorption ratio (SAR), and potassium intensity factor (KIF) were also measured from the measured CC values (Figures 4.4.1c,d). The SAR values increased from 0.43% to 9.40% and the KIF values increased from 0.07% to 17.15%. In this study, water sample testing showed that the Na^+ ion concentration ranged between 10.53 mg/L and 16.44 mg/L, and the concentration of K^+ ion ranged between 1.67 mg/L to 2.38 mg/L after the first flow rate. Overall an increasing trend was observed for Na^+, K^+, Ca^{2+} and Mg^{2+} ionic concentrations (Figure 4.4.2). Variations in these chemical parameters are presented in Table 4.4.2.

Table 4.4.2 Range variation of water chemistry during the conduit flume tests

Parameters	Range after first operated flow rate	Range after final operated flow rate	Range in percentage change
Na^+ (mg/L)	10.53 – 16.44	11.67 – 17.05	0.14% – 13.97%
K^+ (mg/L)	1.67 – 2.38	1.70 – 2.76	0.93% – 30.51%
Ca^{2+} (mg/L)	16.70 – 27.46	18.77 – 29.20	0.69% – 25.36%
Mg^{2+} (mg/L)	5.06 – 7.76	5.26 – 8.09	0.14% – 19.61%
SAR	3.12 – 3.96	3.31 – 4.01	0.07% – 17.16%
KIF	0.34 – 0.42	0.33 – 0.46	0.43% – 9.40%
Conductivity, EC (µS/cm)	189.8 – 282.98	201.56 – 297.29	0% – 3.77%
pH	7.71 – 8.10	7.75 – 8.12	0% – 22.86%

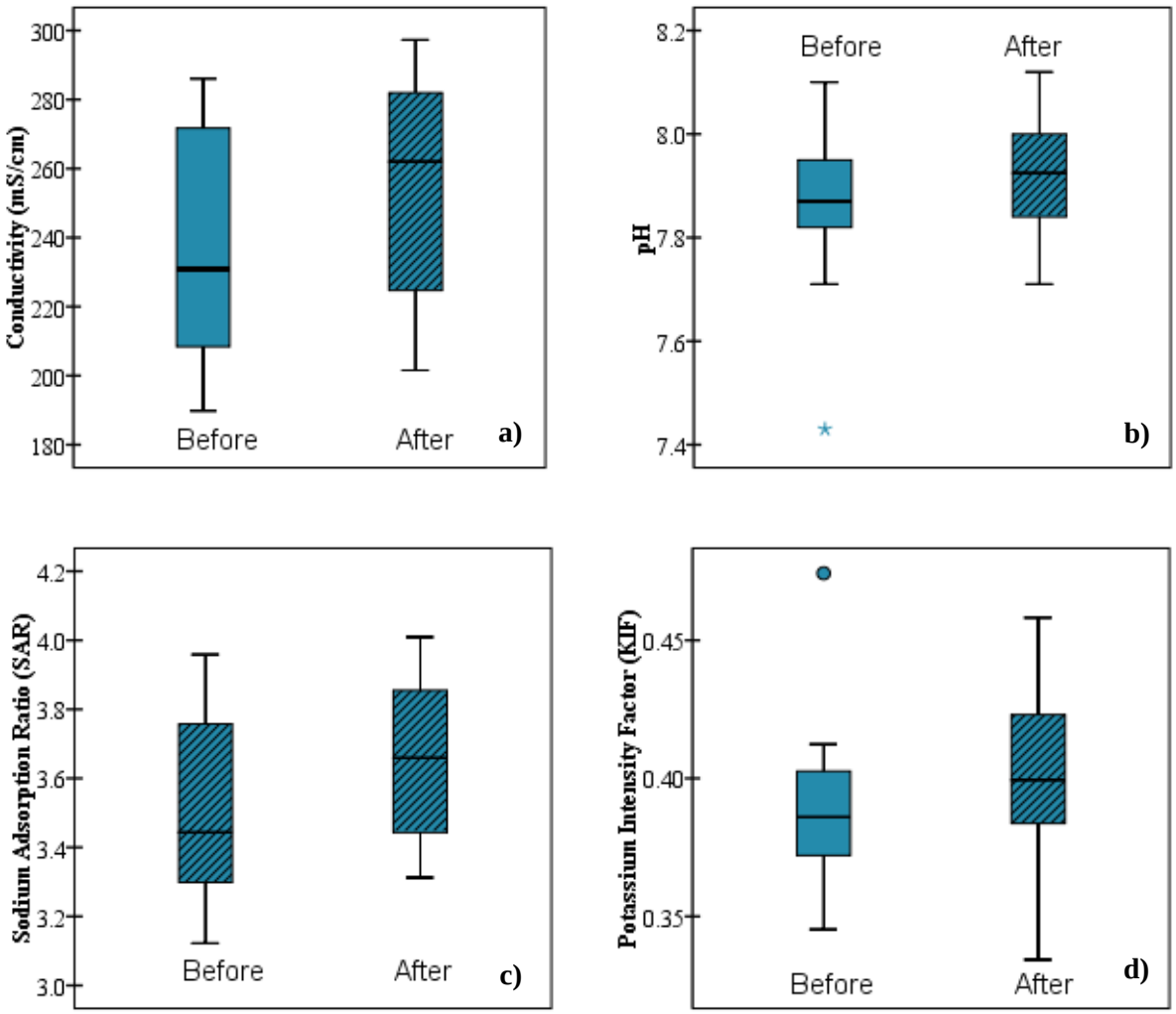


Figure 4.4.1: Variation of a) electric conductivity, b) water pH, c) SAR, and d) KIF. Here "Before" stands for after completing test with first flow rate and "After" stands for after completing test with last flow rate

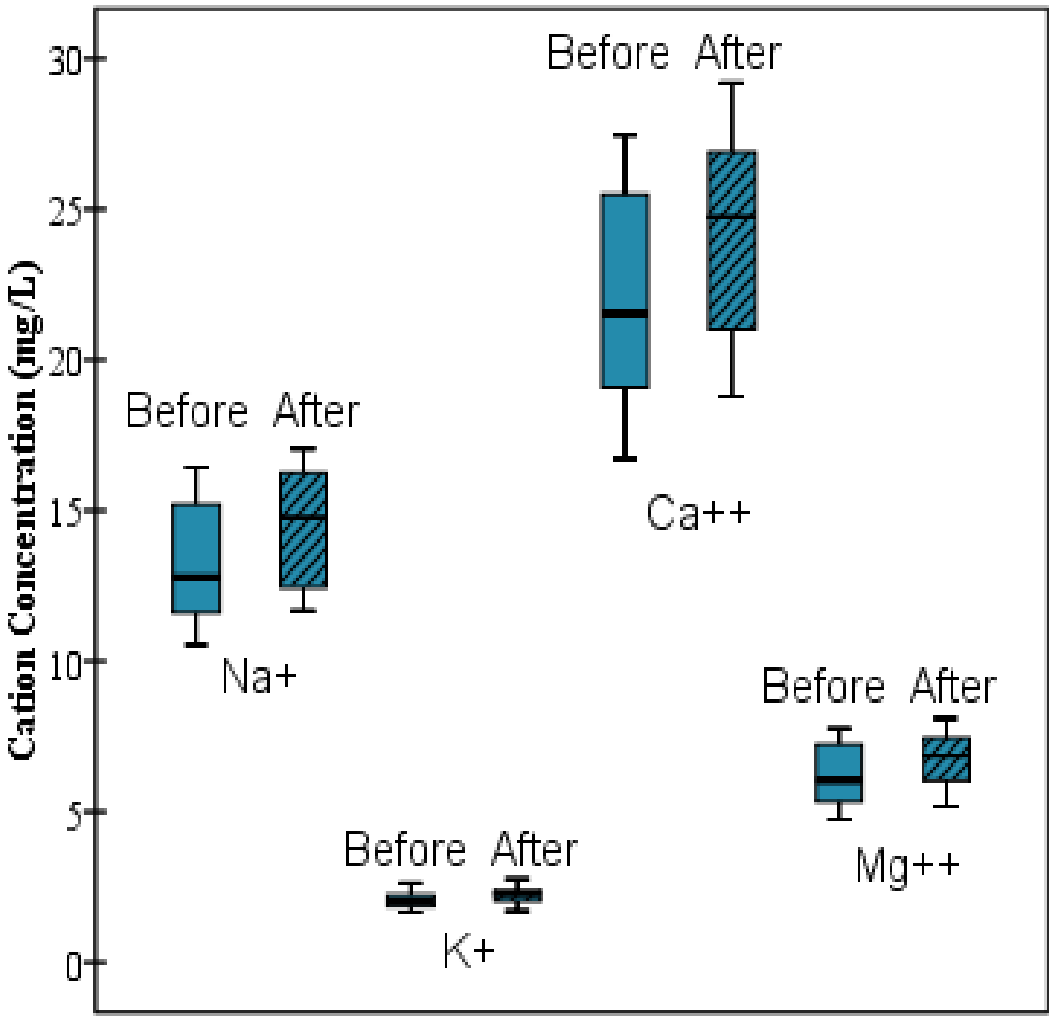


Figure 4.4.2: Variation of ion concentrations of conduit flume water during sample testing, where "Before" represents for the period after completing test with first flow rate and "After" represents the period for after completing test with last flow rate

4.4.3 Critical shear stress measurement

For this comparative study, mini-jet test data were analyzed using four different methods as discussed above. Jet test results using the MPS method showed τ_c ranged between 0.09 Pa to 23.50 Pa. Data range from the other three methods were found as follows: 0.013 Pa to 14.97 Pa; 0 Pa to 25.38 Pa; and 5.08 Pa to 20.68 Pa for BL, SDP and IP methods, respectively. Data collected for the conduit flume tests included the specific flow rates, which correspond to the applied shear stresses, and SSCs and were utilized to compute C_{avg} and erosion rates (Table 4.4.3). Table 4.4.3 represents example calculations for four test runs with the conduit flume. Results from the conduit flume tests showed that τ_c ranged between 1.75 Pa to 20.50 Pa. Four representative plots for τ_c calculation among 26 samples tested are presented in Figure 4.4.3. In these plots, the y-intercept corresponding to E = 0 was identified as the τ_c for a soil sample. Results from the jet tests using the above mentioned four methods and the conduit flume are presented in Table 4.4.4.

4.4.4 Statistical data analysis

Measured τ_c values using the jet device and the conduit flume were compared using a mean separation ANOVA test to identify possible differences in mean values among these results (n = 26). The mean value of τ_c were found 8.44 Pa from conduit flume test, 9.58 Pa from in-situ jet test (MPS), 6.79 Pa for the BL, 9.72 Pa for the IP, and 13.11 Pa for the SDP methods, respectively (Figure 4.4.4a). It was also found that the SDP method results showed wide variation in the predicted τ_c values (σ = 8.27) and the IP method showed the least variation (σ = 3.65) in the dataset. The mean separation ANOVA analysis showed that mean values among these five analyses methods were statistically different for an α of 0.05 (p = 0.013).

Table 4.4.3 Experimental conditions from the conduit flume test for four example samples and the corresponding parameter calculations

Sample identifier	**Q (gpm)**	$Q \times 10^{3}$ **(m^3/s)**	**U (m/s)**	R_{def}	τ_w **(Pa)**	u_* **(m/s)**	$C_{avg} \times 10^{2}$ **(kg/m^3)**	$\Delta C_{avg} \times 10^{2}$ **(kg/m^3)**	$E \times 10^{3}$ **($kg/m^2/s$)**
COCRSP-2	93	5.86	1.17	79743	4.73	0.069	0.33	0.33	0.77
	128	8.08	1.62	109754	8.84	0.094	3.40	3.07	9.74
	154	9.72	1.94	132048	12.71	0.113	6.93	3.52	13.44
	185	11.67	2.33	158629	18.23	0.135	18.01	11.08	50.79
	203	12.81	2.56	174063	21.90	0.148	41.98	23.97	120.57
COCRSP-3	136	8.58	1.72	116614	9.95	0.010	1.36	1.36	4.60
	156	9.84	1.97	133763	13.03	0.114	3.36	2.00	7.61
	180	11.36	2.27	154342	17.28	0.131	9.00	5.64	25.16
	205	12.93	2.59	175778	22.33	0.149	15.32	6.32	32.11
	223	14.07	2.81	191212	26.37	0.162	25.15	9.82	54.27
COCRSP-7	126	7.95	1.59	108039	8.57	0.093	3.48	3.48	10.86
	145	9.15	1.83	124331	11.29	0.106	12.93	9.45	33.95
	167	10.54	2.11	143195	14.90	0.122	20.94	8.01	33.13
	189	11.92	2.38	162059	19.02	0.138	34.65	13.71	64.24
	207	13.06	2.61	177493	22.76	0.151	53.80	19.15	98.19
CRCRSP-5	170	10.72	2.15	145767	15.40	0.124	0.38	0.38	1.47
	186	11.74	2.35	159486	18.43	0.136	1.82	1.44	6.64
	206	12.99	2.60	176635	22.56	0.150	4.45	2.63	13.41
	221	13.94	2.79	189497	25.91	0.161	6.54	2.09	11.45
	232	14.63	2.93	198929	28.51	0.169	11.88	5.34	30.69

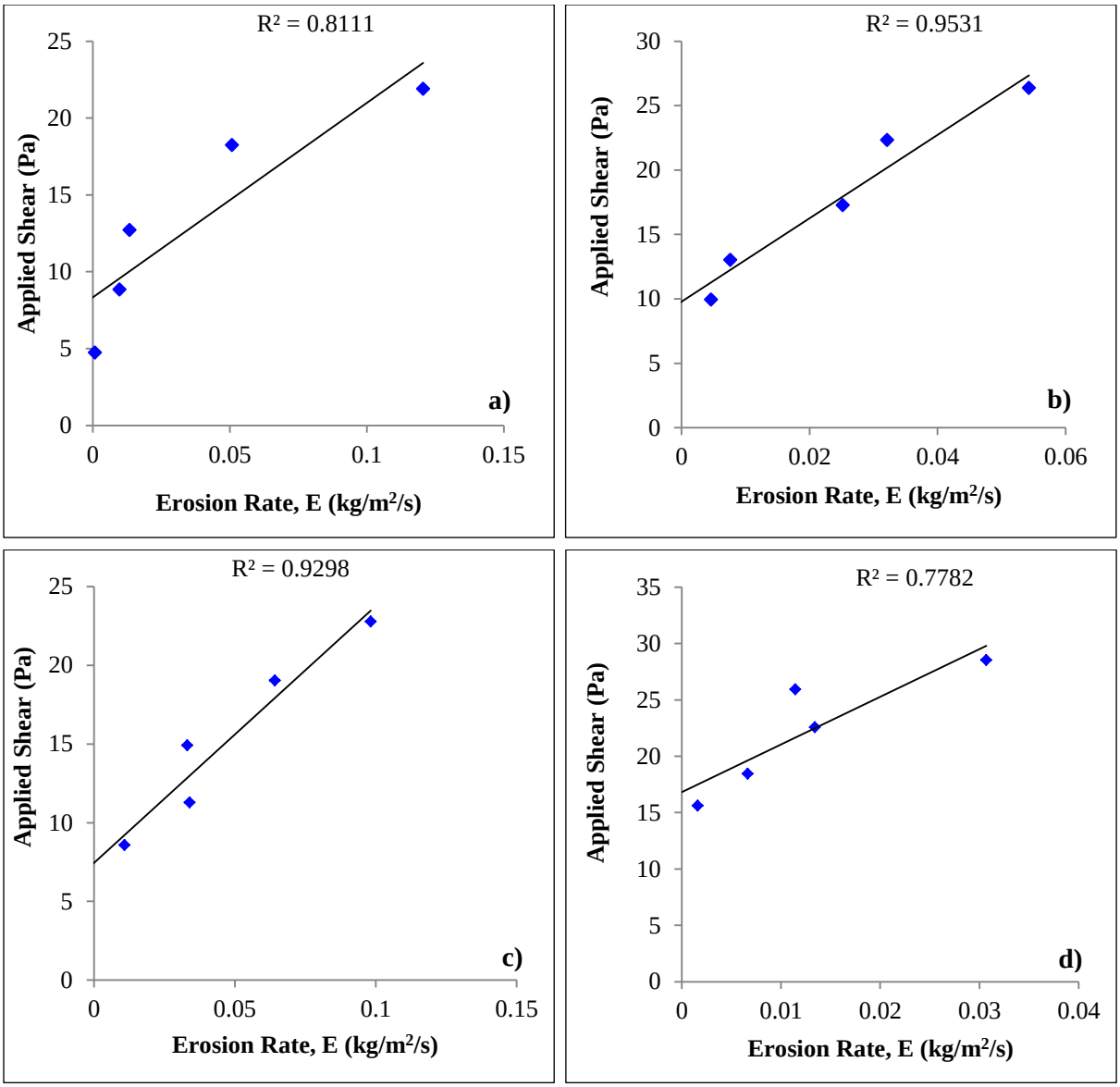


Figure 4.4.3: Conduit flume test results from four samples as presented in Table 4.4.3; the τ_c is determined as the y-intercept where E = 0. These plots represent the sample identifier: a) COCRSP-2, b) COCRSP-3, c) COCRSP-7, and d) CRCRSP-5

Table 4.4.4 Estimated critical shear stress (τ_c) using jet test and conduit flume test for four West Tennessee study sites

Study Site Creek Name	Sample identifier	Critical shear stress, τ_c (Pa)				
		Conduit flume test	Jet test (MPS)	Jet test (BL)	Jet test (IP)	Jet test (SDP)
Coal Creek	COCRSP-1	12.4	11.90	5.60	6.39	0.00
	COCRSP-2	8.20	7.74	5.02	6.67	21.50
	COCRSP-3	9.50	4.95	4.05	6.69	15.56
	COCRSP-4	4.20	4.90	6.00	6.16	4.01
	COCRSP-5	4.82	4.08	8.90	8.26	20.61
	COCRSP-6	11.50	4.53	6.23	6.32	13.19
	COCRSP-7	7.50	7.74	6.22	6.12	0.00
Crooked Creek	CRCRSP-1	8.17	1.90	0.06	8.82	2.40
	CRCRSP-2	13.90	11.10	10.47	8.57	16.92
	CRCRSP-3	7.90	9.00	10.18	9.95	16.80
	CRCRSP-4	5.00	7.76	1.63	11.60	13.32
	CRCRSP-5	16.90	17.90	11.96	11.48	18.65
	CRCRSP-6	13.20	12.22	8.43	8.56	14.36
	CRCRSP-7	5.00	11.03	6.54	8.91	15.62
Pond Creek	POCRSP-1	1.75	6.00	4.08	8.26	9.47
	POCRSP-2	15.20	15.20	8.10	6.54	19.21
	POCRSP-3	20.50	23.50	14.46	13.91	25.38
	POCRSP-4	4.00	0.09	0.01	5.08	3.59
	POCRSP-5	1.80	7.10	0.95	11.27	10.03
	POCRSP-6	3.20	4.50	1.45	12.09	0.20
Black Creek	BLCRSP-1	3.00	8.50	10.05	14.42	23.85
	BLCRSP-2	15.90	22.20	13.88	13.90	19.27
	BLCRSP-3	6.40	14.97	14.97	14.95	25.31
	BLCRSP-4	2.00	3.21	0.35	20.68	0.00
	BLCRSP-5	1.75	8.51	8.11	9.78	18.52
	BLCRSP-6	14.50	18.50	8.76	7.23	13.14

The Tukey HSD comparison methods showed that the statistical differences among the mean values were found between conduit flume and SDP methods ($p = 0.035$), and between BL and SDP methods ($p = 0.001$). Similar to τ_c, SDP method predicted k_d values showed wide variation ($\sigma = 8.92$) in the dataset. Mean values of k_d were found to vary widely among these five methods as: 2.99 $cm^3\ N^{-1}\ s^{-1}$($\sigma = 2.63$), 1.80 $cm^3\ N^{-1}\ s^{-1}$ ($\sigma = 2.62$), 1.97 $cm^3\ N^{-1}\ s^{-1}$ ($\sigma = 2.81$), 7.15 $cm^3\ N^{-1}\ s^{-1}$ ($\sigma = 8.92$), and 13.94 $cm^3\ N^{-1}\ s^{-1}$ ($\sigma = 7.13$) for conduit flume, MPS, BL, SDP, and IP method, respectively (Figure 4.4.4b). The mean separation ANOVA analysis also showed that k_d values were statistically different for an α of 0.05 ($p < 0.001$) among these methods. The IP method estimated mean k_d value was statistically different when compared to the mean from other four methods ($p < 0.001$). Statistical differences for mean values between MPS and SDP ($p = 0.008$), BL and SDP ($p = 0.008$) were also observed using Tukey HSD comparison methods.

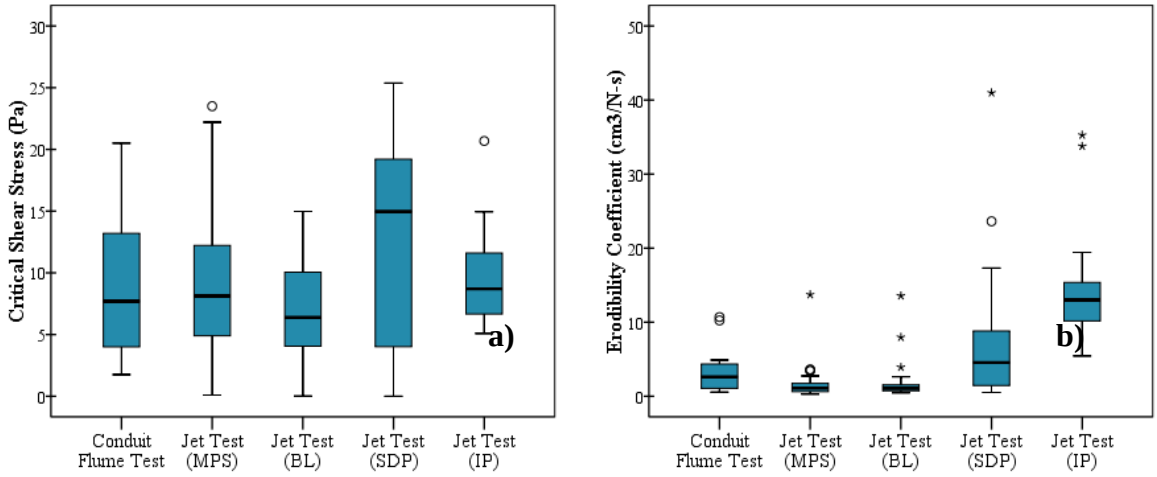


Figure 4.4.4: a) Critical shear stress (τ_c), and b) erodibility coefficient (k_d) comparisons using conduit flume test and jet test results

In Figure 4.4.5, linear prediction models for τ_c using the conduit flume results as the dependent variable and the jet test results using the MPS as independent variable showed that the

correlation value was 0.58 and adjusted R^2 value of 0.56 ($p < 0.001$). Similar significant results with the BL method showed R^2 value was 0.35 and adjusted R^2 value was 0.32 (Figures 4.4.5a,b).

Data normality was checked by plotting the residuals, which showed normal distribution in the dataset. However, using both the SDP ($p = 0.08$) and IP ($p = 0.60$) methods the correlations were not statistically significant as R^2 values were found 0.12 for SDP and 0.01 for IP, respectively (Figures 4.4.5c,d). It is also important to note that the SDP method predicted τ_c values were consistently higher with some exceptions, whereas the IP method predicted values showed mixed results. Similar linear prediction models for the k_d values were also developed in this study as mentioned in the Methodology. Correlation value was found 0.42 ($p < 0.001$) between the conduit flume and the MPS method data and the R^2 value was 0.32 using BL method data (Figures 4.4.6a,b). However, similar to τ_c results, correlations for k_d values using both the SDP and IP showed very low R^2 values (Figures 4.4.6c,d). It was also found that both the SDP and IP methods predicted k_d values were consistently higher with some exception compared to the flume data.

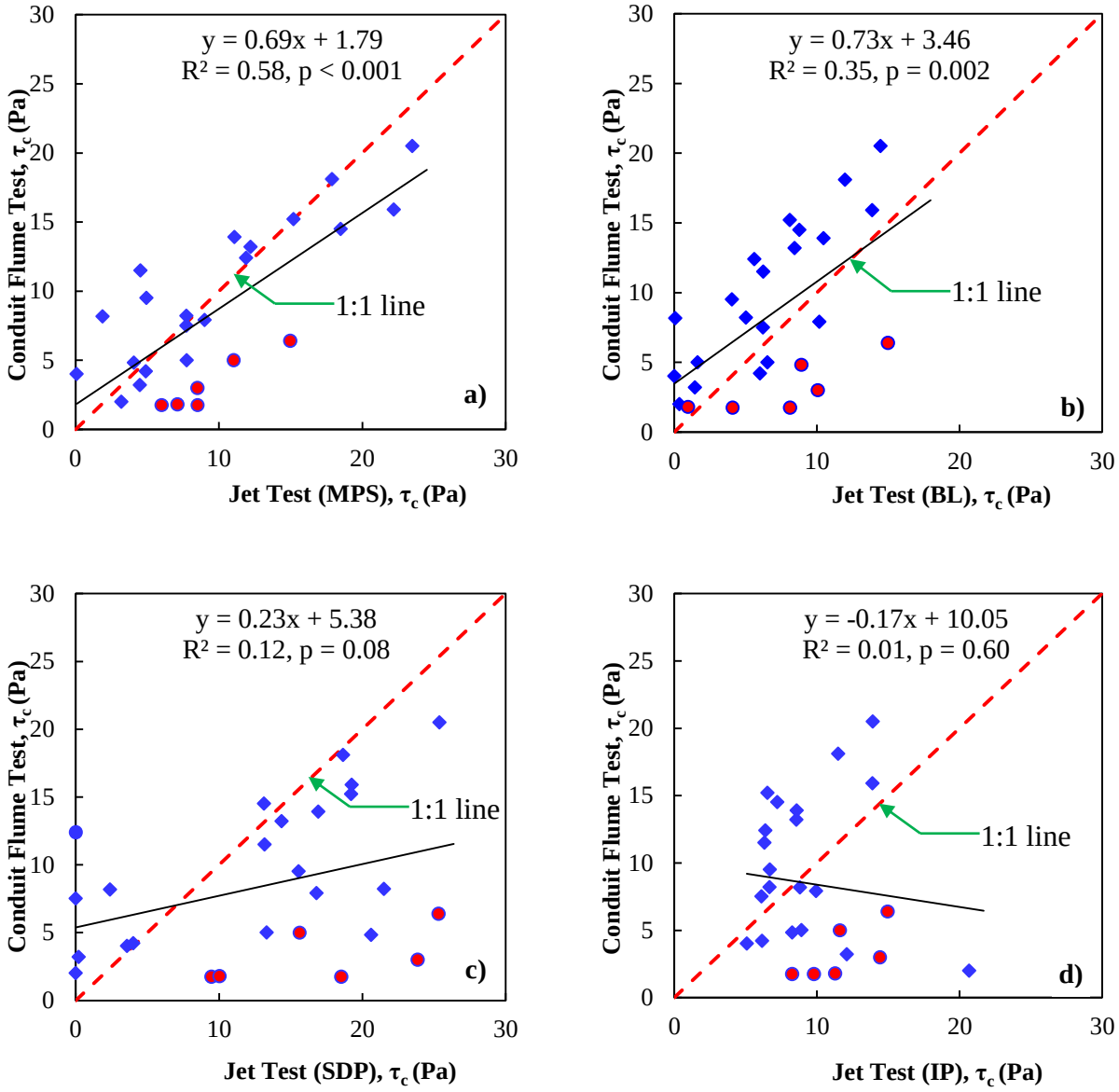


Figure 4.4.5: Critical shear stress comparison with conduit flume test results: a) using multiple pressure settings (MPS), b) using Blaisdell method (BL), c) using scour depth principle (SDP), and d) using iterative principle (IP). Red circles in a) indicate the samples with WC < 18.5%

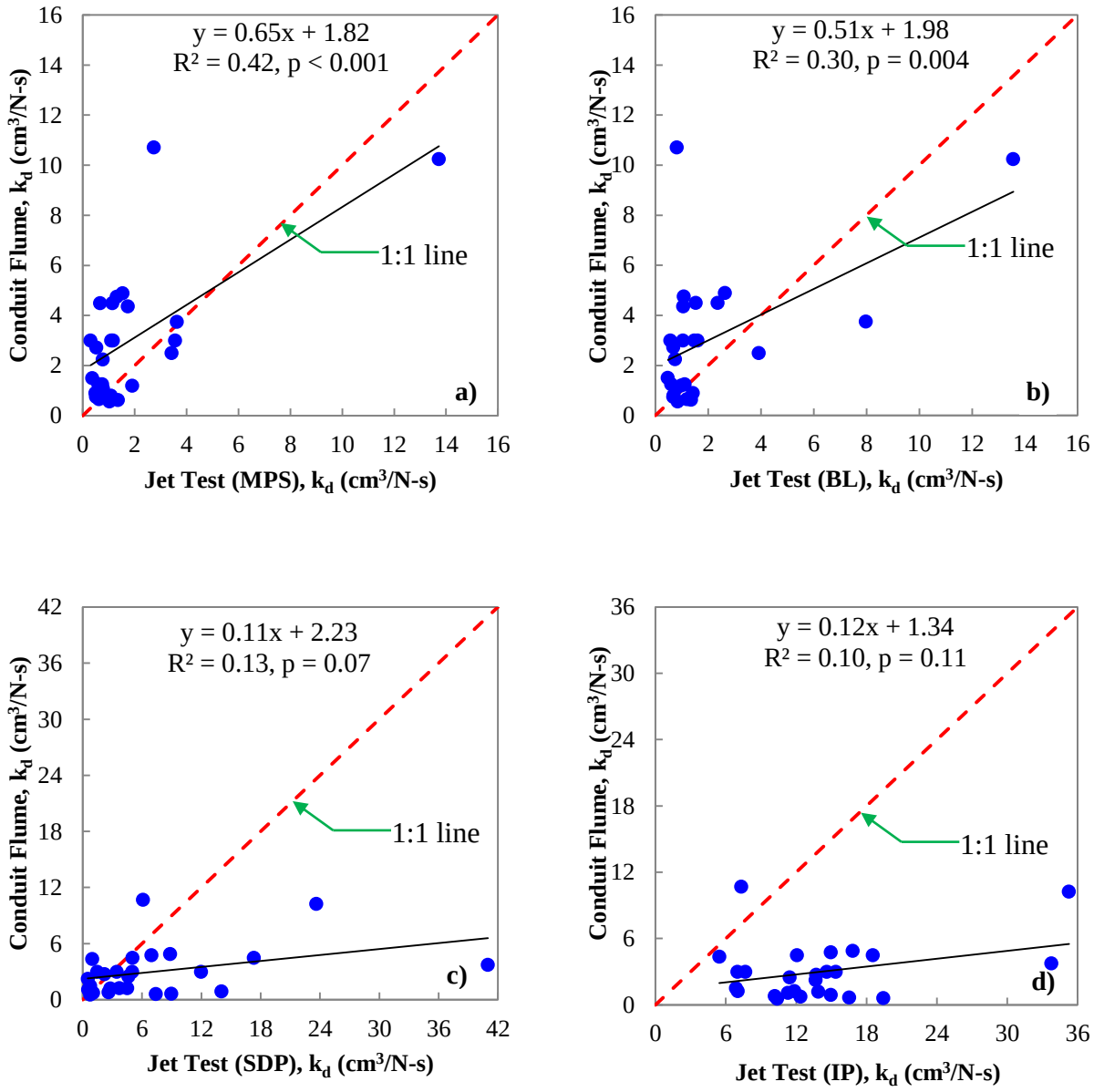


Figure 4.4.6: Erodibility coefficient comparison with conduit flume test results: a) using multiple pressure settings (MPS), b) using Blaisdell method (BL), c) using scour depth principle (SDP), and d) using iterative principle (IP)

4.5 Discussion

Previously published research studies have focused on improving methods for estimating τ_c and k_d with the in-situ jet tests and laboratory flumes being the predominant methods applied. In-situ methods can better represent the actual stream conditions because the soil is undisturbed prior to testing; however, a hydraulic jet is applied normal to the erodible surface with shear stress derived by diffusion relationships. During the impingement, the nature of the force exerted transitions from normal to shear as the scour evolves (Ghaneeizad, 2016). In contrast, the pressurized conduit flume creates a shear stress exerted atop of the erodible surface representing closely the shearing action exerted to the soil surface by the flow in field conditions along a bank/bed profile; however, care should be given, as is the case here, with the improvements made in the Sutarto et al. (2014) approach that there is minimal soil sample disturbances during field collection. Therefore, the device dependent variability in τ_c and k_d are expected since the stress distribution procedures and the erosion mechanism are different in these two devices.

In general, results from our study indicated that τ_c estimates compared better between devices than k_d, in general (Figures 4.4.4-4.4.6). Depending on the jet test analyses methods, MPS method estimated erodibility parameters from this device were more closely correlated with the conduit flume. It is hypothesized that since both the conduit flume test and the MPS methods test hydraulics better replicate each other, better correlation was found. In addition, when either the MPS or the BL data analysis approach are used, erodibility parameters were comparable from a broad perspective, though differences were observed and provided valuable insight to erosion behavior of cohesive soils and the testing methods which are described below. Median τ_c values for the conduit flume, MPS and BL jet test methods including all tests ranged from 0 Pa to 25.38 Pa (Figure 4.4.4a). The τ_c correlations less than 5 Pa were highly variable between the conduit flume and the jet test MPS and BL methods, though significant linear relations were

observed for τ_c for the entire testing range (Figure 4.4.5). This suggests that for lower strength samples mostly operational differences controlled the identified differences. It is also possible that the choice of *Jp* is quite sensitive for weaker soils. Above 5 Pa, the MPS jet test method correlated the best with the conduit flume results thereby suggesting that stronger samples exhibit less variability than the weaker ones and operational differences of the two methods get masked (i.e., in this case the choice of J_p is less sensitive). Study results also showed that at lower WC (usually stronger soils as WC is inversely related to strength), jet test data showed higher τ_c values compared to the conduit flume results using the MPS, BL, IP, and SDP method represented as small circles in the graph (Figure 4.4.5). It is interesting to note that comparable results from these two devices were identified especially for consolidated cohesive soils with relatively higher moisture content (> 20%). However, for relatively dry soils, statistically non-significant correlation was identified due to the challenges associated with the sample collection. Based on field observations, it was hypothesized that during sample collection, micro-cracks developed around the edges of the sample collecting rectangular boxes. The weakened soil may have eroded more quickly from those areas during the conduit flume tests, resulting in lower τ_c values.

Results also showed that estimating k_d values was challenging since lower correlations were found from these two devices using any jet test solution method (Figure 4.4.5). Similar findings have also been reported in several studies using jet test data (Hanson and Simon, 2001, Simon et al., 2010; Daly et al., 2015; Mahalder et al., 2017). Findings for k_d values using jet device showed this parameter was greater than the estimates from the conduit flume (Figure 4.4.6). However, the MPS and the BL analysis methods for the jet test data were better correlated than the SDP and IP methods. Regardless of any methods, the range of k_d values from this study

was found between 0.30 to 40.98 $cm^3 N^{-1} s^{-1}$. Similar to other studies (Hanson and Simon, 2001; Wynn and Mostaghimi, 2006; Simon et al., 2010; Daly et al., 2015), inverse power law relationships with τ_c and k_d were identified using both the conduit flume and jet test data (Figure 4.5.1). Relationship from the SDP method was not developed due to the presence of zero values in the calculated τ_c values. In order to assess better the comparison between the jet test device and the conduit flume in terms of erodibility estimates. A study design would have to be conducted where local bank erosion rates at the sample site are surveyed.

In this study, soil samples that were tested had similar physical characteristics. By the definition of Raudkivi (1990), soil samples were cohesive because clay percentage was greater than 18% by weight and high PI values (Table 4.4.1). The studied stream sites were from the Coastal Plain physiographic province with Neogene and Quaternary rock system, deposited from both marine and non-marine sand, silt and clay with sand dominant (Miller, 1974). Mahalder et al. (2017) identified that in cohesive soils, τ_c predictive equations differed among different geology and reported multiple predictive equations. These studied stream sites were among one of those reported groups, where Pass200, WC, CA, BD and organic content (OC) were found the most significant soil properties among others to predict τ_c. Though, limited soil physical properties (Table 4.4.1) were measured for this case, similar correlation patterns to τ_c were identified. Clay%, CA, BD and Pass200 showed positive correlation to τ_c considering the results obtained from both the conduit flume and the jet test device (using all the four available methods). However, WC did not show any specific correlation to τ_c, which was thought to be influencing the erosion pattern for some of the soil samples as discussed in the earlier section, resulting the variation in the erosion parameters (τ_c. and k_d) estimation.

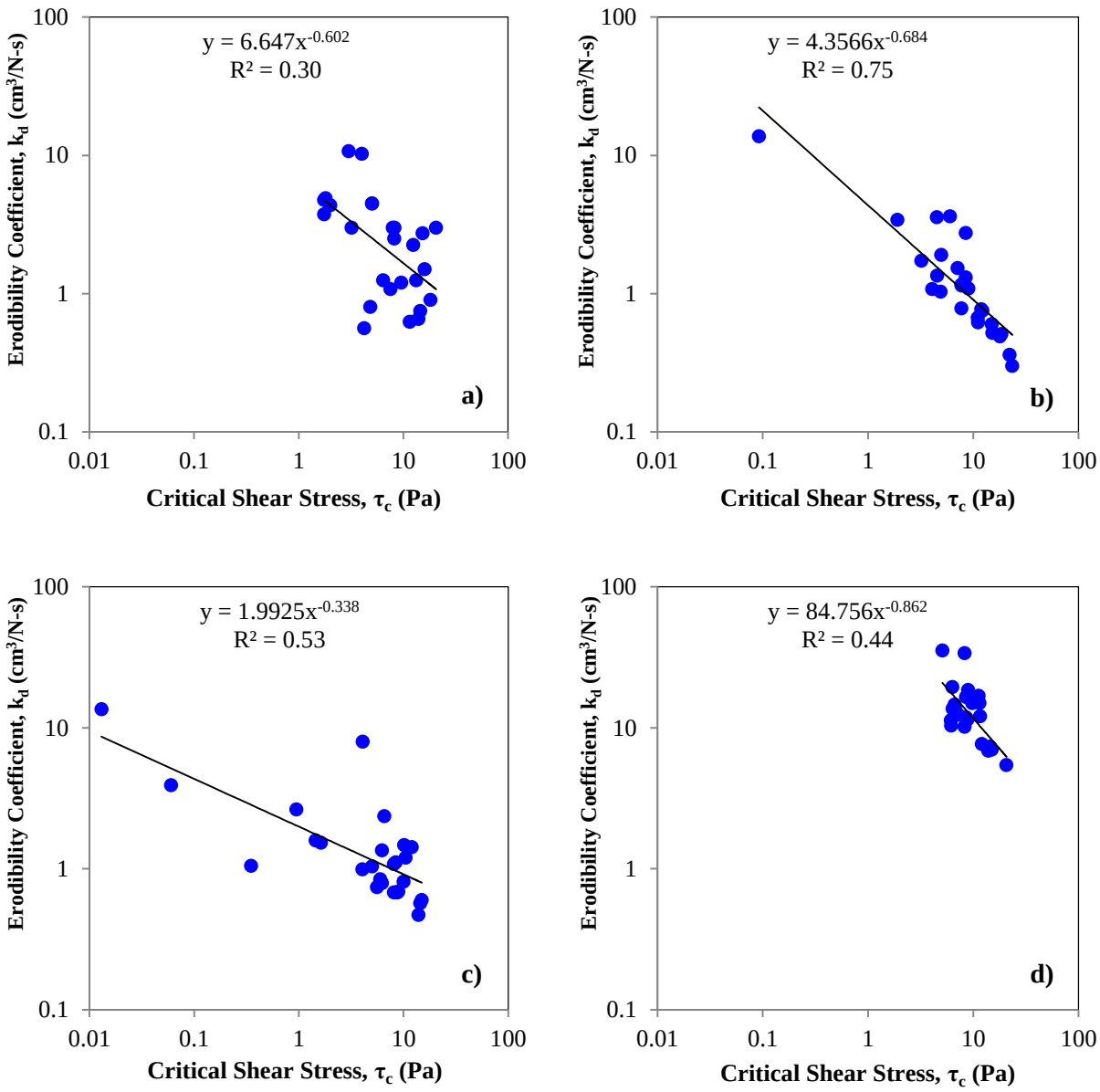


Figure 4.5.1: Relationship between critical shear stress (τ_c) and erodibility coefficient (k_d): a) conduit flume, b) jet test (MPS), c) jet test (BL), and d) jet test (IP)

Both the physical, geochemical, and biological properties can significantly affect the erosional behavior of cohesive soils due to the inter-particle attraction forces (Grabowski et al., 2011). In this study, the physical and biological properties of soil samples were similar. Therefore, the change in water chemistry was measured during sample testing, which can significantly affect the erosional behavior in cohesive soils. With the conduit flume, the water supply is external to instream conditions; therefore, in this study the possible influences on erosion rates or erodibility parameters were explored. Analyses of sediment-water mix samples showed the pH value changed between 0% to 22.86% and EC ranged between 0% and 3.77% for the flowing water during the sample testing (Figures 4.4.1a,b). Erosion of cohesive sediments can be differed in different clay minerals in varying pH and ionic concentrations (Liou, 1970). The relationship between τ_c and soil pore water pH shows that with increasing pH, the concentration of H^+ ions decreases, resulting in an increase in the double layer thickness. Consequently, a greater repulsive force was expected in the soil particles (Winterwerp and van Kesteren, 2004). However, Ravisangar et al. (2005) suggested that at low ionic concentration (lower EC value) erosion rate is higher at higher pH and vise-versa at low pH. They also reported that at higher ionic concentration, pH had no effect on erosion behavior in cohesive sediments. In this study, since both the pH and EC values changed during sample testing in the conduit flume, the effect on erosion behavior is further needed to be studied.

Influence of clay minerals and pore fluid conditions also affect the erosion behavior of cohesive soils. Using different clay minerals and pore fluid conditions, Liou (1970) reported a positive correlation between SAR and τ_c. The influence of SAR on the repulsive forces is positively correlated; consequently influence the erosion potential for cohesive soils based on clay mineral (Liou, 1970; Alizadeh, 1974; Arulanandan, 1975). It was also reported that KIF and

τ_c are negatively correlated. Soils with higher KIF values were typically friable and eroded away easily and a negative correlation is expected (Wynn and Mostaghimi, 2006). During the samples testing in the conduit flume, the SAR values changed from 0.07% to 17.16% and the changes in KIF values were ranged 0.43% to 9.40%. Results from this study showed that water chemistry did change during the test; however, the influence on erosion was not clear. An experimental study design with different flume water chemistry would have to be implemented for better understanding the influence on erosion processes.

Erosion patterns and scour hole development in cohesive soils using a jet device is also dependent on soil physical properties (Mahalder et al., 2018). Mahalder et al. (2018) identified that soils with relatively lower moisture content and lower cohesion showed narrower and deeper scour holes, and for moderately moist consolidated soils with higher cohesion showed shallower and wider scour holes. For the later case, it was hypothesized that layer by layer removal of soil aggregates from the underneath soil column could be prominent as shear forces above the critical are being applied on the soil surface. From field observations and during the sample testing in the conduit flume, comparable incidents were observed to support this hypothesis (Figure 4.5.2).

Therefore, during conduit flume testing, aggregate removal was found prominent for some soil samples. At lower flow rates, those aggregates were found to be unbroken and moving as bedload following both the rolling and saltation movements. Consequently, non-uniform sediment concentrations in the conduit flume may have occurred as those aggregates could have been broken at higher flow rates during the latter stage of the test. These circumstances may have influenced some results as the erosion rate was found to be very high for some intermediate flow rates, influencing the correlations for predicting τ_c and k_d values. This observation might be a future research topic for estimating erodibility parameters using the conduit flume especially for

consolidated cohesive soils. Similar scenarios were also observed for jet device at higher pressure heads broken soil layers underneath the water jet were found stagnant due cracks formation in the soil. However, the depth gage attached to the jet device did not record any changes in the erosion depth though the soil was already broken. In association with the data analysis procedures, this issue must be addressed for the jet device in future for erosion parameters prediction in-situ for cohesive soils.

Findings from this study and field observations also identified that the differences among different devices are not only dependent on the working principles of these devices but the type of soil samples being tested. Working with naturally formed soils, it is always expected a wide variation of heterogeneity in the soil layers affecting the erodibility parameters. Using the jet device, since these parameters are being obtained from a point, it requires multiple tests to obtain an average value. In addition to the jet test data analyses procedures, the jet operation protocol was found another source of possible variation in the correlation. The conduit flume was a more controlled device for predicting erodibility parameters. However, the assumption of uniform sediment concentration across the conduit may not be always correct depending on soil types. It is also important to mention that the applied shear stress calculation procedures during testing might not be always accurate with higher sediment concentration in the flowing water and irregular soil surface due to erosion during testing. These issues are thought to be important and need to be addressed in addition to the sample collection protocol for the conduit flume.

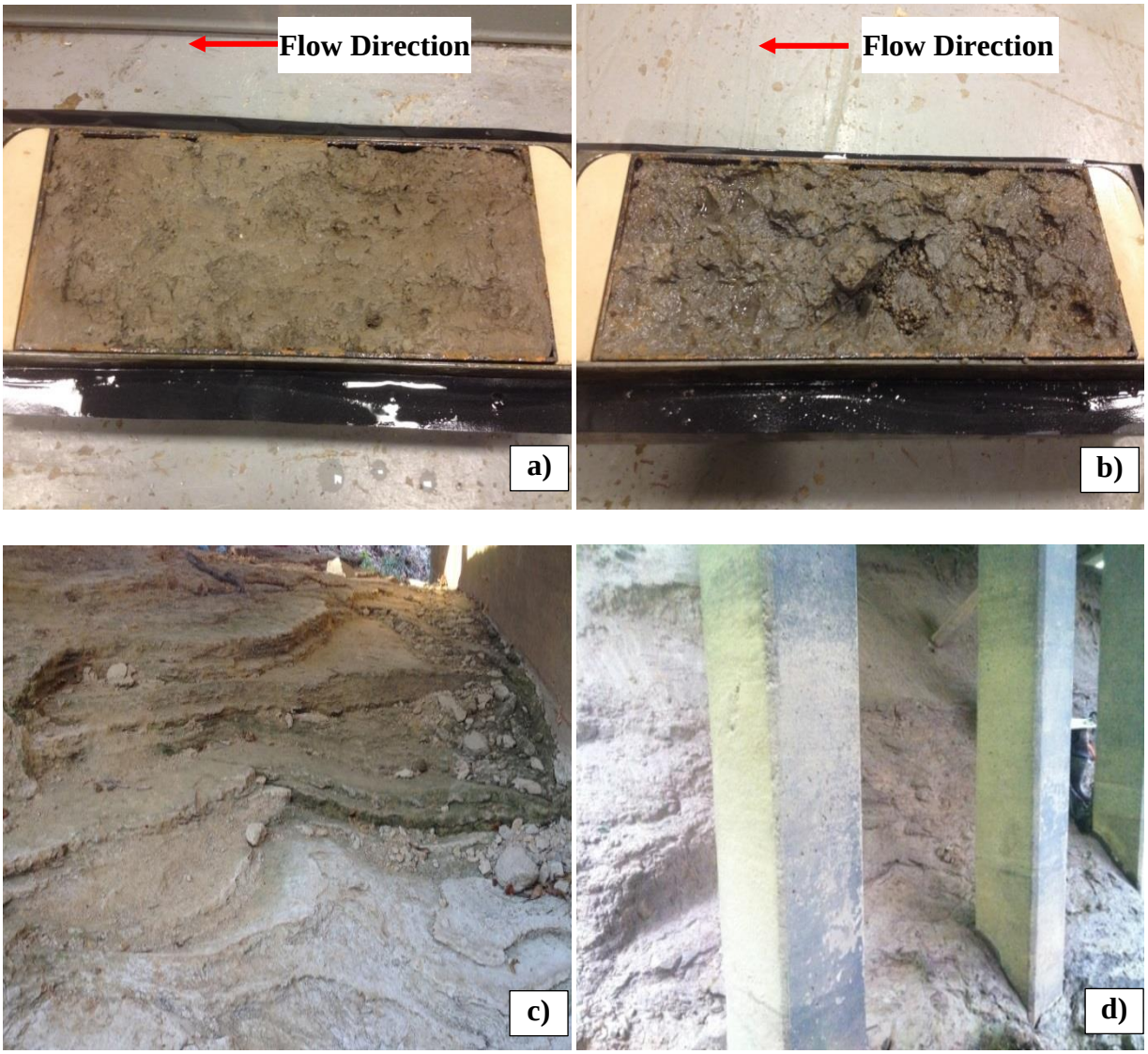


Figure 4.5.2: Erosion pattern of tested soil sample in conduit flume: a) before test, b) after test, erosion pattern from field observations: c) at bottom of creek, and d) around structures

4.6 Conclusions

Device dependent variability for erosion parameters (τ_c and k_d) prediction was studied using a laboratory device: the pressurized conduit flume, and an in-situ device: the submersible mini-jet. Statistically significant correlations for results from conduit flume tests and jet tests data were identified for both the τ_c and k_d values. However, key findings from this study suggests that the operational and data analyses procedures in jet tests were persuasive for these correlations since results from the MPS method showed higher R^2 values for both τ_c ($R^2 = 0.58$) and k_d ($R^2 = 0.42$) values. The variations in k_d estimations were substantial using both these two devices regardless of the data analyses procedures. It is also clear that soil type and soil moisture content have significant impact on the sample collection, which evidently influenced the τ_c and k_d values estimation using the conduit flume tests. Similar scenarios were observed for jet device, where soil heterogeneity may have affected the results since the jet is impacting at a point. From the test hydraulics perspective it is also though that conduit flume and MPS method are similar in nature, which may have influenced the better comparable erodibility parameters as observed in this study.

4.7 References

Aberle J, Nikora V, McLean S, Doscher C, McEwan I, Green M, Goring D, Walsh J. 2003. Straight benthic flow-through flume for in situ measurement of cohesive sediment dynamics. J. Hydraul. Eng. 129 (1): 63-67

Alizadeh A 1974. Amount and type of clay and pore fluid influences on the critical shear stress and swelling of cohesive sediments. Ph.D. Dissertation, University of California, Davis, CA, USA

Al-Madhhachi AT, Hanson GJ, Fox GA, Tyagi AK, Bulut R. 2013a. Measuring soil erodibility using a laboratory "mini" JET." Trans. ASABE 56 (3): 901-910

Al-Madhhachi AT, Hanson GJ, Fox GA, Tyagi AK, Bulut R. 2013b. Deriving parameters of a fundamental detachment model for cohesive soils from flume and jet erosion tests. Trans. ASABE 56 (2): 489-504

Amos CL, Grant J, Daborn GR, Black K. 1992. Sea carousel - a benthic annular flume. Estuarine, Coastal and Shelf Science 34: 557-577

Arulanandan K 1975. Fundamental aspects of erosion of cohesive sediments. J. Hydraul. Division 101(HY5): 635-639

Arulanandan K, Sargunam A, Loganathan P, Krone RB. 1973. Application of chemical and electrical parameters to prediction of erodibility. Soil erosion: Causes and mechanisms; prevention and control, Special Rep. 135, Highway Research Board, Washington, D.C.: 42-51

Blaisdell FW, Clayton LA, Hebaus CG. 1981. Ultimate dimension of local scour. J. Hydraul. Division 107 (3): 327-337

Bones EJ. 2014. Predicting critical shear stress and soil erodibility classes using soil properties. M.Sc. Thesis, Georgia Institute of Technology, GA, USA

Briaud J, Ting F, Chen HC, Gudavilli R, Kwak K, Philogene B, Han S, Perugu S, Wei G, Nurtjahyo P, Cao Y, Li Y. 2001. SRICOS: Prediction of scour rate at bridge piers. Report 2937-1, Texas Transportation Institute, The Texas A&M University, College Station, Texas, USA

Chapuis RP, Gatien T. 1986. An improved rotating cylinder technique for quantitative measurements of the scour resistance of clays. Can. Geotech. J. 23: 83-87

Chiew YM, Parker G. 1994. Incipient sediment motion on non-horizontal slopes. J. Hydraul. Res. 32(5): 649-660

Craft T, Graham L, Launder B. 1993. Impinging jet studies for turbulence model assessment – II. An examination of the performance of four turbulence models. Int. J. Heat Mass Transfer 36(10): 2685-2697

Daly ER, Fox GA, Al-Madhhachi AT, Miller RB. 2013. A scour depth approach for deriving erodibility parameters from jet erosion tests. Trans. ASABE 56(6): 1343–1351

Daly ER, Fox GA, Enlow HK, Storm DE, Hunt SL. 2015. Site-scale variability of streambank fluvial erodibility parameters as measured with a jet erosion test. J. Hydrological Process 29: 5451-5464

Debnath K, Nikora V, Grace C. 2004. Erosion of cohesive sediments in canterbury streams. The Water Balance, Book of Abstracts of the New Zealand Hydrological Society Symp., Queenstown, New Zealand: 67-68

Debnath K, Nikora V, Aberle J, Westrich B, Muste M. 2007. Erosion of cohesive sediments: resuspension, bed Load, and erosion patterns from field experiments. J. Hydraul. Eng. 133 (5): 508-520

Dey S, Sarker HK, Debnath K. 1999. Sediment threshold under stream flow on horizontal and sloping beds. J. Eng. Mech. 125(5): 545-553

Dey S. 2003. Threshold of sediment motion on combined transverse and longitudinal sloping beds. J. of Hydraul. Research 41(4): 405-415. DOI: 10.1080/00221680309499985

Eaton AD, Clesceri LS, Rice EW, Greenburg AE. 2005. Standard methods for the examination of water and wastewater. AWWA, WEF, American Public health Association, Washington, D.C., USA

Dunn IS. 1959. Tractive resistance of cohesive channels. J. Soil Mechanics and Foundations, ASCE 85(SM3, Part 1): 1-24

Ghaneeizad SM. 2016. Impinging jets in a confined environment: Application for soil erosion. Ph. D. Dissertation, Department of Civil, Structural and Environmental Engineering, State University of New York, Buffalo, NY, USA

Gibson MM, Launder BE. 1978. Ground effects on pressure fluctuations in the atmospheric boundary layer. J. Fluid Mech. 86: 491-511

Grabowski RC, Droppo IG, Wharton G. 2011. Erodibility of cohesive sediment: The importance of sediment properties. Earth Sci. Rev. 105 (1): 101-120

Haaland SE. 1983. Simple and explicit formulas for the friction factor in turbulent pipe flow. J. Fluids Eng. 105(1): 89-90

Hanson GJ. 1990. Surface erodibility of earthen channels at high stresses: II. Developing an in situ testing device. Trans., ASAE 33(1): 132-137

Hanson GJ, Simon A. 2001. Erodibility of cohesive streambeds in the loess area of the midwestern USA. Hydrological Processes 15: 23-38

Hanson GJ, Cook KR. 1997. Development of excess shear stress parameters for circular jet testing. ASAE Paper No. 972227. St. Joseph, Michigan, USA

Hanson GJ, Cook KR. 2004. Apparatus, test procedures, and analytical methods to measure soil erodibility in-situ. Appl. Eng. Agric. 20 (4): 455-462

Hanson GJ, Hunt SL. 2007. Lessons learned using laboratory jet method to measure soil erodibility of compaction soils. Applied Eng. in Agric. 23 (3): 305-312

Hobson PM. 2008. Rheologic and flume erosion characteristics of Georgia sediments from bridge foundations. M.Sc. Thesis, Georgia Institute of Technology, GA, USA

Houwing EJ, van Rijn LC. 1998. In situ erosion flume (ISEF): Determination of bed-shear stress and erosion of a kaolinite bed. J. Sea Research 39: 243-253

Karamigolbaghi M, Ghaneeizad SM, Atkinson JF, Bennett SJ, Wells RR. 2017. Critical assessment of jet erosion test methodologies for cohesive soil and sediment. Geomorphology 295: 529-536. DOI: http://dx.doi.org/10.1016/j.geomorph.2017.08.005

Khanal A, Fox GA, Al-Madhhachi AT. 2016. Variability of erodibility parameters from laboratory mini jet erosion tests. J. Hydro. Eng. 21(10). DOI:10.1061/(ASCE)HE.1943-5548.0001404

Liou YD. 1970. Hydraulic erodibility of two pure clay systems. Ph.D. Dissertation, Colorado State University, Fort Collins, CO, USA

Luque RF, van Beek R. 1976. Erosion and transport of bed-load sediment. J. Hydraul. Res. 14(2): 127-144

Mahalder B, Schwartz JS, Palomino AM, Zirkle J. 2017. Relationships between physical-geochemical soil properties and erodibility of streambanks among different physiographic provinces of Tennessee, USA. Earth Surface Processes and Landforms 43(2): 401-416. DOI: 10.1002/esp.4252

Mahalder B, Schwartz JS, Palomino AM, Zirkle J. 2018. Estimating erodibility parameters for streambanks with cohesive soils using the mini jet test device: A comparison of field and computational methods. Water 10(3), 304. DOI: 10.3390/w10030304

Mallison T. 2008. Comparing in-situ submerged jet test device and laboratory flume methods to estimate erosional properties of cohesive soils for stream bank stability models. M.Sc. Thesis, University of Tennessee, Knoxville, TN, USA

McNeil J, Taylor C, Lick W. 1996. Measurement of erosion of undisturbed bottom sediments with depth. J. Hydraul. Eng. 122(6): 316-324. DOI: http://dx.doi.org/10.1061/(ASCE)0733-9429(1996)122:6(316)

Mercier F, Bonelli S, Pinettes P, Golay F, Anselmet F et al. 2014. Comparison of CFD simulations with experimental jet erosion tests results. J. Hydraul. Eng. 140(5). DOI: 10.1061/(ASCE)HY.1943-7900.0000829, 04014006

Miller RA. 1974. The geologic history of Tennessee. Tennessee Division of Geology, Bulletin 74

Moore WL, Masch Jr. FD. 1962. Experiments on the scour resistance of cohesive sediments. J. Geophys. Res. 67(4): 1437-1449

Mostafa TMS, Imran J, Chaudhry MH, Khan IB. 2008. Erosion resistance of cohesive soils. J. Hydraul. Research 46 (6): 777-787

Papanicolaou AN. 2001. Erosion of cohesive streambeds and banks. State of Washington Water Res. Cent. Rep. WRR-08, Washington. State University, Pullman, Washington, USA

Papanicolaou AN, Elhakeem M, Hilldale R. 2007. Secondary current effects on cohesive river bank erosion. Water Resour. Res. 43 (12). DOI: 10.1029/2006WR005763

Raudkivi AJ. 1990. Loose boundary hydraulics. 3rd edition, Pergamon Press, New York, USA

Ravisangar V, Sturm TW, Amirtharajah A. 2005. Influence of sediment structure on erosional strength and density of kaolinite sediment beds. J. Hydraul. Eng. 131 (5): 356-365

Regazzoni PL, Marot D. 2013. A comparative analysis of interface erosion tests. Nat Hazards, 67: 937-950

Simon A, Thomas RE, Klimetz L. 2010. Comparison and experiences with field techniques to measure critical shear stress and erodibility of cohesive deposits. In Proc. 2nd Joint Federal Interagency Conference. Reston, VA., ASCE

Stein OR, Nett DD. 1997. Impinging jet calibration of excess shear sediment detachment parameters. Trans. ASAE 40(6): 1573-1580

Sutarto T, Papanicolaou AN, Wilson CG, Langendoen EJ. 2014. Stability analysis of semicohesive streambanks with CONCEPTS: Coupling field and laboratory investigations to quantify the onset of fluvial erosion and mass failure. J. Hydraul. Eng. 140(9). DOI: 10 .1061/(ASCE)HY.1943-7900.0000899

Tolhurst TJ, Black KS, Paterson DM, Mitchener HJ, Termaat GR, Shayler SA. 2000. A comparison and measurement standardisation of four in situ devices for determining the erosion shear stress of intertidal sediments. Continental Shelf Research 20: 1397-1418

Wahl T, Regazzoni PL, Erdogan Z. 2008. Determining erosion indices of cohesive soils with the hole erosion test and the jet erosion test. Dam Safety office report DSO-08-05, US Bureau of Reclamation, Denver, CO, USA

Wahl TL. 2016. The submerged jet erosion test: Past-present-future. USSD International Symposium on the Mechanics of Internal Erosion for Dams and Levees, Salt Lake City, UT, USA

Wan CF, Fell R. 2004. Investigation of rate of erosion of soils in embankment dams. J Geotech. Geoenviron. Eng. 130(4): 373-380

Weidner KL. 2012. Evaluation of the jet test method for determining the erosional properties of cohesive soils: A numerical approach. M.Sc. Thesis, Department of Civil Engineering, Virginia Polytechnic Institute and State University, Blacksburg, VA, USA

White FM. 2008. Fluid mechanics. 6th Ed., McGraw-Hill, New York, USA

Whitehouse RJS, Hardisty J. 1988. Experimental assessment of two theories for the effect of bed slope on the threshold of bed-load transport. Mar. Geol. 79: 135-139

Winterwerp JC, van Kesteren WGM. 2004. Introduction to the physics of cohesive sediment in the marine environment. Elsevier, Amsterdam, The Netherlands

Wynn TM, Mostaghimi S. 2006. The effects of vegetation and soil Type on streambank erosion, southwestern Virginia, USA. Journal of the American Water Resources Association (AWARA) 42(1): 69-82

CHAPTER V
SCOUR DEPTH PREDICTION IN COHEISVE SOIL

A version of this chapter is in preparation for publication by Badal Mahalder, John S. Schwartz, Angelica M. Palomino and Jon Zirkle.

Badal Mahalder, John S. Schwartz, Angelica M. Palomino and Jon Zirkle: **"The influence of cumulative effective stream power on scour depth prediction around bridge piers in cohesive earth material."**

Badal Mahalder, the senior author generated this manuscript as a part of his Ph.D. dissertation, and co-authors John Schwartz, Angelica Palomino, and Jon Zirkle supervised his research, in addition to direct text contributions to his study's manuscript.

Abstract

Scour in cohesive soils is complex where erosion processes depend on soil physical, geochemical, and biological properties; and erosion represented by a slow fatigue behavior. Therefore, repetitive loadings from multiple flow events are necessary for attaining an equilibrium scour depth in cohesive soils in contrast to that observed with non-cohesive soils. Cumulative effective stream power, which is a surrogate measure of effective stream power duration showed substantial impact on scour depth development in cohesive soils at bridge piers. Results from this study identified that a good correlation exists between cumulative effective stream power and the observed scour depths around different bridge piers ($R^2 = 0.56$, $p < 0.001$) with some localized and specific site variations. It was also identified that scour depth development in cohesive soils appeared to be dependent on the effective shear duration rather than number of flow events above the threshold values. Erodibility index (K) value showed a good correlation ($R^2 = 0.61$, $p = 0.017$) with critical stream power, clearly deviating from the Annandale developed empirical relationship for soils with $K < 0.1$. This finding supports that site specific critical stream power should be measured rather using an empirical relationship for cohesive sediments.

5.1 Introduction

Among many factors resulting in bridge foundation failure, local scour at piers and abutment is the most critical (Shirole and Holt, 1991; Wardhana and Hadipriono, 2003; Cook et al., 2015). Local scour is caused when the instream structure diverts turbulent hydraulic forces towards the streambed and these forces exceed the erosive resistance of earthen bed material. There are approximately 500,000 bridges in the United States that span over waterbodies (FHWA, 2017). During the past 30 years more than 1,000 bridges have failed and about 50-60% of those failures were due to hydraulic forces and bed scour (Shirole and Holt, 1991; Wardhana and Hadipriono, 2003; Cook et al., 2015). In Tennessee, among 20,169 highway bridges about 989 bridges have been designated as scour critical, which is about 5% of the existing bridges

(FHWA, 2017). Wu (2010) reported that older bridges constructed before 1960 are more susceptible to scour critical. Though design and construction of riverine bridge piers and abutments have improved, maintenance and replacement is currently a national priority (ASCE Infrastructure Report Card, 2017). Better predictive equations for local scour at bridge piers further improve on cost-effective designs.

Design equations for equilibrium scour depth at bridge piers most commonly applied and based on granular-type alluvial material (Richardson and Davis, 2001). Equations incorporated into HEC-18, developed for non-cohesive sediments have been extensively used for scour depth prediction regardless of soil type. An equation for pier scour on cohesive sediment has been developed by the Federal Highway Administration (FWHA), expressed as:

$$y_s = 2.2K_1K_2D^{0.65}\left(\frac{2.6V-V_c}{\sqrt{g}}\right) \quad (5.1)$$

where y_s is the maximum scour depth, K_1 and K_2 are the correction factor for pier shape and angle of attack, respectively, D is the pier diameter, V is the flow velocity, V_c is the critical flow velocity for scour initiation, and g is the gravitational acceleration. It has been reported that these equations can grossly under- and over-predict scour depth, which emphasizes the need for further research when the stream bed is composed of cohesive sediments (Benedict 2003, Brubaker et al. 2004, Pierce et al. 2011). Recently, a study conducted by the South Carolina Department of Transportation (SCDOT) and the US Geological Survey found HEC-18 equations over-predicted scour depth in cohesive sediments for 84% of bridge sites surveyed, with over-predicted depths ranging from 0.1 to 13.4 ft (Benedict and Caldwell, 2009). The study also showed 16% of the surveyed sites under-predicted the scour depth, which were a function of local bed sediment and geological conditions with high hydraulic resistance properties.

Erosion behavior of cohesive sediment is more complicated than non-cohesive soils due to chemical bonding forces of a consolidated mass, which leads to the uncertainty in scour prediction. The properties of cohesive sediment are analogous to a chemical gel, which erosion process is complex as both aggregates (clods) of materials and particles are detached from the sediment surface (Croad, 1981; Tan, 1983; Mehta et al., 1989; Annandale, 2006). Flow turbulence generated at the pier or other structures causes a positive pressure pulse acting on the sediment boundary enhancing pore pressure within the bed sediment. Over time the fixed chemical bonds between clay elements are broken down due to the repeated pressure fluctuations leading to clay aggregate removal known as the "plucking" phenomenon (Croad, 1981; Tan, 1983; Briaud et al., 2001; Annandale, 2006). The "plucking" erosion mode is common for both in consolidated cohesive sediments and rocks, though rocks also erode in other forms such as: dissolution, cavitation, and abrasion (Keaton, 2013). From field observations among sites in Tennessee, similarities of stream bed/bank erosion between rock and cohesive sediments were also identified (Figure 5.1.1).

Both in rocks and cohesive soils, the scour rate is slow and takes days to years for equilibrium scour depth and time dependent (Briaud et al., 1999; Ting et al., 2001; HEC-18, 2012). The time-dependent scour behavior of cohesive sediments identifies the necessity to consider the influence of long-term hydraulic history from multiple flow events over many years rather than considering a single flood event for maximum scour depth design as typically applied for non-cohesive sediments. This scour behavior with rock and cohesive boundary materials demonstrate the complexity associated with these types of material.

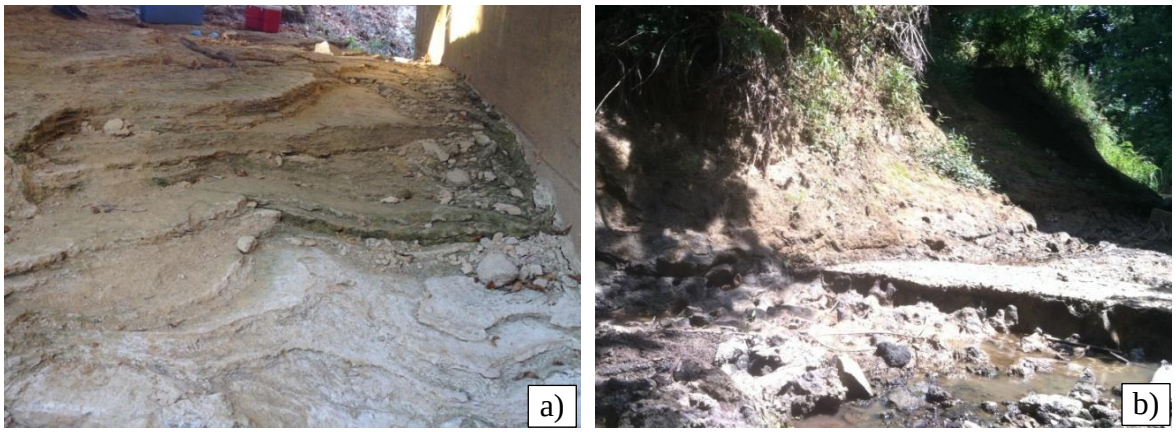


Figure 5.1.1: Erosion in cohesive soils: a) around bridge piers in Crooked Creek, Shelby County, TN, b) undercutting at the bottom of creek in Coal Creek, Tipton County, TN

Annandale (1995) introduced the concept of stream power (erosion capacity of water) and erodibility index (erosion resistance for earth material) for bridge scour study. The concept of erodibility index was first introduced by (Kirsten, 1982) and in the early 1990s number of researchers analyzed field and laboratory scour data for identifying relationship between stream power and erodibility index value (Annandale, 1995, 2006). This concept has been used for bridge foundation on rocks and head-cut erosion studies in spillways. In those studies, critical stream power has been calculated based on the functional relationship between erodibility index and stream power. Because the cohesive soil erosion process is complex; the use of an empirical relationship for critical stream power calculations could be problematic. Furthermore, previous scour studies with cohesive sediment around bridge piers and abutments have not related critical stream power and duration history to pier scour development. The possible lack of published studies could be due to availability of long-term scour data, and the difficulty of measuring the critical shear stress (τ_c) of the soil/sediment near bridge sites. To date, no study has quantified the relationship between erodibility index and the effective cumulative stream power in cohesive sediments, only observed time-independent direct scour relations to stream power.

This study uniquely measured τ_c and modeled long-term flow history to estimate cumulative effective stream power and its relation on pier scour depth on cohesive sediments. The objectives were to examine whether bed scour rates are a function of erosive flood history quantified as effective cumulative stream power (sum of stream power duration over critical shear stress), in addition, whether an erosion index (*K*) (proposed by Annandale (1995)) for cohesive soil erodibility correlates with critical stream power. The hypothesis is that bed scour on cohesive soils is a time-dependent function which can be associated with effective cumulative stream power. Other factors also affect scour rates such as the geophysical characteristics of the soil, bridge pier configuration, and channel geometry at and upstream of the structure. Secondarily, this study provides some insight on the time-dependency scour behavior in terms of scour depth equilibrium at bridge piers.

5.2 Methods

5.2.1 Study Design

The study utilized bridge scour data collected at nine bridge sites on streams in western Tennessee where the bank/bed materials are predominantly composed of cohesive (silt/clay) soils (Figure 5.2.1). Long-term scour data around bridge piers and abutments were collected from the Tennessee Department of Transportation (TDOT) bridge inventory database (Table 5.2.1). Scour data were not available from the period immediately following bridge construction, except for the Pond Creek bridge site. The drainage basin size varied among the nine study sites ranging from 19 to 151 km^2.

In order to compute the cumulative effective stream power and number of days exceeding τ_c, each site required long-term hydrological modeling from the time of bridge construction completion through the dates in which bridge scour data were collected. Hydrological modeling estimated the flow record for each site applying climatic variable inputs. In addition to flow,

stream power (Ω) and reach-scale hydraulic shear stress (τ) calculations required channel slope and cross-sectional geometry. The mini-jet tester, an in situ field device was used to estimate τ_c of the streambed/bank cohesive soils near the bridge site (Mahalder et al. 2017, 2018). Per site, the flow discharge (Q) where $\tau > \tau_c$ was used as the threshold Q to estimate effective stream power (Ω_e), in other words the critical stream power (Ω_c) that can scour the local cohesive soils. The cumulative effective stream power sums the Ω over a unit time interval where $\Omega_c > \Omega$. Calculation of site K, τ_c, Ω_c, and effective cumulative stream power, and measured scour depths (Δy_s) at bridge piers were used to examine the following relationships: 1) K vs Ω_c; 2) Δy_s vs cumulative effective stream power, and 3) number of days exceeding Ω_c vs $\Delta y_s/y_t$, where y_t is the total measured scour depth.

In the TDOT bridge inventory dataset among these nine stream sites, Pond Creek site had scour data available from the beginning of bridge construction. These scour depth data over 20 years provided the information to observe the temporal variability of pier scour depth over the long-term flow history and estimate the equilibrium condition for scour depth. Qualitative assessment of scour behavior was conducted with the hydrological and scour data for this stream site. It also provided a context to evaluate the results relating Δy_s vs cumulative effective stream power suggesting which measurements represent equilibrium depths. Pond Creek is a 3rd order stream with contributing watershed area of 139.96 km^2 at the bridge site and the bankfull width is 31.27m, which is an undeveloped/rural ungaged watershed. In the watershed, 84.63% of the total area is agricultural land, 8.03% medium residential area, 4.75% water body, and 2.59% forest area. The bridge length is 35.50 m with two abutments and two piers both in the channel with flow and substantial scour at Pier#1 was observed.

Table 5.2.1 Study sites characters including the watershed and bridge

Creek Name	County	Latitude	Longitude	Watershed Area (km^2)	Bridge Construction Year	Highway No.	Bridge Pier type	Bridge Length (m)	No. of scour data points	Percent impervious	USGS data availability
Beaver Creek	Carroll	36.01304	-88.445056	151.23	1969	SR 77	Square Bent	106.70	6	1.53	1962-1994
Black Creek	Crockett	35.815902	-89.320778	70.12	1974	SR 88	Circular	78.30	10	1.13	N/A
Pond Creek	Dyer	35.921027	-89.325277	139.96	1990	0A 443	Round Nose	35.50	6	1.33	N/A
Mud Creek	Haywood	35.678261	-89.132721	64.60	1934	SR 076	Square Bent	95.40	5	1.24	N/A
Cane Creek	Lauderdale	35.75975	-89.522583	87.60	1982	SR 209	Rectangular	33.80	11	2.33	1957-1987
Richland Creek	Obion	36.262007	-89.212328	45.28	1980	SR 183	Round Nose	46.60	8	0.51	N/A
Big Creek	Shelby	35.342108	-89.806569	83.29	1966	SR 205	Square Bent	51.20	8	3.17	N/A
Crooked Creek		35.323894	-89.807139	44.63	1952	SR 14	Round Nose	65.20	6	1.37	N/A
Coal Creek	Tipton	35.5526	-89.585556	19.00	1986	SR54	Round Nose	43.00	5	0.95	N/A

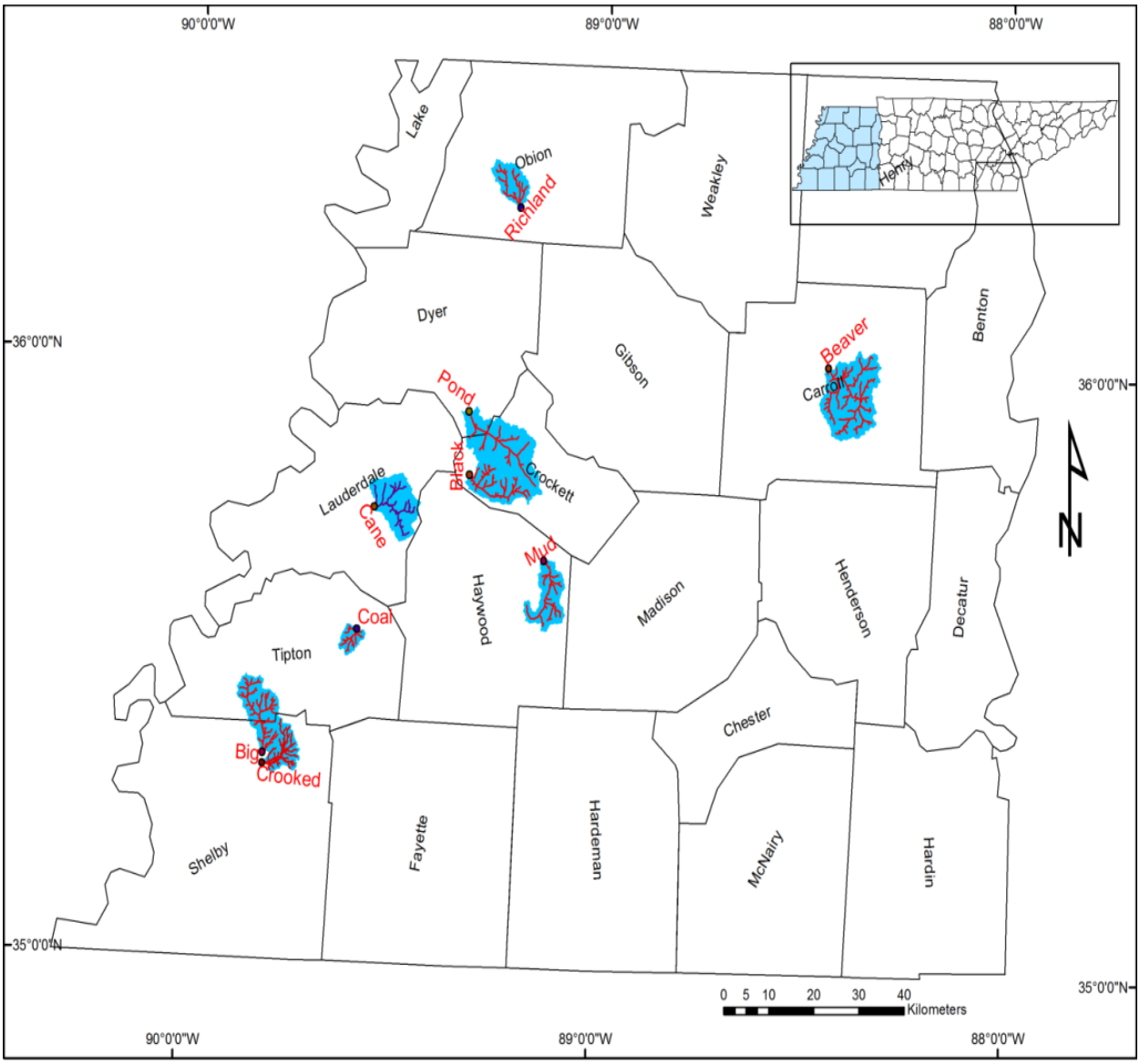


Figure 5.2.1: Study watersheds showing locations of bridge sites in western Tennessee

5.2.2 Erodibility index calculation

The erodibility index *K* is a geomechanical property of earthen material, which is used to quantify the relative resistance of rock and other materials from the erosive capacity of flowing water (Annandale, 2006). Annandale (1995, 2006) reported an empirical relationship between stream power and erodibility index for soils with lower erodibility index values. The erodibility index is defined as:

$$K = M_s \cdot K_b \cdot K_d \cdot J_s \quad (5.2)$$

where M_s is the mass strength number; K_b is the block size number; K_d is the discontinuity bond shear strength number; an J_s is the relative ground structure number. M_s for cohesive sediments can be calculated based on either the vane shear strength value or UCS values (Moore, 1997; Annandale, 2006).

$$M_s = 0.78(UCS)^{1.09} \text{ for } UCS \leq 10 MPa, \text{and } M_s = UCS \text{ for } UCS > 10 \text{ MPa} \quad (5.3)$$

The K_b value for intact cohesive soil is used as 1 and the K_d value is calculated using the drained residual friction angle (φ).

$$K_d = \tan \varphi \quad (5.4)$$

φ can be calculated using the liquid limit (*LL*) of tested cohesive soils and three ranges of clay size fraction (USDS-NRCS, 1997).

$$\text{For } \leq 20\% \text{ clay}, \varphi = 169.58(LL)^{-0.4925} \quad (5.5)$$

$$\text{For } 25 - 45\% \text{ clay}, \varphi = 329.56(LL)^{-0.7100} \quad (5.6)$$

$$\text{For } \geq 45\% \text{ clay}, \varphi = 234.73(LL)^{-0.6655} \quad (5.7)$$

Cohesive soil material is considered intact (without structure), so J_s = 1 (Moore, 1997; Annandale, 2006). In this study, all of these parameters were calculated based on the measured soil properties according to above mentioned guidelines.

5.2.3 Hydrologic flow simulation

Daily flow data was necessary for stream power calculations, which were obtained from the USGS gage stations when data were available. Only two of the sites had limited USGS data. With most study streams being ungaged, hydrological flow simulations were required (Table 5.2.1). The hydrological model HEC-HMS 4.0 was used for the long-term daily flow simulation. Necessary supporting files for HEC-HMS 4.0 were generated using ArcGIS 10.1, where HEC-GeoHMS tool was used for watershed delineation. Long-term flow simulations required climatic variables inputs including: precipitation, air temperature, and evapotranspiration were collected from the NOAA website (https://gis.ncdc.noaa.gov/). DEM, land cover, percent impervious data were collected from USGS TNM 2.0 viewer (https://viewer.nationalmap.gov/) website. SSURGO soil database was collected from web soil survey of USDA (https://websoilsurvey.sc.egov.usda.gov/) for necessary watershed parameters calculation.

In the ungaged watersheds, parameters obtained from another hydrologically and geologically similar gaged watershed were used for the long-term flow simulations. Pond Creek is an ungaged watershed, which is hydrologically and geologically similar to the Stokes Creek watershed (USGS gage station 07029035) of Crockett County (Figure 5.2.1). From the available daily flow data, model was calibrated (data from January 1999 to December 31, 1999), and for model validation, data from January1, 2000 to May 31, 2000 were used for Stokes Creek watershed. The yearlong data was used for model calibration to account the seasonal variation in the watershed for estimating different parameters used in HEC-HMS simulation for Pond Creek watershed. The calibrated results illustrated in Figure 5.2.2a were in good agreement with the observed and simulated daily flow data.

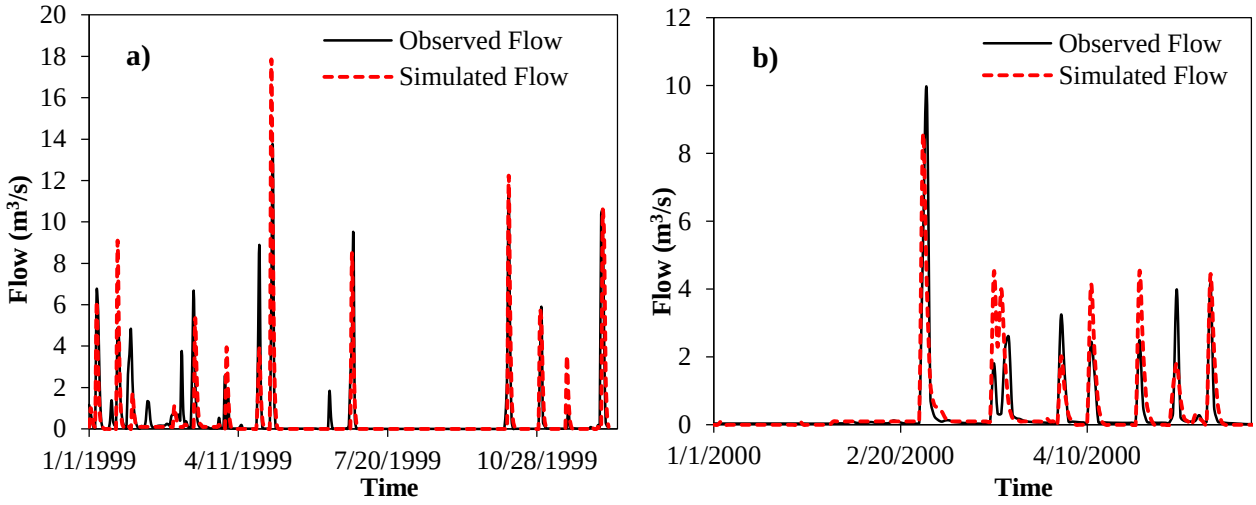


Figure 5.2.2: Simulated flow for gaged watershed (Stokes Creek): a) model calibration, b) model validation

However, two peaks: one in March 1999 and another one in June 1999 were not captured by this model. The differences in peaks were likely due to variations between precipitation station data and actual conditions in the watershed where summer storms can be quite localized. During the model validation, simulated daily flow events demonstrated good agreement with the observed data based on plot inspection (Figure 5.2.2b). The peak flows were captured very well with some deviation as some peaks were over estimating and some peaks were underestimating. The statistical errors were calculated to validate the model further. From the statistical error analysis (Table 5.2.2), it was found that the errors were in an acceptable range for a hydrological modeling similar to this type of watersheds as reported by Fleming and Neary (2004).

Finally, the necessary hydrological model input parameters from the Stokes Creek watershed were used for the ungaged Pond Creek watershed. Flood frequency analysis was also conducted using the simulated flow for the ungaged watershed using the Bulletin 17B method in HEC-SSP and compared with the TDOT regression equations by computing different peak

flows. Figure 5.2.3 demonstrates a typical output from the HEC-HMS model using Pond Creek as the example. Similar procedures were followed for the other ungaged watersheds in this study.

Table 5.2.2 Statistical error calculation and validation targets

Error Type	Calibration	Validation
Mean Absolute Error $(1/n)\sum\lvert(Q_0 - Q_s)\rvert$	1.25	2.53
Root mean square error $\sqrt{\left[\sum(Q_0 - Q_s)^2\right]/n}$	6.99	7.07
Average error in magnitude of peaks (%) $\left[(1/n)\sum\lvert(Q_0 - Q_s)/Q_0\rvert\right] \times 100$	55.50	58.39

5.2.4 Field measurements of stream bank/bed soil critical shear stress

In this study stream bank/bed τ_c measurements of cohesive soils were obtained by the use an in-situ mini-jet test device (Simon et al., 2010; Al-Madhhachi et al., 2013). The submerged jet device was developed for measuring soil erodibility parameters in-situ, but it can also be used in the laboratory. For jet operation, a constant head is necessary, which was maintained using a pump that delivered stream water powered by a 2000 W portable generator. Field operational and computational procedures for jet operation and data analyses are described in detail by Mahalder et al. (2018). Per stream sites, 4 to 5 jet tests were conducted around the bridge piers or at lower bank to find the average τ_c for a stream from May 2015 to August 2015. After completing each test, two core soil samples near the test location were collected using a 5.08 cm dia. cylindrical stainless steel coring instrument. These core samples were used to measure bulk density (BD), water content (WC) and unconfined compression strength (UCS). The core cylinders were immediately end capped and sealed in an air-tight plastic bag to minimize moisture loss. Approximately 1.4 kg of soil was also collected per test site from inside the jet

device's bottom ring for laboratory analyses of other soil physical properties: grain size distribution, LL, plastic limit (PL), plasticity index (PI), and organic content.

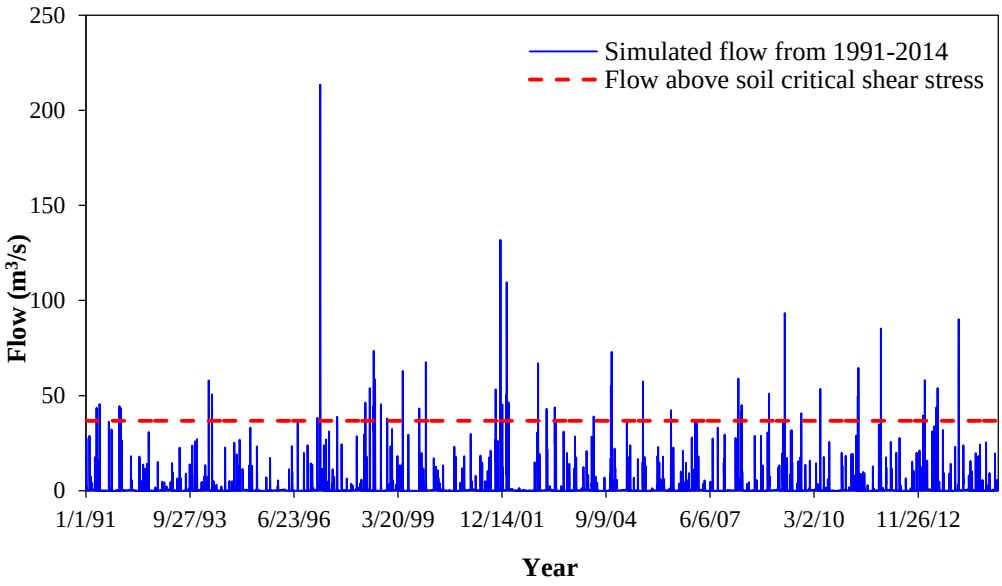


Figure 5.2.3: Example flow simulation for Pond Creek in Dyer County, West Tennessee, and the flow threshold at critical shear stress

5.2.5 Effective stream power calculation

Stream power defines the capability of a stream to transport sediments as bed load and fine sediments in suspension (Bagnold, 1960). Numerous researchers have used stream power (Ω) for sediment movement (Leopold et al., 1964; Hickin and Nanson, 1984; Sklar and Dietrich, 2004; Larsen et al., 2006) based on Bagnold (1960) theory, which is calculated from the stream flow data and channel slope. The excess stream power or Ω_e is the difference between the stream power due to daily flow and Ω_c, which can be calculated using the following equations.

$$\Omega = \rho g Q_n S \quad (5.8)$$

$$\Omega_c = \rho g Q_c S \quad (5.9)$$

$$\Omega_e = \Omega - \Omega_c \quad (5.10)$$

where Ω is the stream power per unit width of channel (W/m^2); ρ is the density of water (kg/m^3); g is the gravitational acceleration (m/s^2); Q_n is the daily discharge (m^3/s); Q_c is the threshold stream power per unit width of channel (W/m^2) above which erosion will take place; and S is the channel slope (m/m). In order to calculate the Ω_e, threshold discharge for scour was calculated for each stream sites from the measured τ_c values from jet tests, channel roughness data (Manning's n) and the channel cross-sectional data by assuming uniform flow. In literature, a threshold hydraulic condition for scour is identified through numerous forms, e.g., critical flow velocity, critical shear stress for earth material, critical stream power, or bankfull/channel-forming discharge.

Stream cross-sectional data and scour data around the bridge foundations were collected from the TDOT bridge inventory database. Cumulative effective stream power was calculated based on the scour depth data measurement frequency found in the TDOT bridge inventory database for each stream sites. Flow data was also used for calculating the number of events above the threshold discharge. These data were used to observe the influence on scour pattern at different soil types and pattern of scour development around those bridge sites.

5.3 Results

5.3.1 Behavior of the data

Among the nine study sites, soil were predominantly silty-loam and silty-clay-loam, where LL values were between ~28-37%, BD ranged from 1.79 g cm^{-3} to 2.06 g cm^{-3} and D_{50} was between 9.0 µm and 24 µm (Table 5.3.1). The tested soil samples were characterized as cohesive since plasticity index values were >10% and clay content was >10% by weight (Raudkivi, 1990). However, the cohesion values showed wide range in the dataset.

Measured τ_c from in-situ jet test were used to calculate the threshold discharge or termed the effective flow per study stream sites, which are the flows that generate reach-scale shear

stress (τ) over τ_c. Measured τ_c are in Table 5.3.1. The bridge at Mud Creek was the oldest studied bridges in this study, though in 2010, major repair works have been conducted on this bridge sites. Average τ_c values ranged between 4.20-17.67 Pa among these stream sites and the corresponding critical flow was between 7.05-50.30 m^3/s. The channel slope was mild around the bridge location and varied between 0.000123 (m/m) to 0.000976 (m/m). Calculated Ω_c varied between 37.31 W/m^2 to 482.84 W/m^2. Contributing watersheds of the studied streams were undeveloped as percent impervious area among these watersheds was between 0.51 and 3.17%.

Table 5.3.1 Soil properties, erodibility index parameters, critical shear stress and critical stream power per unit width of channel, and channel slope for the nine study sites

Creek Name	BD (g/cm^3)	D_{50} (μm)	Cohesion (kPa)	Clay%	LL	Erodibility Index, K	Average critical shear stress, τ_c (Pa)	Critical flow (m^3/s)	Critical Stream Power (W/m^2)	Average Channel Slope at bridge location (m/m)
Beaver Creek	2.06	13.00	88.08	28	27.80	0.082	10.15	50.30	443.12	0.000604
Black Creek	1.96	14.60	59.81	24	35.40	0.046	12.00	20.56	314.98	0.000976
Pond Creek	2.02	9.00	61.01	39	35.00	0.050	5.72	36.80	272.46	0.000694
Mud Creek	1.86	11.50	31.51	25	28.60	0.017	10.10	12.60	207.18	0.000123
Cane Creek	1.79	18.00	38.61	18	29.00	0.027	4.20	10.81	98.84	0.000932
Richland Creek	1.81	24.00	22.06	14	29.40	0.013	5.45	7.98	37.31	0.000261
Big Creek	2.01	15.80	67.05	22	27.80	0.073	14.80	16.97	160.32	0.000963
Crooked Creek	2.05	12.00	67.56	25	29.00	0.078	17.67	27.78	482.84	0.000285
Coal Creek	1.89	15.00	70.46	29	36.60	0.062	13.40	7.05	322.69	0.000970

The relationship between K and Ω_c was developed from the data analysis for these nine stream sites. A good functional correlation between critical stream power and erodibility index was observed (R^2 = 0.61, p = 0.017) with a power function (Figure 5.3.1). However, this observed power function deviated from the proposed relationship developed by Annandale (1995, 2006) for soil with erodibility index value less than 0.10. (Wibowo et al., 2005) developed

a probabilistic approach by logistic regression method to quantify the erosion probability based on the Annandale (1995, 2006) threshold line. Findings from this analysis showed that all the data for these studied stream sites were enclosed between the 99% probability and 1% probability lines (Figure 5.3.1).

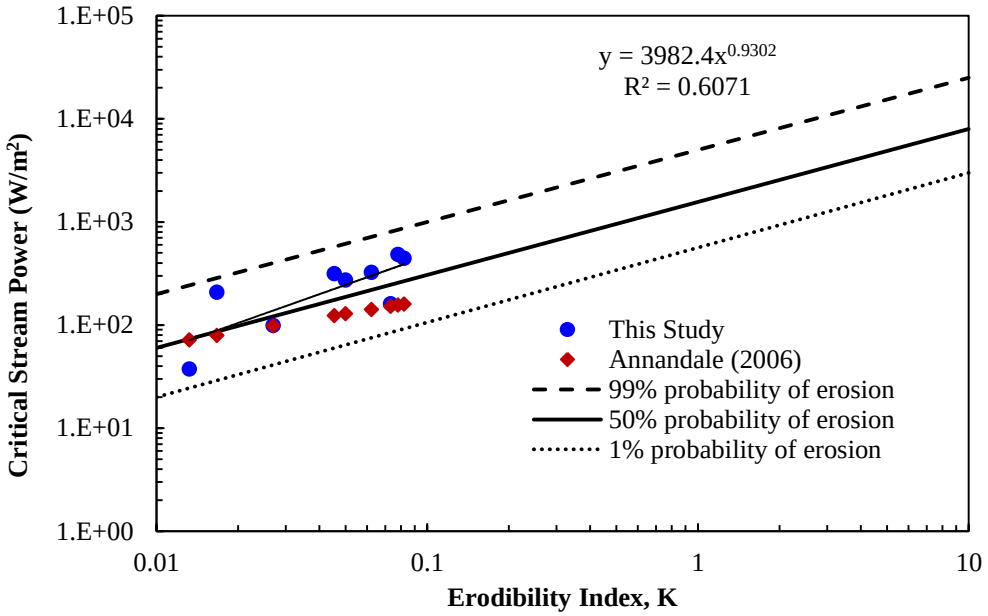


Figure 5.3.1: Relationship between critical stream power and erodibility index. Where probability of erosion was calculated using the Wibowo et al. (2005) proposed probabilistic approach using logistic regression method

The scour depths (Δy_s) was computed and compared with the cumulative effective stream power for the specified duration in which bridge scour depth was measured (Figure 5.3.2). The pattern of this dataset shows that a good correlation exists between effective cumulative stream power and the depth of scour ($R^2 = 0.56$, $p < 0.001$). However, in some cases at lower cumulative stream power, very high erosion rate was observed. The influence of flow history on scour development among these studied streams sites over multiple years and flood events was also analyzed by examining the number of days above critical flow and a non-dimensional scour

depth value $\Delta y_s / y_t$ (Figure 5.3.3). This result showed three distinct areas (Area "A", "B", "C") in the dataset, which were found dependent on the soil properties, number of continuous flow events above critical value, and the age of a bridge.

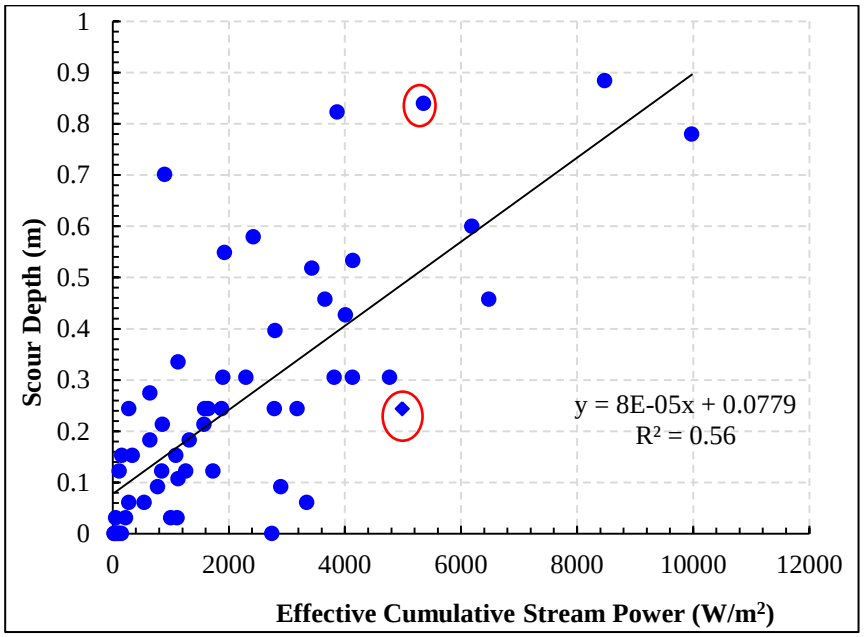


Figure 5.3.2: Relationship between cumulative effective stream power and scour depth measurement. Circled data points represent measurements at the Crooked Creek site

Analyzing the characteristics of the dataset in those zones, it was observed that in the enclosed area "A", at lower number of flow events (< 20 events) relative scour depths were higher compared with the enclosed area "B" on the same figure. Soil physical properties and erodibility data showed that both the τ_c values (4.20-6.10 Pa) and the soil cohesion (22.06-38.61 kPa) values were low expect for Pond Creek where τ_c was 5.72 Pa and cohesion was 61.01 kPa (Table 5.3.1). Area "C" in Figure 5.3.3 represents the more recent scour depths data, where both the short duration higher peak flow events and the longer duration moderate flow events were observed.

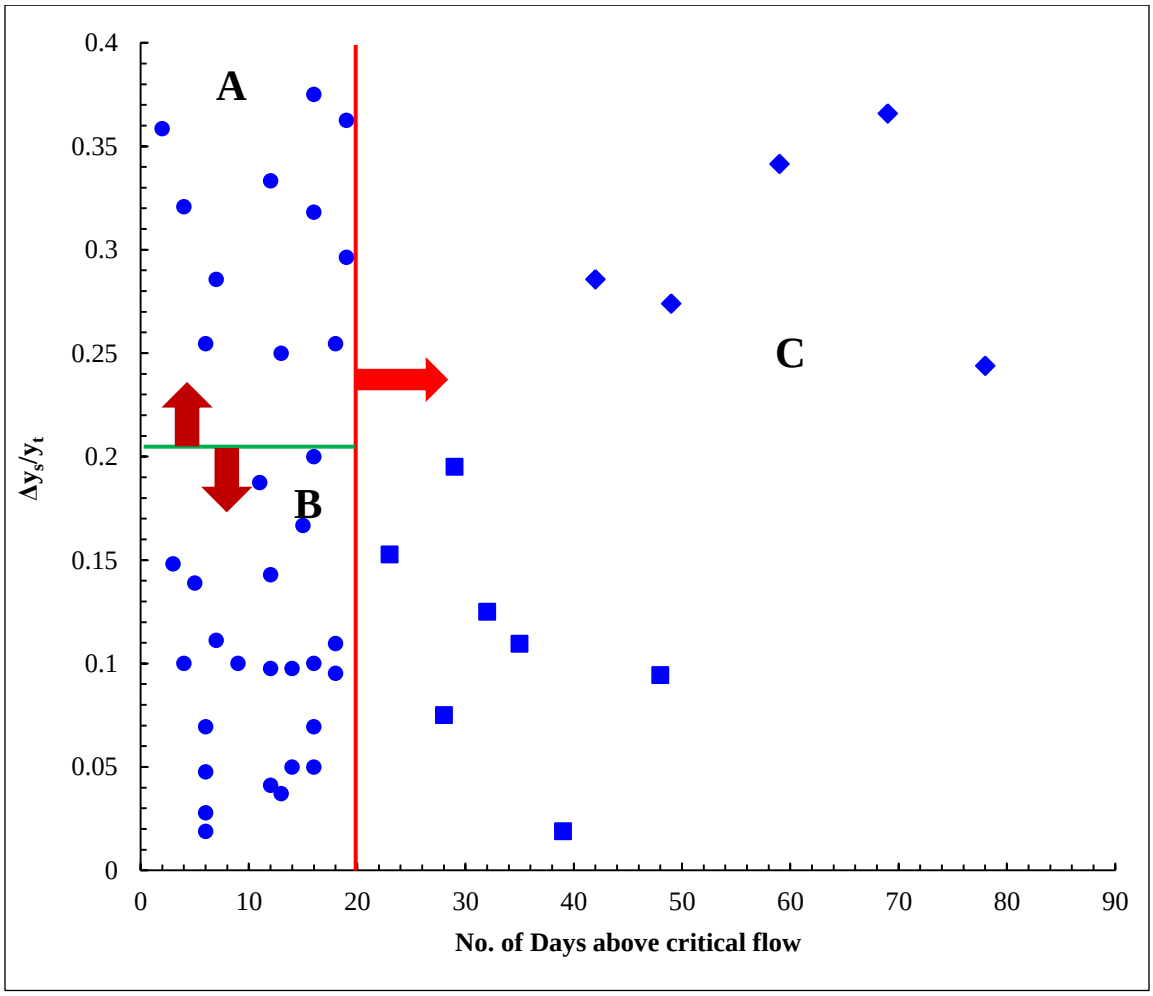


Figure 5.3.3: Relationship between relative scour depth and the number of flow events above the critical flow for the studied stream sites. Solid circles = regular scour data points, diamonds = scour data before 2004 with longer duration flow events; and squares = scour data after 2004 with short duration flow events

5.3.2 Case study for Pond Creek site on scour pattern

At the Pond Creek bridge site, TDOT measured scour depths over 20 years showed some interesting trends with three different scour rates (Figure 5.3.4). Computing the critical flow from channel geometry and measured average τ_c data, it was observed that both short duration high peak and continuous moderate flow events occurred between the year 1991 and 1999 (Figure 5.2.3), consequently very high scour rate (0.25 m/year) was observed (Figure 5.3.4, Zone-A). After the year 1999, scour rate receded (0.07 m/year) substantially (Zone-B). In the year 2000, no flow events were observed above the critical and possible deposition took place since elevated bed profile was observed (Figure 5.3.4, Zone-B). Number of flow events above the critical flow was plotted on the same graph (Figure 5.3.4). Analyzing the graph, it was found that even though several flow events were above critical, no significant scour rate was observed. Specifically, the erosion rate reduced dramatically after the year 2002.

5.4 Discussion

For equilibrium scour depth calculation, the erosive capacity of flowing water has been calculated by several methods including average flow velocity, shear stress, peak flow, and stream power. The FHWA developed three technical guidance for bridge foundation design; they are: HEC-18 (for developing scour evaluation program and 0analyzing bridges for scour), HEC-20 (for analyzing the effect of stream instability on bridges), and HEC-23 (countermeasures for mitigating potential damage to bridges and highways at stream crossings). The FHWA applies risk-based approaches for bridge scour assessment and design by considering the structural safety and reliability, and corresponding economic consequences of failure. In this approach, bridges are designed for 100-year flood and checked with the 500-year flood event (HEC-18, 2012).

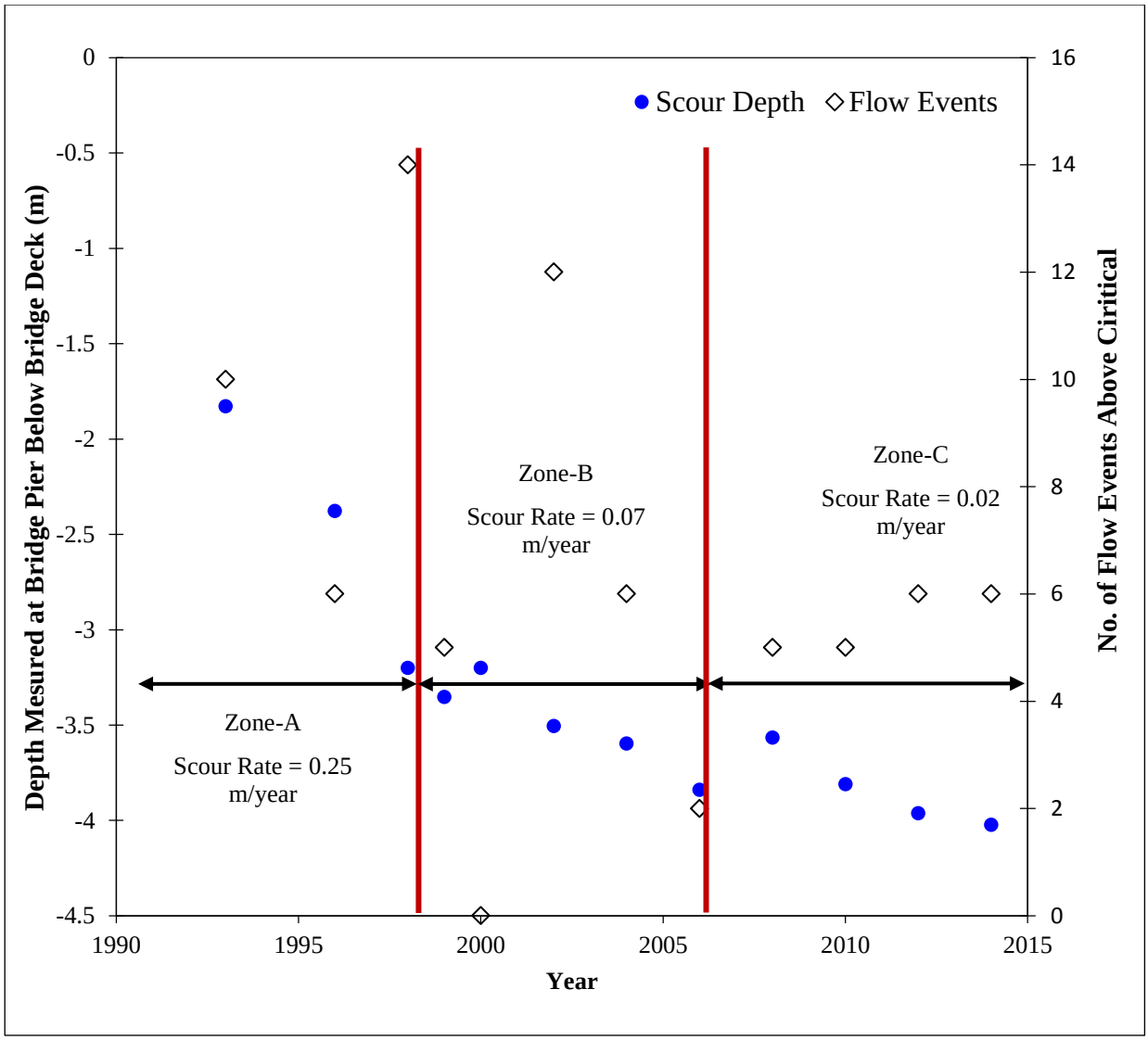


Figure 5.3.4: Long-term scour depth data and the number of flow events above critical flow at the bridge pier for Pond Creek showing three different scour rate over a 20-year period

Pier scour in cohesive soils are slow and time dependent, where many factors influence scour development rates and equilibrium depth. The cumulative effect of long-term flow history from many flood events over many years is required to predict scour depth rates to reach equilibrium, rather than applying hydraulic loading from a single flood event (Kwak, 2000; Briaud et al., 2001; HEC-18, 2012'; Keaton et al., 2012).

Numerous studies reported relationships between stream power and various forms of sediment detachment and transport (Bagnold, 1960; Yang, 1972; Yang, 1973; Chang, 1979; Annandale, 1995; van den Berg, 1995; Annandale, 2006). It has been reported that erosion behavior soil with high silt-clay content or cohesive sediments is dominated by subaerial processes or excess shear stress duration in the flow hydrograph (Costa and O'Connor, 1995; Julian and Torres, 2006). However, sediment encroachment and movement around bridge piers and abutments are fundamentally different from the fluvial erosion process. HEC-18 (2012) introduced an equation for predicting equilibrium scour depth in cohesive soils based on mean and critical flow velocity. This time-dependent phenomenon has been introduced in the scour prediction procedures based on a proposed method by Briaud et al. (2011). This proposed method was developed based on laboratory experiments with commercially available clay soil. However, it is understood that the complex interaction between soil physiochemical and biological properties is not possible to develop in the laboratory. It is also understood that numerous number of flow events above critical might occur for natural streams. It was hypothesized that in cohesive soils, cumulative shear stress duration/cumulative stream power over a critical value for scour initiation could be valuable. Similarities exist between rock erosion and the cohesive soil erosion behavior, though orders of magnitude higher erosive capacity of flowing water is required for rock compared with the consolidated cohesive sediments.

Therefore, possible deviations from the empirical relationship between K and Ω_c for cohesive soils were also studied.

Annandale (1995, 2006) estimated the critical stream power/erosive power required for scour initiation based on a functional relationship with the K value. In this method, only three soil properties, USC, clay content and LL are necessary to calculate the K value. Based on published data from numerous studies, Annandale (1995, 2006) proposed a power relationship to predict Ω_c for earth material when K value is less than 0.1 (Figure 5.3.1). Data from this study as calculated from the in-situ τ_c measurement and the channel geometry showed a clear deviation from the Annandale (1995, 2006) proposed empirical relationship. Non-parametric Mann-Whitney U test also identified that the median values were statistically different ($p = 0.024$). It is important to note that Ω_c calculated from the in-situ measurement showed a good correlation with the K value (Figure 5.3.1). It was assumed that variation in these data could be related to simplified analysis procedures and fundamentally different inherent erosive resistance properties of the tested cohesive earth material. Wibowo et al. (2005) identified that a probabilistic approach better quantifies erosion behavior of highly variable earthen material based on Annandale (1995, 2006) study. Data from this study also fits well in between those proposed erosion probability lines of 99% and 1% as per the Wibowo et al. (2005) equation. It is hypothesized that the influence of erosion properties or prediction of τ_c values for cohesive earth material could have significant influence on the threshold stream power calculation, consequently influenced the observed variation from the Annandale (1995, 2006) proposed relationship. Therefore for calculating Ω_c, the in-situ τ_c measurement could be an alternative approach for cohesive sediment as developed in this study.

Effective stream power acting on soil surface is a surrogate measure for shear duration or excesses shear stress above critical value in erosion study where hydraulic loading is critical for maximum scour depth development. A total of 65 scour depth measurements at bridge piers were available from TDOT bridge inventory database among this study sites. Measured scour depth data over time were directly correlated with cumulative effective stream power among these studied stream sites ($R^2 = 0.56$, $p < 0.001$) (Figure 5.3.2). In Figure 5.3.2 a few high scour depths were associated with lower cumulative stream power estimates. From field observations during the in-situ jet test operations, it was identified that in some streams a non-cohesive granular material layer blanketed cohesive soil layer at the stream bottom, and among the other cases stream beds were exposed with the cohesive sediment layer. It is hypothesized that during low flow events as sediment capacity of the flowing water receded, transported granular (non-cohesive) sediments were deposited on the streambed and presumably within the scour holes. Consequently, during short peaked flow events above the erosion threshold might have eroded those granular materials around bridge piers and a big jump in scour depth was observed (Figure 5.3.2). Further analyzing the daily flow data for each stream and the corresponding scour depth value, it was identified that not only the number of flow events flow duration over critical had significant influence on the observed scour depth pattern.

Several studies identified the influence of flow duration, flow magnitude and flow frequency on erosion behavior in different earth materials for both the bank erosion, fluvial erosion (channel incision) and localized scour around structures (Wolman, 1959; Costa and O'Connor, 1995; Julian and Torres, 2006; Keaton et al., 2012). Costa and O'Connor (1995) showed that short duration spikes with higher flow intensity might not generate sufficient erosive power for cohesive soils to be scoured compared with long duration medium intensity flood

events. Similar observations were also reported by Julien and Torres (2006) for bank erosion estimation in cohesive sediments. In this study, it was identified that at lower cumulative effective stream powers (< 2000 W/m^2) generally produced lower scour depths with some exception as for Richland Creek and Mud Creek data (Figure 5.3.2). In those two streambeds, substantial amounts of granular material (sand and gravel) were observed on the top of cohesive sediment layer during field tests. Therefore, short duration flashy flow events could have removed the granular material from the vicinity of the pier and higher scour depths readings were recorded.

A major disparity among this study's dataset was observed when the cumulative effective stream power range was between 2000-5200 W/m^2 (Figure 5.3.2). In this stream power range, both the flow and the soil physical properties influenced the erosional behavior. Specifically with soils having a higher *K* values per Beaver Creek, Big Creek, Coal Creek, and Crooked Creek data had lower scour depths and represent those data points below the regression line as presented in Figure 5.3.2. Among the other studied streams, higher scour depths were observed. For both of these cases, the influence of flow duration was also identified as the key controlling variable. Cumulative effective stream power above 5200 W/m^2 showed an interesting trend in the dataset. In this region, the longer flow duration above critical value could have influenced for the higher scour depths, since more continuous flow events were observed in the flow hydrograph except for Crooked Creek data (represented in a circle above the best fit line in Figure 5.3.2). In Crooked Creek, several wooden logs were found driven into the stream bed close to the pier foundation for protecting bank failure (Figure 5.4.1). It is hypothesized that the local turbulence due to wooden logs near the pier could have influenced the higher scour depth

since after that measurement very low scour depth was observed (data points in a circle below the best fit line in Figure 5.3.2).



Figure 5.4.1: Protective wooden logs at the vicinity of the pier in Crooked Creek

For investigating the influence of shear stress duration above critical threshold for erosion, relative scour depth values were plotted against the number of flow events above critical flow using the simulated flow data (Figure 5.3.3). In this analysis, three distinct zones were identified. Higher relative scour depths were observed inside the enclosed area "A" compared with the enclosed area "B". As expected, lower relative scour depths were observed for the stream sites with higher τ_c and higher cohesion values at lower number of flow events above the critical flow (area "B" of Figure 5.3.3). However, in the area "C" in Figure 5.3.3, the influence of both the flow duration and the time of scour depth measurement were identified. It was observed that for higher relative scour depth data, several continuous flow events were observed during the scour depth measurement periods (diamond-shaped points, Figure 5.3.3), consequently higher relative scour depth values were observed. Conversely, short duration and isolated flow events above a critical value showed lower relative scour depths though the number of flow

events was higher (square points in figure 5.3.3). These observations were supported by other studies for fluvial erosion process of cohesive earthen material (Costa and O'Connor, 1995; Julien and Torres, 2006; NRCHP, 2012).

The combination of number of flow events and the influence of flow duration on scour rate propagation was observed from the Pond Creek data (Figure 5.3.4). Though cohesion for Pond Creek was high (61.01 kPa), at lower number of effective flow events, relatively higher scour depths were observed during the early age of the bridge. It is hypothesized that channel geomorphology was still adjusting from the local hydrodynamics at the vicinity of the bridge, consequently higher relative scour depths were observed. It was also observed that, scour depths reduced significantly after 1999, even though several continuous high to moderate daily flow events were observed. After 2006, scour rates was reduced significantly. The probable explanation could be the state of equilibrium might have been attained due to the repeated flood events above critical for this bridge site. Observing the evolution of scour depth around the pier of this these bridge and the corresponding flow events, an agreement with the previously stated hypothesis was established, where both the cumulative effective stream power and the number of flow events above critical flow had substantial influence on scour depth propagation in cohesive soils. Flow duration is also found significantly influencing the scour pattern as identified by other studies.

In this study, some limitations were identified to achieve an outcome of a predictive relationship between cumulative effective stream power and an equilibrium scour depth in cohesive sediment beds. They included a lack of channel cross-sectional data over time which could have influenced the critical flow calculation, since one cross-sectional data was used for the calculation by assuming uniform flow depth. Also scour data were collected by several

TDOT operators without a standard operating procedure. Further research is needed to development predictive relationships through a well-designed and long-term field study initiated immediately following completion of a constructed bridge.

5.5 Conclusions

The influence of shear stress duration for scour prediction in cohesive earthen material around bridge piers was investigated in this study. Cumulative effective stream power is thought to be a surrogate measure to the shear stress duration over a τ_c threshold for erosion. Using the in-situ measured τ_c values and the recent measured channel geometry data, critical/threshold steam power was computed for the studied stream sites. Calculated erodibility index values and the corresponding critical stream power estimates were significantly correlated ($R^2 = 0.61$, $p = 0.017$). Data from this study showed a clear deviation from the Annandale (1995, 2006) developed empirical relationship for soils with erodibility index value less than 0.1. Although these values were fitted in between the 99% and 1% erosion probability lines as suggested by Wibowo et al. (2005) using logistic regression approach. This finding supports the hypothesis that erosion behavior in cohesive sediments should be considered for the critical stream power calculation rather using an empirical relationship.

It was also hypothesized that the flow duration in association with the cumulative stream power over a scour depth measurement period could have significant impact on scour depth development. Collecting long-term scour depth data from the TODT bridge inventory for the selected nine stream sites this study has been conducted. It appeared that cumulative effective stream power showed a reasonable correlation with the observed scour depths around different bridge piers among these stream sites with some localized and site specific variations ($R^2 = 0.56$, $p < 0.001$). Scour depth development in cohesive soils appeared to be dependent on the effective

shear stress duration rather than number of flow events above the critical threshold values. The influence of flow history on scour rate propagation in cohesive earth material from multiple flow events was observed from the Pond Creek data where continuous scour depths were recorded from the time of bridge construction.

Overall, it appears that scour depth can be predicted by calculating the critical stream power from the τ_c values and channel geometric data. Though, the erodibility index method for scour prediction is not a new concept, cautions should be taken for predicting the critical stream power from empirical relationships for cohesive soils. Findings from this study also suggest further research is needed to investigate the acceptability of effective stream power on the scour depth prediction in a detail continuous monitoring stream site or in a controlled laboratory environment.

5.6 References

Annandale GW. 1995. Erodibility. Journal of Hydraulic Research 33:471–94

Annandale GW. 2006. Scour technology: Mechanics and engineering practice. McGraw-Hill, New York, USA

Bagnold RA. 1960. Sediment discharge and stream power: a preliminary announcement, U.S. Geological Survey

Benedict ST. 2003. Clear-water abutment and contraction scour in the Coastal Plain and Piedmont Provinces of South Carolina, 1996-99. U.S. Geological Survey, Water-Resources Investigations Report 03-4064, Reston, Virginia.

Benedict ST, Caldwell AW. 2009. Development and evaluation of live-bed pier and contraction scour envelope curves in the coastal plain and piedmont provinces of South Carolina, USA. Geological Survey Scientific Investigations, Report 2009-5099

Briaud JL, Ting FC, Chen H, Gudavalli R, Perugu S, Wei G. 1999. SRICOS: Prediction of scour rate in cohesive soils at bridge piers. Journal of Geotechnical and Geoenvironmental Engineering 125:237-246

Briaud J, Ting F, Chen H, Cao Y, Han S, Kwak K. 2001. Erosion function apparatus for scour rate predictions. Journal of Geotechnical and Geoenvironmental Engineering 127:105-113

Brubaker KL, Ghelardi V, Goodings D, Guy L, Pathak P. 2004. Estimation of long-term scour at Maryland Bridges Using EFA/SRICOS. Maryland Department of Transportation, Final Report, Project SP107B4E, University of Maryland, College Park, MD

Chang HH. 1979. Minimum stream power and river channel patterns. Journal of Hydrology 41:303-327

Cook W, Barr PJ, Halling MW. 2015. Bridge failure rate. Journal of Performance of Constructed Facilities 29:04014080. DOI:10.1061/(asce)cf.1943-5509.0000571

Costa JE, O'Connor JE. 1995. Geomorphically effective floods. In Natural and Anthropogenic Influences in Fluvial Geomorphology 89:45-56

Croad RN. 198). Physics of erosion of cohesive soils. PhD Thesis, Department of Civil Engineering, University of Auckland, New Zealand

Federal Highway Administration (FHWA) 2017. National bridge inventory. (http://www.fhwa.dot.gov/bridge/nbi/ascii.cfm) (last accessed on February 02, 2018)

Fleming M, Neary V. 2004. Continuous hydrologic modeling study with the hydrologic modeling system. ASCE Journal of Hydrologic Engineering 9(3): 175-183

Hickin EJ, Nanson GC. 1984. Lateral migration rates of river bends. Journal of Hydraulic Engineering 110(11):1557- 1567

Hydraulic Engineering Circular No. 18 (HEC-18) 2012. Evaluating scour at bridges. Fifth Edition, U.S Department of Transportation, Federal Highway Administration, Washington D.C.

Julian JP, Torres R. 2006. Hydraulic erosion of cohesive riverbanks. Geomorphology 76:193-206. doi:10.1016/j.geomorph.2005.11.003

Keaton JR, Mishra SK, Clopper PE. 2012. Scour at bridge foundations on rock. National Cooperative Highway Research Program (NCHRP), Report 717, Transportation Research Board of National Academics, Washington, D.C.

Keaton JR. 2013. Estimating erodible rock durability and geotechnical parameters for scour analysis. Environmental & Engineering Geoscience 19:319-343

Kirsten H. 1982. A classification system for excavating in natural materials, Civil Engineering South Africa 24:293-308

Kwak K. 2000. Prediction of scour depth versus time for bridge piers in cohesive soils in the case of multi-flood and layered soil systems. Ph.D. Dissertation, Texas A&M University, College Station, TX, USA

Lagasse P, Schall J, Johnson F, Richardson E, Chang F. 1995. Stream stability at highway structures (2d ed.): Federal Highway Administration, Hydraulic Engineering Circular No. 20. Publication FHWA-IP-90-014

Larsen EW, Fremier AK, Greco SE. 2006. Cumulative effective stream power and bank erosion on the Sacramento River, California, USA. Journal of the American Water Resources Association 42:1077-1097

Leopold LB, Wolman MG, Miller JP. 1964. Fluvial processes in geomorphology. W. H. Freeman and Company, San Francisco, California, USA

Mehta AJ, Hayter EJ, Parker WR, Krone RB, Teeter AM. 1989. Cohesive sediment transport. I: Process description. Journal of Hydraulic Engineering 115:1076-1093

Moore JS. 1997. Field procedures for the head-cut erodibility index. Transactions of the ASAE 40:563-574. doi:10.13031/2013.21315

Pierce CE, Gassman SL, Ray RP. 2011. Geotechnical materials database for embankment design and construction. Federal Highway Administration, Final Report. FHWA/SCDOT Report No. FHWA-SC-11-02

Raudkivi AJ. 1990. Loose boundary hydraulics. 3rd Edition, Pergamon Press, Oxford.

Richardson EV, Davis SR. 2001. Evaluating scour at bridges. 4th Edition, U. S. Department of Transportation, Federal Highway Administration, Washington D.C.

Shirole A, Holt R. 1991. Planning for a comprehensive bridge safety assurance program. Transportation Research Record 1290:39-50

Sklar LS, Dietrich WE. 2004. A mechanistic model for river incision into bedrock by saltating bed load. Water Resources Research 40:W06301

Tan SK. 1983. Erosion of cohesive soils. PhD Thesis, Department of Civil Engineering, University of Auckland, New Zealand

Ting FC, Briaud JL, Chen H, Gudavalli R, Perugu S, Wei G. 2001. Flume tests for scour in clay at circular piers. Journal of Hydraulic Engineering 127:969-978

Van den Berg JH. 1995. Prediction of alluvial channel pattern of perennial rivers. Geomorphology 12:259-279

Wardhana K, Hadipriono FC. 2003. Analysis of recent bridge failures in the United States. Journal of Performance of Constructed Facilities 17:144-150

Wibowo J, Yule D, Villanueva E, Temple D. 2005. Earth and rock surface spillway erosion risk assessment. The 40th US Symposium on Rock Mechanics (USRMS), American Rock Mechanics Association, Alaska, USA

Wu NC. 2010. An exploratory data analysis of national bridge inventory. M.Sc. Thesis, Department of Civil Engineering, University of Virginia, USA

Yang CT. 1972. Unit stream power and sediment transport. Journal of the Hydraulics Division 98:1805-1826

Yang CT. 1973. Incipient motion and sediment transport. Journal of the Hydraulics Division 99:1679-1704

USDA-NRCS 1997. Field procedures guide for the head-cut erodibility index. Chapter 52, Part 628 Dams, 210-VI-NEH. Washington D.C.: USDA Natural Resources Conservation Service.

CHAPTER VI
SCOUR STUDY IN COHESIVE SOILS

This chapter is in preparation for publication by Badal Mahalder, John S. Schwartz, Angelica M. Palomino and Jon Zirkle.

Badal Mahalder, John S. Schwartz, Angelica M. Palomino and Jon Zirkle: **"Evolution of scour depths around cylinder in natural cohesive soil from multiple flow events."**

Badal Mahalder, the senior author generated this manuscript as a part of his Ph.D. dissertation, and co-authors John Schwartz, Angelica Palomino, and Jon Zirkle supervised his research, in addition to direct text contributions to his study's manuscript.

Abstract

Channel bed scour evolution and erosional behavior around a vertically-positioned cylinder in natural cohesive sediment was investigated under multi-flow event scenarios. Published local scour studies in cohesive sediments describe scour around cylinders for either commercially available clay or mixing sand or gravel with clay at different proportions and a single flow velocity. In natural streams, flow hydrographs vary by peak magnitude and duration, which variability in characteristics appears to influence evolution patterns of bed scour adjacent to a structure. The purpose of this study was to investigate the behavior of scour development with different combinations of flow events and observe the final scour depths within a large open channel flume. It was identified that with any flow sequence, the final scour depths were similar; however, time dependency on scour initiation was observed for higher bulk density soil (1.81-2.04 gm/cm^3) regardless flow sequence. Results from of studies also suggest that similar scour depths can be expected for both non-cohesive and cohesive soils. However, this study did not support those findings for soil with similar field bulk density conditions. It was also identified that at field bulk density conditions, the scour rate was slow and produced smaller scour depths compared with the lower bulk density condition.

6.1 Introduction

Local scour around bridge piers are dependent on several factors including flow conditions, stream bed material, pier characteristics, and time of scour (Hosny, 1995; Melville and Chiew, 1999; Kwak, 2000; Devi and Barbhuiya, 2017). Many scour studies involving circular bridge piers in non-cohesive soils have been completed by numerous researchers to date. However, very few scour studies focusing on cohesive sediments have been conducted, likely due to the complex erosion processes of cohesive sediments (Briaud et al., 1999; Molinas and Hosny 1999; Ting et al., 2001; Ansari et al. 2002; Debnath and Chaudhuri, 2010a,b; Debnath and Chaudhuri, 2012; Kothyari et al., 2014). Erosion processes in cohesive sediments are complex. particles from cohesive sediment beds starts to move when inter-particle bonds connecting aggregate, floc or individual particle breaks due to the applied stress from the flowing water

(Debnath and Chaudhuri, 2010a). Reported scour studies in cohesive sediments have been conducted using the mixture of non-cohesive sediments with clay at different proportions. The presence of clay content (C) and antecedent moisture content (WC) have been reported the most critical parameters on equilibrium scour depths prediction (Molinas and Hosny, 1999; Ansari et al., 2002; Debnath and Chaudhuri, 2010a,b; Debnath and Chaudhuri, 2012).

Scour rates in cohesive soils are slow and represent a fatigue failure behavior compared to non-cohesive sediments represented by an incipient motion theoretical basis, where for cohesive soils it has been reported that it takes several days with multiple flow events for attaining equilibrium scour depths (Briaud et al., 2001; Ting et al., 2001). Several studies identified the influence of flow duration, flow magnitude and flow frequency on erosion behavior in different earth materials for both the bank erosion, fluvial erosion (channel incision) and localized scour around structures (Wolman, 1959; Costa and O'Connor, 1995; Julian and Torres, 2006; Keaton et al., 2012). The assumption of constant flow velocity as considered in cohesive soil scour studies is does not represent a natural stream/river flow hydrograph. The flow hydrograph for a stream shows three parts: a rising limb, a constant peak flow and a falling limb. Based on storm duration and the characteristics of the watershed, the constant peak flow duration may vary and recede afterwards. Therefore, a sequence of low-medium-high flow or vice versa is expected for a flow hydrograph over the life span of a bridge, which will generate scour around the piers or abutments. Since the scour rate in cohesive soil is slow; it is hypothesized that the influence of stress history from multiple flow events could have significant influence on scour depth evolution around bridge piers.

Gudavalli (1997) conducted an experimental study on commercially available pure clay soils to observe the influence of multiple flow events on scour depth evolution around circular

bridge piers and developed a conceptual model for ultimate scour depth predictions using two sets of experiments. Later, the method was modified by Briaud et al. (2001). However, in natural sediments, sand, silt, and clay are present at different proportions. In addition to the inherent attractive forces between the clay particles, the biological properties developed over time in the sediments also influence the cohesive characteristics of the cohesive sediments, consequently the erosive behavior (Black et al., 2002; Grabowski et al., 2011). It is nearly impossible to develop the biological parameters in the soil during the experimental period in the laboratory. Therefore, the objective of this study was to observe the evolution of scour depths around a cylinder from multiple flow events in natural cohesive sediments. The influence of stress history or memory effect was also studied under higher flow velocity conditions from laboratory flume experiments.

6.2 Experimental Set-up and Procedures

6.2.1 Flume construction

For this experimental study, a 12.20m long, 1.22m wide and 0.61m deep outdoor flume was constructed at the University of Tennessee, Knoxville on the ETREC Plant Sciences Unit premises (Figure 6.2.1). The sides and bottom of this flume were constructed with plywood material and a geo-liner was used as a water seal. A test section (1.22m X 1.22m X 0.3m) was constructed 8.23m downstream from the flume entrance (Figure 6.2.1). Water was pumped from a nearby slough using a 6 inch suction pump (0.13 m^3/s maximum flow capacity; United Rental Inc.). The desired flow velocity was maintained with the variable control system attached to the pump. The slope of the flume was kept constant (0.85%).

6.2.2 Properties of natural cohesive sediment

In this experimental study, natural cohesive sediments were used for the each flow condition. The sediment samples were collected from Crooked Creek of Shelby County (Tennessee, USA). The geological properties of this stream site are described in detail in

Mahalder et al. (2017). In-situ WC and bulk density (BD) were 23.82% and 2.04 gm/cm^3, respectively, which were measured for the undisturbed condition prior to collecting the soil sample. The details of other soil properties are reported in Table 6.2.1. The natural cohesive soil has approximately 72% silt and 25% clay. A standard proctor test was conducted on the collected soil after remolding, which showed that the maximum density was attained at a much lower WC than the field WC. Replicating the exact in-situ soil conditions (e.g. in-situ density at the in-situ WC) is difficult given the variations of physical properties between remolded and in-situ soils. Therefore, the test sediment beds were prepared by targeting the desired BD values and measuring the corresponding WC values rather than compacting the soil at the optimum water content.

6.2.3 Sediment bed preparation

Three different compaction efforts were applied to prepare the sediment beds for the experiments. For matching the field BD of the sediment bed, water was spread over the dry soil and covered for 24 hours hydrate the soil uniformly. The moist soil was then placed in the test box and compacted in three approximately equal lifts. Each lift was compacted with a 25.4cm x 25.4cm cast iron tamper dropped manually ~30 cm above the lift surface. After compaction, a 16 kg roller was used to smooth out the surface and avoid any possible kneading in the soil for attaining desired BD. Two core samples were collected from each lift for WC and BD measurements using the standard method. A 101.6 mm diameter clear Plexiglass cylinder was inserted in the middle of the test section. Figure 6.2.2-a shows the locations of vertical graduated tank tape strips glued to the inner surface of the cylinder at different circumference locations (counter-clockwise: 0° (front), 45°, 90° (right side), 135°, 180° (back), 270° (left side), 225°, and 315°) for periodic scour depth measurements.

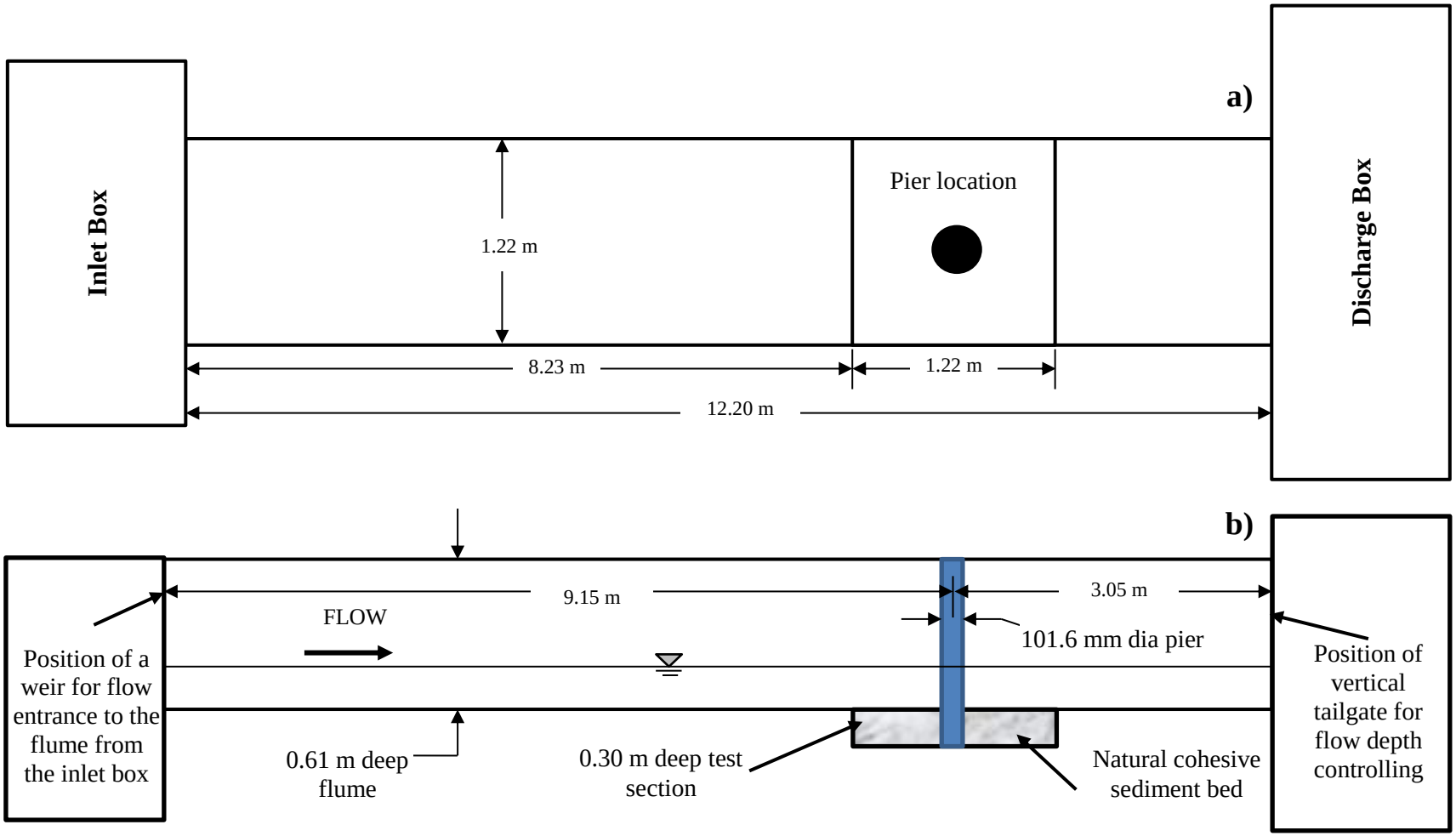


Figure 6.2.1: Detail of the flume: a) plan view, and b) long section of the flume (not to scale)

Table 6.2.1 Properties of Crooked Creek sediment

Properties	
Median grain size (μm)	12.00
Liquid limit, LL	29.00
Plastic limit, PL	18.95
Plasticity index, PI	10.05
In-situ moisture content	23.82
In-situ cohesion (kPa)	67.56
Sand %	3.00
Silt %	72.00
Clay %	25.00
Clay activity	0.41
Specific surface area (m^2/g)	46.49
Sodium adsorption ration (SAR)	5.34
Potassium intensity factor (KIF)	0.07
Field bulk density, BD (gm/cm^3)	2.04
Specific gravity	2.658
Geometric standard deviation (σ_g)	9.83

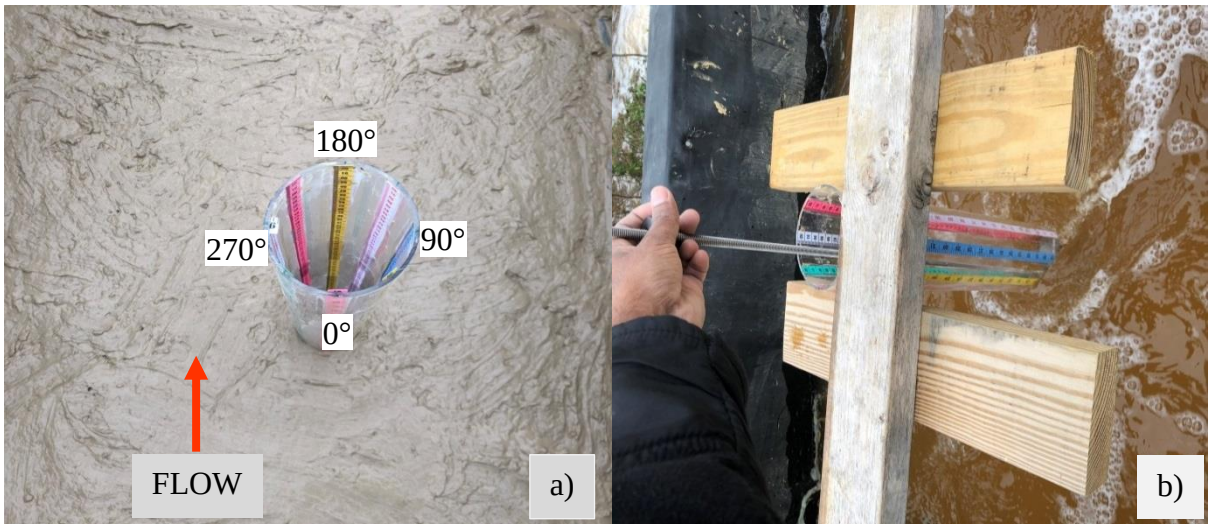


Figure 6.2.2: a) Prepared sediment bed with the Plexiglas circular pier, b) placement of underwater camera during experiments for periodic scour depth measurement

Experiments were also conducted on sediment beds with three other BD values: BD = 1.81-1.86 g/cm^3, BD = 1.69-1.71 g/cm^3 and BD = 1.52-1.56 g/cm^3. For the first set of targeted BD values, the soil was mixed thoroughly by hand by adding water and then placing the moistened soil into the test section. The soil was then compacted using the tamper for attaining the desired BD. The low density sediment bed was prepared by adding more water to the soil and compacting by hand using a wooden board to achieve the target density. The sediment beds were compacted in three lifts. After preparing the sediment bed, the critical shear stress (τ_c) was measured at two downstream locations using a mini-jet device following the procedure described in Mahalder et al. (2018). Soil shear strength was also measured using a hand-held vane shear instrument (E-286 Inspection Vane, Omnimetrix, Canada) at four to five locations (ASTM D2573). The top surface of the prepared sediment bed was levelled gently by hand using a trowel. The prepared sediment bed was then kept covered for 16-24 hours before starting a test. For each experimental set (Table 6.2.2) a fresh sediment bed was prepared following similar procedures.

Table 6.2.2 Experimental condition

Experiment Set	Run No	Flow Condition	Flow velocity (cm/s)	Duration (Hours)	BD (gm/cm^3)	WC
1	1	Low	81.25	36	2.04	25.31
	2	High	102.20	36	2.03	25.31
2	3	Low	79.98	12	1.84	30.16
	4	Medium	89.41	12	1.84	30.16
	5	High	100.34	12	1.84	30.16
3	6	Low	80.40	12	1.71	37.86
	7	Medium	91.25	12	1.71	37.86
	8	High	100.60	12	1.71	37.86
4	9	High	102.40	12	1.86	31.25
	10	Medium	90.26	12	1.86	31.25
	11	Low	80.36	12	1.86	31.25
5	12	High	101.40	12	1.69	38.12
	13	Medium	89.52	12	1.69	38.12
	14	Low	80.10	12	1.69	38.12
6	15	Low	81.25	36	1.81	31.24
7	16	Low	80.68	36	1.56	37.45
8	17	High	99.89	36	1.83	30.65
9	18	High	100.26	36	1.52	37.90

*Approach flow depth, h = 15.25 cm and cylinder diameter = 10.16 cm

6.2.4 Procedure of experiment

In this experiment, shallow water condition (h/D = 1.50) was maintained for attaining higher velocities during experiments. During the trial run, it was identified that at least 70 cm/s depth average velocity was required for observing any scour depth over 12 hours. For attaining flow velocities higher than 70 cm/s, 15.25 cm water depth was maintained throughout the experiments at subcritical flow condition by controlling the tailgate height. Since the flume boundary was smooth, the mean velocity profile was approximated by the log law (Nezu and Nakagawa, 1993). A handheld SonTek/YSI ADV (Version 2.5) was used for velocity measurement at different points during the experiments. Depth average mean velocity was approximated by measuring the velocity using the handheld ADV at 0.2y and 0.8y depths and averaging the values (e.g., Ting et al., 2001; Debnath and Chaudhuri, 2012). Velocity distribution with depth for three different flow conditions is presented in Figure 6.2.3.

The goal of this experiment was to observe the scour depth evolution under multiple flow condition using different flow sequences. During each experiment, flow depth was monitored throughout the experimental run using graduated tape attached to the sides at different locations of the flume. For the above mentioned BD conditions, four flow velocity sequences were used in this experimental study as presented in Table 6.2.2. A total of 18 experimental runs were conducted comprising nine different scenarios using natural cohesive soil. During experiments, an underwater camera was used for taking periodic pictures and videos of scour depths on the graduated tapes attached inside the cylinder. After finishing each experimental run, the water was drained out from the scour hole and the detail measurements were conducted using a point gage mounted on the top of the flume.

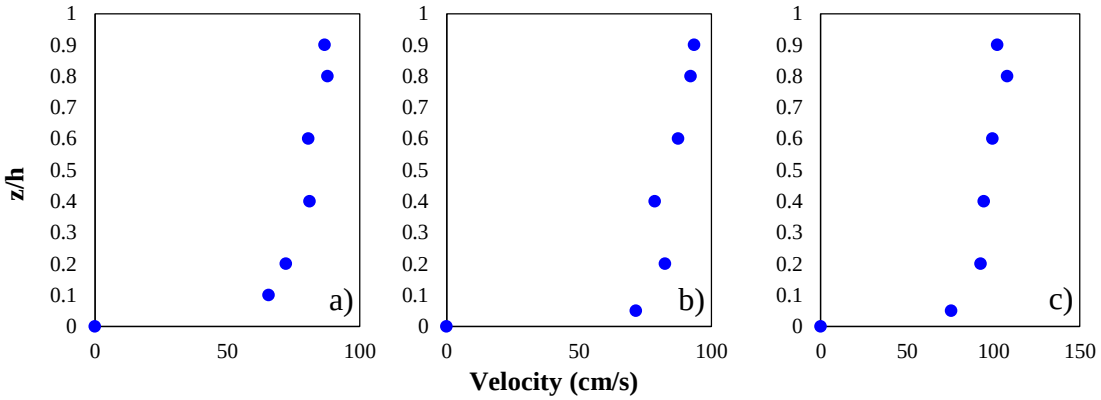


Figure 6.2.3: Velocity distribution with depth: a) low flow (run no. 3), b) medium flow (run no. 4), and b) high flow (run no. 5)

6.2.5 Available equilibrium scour depth predicting equations for cohesive soil

Several equations are available for equilibrium scour depth prediction in cohesive soils. Those equations were developed with different flow and soil conditions using commercially available clay or mixture of clay-sand at different proportions. From those studies, it was identified the relative slowness in scouring processes compared with non-cohesive soils. Contradictory findings have been reported on equilibrium scour depths prediction. Some of those studies reported similar maximum scour depths for both non-cohesive and cohesive sediments under similar flow conditions, whereas some studies reported lower or even higher maximum scour depths for cohesive soils compared to non-cohesive soils.

Molinas and Hosny (1999) developed equations for estimating geometric dimensions of scour hole and maximum scour depths based on the observed scour volume using three sets of laboratory flume experiments. They proposed an equation for clay-sand mixture with less than 31% clay-silt proportions:

$$\frac{y_s}{D} = 18.92\left(\frac{F_r^{2.08}}{(1+C)^{1.88}}\right) \qquad (6.1)$$

where y_s is the maximum scour depth, D is the pier diameter, C is the fraction of cohesive soil, and F_r is the Froude number, which should be in between 0.18-0.33.

Briaud et al. (1999) introduced a new method for scour prediction in cohesive soils by introducing the time dependent scour depth prediction using a hyperbolic equation. In this method, maximum shear stress at pier is calculated and based on the value initial erosion rate is estimated from erosion function apparatus (EFA) tests. Later, a generalized curve was developed based on different soil type to predict the initial erosion rate for different maximum shear stress (τ_{max}) values at pier. The proposed equation for estimating τ_{max} value is:

$$\tau_{max} = 0.094\rho V^2 \left(\frac{1}{\log R_p} - \frac{1}{10}\right) \quad (6.2)$$

where τ_{max} is the maximum shear stress at the pier. ρ is the density of water, V is the approach flow velocity, and R_p is the pier Reynolds number. The time dependent scour depth is then calculated using the following formula:

$$y_t = \frac{t}{\frac{1}{z_i} + \frac{t}{y_s}} \quad (6.3)$$

where t is the time of scour, z_i is the initial erosion rate calculated using the τ_{max} value, and y_s is the maximum scour depth calculated using the following functional relationship with R_p:

$$y_s = 0.018R_p^{0.635} \quad (6.4)$$

This method is applicable for circular pier with deep water condition and constant flow velocity. Considering the flow variation in natural streams, this method was modified by them later based on series of experiments.

Briaud et al (2001) modified the equation for incorporating the influence of shallow water effect, attack-angle effect, pier shape effect and pier spacing effect. The modified equations of maximum shear stress and maximum scour depth with the correction factors are as follows:

$$\tau_{max} = k_w k_{sp} k_{sh} k_a 0.094 \rho V^2 \left(\frac{1}{\log \frac{Vb}{\nu}} - \frac{1}{10} \right) \quad (6.5)$$

$$y_s = k_w k_{sp} k_{sh} 0.018 R_p^{0.635} \quad (6.6)$$

where b is the projected pier width perpendicular the flow, k_w, k_{sp} and k_a are the correction factor for shallow water, pier spacing and angle of attack, respectively.

$$k_w = \begin{cases} 0.85 \left(\frac{h}{b} \right)^{0.34} & \text{for } {}^{h}/_{b} < 1.62 \\ 1 & \text{for } {}^{h}/_{b} > 1.62 \end{cases} \quad (6.7)$$

Debnath and Chaudhuri (2010 a,b, 2012) conducted series of flume experiments on clay-sand mixed sediment at different WC and clay content condition. Based on the experimental data, Debnath and Chaudhuri (2010a) proposed regression equations to estimate the dimensionless maximum scour depth at circular pier founded in clay sand mixed bed:

$$\hat{y}_s = 2.05 {F_{rp}}^{1.72} C^{-1.29} {\hat{\tau}_s}^{-0.37} \text{ for } WC = 20 - 23.22\% \text{ and } 20\% \leq C \leq 85\% \quad (6.8)$$

$$\hat{y}_s = 3.64 {F_{rp}}^{0.22} C^{-1.01} {\hat{\tau}_s}^{-0.69} \text{ for } WC = 27.95 - 33.55\% \text{ and } 20\% \leq C \leq 50\% \quad (6.9)$$

$$\hat{y}_s = 20.52 {F_{rp}}^{1.28} C^{0.19} {\hat{\tau}_s}^{-0.89} \text{ for } WC = 27.95 - 33.55\% \text{ and } 50\% \leq C \leq 100\% \quad (6.10)$$

$$\hat{y}_s = 3.32 {F_{rp}}^{0.72} C^{-0.62} WC^{0.36} {\hat{\tau}_s}^{-0.29} \text{ for } WC = 33.60 - 45.92\% \text{ and } 20\% \leq C \leq 70\% \quad (6.11)$$

$$\hat{y}_s = 8 {F_{rp}}^{0.61} C^{058} WC^{1.24} {\hat{\tau}_s}^{-0.19} \text{ for } WC = 33.60 - 45.92\% \text{ and } 70\% \leq C \leq 100\% \quad (6.12)$$

where $\hat{y}_s$ is the non-dimensional maximum scour depth $\left(\hat{y}_s = \frac{y_s}{D} \right)$, F_{rp} is the pier Froude number, C is the clay content, $\hat{\tau}_s$ is the non-dimensional bed shear stress $\hat{\tau}_s = \frac{\tau_s}{\rho V^2}$, and τ_s is the vane shear strength of the soil.

Briaud et al. (2011) updated the pier scour equation for cohesive material by incorporating the critical velocity for initiation of erosion, which was added to HEC-18 (2012) report and expressed as:

$$y_s = 2.2 K_1 K_2 D^{0.65} \left(\frac{2.6V - V_c}{\sqrt{g}} \right) \quad (6.13)$$

where y_s is the maximum scour depth, K_1 and K_2 are the correction factor for pier shape and angle of attack, respectively, D is the pier diameter, V is the flow velocity, V_c is the critical flow velocity for scour initiation, and g is the gravitational acceleration. However, for calculating the time dependent scour development, Equation 6.3 should be used.

Milonas and Hosny (1999), and Debnath and Chaudhuri (2010a) equations were developed for maximum scour depth prediction only. Briaud et al. (2001, 2011) equations considered the time dependent scour development in addition to the maximum scour depth prediction. In the later stage, a generalized curve developed by Briaud et al. (2011), which was used for estimating initial erosion rate (z_i) based on soil type. However, they recommended to apply the EFA for developing erosion rate curve for tested soil. In this study, the observed scour depths from each flow events were compared with the predicted scour depths using the hyperbolic time dependent scour formula developed by Briaud et al (1999). The HEC-18 equation was also used for maximum scour depth prediction with the experimental condition to observe the possible variations among these sets of equations.

6.3 Results and Discussion

6.3.1 Scour depth evolution

Periodic scour depths measurements around the cylinder showed that for each experimental run, scour initiated at the sides of the cylinder. It was also observed that maximum scour developed at the sides except for one scenario (experimental set 4), where maximum scour depth was observed between 45° and 90° of the cylinder (Table 6.3.1). Similar findings have been reported in the literature from other studies (Ting et al., 2001; Debnath and Chaudhuri, 2010a,b; Chaudhuri and Debnath, 2013). Since all of the experiments were conducted in shallow water depth, faster scour depth was expected (Briaud et al., 2001). Experimental results from this study also demonstrated that the progression of scour depths was also dependent on the BD

values. It was observed that in the wake zone (downstream side of the cylinder), the lateral and transverse extent of the scour hole was much higher compared with other sides of the cylinder (Figure 6.3.1). Further analyzing the scouring processes around the cylinder, it was identified that scouring initiated at the sides and gradually propagated either upstream or downstream directions for all cases. Overall, scour depths at the nose of the pier (0°) were higher compared with the scour depths at the wake zone (180°) for each experimental condition.

Ting et al. (2001) reported that at lower R_d values the scour depth at downstream and upstream side of pier is similar, whereas for higher R_d values, downstream side scour depth is more compared with the upstream side. However, Debnath and Chaudhuri (2010a) reported that this hypothesis was not always valid. They argued that in addition to the R_d values, τ_{max} (calculated using equation 6.5) has strong influence on the scour depth propagation towards either the downstream or the upstream direction of cylinder.

In this experiment τ_{max} values were significantly higher compared with Ting et al. (2001) study and R_d values were in between 66265 to 98087. The scour depths were found propagating more towards the downstream direction of the cylinder at all flow and BD conditions compared to upstream direction. This observation was clearly deviating from the hypothesis developed by Debnath and Chaudhuri (2010a) but followed the Ting et al. (2001) observations for scour hole propagation. However, higher scour depths were observed at the nose of the cylinder compared with back side of the cylinder. It was hypothesized that since the flow depth was shallow, the horse shoe vortex was not fully developed. The upstream turbulent flow was also forcing the horse vortex to move around the downstream side of the pier; consequently soil layer was removed from a wider downstream area compared with other locations (Figure 6.3.2).

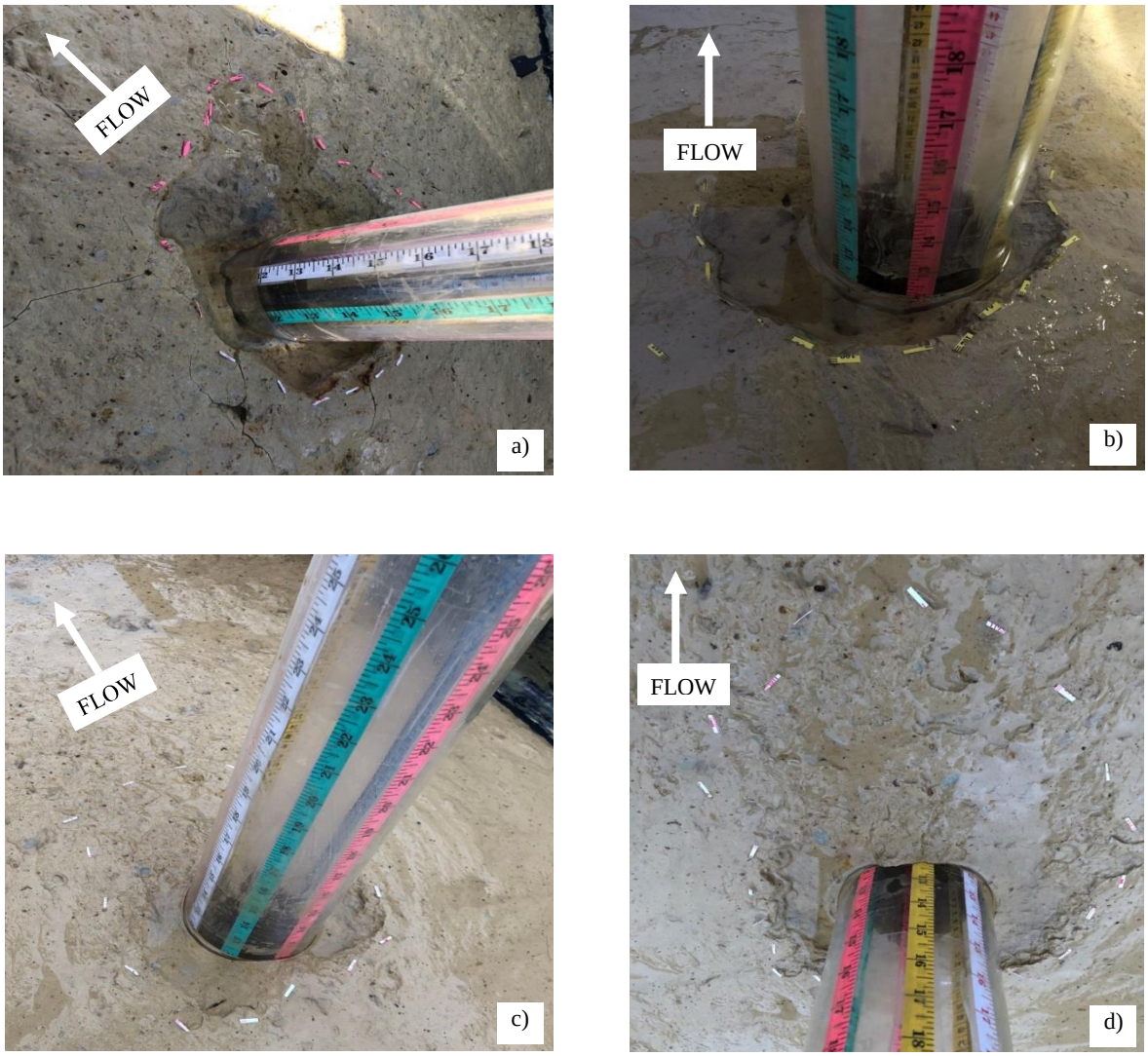


Figure 6.3.1: Scour hole development for: a) run 16, V = 80.68 cm/s, WC = 37.45%, b) run 14, V = 80.10 cm/s, WC = 38.12%, c) run 10, V = 90.26 cm/s, WC = 31.25%, and d) run 9, V = 102.40 cm/s, WC = 31.25%

It is also important to note that the behavior of cohesive sediment could have also influence on scour propagation. In this experiment since natural cohesive sediments were used it was expected to develop cohesion in the soil quicker than the commercially available completely remolded clay soils.



Figure 6.3.2: Scour hole development and the soil removal erosion pattern at the wake zone of the pier: run 14, V = 80.10 cm/s, WC = 38.12%

Analyzing the scour depth data around the cylinder, it was also observed that scour depths were not propagating at the same rate along the entire experiment duration (Table 6.3.1). Both down-cutting and widening in scour holes were observed with time rather than deepening at the same location. It was hypothesized that pressure gradient and the uneven shear stress distribution in the scour hole influenced the growth of scour holes. The maximum scour hole developed at a side of the cylinder after initial flow condition influenced the scour propagations on other adjacent sides during the intermediate flow condition. Resulting higher scour depth readings were recorded at other attached graduated tapes rather than deep scour hole formation in the same position. This was identified as a dynamic processes as for the next flow condition

higher scour depth was recorded at the previous maximum scour depth position. It was also envisaged that if another set of flow sequence was applied, similar scenarios could have been observed. However, due to the some constrains, another set of flow sequence was not tested in this experiment, which is thought to be a future research area for completely understanding the scour behavior in cohesive soils.

6.3.2 Influence of multi-flow on scour propagation

Similar to non-cohesive sediment, most of the previous research in bridge scour was concerned about single flow event without considering sequence of flow events. In reality, during the design life of a bridge, it is expected to observe multiple flow events above critical with different magnitudes, frequency and duration. It is expected that scour depth development could be affected by the sequence of different flow events. Briaud et al. (2001) studied and reported the significance of multi-flow events based on two laboratory experiments in commercially available clay material. They developed a hyperbolic equation for predicting the time dependent scour depth for different flow events as discussed in the previous section. In this study, two sequences of flow events were used: i) Low-Medium-High (L-M-H), and ii) High-Medium-Low (H-M-L) on different soil BD conditions (Table 6.2.2). Results from this experimental study showed that flow sequence had notable influence on scour depth evolution for different soil BD conditions (Figure 6.3.3).

Regardless of the flow sequence, similar scour depths were observed for the natural cohesive soil with BD 1.69-1.86 gm/cm^3 at the end of experiment set. It was observed that for H-M-L flow sequence (Figure 6.3.3a) initially a big jump in the scour depth, then it slowed down for medium flow, which was again increased for low flow condition. The scour rate for higher BD soil (1.86 gm/cm^3) reduced substantially at the end of high flow events. For lower BD soil

(1.69 gm/cm^3), higher scour rate was observed at high flow and reduced significantly for medium flow, which was picked up again at lower flow events.

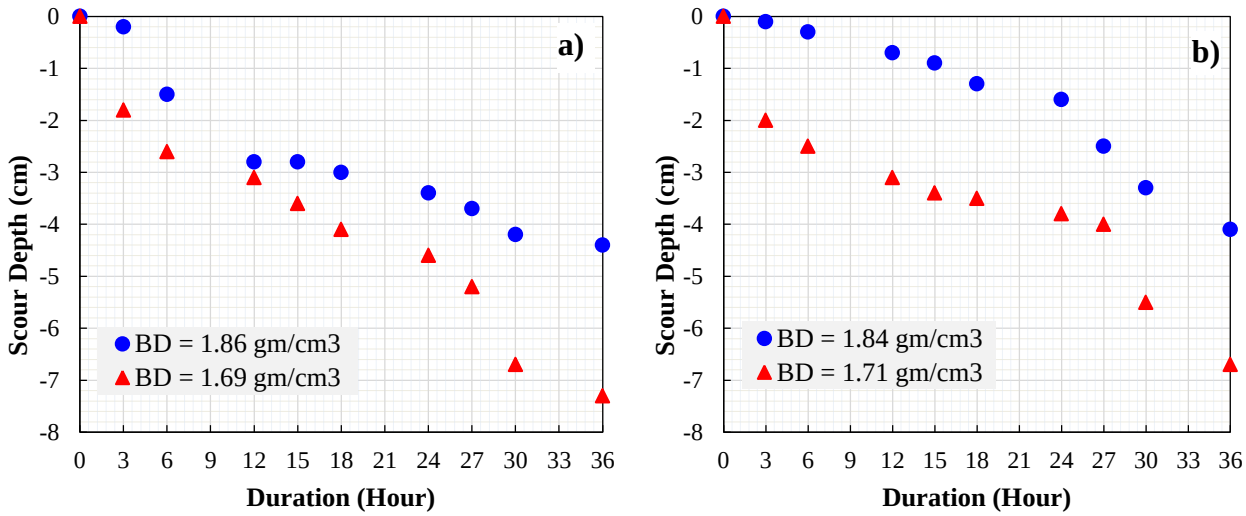


Figure 6.3.3: The evolution of maximum scour depth: a) for High-Medium-Low (H-M-L) flow sequence at 270° and 90° of the pier, b) for Low-Medium-High (L-M-H) flow sequence at 90° and 45° of the pier

Mechanism of scour depth evolution was also studied for very dense (BD = 2.03-2.04 gm/cm^3), medium dense (BD = 1.81-1.83 gm/cm^3) and low dense (BD = 1.52-1.56 gm/cm^3) condition of the natural sediments using low and high flow conditions (Figure 6.3.4). In these experiments, after each 12 hours, experiment was stopped for necessary scour hole measurement without disturbing the soil surface and restarted the experiment. Temporal scour depths measurements showed that for each soil density condition the scour rates were reduced after 24 hours except for low density soil at high flow (Figure 6.3.4 a).

Table 6.3.1 Scour depth development around circular pier for different flow and soil condition

Run No	Location of max scour depth		Observed scour depth around the sides of pier (cm)								Lateral extent of scour hole around the pier, x_L (cm)							
	After each flow	End of test	0°	45°	90°	135°	180°	225°	270°	315°	0°	45°	90°	135°	180°	225°	270°	315°
1	90°	90°	0.50	1.40	2.20	2.00	1.20	0.60	0.60	0.30	4.57	7.62	11.43	5.08	10.16	3.81	4.10	4.57
2	90°	270°	0.50	2.90	3.10	3.00	1.10	1.50	1.00	1.60	3.60	7.25	9.80	10.26	17.00	12.25	5.60	6.25
3	90°		0.20	0.60	0.70	0.40	0.40	0.60	0.60	0.40	2.60	2.51	2.60	3.50	6.60	3.60	2.40	3.20
4	270°	90°	1.00	1.30	0.90	1.10	0.30	0.80	1.40	1.00	2.70	3.20	3.00	3.50	7.12	4.00	3.60	3.50
5	90°		0.50	1.50	2.50	1.30	0.80	0.80	2.20	1.40	3.50	5.00	4.00	4.00	8.15	7.25	4.20	4.00
6	45°		1.70	3.10	1.90	0.20	0.50	0.50	1.70	1.20	3.00	4.50	3.00	4.50	4.00	8.00	6.00	3.00
7	270°	45°	0.40	0.70	0.90	1.30	0.50	1.00	1.50	0.90	3.00	4.50	6.00	8.00	14.00	9.00	7.00	5.50
8	45°		0.70	2.90	1.50	1.20	0.30	1.50	1.00	1.00	4.50	5.00	6.50	11.00	17.00	13.00	8.00	8.00
9	270°		1.30	1.50	2.00	1.80	1.50	1.50	3.00	2.00	1.50	2.00	3.00	9.00	12.00	4.00	3.00	2.00
10	90°	270°	0.20	1.00	1.00	1.10	0.90	1.60	0.60	1.00	4.00	2.50	5.00	14.00	23.00	8.00	6.00	4.00
11	270°		0.30	1.20	0.80	0.80	1.00	1.40	1.50	0.90	4.50	4.60	6.50	14.00	23.00	8.50	6.50	4.60
12	270°		2.10	3.50	4.00	0.70	1.20	2.00	4.30	4.20	4.00	2.00	2.60	6.00	9.00	8.00	6.00	5.00
13	90°	90°	0.20	0.70	1.10	1.00	0.30	1.00	1.00	1.00	5.00	2.00	3.50	11.00	11.00	9.00	7.00	6.00
14	90°		1.00	0.50	2.20	1.50	0.70	1.00	0.70	0.50	5.00	3.00	6.00	12.00	12.00	12.00	8.00	6.00
15	90° and 270°		1.10	2.10	3.20	1.20	1.50	2.10	3.20	2.20	3.50	6.20	8.00	10.80	11.30	8.60	6.20	5.00
16	90°		2.60	5.80	6.40	3.90	2.70	5.30	4.80	4.80	6.00	10.00	8.50	14.00	9.00	4.50	5.00	4.00
17	90° and 270°		2.00	3.70	5.30	4.10	2.60	3.00	5.30	3.40	6.00	5.50	11.50	18.50	13.00	12.00	8.00	5.00
18	90°		4.50	6.80	9.00	8.00	1.40	5.20	6.60	4.80	6.50	9.00	14.00	11.00	7.00	5.00	5.50	5.00

Note: Approach flow depth, h = 15.25 cm and cylinder diameter, D = 10.16 cm

In case of lower BD conditions (1.51-1.71 gm/cm^3) scour depths were found initiated at each flow condition. Analyzing the recorded videos during experiments, it was observed that for soft sediment bed both particle by particle and flocs removal patterns were prominent. As experimental time progressed and the scour holes deepened, the soil saturation played influential part in removing the soil aggregates from the hole at higher flow condition. Whereas at lower flow velocity, it was assumed that the erosive capacity of the flowing water was not higher enough in the deeper scour hole as very few aggregates removal were observed. The reduction of effective shear stress in the scour hole could have also influenced the slower scour rate at low flow velocities. It was also assumed that during the lower shear stress condition more particles were eroded away since consequently smoother scour hole was observed. At high flow velocity the surface of scour hole was rough suggesting the possible aggregate removal. Due to pump capacity, flow sequences (L-M-H and H-M-L) were not used for dense soil since at low flow no scour was observed after 12 hours of run (Figure 6.3.4b).

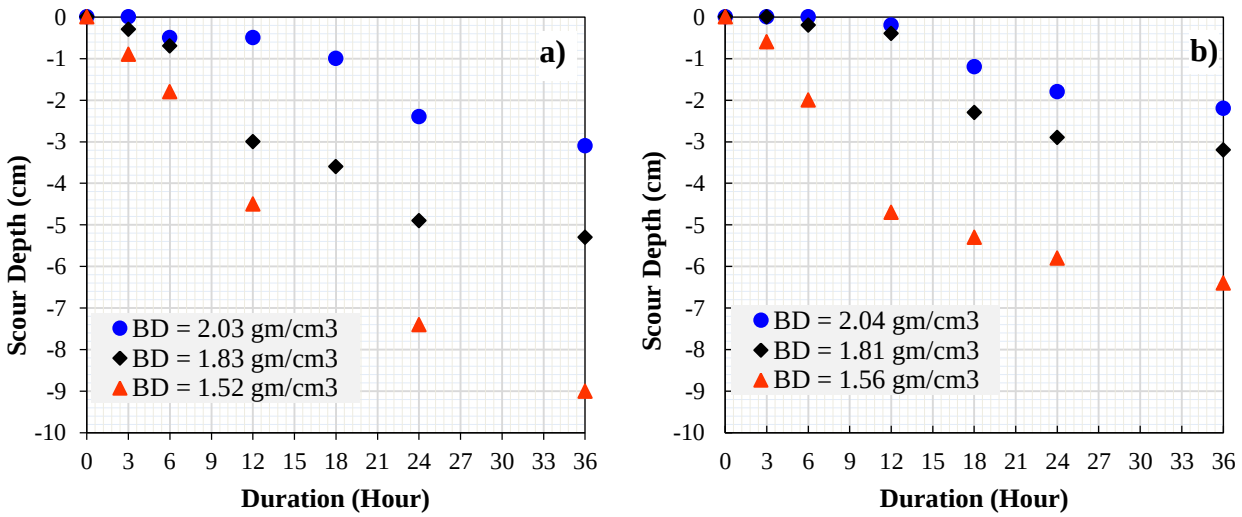


Figure 6.3.4: The evolution of maximum scour depth: (a) for High-High-High (H-H-H) flow sequence at 270° and 90° of the pier, b) for Low-Low-Low (L-L-L) flow sequence at 90° and 270° of the pier

6.3.3 Influence of stress history on scour propagation

It has been reported that erosion behavior of soil with high silt-clay content or cohesive sediments is dominated by subaerial processes or excess shear stress duration in the flow hydrograph (Costa and O'Connor, 1995; Julian and Torres, 2006). Though the sediment encroachment and movement around bridge piers and abutments are fundamentally different from the fluvial erosion process, it was expected that the stress history could have influence on the scour propagation around bridge piers. It is interesting to note that the effect of stress history on scour development was observed from these experimental results since scour depths were not visible immediately after starting the experiment for higher BD conditions. Results from this study revealed that scour initiated immediately after starting an experiment for low BD soil, which is reported in the previous section. Soil with higher BD condition (1.81-2.04 gm/cm^3) scour depth initiation time was found dependent on flow velocity. At lower flow velocity, scour depths were observed usually after 12 hours, whereas at high flow velocity scour depths were observed after 3-6 hours of experimental run.

It was also observed that after the initial scour depth formation, rate of scour slowed down for both the H-M-L and L-M-H flow sequences for each BD condition (from 12-24 hours in Figure 6.3.3). Scour rate increased significantly after that period regardless of flow condition, though at higher flow velocity sequence greater scour depths were observed for both BD conditions. It was hypothesized that at the end of initial flow condition, some intermediate equilibrium state was attained. During the intermediate flow events, the developed scour hole from the previous flow event was exposed to either higher or lower shear stresses. Previous stress history influenced the scour rate for this intermediate flow condition, though relatively lower scour rates were observed for each BD conditions. In the H-M-L flow sequence, since the previous stress history was higher, lower scour rate was observed compared with the L-M-H

flow sequence. It was also observed that at the end of intermediate flow velocity, scour rate picked up again regardless of the flow condition for the last stage of the experiment. It was thought that since the scour hole was exposed to a certain shear stress history for a longer period of time, introduction of higher flow events could have influence the higher scour rate. In each case, both the shear duration and saturation during the experimental period could have influenced the scouring processes. It was also observed that the sour rate was not linear at any stage of the flow sequence.

The influence of repetitive action of shear force due to water velocity on the soil surface for both the low and high flow conditions were also observed at field BD condition (2.03-2.04 gm/cm^3). It was observed that at higher flow velocity, less time was required for aggregate entrainment around the cylinder compared with low flow velocity, where higher time was required. This observation reveled that higher exposer time is required for breaking the inter-particle attractive forces between cohesive sediments at lower flow velocity and vice versa for higher flow velocity. However, soil with lower BD behaved somehow as non-cohesive sediment particle as scour initiated from the beginning of the experiment. Working with complete remolded sediment could have also influenced the scour behavior at lower BD, since higher WC played role in sediment dislodgement as the shear strength reduced significantly. Hotz and Kovacs (1981) showed that clay soils can behave as a liquid when thoroughly remolded at field same moisture content. Therefore, scour rate in remolded cohesive soil could be significantly different from the in-situ undisturbed consolidated cohesive soil.

6.3.4 Comparison between different scour depth equations

Using the flow hydraulics around the cylinder and soil properties, maximum scour depths were estimated using different equations and compared with HEC-18 equation. It was observed that all of these equations estimated similar maximum scour depths as HEC-18 equation except

Molinas and Hosny (1999) equation (Table 6.3.2). It is interesting to note that Debnath and Chaudhuri (2010a) estimated less equilibrium scour depths when the soil shear strength was higher compared with other methods. In other methods, soil properties were not considered for developing maximum scour depth equation except Briaud et al. (2011) equation. It is also important to note that Briaud et al. (2001, 2011) considered the time dependency and multi-flow condition for scour estimation using a hyperbolic time dependent formula. Depending on the duration of experimental run and other flow properties, therefore, the scour depths were estimated at each experimental run and compared with the time dependent scour depth equation (Table 6.3.2).

Results showed that overall the Briaud et al.(2001, 2011) methods predicted higher scour depths after each flow condition (Figure 6.3.5). Further analyzing the data, it was observed that at lower BD condition (1.51-1.86 gm/cm^3) the low flow sequence closely predicted the time dependent scour depths in both L-M-H and L-L-L flow sequences. It was also observed that predicted scour depths (using time dependent formula) deviated mostly for the intermediate flow condition for higher soil BD values. The deviation was also observed for the H-M-L flow sequence, though in this sequence at low flow the predicted scour depths were close. At higher flow conditions, probably the incorrect erosion rate estimation from the generalized curve developed by Briaud et al. (2011) could have influenced the scour depths estimation (Equation 6.3).

Table 6.3.2 Comparison of observed and predicted scour depth

Run No	τ_c (Pa)	τ_s (kPa)	Water Temp (°C)	Pier Reynolds No. (R_d)	Froude No. (Fr)	Observed max scour from this experiment after each flow (cm)	Total maximum scour after each experiment set (cm)	Estimated scour depth (cm)						
								Molinas and Hosny (1999)	Briaud et al. (2001)		Briaud et al. (2011)		Debnath and Chaudhuri, (2010a)	HEC-18
									After each flow	Max Scour	After each flow	Max Scour		
1	6.65	1.36	16.50	75429	0.743	2.20	2.20	64.16	9.65	23.97	9.77	21.19	13.08	20.61
2	6.52	1.40	17.80	98087	0.934	3.10	3.10	103.38	11.01	28.32	11.23	29.85	9.82	22.75
3	3.85	0.93	15.60	72521	0.731	1.00		62.09	2.15	23.38	2.17	22.93	17.31	20.47
4	3.85	0.93	12.60	74759	0.817	1.30	4.10	78.28	3.13	23.84	3.17	26.82	15.21	21.48
5	3.85	0.93	14.40	88127	0.917	2.50		99.51	4.89	26.46	5.04	31.34	13.31	22.57
6	2.35	0.62	16.50	74640	0.735	3.10		62.76	2.18	23.81	2.20	25.81	29.51	20.52
7	2.35	0.62	12.10	75245	0.834	1.50	6.70	81.67	3.13	23.93	3.22	30.29	30.04	21.67
8	2.35	0.62	10.90	80183	0.920	2.90		100.05	4.84	24.92	5.10	34.15	30.45	22.59
9	3.86	0.96	9.60	78614	0.936	3.00		103.81	4.83	24.61	5.06	32.17	12.72	22.77
10	3.86	0.96	10.20	70509	0.825	2.00	4.40	79.84	3.11	22.97	3.18	27.16	14.73	21.57
11	3.86	0.96	12.10	66265	0.735	1.40		62.70	2.16	22.08	2.17	23.07	16.85	20.51
12	2.10	0.65	14.40	89058	0.927	4.70		101.71	4.90	26.64	5.12	34.99	29.58	22.67
13	2.10	0.65	11.60	72785	0.818	1.30	7.30	78.48	3.12	23.43	3.22	30.09	30.11	21.49
14	2.10	0.65	13.40	68468	0.732	2.50		62.28	2.17	22.54	2.20	26.20	30.53	20.49
15	3.67	0.96	10.20	63470	0.743	2.50	2.50	64.15	5.39	21.48	5.53	23.75	16.63	20.61
16	2.05	0.48	13.40	68964	0.738	3.20	3.20	63.22	5.46	22.65	5.66	26.54	30.33	20.55
17	3.83	1.10	12.60	83522	0.913	5.30	5.30	98.58	9.92	25.58	10.66	31.19	11.91	22.53
18	2.28	0.48	10.60	79228	0.917	9.00	9.00	99.34	10.42	24.73	11.79	34.15	30.46	22.56

Note: Approach flow depth, h = 15.25 cm and cylinder diameter, D = 10.16 cm

Soil consistency, which is also known as Liquidity index (LI) is the relative ease to deform soil and dependent on the clay minerals and water content. LI is calculated based on field WC, LL, and PL. If LI < 0, soil will be brittle fracture if shredded, if LI = 0-1, is acts as plastic and if LI > 1 it acts as viscous liquid. Soil with LI > 1 is very sensitive to breakdown, though in undisturbed condition the soil is really strong (Hotz and Kovacs (1981). Henceforth, the behavior of remolded soil could be drastically different from the undisturbed field sample used for scour study. For this natural soil, LI value was 0.49, so soil was plastic type. However, at low BD condition, the soil was completely remolded, consequently affected the erosion behavior and higher erosion rate was observed.

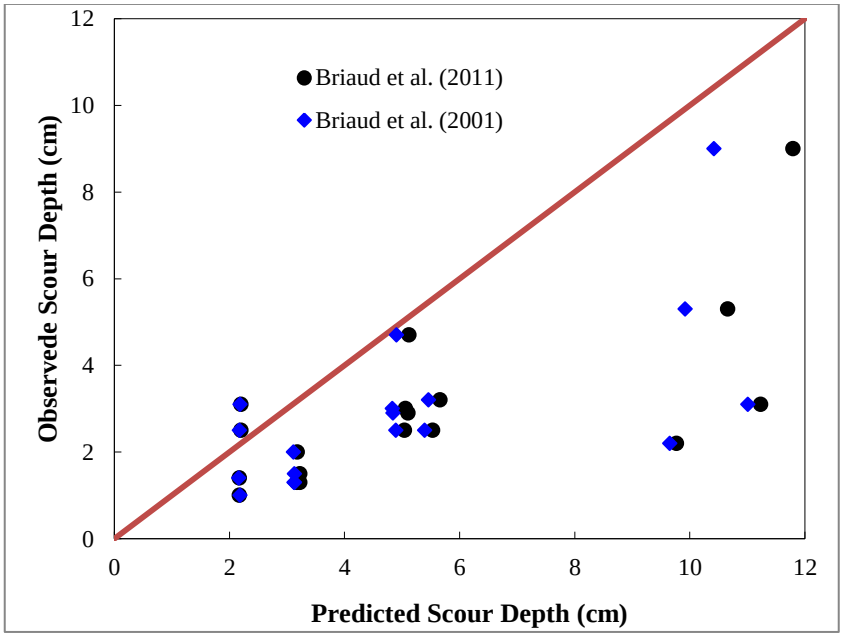


Figure 6.3.5: Observed and predicted scour depths after each experimental run

It was also important to note that prior collecting soil samples, in-situ mini-jet tests were conducted to estimate average critical shear stress, which ranged between 8.68 to 10.76 Pa. Measured critical shear stress of the prepared sediment bed at field BD condition was found

6.52-6.65 Pa, which was thought comparable to the field condition. This result also revealed the influence of soil physical properties on scour studies. Briaud et al. (1999, 2001, 2011) and Ting et al. (2001) also identified the issue and reported that soil should be tested in EFA for erosion rate measurement. In those studies, ultimate scour depth prediction equations were developed based on the commercially available clay soil, which was remolded completely. However, as we observed that the properties of field soil samples could be significantly different from those commercially available clay soils, consequently the erosion behavior could be different. Debnath and Chaudhuri (2010a) used field soil samples in their study, which was completely remolded and mixed with sand at different proportions at different WC conditions. They did not report any specific scour pattern rather reported higher shear strength for the field sample. It was expected that due to variation in shear strength of soil, the scour pattern should be different.

6.4 Conclusions

This study reports new data on scour around a vertically positioned cylinder in natural cohesive sediments under multi-flow conditions. The natural cohesive soil consist 3% sand, 72% silt and 25%. The influence of multi-flow events on scour evolution, the influence of previous stress history, and the time dependent scour developments were investigated. Contradictory findings have been reported in literature for local scour study around cylinders in cohesive beds, where either pure clay or mixture of clay-sand-gravel was used in those studies. The present study suggested that scour commenced at the lateral sides of the cylinder and maximum scour depth also occurred at sides irrespective of flow velocity and BD condition. For each flow and BD conditions both the τ_{max} and R_d values were higher, and larger downstream direction scour propagations were observed. It was also observed that shallow water condition (since $h/D < 2.0$)

influenced the lateral and transverse scour hole formation at the downstream side of the cylinder compared with the sides and upstream of the cylinder.

Scour propagation under multi-flow condition showed that depending on the soil BD conditions, almost similar maximum scour depths were observed for both the L-M-H and H-M-L flow sequence. The rate of scour rate was found dependent on initial flow and BD, where regardless of flow sequence scour rate was always slow at medium flow velocity. It was also observed that at higher BD condition (1.81-2.04 gm/cm^3) scour depths initiated after 3-12 hours of flow. Analyzing the time dependent scour development, it was observed that the available equations over predicted the equilibrium depths. For the field BD condition, those equations were estimating substantially higher scour depths, compared with observed scour depths from this study. This finding identified that the predicted equilibrium depth for this natural cohesive sediment was not similar to the non-cohesive sediments, which was reported by previous studies. Further research through a similar study design specifically targeting more flow events are necessary to better understand the scour development in natural cohesive soils and development of equilibrium scour depth equation.

6.5 References

Ansari SA, Kothyari UC, Ranga Raju KG. 2002. Influence of cohesion on scour around bridge piers. J. Hydraul. Res. 40(6): 717–729. DOI: DOI: 10.1080/00221680209499918

Black KS, Tolhurst TJ, Paterson DM, Hagerthey SE. 2002. Working with natural cohesive sediments. J. Hydraul. Eng., ASCE 128(1): 2-8

Briaud JL, Ting FCK, Chen HC, Gudavalli R, Perugu S, Wei G. 1999. SRICOS: Prediction of scour rate in cohesive soils at bridge piers. J. Geotech. Geoenviron. Eng. 125(4): 237–246

Briaud JL, Chen HC, Kwak KW, Han SW, Ting FCK. 2001. Multiflood and multilayer method for scour rate prediction at bridge piers. J. Geotech. Geoenviron. Eng. 127(2): 114–125

Briaud JL, Chen HC, Chang KA, Oh SJ, Chen S, Wang J, Li Y, Kwak K, Nartjaho P, Gudaralli R, Wei W, Pergu S, Cao YW, Ting F. 2011. The SRICOS-EFA Method. Summary Report, Texas A&M University, TX, USA

Chaudhuri S, Debnath K. 2013.Observations on initiation of pier scour and equilibrium scour hole in cohesive sediments. ISH J. Hydraulic Engineering 19(1): 27-37. DOI: http://dx.doi.org/10.1080/09715010.2012.749011

Costa JE, O'Connor JE. 1995. Geomorphically effective floods. In Natural and Anthropogenic Influences in Fluvial Geomorphology 89:45-56

Debnath K, Chaudhuri S. 2010a. Laboratory experiments on local scour around cylinder for clay and clay–sand mixed bed. Elsevier, Eng. Geol. 111(12): 51–61. DOI: 10.1016/j.enggeo.2009.12.003

Debnath K, Chaudhuri S. 2010b. Bridge pier scour in clay–sand mixed sediments at near-threshold velocity for sand. J. Hydraul. Eng. 136(9): 597–609. DOI: 10.1061/(ASCE)HY.1943-7900.0000221

Debnath K, Chaudhuri S. 2012. Local scour around noncircular piers in clay-sand cohesive sediment beds. Eng. Geol. 151(10): 1–14. DOI: http://dx.doi.org/10.1016/j.enggeo.2012.09.013

Devi YS, Barbhuiya AK. 2017. Bridge pier scour in cohesive soil: a review. Sadhana 42 (10): 1803–1819. DOI: https://doi.org/10.1007/s12046-017-0698-5

Grabowski RC, Droppo IG, Wharton G. 2011. Erodibility of cohesive sediment: the importance of sediment properties. Earth Sci. Rev. 105(1): 101-120. DOI:10.1016/j.earscirev.2011.01.008

Holtz RD, Kovacs WD. 1981. An introduction to geotechnical engineering. Prentice Hall Inc., Englewood Cliffs, NJ, USA

Hosny MM. 1995. Experimental study of local scour around circular bridge piers in cohesive soils. Ph.D. Dissertation, Civil Engineering Department, Colorado State University, Fort Collins, Colorado, USA

Julian JP, Torres R. 2006. Hydraulic erosion of cohesive riverbanks. Geomorphology 76:193-206. DOI:10.1016/j.geomorph.2005.11.003

Kothyari UC, Kumar A, Jain RK. 2014. Influence of cohesion on river bed scour in wake region of piers. J. Hydraul. Eng. 14(1): 1–13

Kwak K. 2000. Prediction of scour depth versus time for bridge piers in cohesive soils in the case of multi-flood and layered soil systems. Ph.D. Dissertation, Department of Civil Engineering, Texas A&M University, College Station, TX, USA

Mahalder B; Schwartz JS; Palomino AM; Zirkle J. 2017. Relationships between physical-geochemical soil properties and erodibility of streambanks among different physiographic provinces of Tennessee, USA. Earth Surface Processes and Landforms 43(2):401-416. DOI: 10.1002/esp.4252

Mahalder B, Schwartz JS, Palomino AM, Zirkle J. 2018. Estimating erodibility parameters for streambanks with cohesive soils using the mini jet test device: A comparison of field and computational methods. Water 10(3), 304. DOI:10.3390/w10030304

Melville BM, Cheiw YM. 1999. Time scale for local scour at bridge piers. J. Hydraul. Eng. 125(1): 59-65. DOI: https://doi.org/10.1061/(ASCE)0733-9429(1999)125:1(59)

Molinas A, Hosny MM. 1999. Experimental study on scour around circular piers in cohesive soil. Publication No. FHWA-RD- 99-186, Federal Highway Administration, U.S. Department of Transportation, McLean, VA, USA

Nezu I, Nakagawa H. 1993. Turbulence in open-channel flows. Balkema, Rotterdam, The Netherlands

Ting FCK, Briaud JL, Chen HC, Gudavalli R, Perugu S, Wei G. 2001. Flume tests for scour in clay at circular piers. J. Hydraul. Eng. 127(11): 969–978

CHAPTER VII
CONCLUSIONS AND FUTURE RECOMMENDATIONS

7.1 Summary and Conclusions

In this dissertation, erosion behavior in cohesive sediments has been investigated through intensive field tests and laboratory experiments. It was identified that several conditional factors were related to the erodibility parameters estimation for cohesive sediments: i) variability related to the device operation, ii) variability related to sediment source, iii) device dependent variability, and iv) soil heterogeneity are some of the few investigated in this study. Local scour depth propagation around cylinder was also investigated using natural cohesive sediments. In the following section general conclusions related to specific research question have been reported.

1. New MPS field operational and computational procedures for estimating the τ_c and k_d values provide some insight into the variability associated with previous jet operational and data analyses procedures. MPS method may better reflect fluvial erosion processes along a streambank/bed as multiple pressure heads have been used during tests. So MPS method estimates average erodibility parameter values of different soil layers rather than that of the surficial soil layer.
2. The MPS field methodology also provides better control on device operation and data analysis, which could help to avoid using any reduction factor (α) suggested by others to be incorporated in the excess shear stress equation for calculating erosion rate.
3. Extensive in-situ mini-jet tests in diverse geological origin revealed that no single soil property, or a common group of a select few properties will form an universal equation for predicting τ_c rather regional surficial geology influence the predictive

equations for τ_c and k_d estimation. It also appeared that individual equations need to be developed based on physiographic provinces as four different predictive equations have been identified among the diverse geology of Tennessee, USA.

4. Soil properties, WC and Pass200 were found to control τ_c prediction. Other soil properties: CC, DR, LL, SAR, and OC were also found to be dominant variables within the predictive models. D_{50} was found the least significant variable in predicting τ_c for cohesive soils.
5. Device dependent variability was studied for erosion parameters (τ_c and k_d) prediction using a laboratory device: the pressurized conduit flume, and an in-situ device: the submersible mini-jet. Results suggested that the operational and data analyses procedures in jet tests were persuasive, which also justify the needs to develop a new methodology (the MPS method) for jet operation.
6. It was identified that k_d estimations was challenging regardless of the device been used. It was also identified that soil type and present soil moisture content had significant impact on the τ_c and k_d values estimation.
7. Estimating equilibrium scour depths around bridge piers in cohesive soils was identified as a challenging topic for hydraulic engineers. Combining the field tests and hydrologic flow simulation, it was identified that cumulative effective stream power correlated well with the observed bridge pier scour data. Scour depth development in cohesive soils appeared to be dependent on the effective shear stress duration rather than number of flow events above the critical threshold values. The influence of flow history on scour rate propagation in cohesive earth material from multiple flow events was also observed.

8. Erodibility index (*K*), a surrogate measure to scour resistance of earth material was significantly correlated to critical stream power (R^2 = 0.61, p = 0.017). Data from this study showed a clear deviation from the Annandale (1995, 2006) developed empirical relationship for soils with erodibility index value less than 0.1. This finding implied that direct in-situ measurements of erosion parameters are necessary for the critical stream power calculation rather using an empirical relationship.
9. Formulating a conceptual study design by mimicking the natural flow condition, scour study in natural cohesive sediments around cylinders under multi-flow condition was conducted. Study findings suggested that scour commenced at the sides of the cylinder and maximum scour depth also occurred at sides irrespective of flow velocity and BD condition. It was also observed that shallow water condition (since $h/D < 2.0$) influenced the lateral and transverse scour hole propagation at the downstream side of the cylinder compared with the sides and upstream of the cylinder.
10. Scour propagation under multi-flow condition showed that depending on the soil BD conditions, almost similar maximum scour depths were observed for both the L-M-H and H-M-L flow sequence. It was also observed that at higher BD condition (1.81-2.04 gm/cm^3) scour depths initiated after 3-12 hours of flow, which supported the hypothesis that memory effect could have influence on scour propagation in cohesive soils.
11. Analyzing the time dependent scour development, it was observed that the available equations over predicted the equilibrium depths. For the field BD condition, those equations were estimating substantially higher scour depths. However, at lower BD

condition the observed scour depths were comparable to the predictive equations. This finding suggested that physical properties of the sediment among those studies could have influenced the scour prediction equation since relatively lower BD values have been reported by those studies.

7.2 Limitations and Recommendations

Soil heterogeneity is common when working with natural undisturbed sediments, consequently, biasness is expected in some of these findings. Predictive τ_c equations were not also validated from more field test in similar geological formations. It is also important to note that in Chapter V, lack of channel cross-sectional data over time which could have influenced the critical flow calculation, since one cross-sectional data was used for the calculation by assuming uniform flow depth. Also scour data were collected by several TDOT operators without a standard operating procedure. Due to limited resources and time, limited numbers of flow sequences were tested for the laboratory flume scour experiments. No predictive equation was also developed using this limited data. Considering these, the following recommendations are proposed for future research:

1. More field tests should be conducted to verify the critical shear stress predictive equations among similar geological locations.
2. By preparing homogenous sediment bed using natural cohesive sediment tests should be conducted, where soil should be consolidated to the field condition and placed in a controlled environment to develop necessary organic matter for the necessary strength development.
3. Some pilot study bridge sites which foundations are on cohesive soils should be selected to monitor both the scour depths and the corresponding flow parameters

over time. Based on the collected data, scour prediction equations could be improved since in laboratory flume it is not always possible to develop all the complex hydrodynamics.

4. Flume experiments should be extended by incorporating more flow sequences and soil types, where prepared sediment should be kept under same field condition for long time for attaining necessary cohesive strengths and consolidation. Based on those experiments, scour depth prediction equations could be improved for greater accuracy.

APPENDIX

Appendix A.1 Cluster Data

Table A.1.1 Custer 1 data

Location	τ_c (Pa)	K (cm^3/N-s)	WC %	BD (g/cm^3)	DD (g/cm^3)	D_{50} (µm)	DR	SG	Cu (Psi)	Str %	e	n	LL %	PL %	PI %	OC %	SAR	KIA	Pass200 %	σ_g	Sand %	Silt %	Clay %	pH	SS (m^2/g)	T (C)	CA	EC (µS)	Con
90' d/s Lower Bank L/B (Gist Creek)	8.10	1.5	27.5	1.96	1.53	26.0	0.45	2.68	8.00	3.15	0.75	0.43	29.6	21.35	8.27	2.69	2.68	0.05	77	10.54	33	44	23	6.98	25.7	25.4	0.36	258	0.26
55' d/s Middle Bank L/B (Gist Creek)	3.65	2.04	34.1	1.84	1.37	40.0	0.40	2.65	1.27	9.00	0.95	0.49	27.8	20.35	7.45	3.93	2.15	0.13	60	17.00	50	30	20	7.07	32.4	26.4	0.37	506	-0.84
50' d/s Upper Bank L/B (Gist Creek)	5.87	0.89	38.1	1.72	1.24	30.0	0.37	2.65	3.24	4.50	1.13	0.53	26.3	17.63	8.65	4.10	3.36	0.04	61	15.97	43	37	20	7.27	26.3	27.4	0.43	520	-1.37
20' d/s Lower Bank R/B (Gist Creek)	7.55	1.23	35.1	1.81	1.34	27.0	0.49	2.68	3.88	13.10	0.64	0.39	29.2	22.35	6.85	4.45	5.05	0.03	72	14.39	38	39	23	7.49	32.4	22.4	0.3	466	-0.86
140' d/s Middle Bank R/B (Gist Creek)	4.12	1.56	35.1	1.81	1.34	29.0	0.29	2.64	6.05	4.10	0.97	0.49	34.8	27.20	7.60	4.87	3.16	0.04	67	15.17	42	37	21	7.16	30.6	21.4	0.36	410	-0.03
160' d/s Upper Bank R/B (Gist Creek)	5.50	1.15	34.8	1.73	1.28	35.0	0.29	2.66	3.13	3.65	1.07	0.52	32.8	26.32	6.48	6.55	3.8	0.07	68	12.57	42	38	20	7.28	30.6	24.6	0.32	612	-0.31
150' u/s Lower Bank L/B (Pistol Creek)	6.21	1.27	39.5	1.93	1.49	4.7	0.38	2.68	4.83	14.65	0.71	0.41	34.2	21.97	12.23	4.49	1.58	0.33	90	17.28	12	49	39	6.4	19.0	18.6	0.31	353	-0.43
200' u/s Middle Bank L/B (Pistol Creek)	6.36	1.35	34.1	1.85	1.38	3.8	0.29	2.65	3.25	4.81	0.92	0.48	37.2	23.36	13.84	5.78	1.23	0.05	92	16.67	8	51	41	7.25	19.6	19.2	0.34	342	0.23
200' u/s Upper Bank L/B (Pistol Creek)	3.69	1.38	38.1	1.65	1.20	5.3	0.20	2.65	3.00	2.68	1.28	0.56	41.7	25.71	15.99	8.21	1.1	0.12	91	10.49	12	50	38	7.35	42.8	17.6	0.42	590	0.22
Under Bridge Lower Bank R/B (Pistol Creek)	3.92	2.67	28.3	1.79	1.30	6.8	0.43	2.68	1.78	20.20	1.06	0.51	39.4	22.63	16.77	8.65	3.53	0.24	80	25.82	21	47	32	6.89	50.8	18.8	0.52	647	0.66
15' u/s Middle Bank R/B (Pistol Creek)	3.39	1.98	27.9	1.73	1.19	9.6	0.43	2.64	1.40	11.55	1.13	0.53	38.6	24.26	14.34	7.01	8.21	0.28	82	20.00	19	48	33	7.16	50.2	20.2	0.43	608	0.75
5' d/s Upper Bank R/B (Pistol Creek)	3.95	1.87	21.2	1.57	1.17	7.0	0.26	2.66	2.47	2.90	1.30	0.57	41.0	25.71	15.29	4.52	1.54	0.09	87	11.18	16	47	37	7.36	50.8	24.1	0.41	535	1.29
5' u/s Lower Bank L/B (Nine Mile Creek)	2.94	3.96	25.7	1.85	1.40	8.3	0.30	2.60	1.55	8.23	0.85	0.46	36.7	20.54	16.16	4.35	4.75	0.03	82	27.29	19	50	31	6.4	45.9	24.6	0.52	22.3	0.68
30' u/s Middle Bank L/B (Nine Mile Creek)	2.77	2.24	25.9	1.72	1.25	12.0	0.31	2.50	2.15	5.99	1.00	0.50	37.0	25.50	11.5	7.22	2.33	0.05	76	21.21	26	45	29	6.66	45.9	28.6	0.4	48	0.97
15' d/s Top Bank L/B (Nine Mile Creek)	2.87	2.64	18.7	1.70	1.23	7.8	0.30	2.55	3.08	5.34	1.08	0.52	41.5	29.37	12.13	6.93	0.99	0.03	87	24.49	16	51	33	6.57	45.9	23.7	0.37	40.6	1.88
20' u/s Lower Bank R/B (Nine Mile Creek)	9.13	1.05	36.4	1.52	0.98	12.0	0.34	2.53	8.56	5.64	1.61	0.61	39.2	29.84	9.36	7.51	0.6	0.15	81	12.91	23	50	27	6.77	52.0	16.8	0.35	55.3	0.30
10' d/s Middle Bank R/B (Nine Mile Creek)	3.65	3.72	34.6	1.72	1.29	14.0	0.32	2.57	2.30	3.10	0.99	0.50	34.3	24.81	9.49	5.55	1.75	0.09	79	12.37	27	50	23	6.55	49.5	22.3	0.41	32.2	-0.03
15' d/s Upper Bank R/B (Nine Mile Creek)	3.25	2.68	31.8	1.72	1.23	10.0	0.36	2.58	2.70	5.50	1.10	0.52	42.5	30.65	11.85	1.6	0.7	0.18	86	10.80	21	54	25	6.67	50.8	17.9	0.47	29.5	0.90

Table A.1.1 (continued)

Location	τ_c (Pa)	K (cm^3/N-s)	WC %	BD (g/cm^3)	DD (g/cm^3)	D_{50} (µm)	DR	SG	Cu (Psi)	Str %	e	n	LL %	PL %	PI %	OC %	SAR	KIA	Pass200 %	σ_g	Sand %	Silt %	Clay %	pH	SS (m^2/g)	T (C)	CA	EC (µS)	Con
100' d/s Lower Bank L/B (South Chickamauga)	8.56	0.90	27.2	2.03	1.68	7.9	0.31	2.57	6.53	11.57	0.54	0.35	31.4	18.58	12.82	3.33	1.36	0.02	91	20.98	12	54	34	6.15	55.0	21.6	0.38	7.07	0.33
150' d/s Middle Bank L/B (South Chickamauga)	6.29	1.25	20.7	1.95	1.58	9.0	0.36	2.60	5.71	13.47	0.64	0.39	28.2	18.64	9.56	3.59	0.38	0.03	84	20.00	19	47	34	6.09	49.5	20.6	0.28	7.92	0.78
20' u/s Lower Bank R/B (South Chickamauga)	4.26	3.12	29.1	1.88	1.41	3.7	0.32	2.61	2.60	15.45	0.85	0.46	36.6	21.30	15.3	6.66	1.63	0.03	97	10.90	4	53	43	5.96	53.2	21.2	0.36	9.98	0.49
0' u/s Middle Bank R/B (South Chickamauga)	3.75	3.27	28.7	1.91	1.46	6.2	0.26	2.58	3.66	6.67	0.77	0.44	30.2	19.21	10.99	4.58	3.09	0.02	82	19.36	19	47	34	6.24	51.4	19.6	0.32	15.1	0.14
10' u/s Lower Bank L/B (Oostanaula Creek)	5.05	1.93	29.5	1.96	1.53	15.0	0.34	2.61	2.91	7.61	0.71	0.41	27.3	16.89	10.41	4.51	0.99	0.03	74	25.82	27	46	27	6.75	44.7	22.5	0.39	25.9	-0.21
Below bridge Middle Bank L/B (Oostaunaula)	2.88	4.27	23.5	2.02	1.71	9.5	0.30	2.62	4.83	5.32	0.54	0.35	36.0	17.74	18.26	5.25	0.59	0.26	80	24.81	21	49	30	6.53	48.3	22.9	0.61	22	0.68
30' d/s Upper Bank L/B (Oostaunaula Creek)	2.27	4.4	17.6	1.84	1.50	17.0	0.30	2.66	5.26	3.91	0.76	0.43	28.7	17.43	11.27	3.89	0.38	0.03	69	22.91	32	40	28	6.3	52.0	25.6	0.4	9.87	0.98
30' d/s Lower Middle L/B (Cane Creek)	2.14	2.93	26.3	1.91	1.51	18.0	0.29	2.61	7.50	11.59	0.73	0.42	29.9	24.13	5.77	2.4	1.62	0.07	95	5.00	8	74	18	7.35	53.2	22.9	0.32	234	0.63
5' d/s Middle L/B (Cane Creek)	2.50	4.25	32.3	1.79	1.35	24.0	0.38	2.59	2.50	13.61	0.91	0.48	31.2	25.08	6.12	3.81	1.63	0.17	75	10.58	31	52	17	7.5	57.5	24.3	0.36	370	-0.19
35' d/s Lower L/B (Cane Creek)	4.20	1.8	26.1	1.95	1.55	18.0	0.44	2.57	7.01	12.45	0.66	0.40	28.8	21.90	6.90	2.68	1.69	0.13	93	5.77	5	77	18	7	61.2	22.4	0.38	243	0.40
30' u/s Middle R/B (Cane Creek)	1.68	6.3	33.0	1.75	1.32	19.0	0.25	2.61	2.87	14.85	0.98	0.50	34.2	28.28	5.92	3.66	4.44	0.25	92	5.96	10	72	18	7.61	39.8	21.5	0.33	584	0.20
215' d/s Top R/B (Lewis Creek)	0.78	10.07	29.8	1.83	1.41	20.5	0.49	2.63	2.46	12.86	0.86	0.46	30.4	24.94	5.457	2.04	0.79	0.1	93	4.06	10	73	17	7.82	22.6	22.4	0.32	195	0.11
90' u/s Top Middle R/B (Reed Creek)	0.002	14.95	34.2	1.80	1.34	18.0	0.15	2.58	2.61	13.25	0.92	0.48	29.8	22.71	7.09	2.76	2.13	0.77	94	7.01	5	72	23	7.44	56.3	29.2	0.31	164	-0.62
0' d/s Lower R/B (Richland Creek)	4.00	2.5	32.4	1.68	1.27	24.0	0.22	2.60	2.55	7.67	1.05	0.51	28.2	24.48	3.72	3.38	6.27	0.23	88	4.13	15	70	15	7.56	36.7	29.7	0.25	496	-1.14

Table A.1.2 Cluster 2 data

Location	τ_c (Pa)	K (cm^3/N-s)	WC %	BD (g/cm^3)	DD (g/cm^3)	D_{50} (µm)	DR	SG	Cu (Psi)	Str %	e	n	LL %	PL %	PI %	OC %	SAR	KIA	Pass200 %	σ_g	Sand %	Silt %	Clay %	pH	SS (m^2/g)	T (C)	CA	EC (µS)	Con
0' u/s Middle Bank R/B (South Chickamauga)	3.75	3.27	28.7	1.91	1.46	6.2	0.26	2.58	3.66	6.67	0.77	0.44	30.2	19.21	10.99	4.58	3.09	0.02	82	19.36	19	47	34	6.24	51.4	19.6	0.32	15.05	0.14
10' d/s Lower R/B (Cane Creek)	2.70	2.14	36.6	1.78	1.31	24.0	0.21	2.58	2.20	10.48	0.98	0.49	33.0	27.82	5.18	3.58	1.53	0.21	84	3.67	22	66	12	7.67	55.0	22.4	0.43	432	-0.70
210' d/s Middle L/B (Lewis Creek)	0.13	13.95	37.6	1.76	1.27	30.0	0.46	2.65	1.24	22.45	1.07	0.52	32.6	27.38	5.22	2.42	0.91	0.19	82	2.70	30	60	10	8.11	59.3	21.4	0.52	478	-0.95
215' d/s Middle L/B (Lewis Creek)	0.36	24.28	37.3	1.75	1.28	24.0	0.46	2.63	1.96	13.50	1.08	0.52	32.6	27.65	4.95	2.70	0.69	0.26	92	2.53	12	75	13	7.14	28.1	21.2	0.38	243	-0.96
220' d/s Middle L/B (Lewis Creek)	0.09	6.92	38.0	1.76	1.27	28.0	0.47	2.62	2.88	12.60	1.06	0.51	32.3	27.13	5.17	2.21	0.69	0.18	89	2.04	16	74	10	8.12	39.1	23.4	0.52	336	-1.11
90' u/s Middle R/B (Lewis Creek)	1.47	6.70	41.0	1.69	1.20	22.0	0.45	2.60	2.05	6.68	1.16	0.54	34.8	28.74	6.06	3.04	0.67	0.45	91	2.59	17	70	13	7.91	37.3	23.5	0.47	415	-1.02
200' d/s Lower R/B (Lewis Creek)	6.90	1.79	30.7	1.94	1.48	14.0	0.54	2.66	5.85	14.40	0.80	0.44	29.6	23.98	5.62	2.00	2.85	0.28	98	4.71	3	79	18	6.91	47.1	22.8	0.31	195.5	-0.20
210' d/s Middle R/B (Lewis Creek)	4.00	1.90	33.3	1.87	1.40	16.0	0.46	2.59	4.13	22.90	0.87	0.46	33.8	26.07	7.73	1.99	3.40	0.09	98	6.44	4	74	22	7.08	68.5	22.5	0.35	165.3	0.07
80' u/s Top Middle R/B (Lewis Creek)	2.20	5.90	33.2	1.68	1.26	29.0	0.62	2.62	2.72	8.23	1.07	0.52	32.9	27.27	5.63	2.60	0.38	0.31	88	2.57	18	67	15	7.72	22.0	23.6	0.38	374	-0.06
70' u/s Middle R/B Slump # 1 (Lewis Creek)	0.18	18.20	36.3	1.80	1.32	29.0	0.59	2.69	2.50	13.85	1.04	0.51	32.6	28.21	4.35	2.69	0.45	0.36	85	2.65	24	64	12	7.95	44.7	22.5	0.36	541	-0.87
70' u/s Middle R/B Slump # 2 (Lewis Creek)	.001	24.40	35.5	1.82	1.34	24.0	0.48	2.60	2.20	12.65	0.94	0.48	32.8	28.74	4.06	3.23	0.90	0.82	95	2.53	9	76	15	7.84	48.3	23.2	0.27	624	-0.68
75' u/s Lower R/B (Lewis Creek)	2.25	6.5	37.7	1.81	1.32	24.0	0.56	2.66	2.66	17.34	1.02	0.50	32.0	26.99	5.01	2.47	0.5	0.26	94	2.20	10	78	12	8.09	52.0	21.5	0.42	350	-1.14
15' u/s Middle L/B (Pond Creek)	3.25	4.215	32.0	1.84	1.39	12.0	0.39	2.59	3.27	14.72	0.87	0.46	31.8	22.23	9.57	2.86	3.48	0.30	99	8.94	2	70	28	5.88	46.5	24.1	0.34	103.9	-0.02
120' d/s Lower L/B (Pond Creek)	5.72	1.72	26.3	2.02	1.60	9.0	0.34	2.57	8.85	16.96	0.61	0.38	39.0	21.37	17.63	3.36	3.27	0.14	97	17.32	4	61	35	6.98	154.1	24.3	0.50	198.1	0.72
10' d/s Top L/B (Pond Creek)	0.94	6.19	29.4	1.76	1.36	18.0	0.33	2.60	2.77	13.72	0.91	0.48	26.4	20.51	5.892	3.07	1.33	0.25	77	14.47	25	58	17	6.73	42.2	25.5	0.35	99.6	-0.52
40' d/s Lower R/B (Pond Creek)	4.86	1.33	26.5	1.99	1.57	8.5	0.32	2.63	9.60	16.72	0.67	0.40	40.6	19.94	20.66	3.28	2.8	0.09	97	16.33	4	59	37	7.03	136.4	23.1	0.56	136.6	0.68
10' d/s Middle R/B (Pond Creek)	2.12	3.45	30.6	1.87	1.43	16.0	0.43	2.63	4.75	16.55	0.84	0.46	30.9	24.43	6.47	2.26	2.9	0.32	96	5.29	7	75	18	6.45	38.5	24.8	0.36	227	0.05
5' u/s Upper Middle R/B (Pond Creek)	1.86	4.91	27.9	1.91	1.50	17.0	0.54	2.64	3.87	10.55	0.76	0.43	30.0	23.56	6.44	2.11	9.13	0.21	97	5.58	5	77	18	7.2	26.9	22.7	0.36	180.6	0.32

Table A.1.2 (continued)

Location	τ_c (Pa)	K (cm^3/N-s)	WC %	BD (g/cm^3)	DD (g/cm^3)	D_{50} (µm)	DR	SG	Cu (Psi)	Str %	e	n	LL %	PL %	PI %	OC %	SAR	KIA	Pass200 %	σ_g	Sand %	Silt %	Clay %	pH	SS (m^2/g)	T (C)	CA	EC (µS)	Con
20' d/s Lower R/B (Pond Creek)	5.15	1.52	27.5	1.96	1.54	7.0	0.22	2.49	7.96	15.20	0.62	0.38	40.0	20.03	19.96	3.48	4.66	0.12	96	18.71	7	54	39	7.08	112.5	28.8	0.51	135	0.63
Under Bridge Lower Bank R/B (Pond Creek)	1.26	2.04	29.5	1.99	1.54	12.2	0.41	2.55	5.60	12.20	0.66	0.40	33.2	20.62	12.57	2.81	4.08	0.16	96	9.49	6	64	30	7.26	71.6	25.2	0.42	232	0.29
50' u/s Lower L/B (Reed Creek)	3.69	1.96	30.6	1.93	1.48	11.5	0.30	2.64	6.38	13.35	0.79	0.44	33.4	19.43	13.97	2.78	2.93	0.35	94	19.64	7	58	35	7.17	92.4	28.5	0.40	133.4	0.20
30' u/s Middle L/B (Reed Creek)	2.96	4.79	30.9	1.90	1.45	16.0	0.22	2.63	3.41	11.72	0.81	0.45	26.8	20.71	6.1	2.38	6.69	0.12	89	8.60	13	64	23	7.49	42.8	28.4	0.27	246	-0.67
70' u/s Lower R/B (Reed Creek)	2.62	3.79	33.5	1.87	1.40	15.8	0.23	2.63	3.95	17.97	0.88	0.47	30.6	23.54	7.06	2.67	3.3	0.23	99	11.96	2	75	23	7.34	58.1	28.4	0.31	205	-0.41
5' d/s Lower R/B (Reed Creek)	5.47	1.85	31.4	1.86	1.42	16.0	0.31	2.60	2.74	17.80	0.83	0.45	29.2	22.56	6.64	2.82	4.16	0.98	94	6.55	7	70.5	22.5	6.03	48.3	29.9	0.29	337	-0.32
15' d/s Lower Middle R/B (Reed Creek)	2.15	4.64	30.5	1.86	1.43	14.0	0.40	2.66	4.64	12.60	0.87	0.46	31.4	23.14	8.26	3.12	5.04	0.23	97	9.54	4	71	25	7.28	71.0	30.1	0.33	285	0.10
30' d/s Lower R/B (Reed Creek)	0.37	8.18	32.5	1.87	1.41	17.0	0.25	2.60	4.13	11.56	0.84	0.46	29.5	23.04	6.42	2.73	4.91	0.58	98	7.55	3	75	22	6.41	55.7	29.5	0.29	304	-0.47
20' u/s Lower L/B (Richland Creek)	5.45	3.02	20.5	2.12	1.76	15.8	0.51	2.63	15.65	6.89	0.50	0.33	23.6	18.17	5.42	2.12	4.78	0.15	93	5.77	9	72	19	7.39	59.9	28	0.28	381	0.56
40' u/s Middle L/B (Richland Creek)	3.63	3.07	32.6	1.87	1.41	24.0	0.22	2.67	3.20	16.75	0.90	0.47	29.4	24.08	5.27	2.02	6.3	0.10	83	4.24	20	66	14	7.29	40.4	28.5	0.377	590	-0.62
10' u/s Top Middle R/B (Richland Creek)	0.17	22.12	28.0	1.85	1.44	24.0	0.15	2.65	4.64	6.30	0.83	0.45	27.6	23.39	4.21	2.37	1.45	0.23	83	4.74	20	65	15	7.69	35.5	30	0.28	540	-0.11
40' d/s Upper Middle R/B (Big Creek)	5.00	2.25	29.3	1.89	1.46	16.0	0.31	2.64	5.93	13.34	0.80	0.44	30.6	24.06	6.54	1.78	20.18	0.04	97	4.83	6	76	18	7.15	66.1	28.6	0.36	489	0.19

Table A.1.3 Cluster 3 data

Location	τ_c (Pa)	K (cm^3/N-s)	WC %	BD (g/cm^3)	DD (g/cm^3)	D_{50} (µm)	DR	SG	Cu (Psi)	Str %	e	n	LL %	PL %	PI %	OC %	SAR	KIA	Pass 200 %	σ_g	Sand %	Silt %	Clay %	pH	SS (m^2/g)	T (C)	CA	EC (µS)	Con
200' d/s Upper Bank L/B (South Chickamauga)	3.34	2.57	31.8	1.74	1.39	7.0	0.29	2.54	5.44	12.36	0.83	0.45	37.4	24.52	12.9	6.91	0.32	0.07	87	14.14	16	50	34	6.72	51.4	24.8	0.38	34.3	0.43
15' d/s Lower R/B (Richland Creek)	8.00	1.31	23.4	2.08	1.68	15.5	0.46	2.65	14.50	8.85	0.58	0.37	27.0	18.40	8.6	1.93	2.59	0.14	85	10.0	12	65	23	7.53	61.8	29.6	0.37	129	0.42
30' d/s Upper Middle R/B (Richland Creek)	2.76	4	29.3	1.89	1.46	22.0	0.28	2.64	3.58	11.98	0.80	0.45	28.6	24.50	4.05	1.97	0.93	0.13	84	2.72	20	66	14	7.72	36.1	28.8	0.29	231	-0.18
40' d/s Lower Middle R/B (Richland Creek)	2.80	2.7	31.2	1.89	1.44	23.0	0.39	2.68	2.94	14.25	0.86	0.46	26.9	22.23	4.67	2.07	1.29	0.1	83	6.32	20	65	15	7.63	34.3	28.2	0.31	276	-0.93
40' d/s Lower L/B (North Reelfoot Creek)	1.59	5.93	29.9	1.92	1.48	22.0	0.33	2.60	4.53	9.21	0.76	0.43	29.4	25.96	3.44	1.74	1.25	0.24	93	4.71	5	78	17	7.6	12.8	29.2	0.2	229	-0.14
30' d/s Middle L/B (North Reelfoot Creek)	2.06	5.46	33.9	1.82	1.36	21.0	0.30	2.59	3.90	9.35	0.91	0.48	31.8	25.18	6.58	2.99	7.69	0.8	94	5.31	8	74	18	7.44	28.7	29.5	0.37	659	-0.33
10' u/s Lower R/B (North Reelfoot Creek)	3.98	1.99	42.4	1.65	1.16	20.0	0.45	2.56	1.39	11.47	1.21	0.55	33.4	29.07	4.33	4.77	1.84	0.76	94	5.28	8	74	18	7.07	40.4	27.8	0.24	532	-2.07
25' u/s Middle R/B (North Reelfoot Creek)	1.79	5.9	27.8	1.89	1.48	21.8	0.45	2.64	5.02	7.34	0.79	0.44	29.8	24.51	5.29	2.08	4.89	0.07	97	5.22	5	78	17	7.72	33.6	27.2	0.31	456	0.38
10' d/s Lower R/B (North Reelfoot Creek)	4.62	2.3	38.2	1.71	1.24	18.0	0.41	2.54	2.83	7.47	1.05	0.51	35.0	29.10	5.9	4.02	0.85	0.44	95	5.22	7	74	19	7.48	34.9	29.2	0.31	417	-0.54
60' d/s Bottom of Creek L/B (Black Creek)	14.00	0.75	29.4	1.97	1.52	14.6	0.39	2.70	8.68	7.84	0.77	0.44	35.4	23.57	11.8	1.77	5.21	0.31	98	13.42	3	73	24	7	80.1	29	0.49	151	0.51
40' d/s Middle L/B (Black Creek)	4.05	2.13	28.5	1.94	1.51	15.0	0.40	2.67	6.68	11.84	0.77	0.44	32.3	21.80	10.5	1.94	14.5	0.06	97	16.73	4	71	25	6.23	78.9	29.2	0.42	570	0.36
15' u/s Top R/B (Black Creek)	2.14	3.76	29.3	1.85	1.43	16.0	0.35	2.66	3.96	7.63	0.86	0.46	29.4	23.38	6.02	1.95	6.79	0.21	97	5.13	5	77	18	6.49	24.5	27.5	0.33	110	0.02
10' u/s Middle R/B (Black Creek)	1.22	3.91	28.1	1.93	1.50	13.0	0.26	2.60	6.20	9.33	0.73	0.42	35.8	22.82	13	2.19	10.2	0.09	98	9.13	3	69	28	6.9	59.9	29.4	0.46	480	0.59
Below Bridge Lower R/B (Black Creek)	10.00	1.1	27.2	1.94	1.52	16.0	0.24	2.63	8.28	10.45	0.73	0.42	30.6	23.00	7.6	1.48	6.69	0.12	98	6.02	4	77	19	6.62	101.5	28.2	0.4	292	0.44
Under Bridge Top R/B (Black Creek)	2.25	6.2	30.1	1.82	1.40	17.0	0.31	2.63	4.42	8.72	0.88	0.47	29.1	23.59	5.51	1.82	10.5	0.17	98	4.43	3	79	18	6.5	20.2	28	0.31	609	-0.19
30' u/s Lower L/B (Beaver Creek)	6.80	1.15	25.0	1.97	1.57	10.0	0.33	2.58	2.52	21.40	0.64	0.39	28.1	18.37	9.73	2.73	23.1	0.14	87	9.62	11	60	29	5.23	35.5	27.8	0.34	131	0.32
15' u/s Top L/B (Beaver Creek)	2.57	2.82	29.7	1.86	1.44	5.4	0.24	2.61	9.30	8.19	0.82	0.45	35.4	24.39	11	3.8	4.04	0.12	91	11.73	10	55	35	4.83	31.8	27.8	0.31	90.8	0.51
30' d/s Middle L/B (Beaver Creek)	9.10	0.82	21.8	2.06	1.69	13.0	0.45	2.60	12.78	5.47	0.54	0.35	27.8	17.99	9.82	2.58	12.6	0.18	83	17.26	20	52	28	4.89	31.8	27.9	0.35	110	0.61
40' d/s Upper Middle L/B (Beaver Creek)	8.20	1	23.1	1.98	1.61	15.0	0.52	2.63	6.33	8.84	0.63	0.39	25.8	19.04	6.76	2.26	3.58	0.18	82	11.70	23	54	23	4.97	20.8	28.9	0.29	59	0.40

Table A.1.3 (continued)

Location	τ_c (Pa)	K (cm^3/N-s)	WC %	BD (g/cm^3)	DD (g/cm^3)	D_{50} (µm)	DR	SG	Cu (Psi)	Str %	e	n	LL %	PL %	PI %	OC %	SAR	KIA	Pass 200 %	σ_g	Sand %	Silt %	Clay %	pH	SS (m^2/g)	T (C)	CA	EC (µS)	Con
25' u/s Lower R/B (Beaver Creek)	7.37	1.23	22.3	2.05	1.68	14.0	0.56	2.61	8.25	8.84	0.56	0.36	24.6	16.76	7.84	2.38	10.7	0.19	81	17.32	20	55	25	5.57	30.0	29.5	0.31	79.8	0.29
Under Bridge Middle R/B (Beaver Creek)	11.20	1.02	23.4	2.02	1.63	8.5	0.45	2.61	8.78	10.86	0.60	0.37	27.4	18.95	8.45	2.67	12.3	0.32	91	8.44	10	60	30	4.93	36.1	28.6	0.28	127	0.47
5' u/s Bottom of Creek L/B (Crooked Creek)	26.80	0.56	24.4	2.05	1.65	12.0	0.36	2.66	9.80	15.63	0.61	0.38	29.0	18.85	10.2	1.98	5.34	0.1	98	20.0	3	72	25	7.11	46.5	27.7	0.41	87.2	0.45
10' u/s Middle L/B (Crooked Creek)	5.31	1.41	24.2	2.02	1.63	15.7	0.45	2.64	5.50	19.07	0.62	0.38	27.5	19.97	7.53	1.74	5.97	0.08	96	6.44	7	72	21	7.2	53.2	28.1	0.36	94.8	0.44
40' u/s Top L/B (Crooked Creek)	9.48	0.92	25.0	2.00	1.60	16.0	0.63	2.69	6.48	15.47	0.68	0.40	27.6	21.42	6.18	1.55	23.7	0.07	97	4.72	5	78	17	7.54	30.0	28	0.36	148	0.41
5' u/s Bottom of Creek R/B (Crooked Creek)	11.20	0.85	23.9	2.04	1.64	15.0	0.44	2.64	9.53	9.43	0.60	0.38	27.6	19.86	7.74	1.74	5.14	0.07	97	9.83	3	75	22	7.42	41.0	30	0.35	189	0.48
30' d/s Lower R/B (Crooked Creek)	15.00	0.59	23.2	2.05	1.66	14.0	0.36	2.67	8.15	7.83	0.61	0.38	28.2	18.44	9.76	2.09	3.76	0.09	96	10.0	6	69	25	7.07	41.6	31.4	0.39	91.9	0.51
45' d/s Upper Middle R/B (Crooked Creek)	6.24	3.35	22.9	2.03	1.65	15.8	0.43	2.68	7.58	12.72	0.63	0.39	27.6	19.96	7.6	1.71	3.47	0.08	96	6.07	6	72	22	7.27	23.2	31	0.35	126	0.61
40' u/s Middle L/B (Big Creek)	14.80	0.62	27.1	1.96	1.54	16.0	0.39	2.62	8.23	11.22	0.70	0.41	29.2	22.56	6.65	1.95	22.5	0.1	97	4.47	7	76	17	7.05	32.4	34.5	0.39	244	0.32
20' u/s Bottom of Creek L/B (Big Creek)	11.20	0.84	24.2	2.01	1.62	15.8	0.35	2.61	9.73	14.38	0.61	0.38	27.8	19.97	7.83	1.69	13	0.07	95	17.03	6	72	22	6.74	64.8	31	0.36	140	0.46
100' d/s Lower R/B (Big Creek)	11.70	0.67	25.5	2.04	1.62	16.0	0.48	2.63	9.83	11.97	0.62	0.38	26.9	20.57	6.33	1.53	6.46	0.11	94	6.95	8	72	20	6.66	78.3	25.3	0.32	189	0.22
80' d/s Middle R/B (Big Creek)	5.13	1.67	28.1	1.96	1.53	18.0	0.28	2.63	7.83	13.60	0.72	0.42	29.0	23.99	5.03	1.87	25.5	0.06	96	3.72	5	80	15	7.05	50.2	25.9	0.34	626	0.19
50' d/s Lower R/B (Big Creek)	9.14	1.01	23.4	2.04	1.65	18.0	0.45	2.61	8.25	11.59	0.58	0.37	26.9	20.10	6.8	1.67	13.4	0.07	91	6.55	10	70	20	6.72	62.4	25.6	0.34	200	0.51
60' u/s Top L/B (Town Creek)	5.20	2.02	27.2	1.95	1.53	17.0	0.50	2.59	8.15	11.56	0.69	0.41	36.7	25.62	11.1	2.22	2.45	0.03	97	10.0	5	73	22	7.51	66.1	32.9	0.5	224	0.85
70' u/s Lower L/B (Town Creek)	5.56	3.12	28.2	1.97	1.54	20.0	0.43	2.65	4.46	12.10	0.72	0.42	30.4	24.57	5.83	1.58	1.49	0.08	95	3.87	8	75	17	7.26	59.9	33.7	0.34	162	0.38
120' u/s Middle L/B (Town Creek)	4.72	2.1	27.5	1.95	1.53	19.0	0.50	2.66	4.96	10.85	0.74	0.43	31.8	24.47	7.33	1.83	2.42	0.03	94	5.77	10	71	19	7.28	95.4	33.7	0.39	226	0.59
125' u/s Lower L/B (Town Creek)	1.74	5.28	27.6	1.94	1.52	18.0	0.42	2.62	5.85	19.10	0.72	0.42	30.8	24.04	6.76	1.7	1.42	0.11	95	3.94	7	76	17	7.45	24.5	33	0.4	146	0.48
5' u/s Middle R/B (Town Creek)	9.25	1.2	33.4	1.86	1.39	17.0	0.40	2.53	3.08	10.15	0.82	0.45	32.2	25.70	6.5	2.65	4.29	0.3	99	5.09	2	78	20	6.97	34.9	32	0.32	253	-0.18
90' u/s Lower Middle R/B (Town Creek)	6.03	1.77	31.4	1.86	1.41	18.0	0.38	2.61	4.10	9.81	0.84	0.46	32.6	25.43	7.17	3.56	1.97	0.16	96	4.84	7	75	18	7.66	27.5	33.1	0.4	347	0.17
240' u/s Middle L/B (Coal Creek)	7.80	1.4	26.5	2.00	1.58	11.5	0.31	2.63	9.40	14.00	0.67	0.40	37.2	20.69	16.5	2.95	7.95	0.06	99	18.03	2	65	33	7.1	115.0	31.2	0.5	366	0.65

Table A.1.3 (continued)

Location	τ_c (Pa)	K (cm^3/N-s)	WC %	BD (g/cm^3)	DD (g/cm^3)	D_{50} (µm)	DR	SG	Cu (Psi)	Str %	e	n	LL %	PL %	PI %	OC %	SAR	KIA	Pass 200 %	σ_g	Sand %	Silt %	Clay %	pH	SS (m^2/g)	T (C)	CA	EC (µS)	Con
30' d/s Bottom of Creek L/B (Coal Creek)	4.74	1.79	32.2	1.93	1.46	15.7	0.26	2.65	5.97	12.00	0.81	0.45	32.0	23.43	8.57	2.07	2.95	0.17	93	7.62	5	72	23	7.12	61.8	31.7	0.37	103	-0.02
20' d/s Upper L/B (Coal Creek)	5.50	2.1	24.0	2.01	1.62	16.5	0.28	2.64	10.23	9.04	0.63	0.39	32.4	23.91	8.49	2.09	7.2	0.04	97	7.26	5	71	24	6.93	77.1	32.1	0.35	454	0.99
200' u/s Bottom of Creek R/B (Coal Creek)	13.40	0.8	31.4	1.89	1.44	15.0	0.42	2.65	4.91	17.50	0.84	0.46	36.6	22.62	14	2.39	2.47	0.36	97	9.49	5	66	29	7.03	102.1	31.1	0.48	137	0.37
180' u/s Upper R/B (Coal Creek)	4.90	2.8	24.9	1.94	1.55	13.0	0.30	2.67	5.60	8.80	0.72	0.42	35.6	21.21	14.4	2.8	3.79	0.05	97	12.04	4	67	29	7.05	96.0	31.2	0.5	189	0.74
140' u/s Middle R/B (Coal Creek)	5.80	2	25.7	1.96	1.56	16.0	0.24	2.67	5.88	12.05	0.71	0.42	31.0	23.54	7.46	1.98	3.96	0.12	96	6.44	7	72	21	6.77	69.1	30.7	0.36	190	0.71
20' u/s Middle L/B (Mud Creek)	2.37	3.1	30.5	1.91	1.46	20.0	0.26	2.61	2.30	14.65	0.79	0.44	24.9	18.80	6.1	1.75	4.63	0.15	84	13.46	18	62	20	7.13	30.0	32.1	0.31	75.2	-0.92
30' d/s Lower L/B (Mud Creek)	4.05	1.53	26.2	1.99	1.58	20.0	0.27	2.63	4.57	12.35	0.66	0.40	25.2	20.11	5.09	1.87	3.78	0.44	84	7.85	18	63	19	7.01	37.3	31.6	0.27	129	-0.19
150' u/s Upper R/B (Mud Creek)	1.34	4.63	31.1	1.81	1.38	10.5	0.38	2.59	3.43	13.35	0.88	0.47	32.4	23.75	8.65	2.74	6.31	0.36	99	6.40	2	72	26	6.66	58.1	31.7	0.33	61.7	0.15
60' u/s Lower R/B (Mud Creek)	10.10	1.1	29.0	1.91	1.48	11.5	0.42	2.57	3.50	14.51	0.73	0.42	28.6	21.56	7.04	3.62	21.7	1.25	95	7.35	6	69	25	6.43	42.2	31.6	0.28	102	-0.06
40' u/s Middle R/B (Mud Creek)	10.00	1.3	27.5	1.90	1.49	9.0	0.27	2.59	4.40	17.77	0.74	0.42	31.4	21.69	9.71	3.74	10	0.5	91	5.48	4	66	30	6.86	48.3	31.4	0.32	224	0.40

Table A.1.4 Cluster 4 data

Location	τ_c (Pa)	K (cm^3/N-s)	WC %	BD (g/cm^3)	DD (g/cm^3)	D_{50} (µm)	DR	SG	Cu (Psi)	Str %	e	n	LL %	PL %	PI %	OC %	SAR	KIA	Pass 200 %	σ_g	Sand %	Silt %	Clay %	pH	SS (m^2/g)	T (C)	CA	EC (µS)	Con
100' d/s Lower Middle R/B (Mud Creek)	8.00	1	24.4	2.03	1.63	12.0	0.30	2.62	7.99	6.05	0.61	0.38	33.0	20.45	12.55	2.4	15.84	0.74	94	13.54	7	63	30	5.97	96.6	28.5	0.42	63.8	0.69
30' u/s Lower L/B (Spring Creek)	7.00	1.523	39.0	1.83	1.32	12.0	0.35	2.61	1.86	12.75	0.98	0.49	29.2	20.71	8.49	4.65	1.47	0.27	94	6.71	7	66	27	7.34	41.6	28.2	0.31	340	-1.15
40' d/s Upper L/B (Spring Creek)	4.13	1.96	19.7	1.78	1.49	15.0	0.22	2.59	6.65	8.20	0.74	0.24	26.4	18.72	7.68	4.35	2.23	0.10	75	15.41	26	51	23	7.29	46.5	29.1	0.33	538	0.88
60' d/s Middle L/B (Spring Creek)	3.96	3.08	32.4	1.73	1.31	12.1	0.29	2.58	5.29	6.60	0.98	0.49	34.0	23.08	10.92	6.10	3.58	0.06	87	7.07	14	59	27	7.45	43.4	29.8	0.40	692	0.15
20' d/s Middle R/B (Spring Creek)	1.20	4.46	24.3	1.77	1.43	12.2	0.22	2.60	3.35	10.15	0.82	0.45	28.6	19.51	9.09	3.74	10.2	0.07	93	6.71	8	65	27	7.36	45.3	30.7	0.34	490	0.47
30' u/s Lower R/B (Spring Creek)	12.13	0.83	24.8	1.98	1.59	12.0	0.37	2.63	6.05	13.60	0.65	0.40	27.9	18.66	9.24	3.40	1.19	0.25	92	7.48	9	65	26	7.4	41.0	31.5	0.36	296	0.33
3' u/s Upper R/B (Spring Creek)	2.85	5.76	19.1	1.78	1.49	12.0	0.26	2.59	5.68	2.45	0.73	0.42	28.2	19.30	8.90	3.33	2.81	0.11	97	6.21	4	71	25	7.65	41.6	31.7	0.36	283	1.02
10' d/s Middle R/B (Red River)	3.94	2.4	20.5	2.04	1.69	15.0	0.45	2.61	7.50	6.50	0.55	0.35	25.6	16.90	8.70	3.10	0.94	0.06	82	22.29	20	56	24	7.37	55.0	25.4	0.36	115	0.59
5' d/s Lower R/B (Red River)	3.70	4.56	23.1	2.00	1.62	13.0	0.33	2.59	2.61	11.51	0.60	0.37	25.2	17.45	7.75	2.99	1.03	0.06	87	9.62	16	59	25	7.36	41.6	25.7	0.31	156.6	0.27
5' d/s Upper R/B (Red River)	3.89	4.78	22.0	1.89	1.55	12.5	0.24	2.62	5.85	3.30	0.69	0.41	27.2	18.53	8.67	3.60	0.98	0.10	87.5	8.80	17	57	26	7.51	50.2	26.5	0.33	319	0.60
30' u/s Lower R/B (Red River)	2.97	3.26	34.1	1.81	1.35	14.0	0.20	2.58	1.52	4.75	0.91	0.48	31.5	23.15	8.35	5.89	0.75	0.32	84	6.32	18	58	24	7.25	51.4	28.5	0.35	669	-0.31
5' u/s Upper Middle L/B (Peyton Creek)	3.50	3.92	25.2	1.88	1.50	5.5	0.28	2.61	6.61	4.70	0.74	0.43	35.0	23.42	11.58	4.64	2.96	0.04	97	15.63	4	59	37	6.61	50.2	26.3	0.31	143.3	0.84
10' u/s Lower L/B (Peyton Creek)	5.60	1.60	30.9	1.89	1.44	5.6	0.35	2.63	2.16	8.35	0.82	0.45	37.2	23.69	13.51	4.65	4.26	0.05	97	18.71	4	57	39	6.58	38.5	25.3	0.35	164.4	0.46
10' u/s Middle L/B (Peyton Creek)	6.00	1.89	29.2	1.87	1.45	6.9	0.31	2.66	3.58	10.60	0.84	0.46	35.4	23.92	11.48	4.60	1.34	0.07	96	16.33	5	59	36	6.99	49.5	25.4	0.32	176.4	0.54
10' u/s Lower R/B (Peyton Creek)	11.95	1.12	29.2	1.90	1.47	7.6	0.30	2.62	3.32	6.90	0.79	0.44	34.6	22.33	12.27	4.60	0.83	0.05	96	15.81	5	61	34	7.13	52.6	22.2	0.36	158.4	0.44
5' u/s Middle R/B (Peyton Creek)	7.79	1.43	28.0	1.88	1.47	8.2	0.36	2.60	6.30	4.90	0.77	0.43	34.2	22.65	11.55	4.32	0.8	0.06	90	13.90	12	56	32	7.36	53.8	24.7	0.36	182.6	0.54
10' u/s Upper R/B (Peyton Creek)	4.49	3.1	22.0	1.94	1.59	6.2	0.22	2.67	9.05	6.60	0.67	0.40	33.4	21.63	11.78	4.26	0.72	0.05	94	15.08	7	57	36	7.15	48.9	26.7	0.33	169	0.97

Appendix A.2 Soil Properties

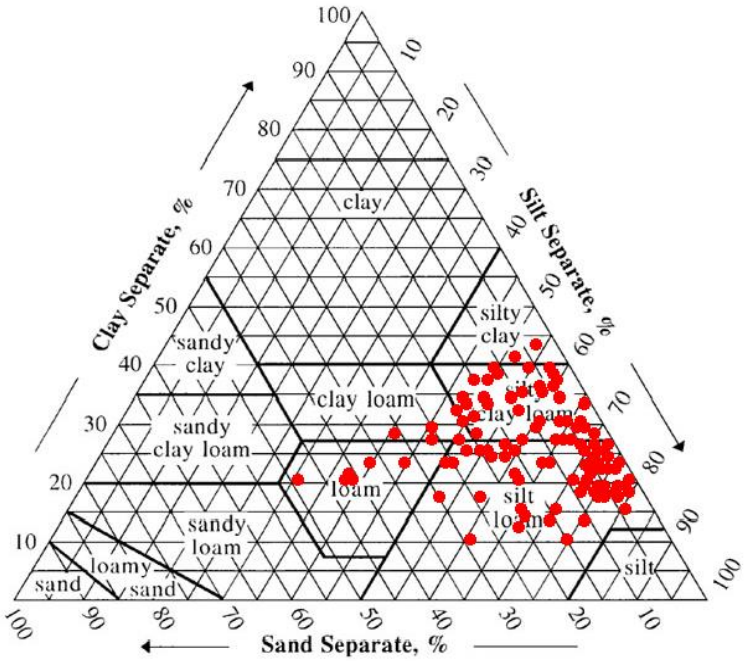


Figure A.2.1: Soil textures for tested soil samples (figure compiled using USDA soil texture calculator, http://www.nrcs.usda.gov/wps/portal/nrcs/detail/soils/survey)

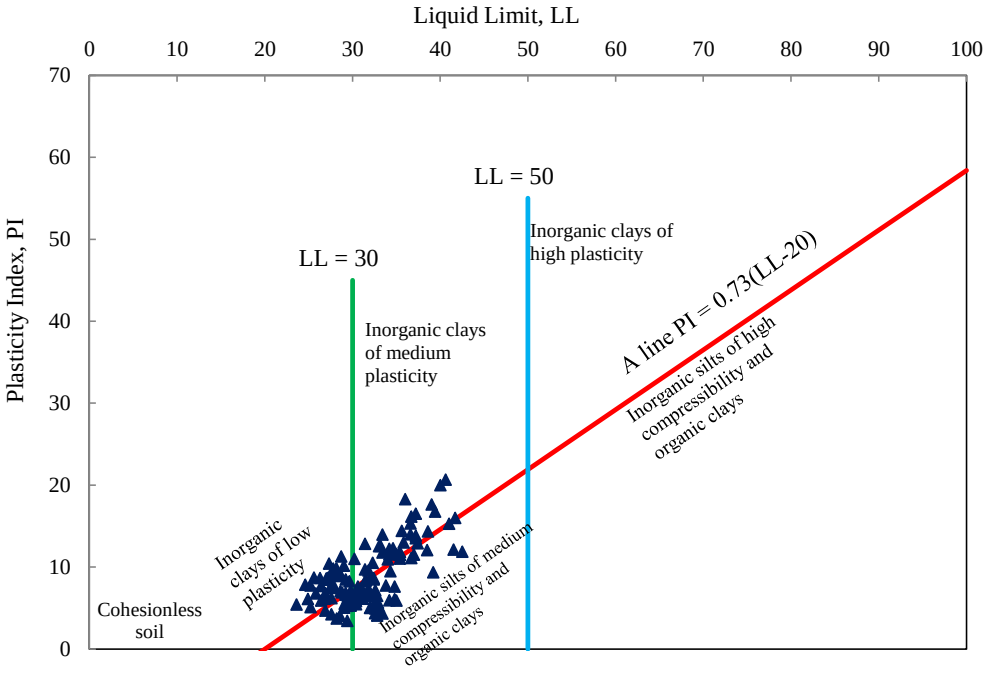


Figure A.2.2: Soil classification according to the Unified Soil Classification System (USCS) Plasticity Chart

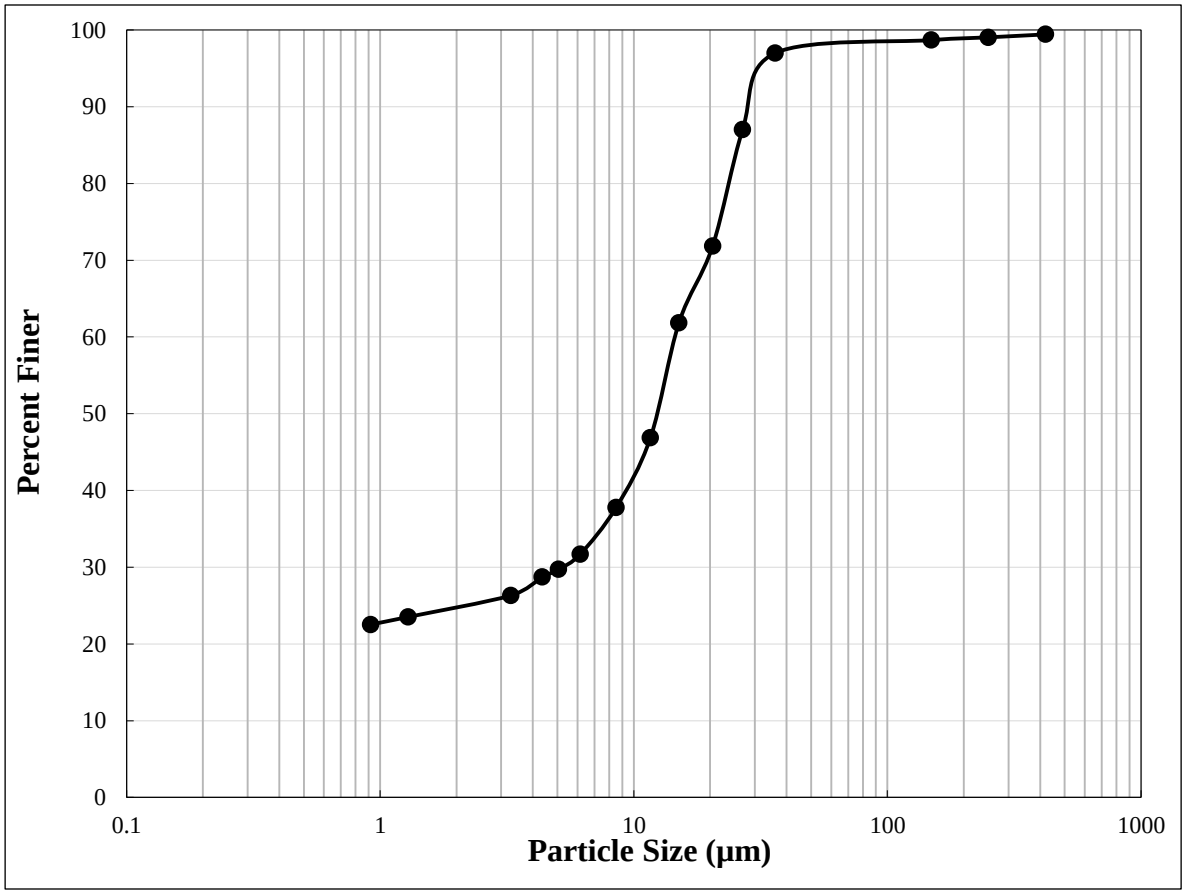


Figure A.2.3: Particle size distribution of the natural cohesive sediment

VITA

Badal Mahalder was born in Bangladesh to the parents of Kanchan and Amar Mahalder. He is the youngest of his three siblings Madhuri and Debabrata. He obtained his Bachelors of Science and Masters of Science degrees from Bangladesh University of Engineering and Technology (BUET), Bangladesh in Water Resources Engineering in January 2008 and January 2011, respectively. After finishing his B. Sc., he was appointed as a Lecturer in the same university and served there for three years and promoted to Assistant Professor. In 2011, he moved to USA for his higher education and received his second MS from the North Carolina State University (NCSU) from Civil, Construction and Environmental Engineering Department. He accepted a graduate research assistantship for pursuing his Ph. D. at the University of Tennessee, Knoxville in the Civil and Environmental Engineering department in 2013 and graduated in March 2018. He is currently working at Pape-Dawson Engineers Inc. as a Water Resources Engineer in Houston, TX.